Proceedings of the 19th European VLBI for Geodesy and Astrometry Working Meeting

G. Bourda, P. Charlot, A. Collioud

Proceedings of the 19th European VLBI for Geodesy and Astrometry Working Meeting

24–25 March 2009

Bordeaux, France

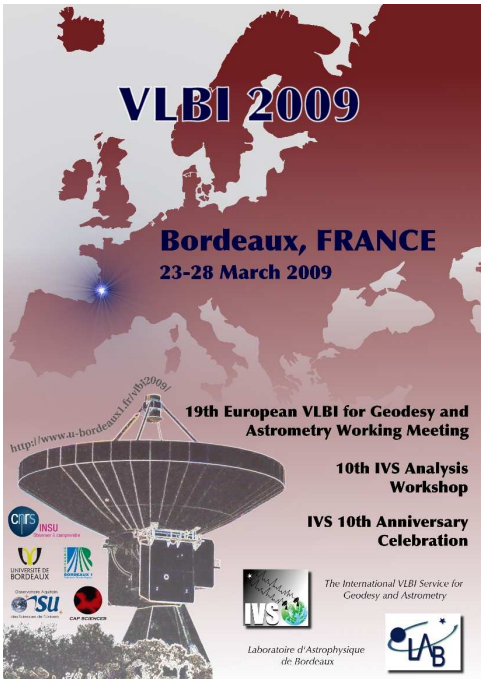

edited by G. Bourda, P. Charlot and A. Collioud

Université Bordeaux 1 – CNRS
Observatoire Aquitain des Sciences de l'Univers
Laboratoire d'Astrophysique de Bordeaux

Responsible for this issue: Géraldine Bourda, Patrick Charlot, and Arnaud Collioud
2009
Bordeaux, France

Printed by: ACSD – Imprimerie Numérique Reprographie – Bordeaux, France

Table of contents

Preface

The Laboratoire d'Astrophysique de Bordeaux (LAB) from the University Bordeaux 1 and CNRS, France, hosted the 19th European VLBI for Geodesy and Astrometry (EVGA) Working Meeting on March 24–25, 2009. This event took place at Cap Sciences (Hangar 20, Quai de Bacalan, F-33300 Bordeaux). The purpose of the EVGA meeting is to report the latest results on astrometric and geodetic VLBI research, including technical developments, applications to geophysics and astrophysics, and the future perspective of VLBI. More than 80 scientists working in all fields of geodetic and astrometric VLBI, from all around the world (20 countries), gathered in Bordeaux for the occasion, which is by far the largest attendance for these meetings. A total of 33 oral and 15 poster presentations were given by participants during the conference.

In addition, a specific symposium was held to celebrate the 10th Anniversary of the International VLBI Service for geodesy and astrometry (IVS) during the afternoon of March 25. This celebration took place in the prestigious Salle Agora of Université Bordeaux 1, a chapel-converted-to-conference-room, giving the event the proper ambience. During the symposium, invited speakers addressed the history of the IVS and its interrelation with the other geodetic services and other VLBI networks. This was complemented by welcome addresses given by Harald Schuh (IVS Chair) and Jean-Baptiste Verlhac (vice-president of University Bordeaux 1), and greetings by representatives from the International Association of Geodesy and the International Astronomical Union. The event was live broadcast over the Internet.

The 10th IVS Analysis Workshop, focused on the discussion of current and future IVS products, was held on March 26, 2009. Meetings from the IVS Working Group on data structure and the IVS/IERS Working Group on the next realization of the International Celestial Reference Frame also took place during the same week, along with a meeting of the IVS Directing Board. The latter was held at the Observatory of Bordeaux in Floirac. Altogether, about 100 scientists attended some or all of the meetings organized during this "VLBI week" in Bordeaux.

Group picture of the participants in the 19th EVGA Working Meeting and IVS 10th Anniversary celebration.

The oral and poster presentations from the 19th EVGA Working Meeting are available from the conference web site at **http://www.u-bordeaux1.fr/vlbi2009** along with the electronic version of these proceedings. Additionally, a recording of the presentations from the IVS 10th Anniversary celebration is available at **http://canalc2.u-strasbg.fr/video.asp?idvideo=8558**.

The papers from this publication should be cited as:

Authors, Title (2009), Proceedings of the 19th European VLBI for Geodesy and Astrometry Working Meeting, 24–25 March 2009, edited by G. Bourda, P. Charlot, and A. Collioud, Université Bordeaux 1 – CNRS – Laboratoire d'Astrophysique de Bordeaux.

Acknowledgements

We are grateful to all the authors for preparing and submitting their manuscripts in time, which facilitated the publication of these proceedings.

We also acknowledge Cap Sciences for hosting this meeting, the University Bordeaux 1 for making available the Agora chapel for the IVS 10th Anniversary celebration, the "Atelier Audiovisuel Multimedia" of the University Bordeaux 1 for arranging the broadcast over the internet, and the CNRS regional offices (Délégration Régionale Aquitaine-Limousin) for providing web registation.

Support was provided by the following organizations: University Bordeaux 1, INSU (Institut National des Sciences de l'Univers), OASU (Observatoire Aquitain des Sciences de l'Univers), LAB (Laboratoire d'Astrophysique de Bordeaux), IPF (Institut de Physique Fondamentale), Conseil Régional d'Aquitaine, and IVS (International VLBI Service for geodesy and astrometry).

We would like to warmly thank the other members of the local organizing committee, namely Reine Bedos for dealing with general logistics, registration issues and contact with participants, Antoine Bellanger, Lydie Durepaire and Ming Zhang for helping with many other aspects which made this conference and the other side meetings organized during the same week run smoothly. We are also grateful to Nicolas Daugey for building and maintaining the conference web site all along.

Géraldine Bourda, Patrick Charlot, and Arnaud Collioud
Editors
Bordeaux, September 2009

Preparations for the Next ICRF: Work at GSFC

D. Gordon, D. MacMillan
NVI Inc., Goddard Space Flight Center

Abstract. In preparation for the second realization of the ICRF, we have investigated VLBI radio source time series behavior and studied the effects of different data options and analysis models. The tests and comparisons made indicate that the full geodetic VLBI data span (1979–present), including mobile VLBI sessions and VCS sessions and the latest analysis models can be safely used with no adverse effects on the celestial reference frame.

Keywords. Reference frames, VLBI

1 Introduction

Generation of the second realization of the International Celestial Reference Frame (ICRF2) at radio wavekengths will be finalized by an IERS/IVS working group over the next few months. ICRF2 will be generated so as to be consistent with the current realization of the ITRF (International Terrestrial Reference Frame) and EOP products. Thus it will be a TRF solution, and use pressure loading, the Vienna Mapping Function (VMF), and an antenna thermal deformation model. In preparation, we have studied source time series and made various tests and comparisons in order to understand the effects of different session types, different data spans, and different analysis models.

2 Time Series Analysis

Time series solutions were made of all sources. For each source observed in 5 sessions or more, we computed the weighted RMS of its R.A. (Right Ascension) and Declination positions, with respect to the mean. Of particular interest is a clear declination dependence of the WRMS's, shown in Fig. 1. There is a steady increase from north to south, with a hump centered at $\sim -35°$ declination. This distribution reflects the distribution of stations (roughly 80% have been in the northern hemisphere) and the resulting observing history. The ICRF2 Working Group will have to select a large set of stable sources to define the axes of the ICRF2. Astrophysically, there is no reason to expect source stability to be declination dependent, therefore, this observed dependence must be taken into account when selecting the set of defining sources.

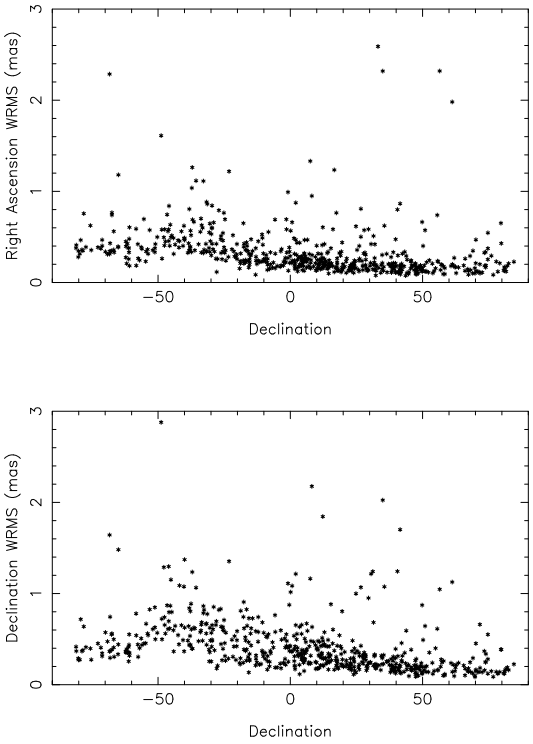

Figure 1. Weighted RMS position variations about the mean in R.A. and declination from a time series solution.

3 Data Comparisons

VLBI data quality has improved significantly since the beginning of the Mark3 era, and a question posed was whether use of the earliest Mark3 data would have any adverse effects on the ref-

erence frame. To study that question we made several comparisons with different data ranges: 1979–2008, 1990–2008, and 1993–2008. The 1979 starting date gives the smallest formal errors and does not appear to degrade or distort the solution, compared to the other two. On the other hand, with the 1993 starting date, we begin to lose significant amounts of data on a few sources observed more in earlier years. Thus, it appears advantageous to use the earliest Mark3 data.

Another question was whether to use only the fixed station sessions, or to include mobile sessions, regional sessions, and other non-standard sessions. To study this question, we made three comparison solutions with different session types: fixed station only sessions; fixed station + mobile sessions; and fixed station + mobiles + small regional sessions. Little change was seen when the Western U.S. and Alaska mobile sessions were added. But larger changes were seen when the regional and other weak sessions were added. The mobile sessions usually had 2 or 3 larger fixed antennas participating, and would be expected to contribute to the reference frame. The regional sessions (mostly Japanese and Canadian sessions) were weaker astrometrically, with smaller networks and often only one large fixed antenna. Thus, it has been decided to use only the fixed station sessions and sessions with mobile antennas that included at least two fixed antennas.

A third data comparison was made in which the VLBA Calibrator Survey (VCS) sessions were added to the solution. There are 24 VCS sessions, from 6 campaigns (Beasley et al. (2002); Fomalont et al. (2003); Petrov et al. (2005, 2006); Kovalev et al. (2007); Petrov et al. (2008)). Their use adds nearly 2200 additional sources, mostly from a single epoch. When they are included, mostly just small positions differences are seen in the non-VCS sources, with no systematic effects. However, a few sparsely observed sources do show large position changes, due to a large increase in the number of observations and to presumably a better position.

4 Model Comparisons

4.1 TRF vs. Baseline Solution

For the first ICRF and its extensions, baseline solutions were made, in which site positions were estimated for each session. However, for consistency with ITRF2008, ICRF2 must be generated as a TRF solution, in which a single site position and velocity will be estimated. Tests were made to see what effect this might have on the reference frame. Matching TRF and baseline solutions were made and compared. Their differences should allow us to assess how much unmodeled site position noise in the TRF solution propagates into other parameter estimates, specifically the source position estimates. The two solutions show mostly only noise-like differences with WRMS's of 10-12 μas, and with no differences greater than around 0.6 mas. There are no declination or R.A. dependent systematic variations in the differences. This comparison gives us confidence that the TRF requirement will not have any adverse effect on ICRF2.

4.2 Gradient Tests

Atmosphere gradients have a strong, declination dependent effect on the celestial reference frame, if not corrected for. The effect can be as much as $\sim$0.5 mas at around -10° declination. For the first ICRF solution, total gradients with no constraints were solved for. The current method in program Solve is to apply an a priori gradient model and solve for a residual. The a priori model in use (MacMillan and Ma (1997)) was derived from a numerical weather model, and essentially gives a fixed N-S gradient for each site. We compared two solutions, one solving for total gradients with no a priori model applied, and the other solving for gradient residuals with the a priori model applied. As long as the constraints are not too tight, agreement between the two methods is very good, and all differences are less that 2.1 times their formal errors.

4.3 Pressure Loading Tests

Comparisons were made with pressure loading applied versus not applied. Many small differences are seen in positions, mostly less than 0.2 mas, with no change in formal errors. Pressure loading has been shown to improve VLBI baseline repeatability (Petrov and Boy (2004)), and it was used in the VLBI contribution to ITRF2008. Our tests show that applying pressure loading has no systematic effect on the celestial reference frame.

4.4 VMF vs NMF Test

The VLBI contribution to ITRF2008 used the Vienna Mapping Function (VMF) for tropospheric delays (Böhm and Schuh (2004)). Therefore, VMF should also be used for ICRF2. The previous standard was the Niell Mapping Function (NMF) (Niell (1996)). We made comparison solutions using VMF and NMF. Source position differences are mostly small, and none are greater than 0.9 formal errors.

4.5 Thermal Deformation Test

The antenna thermal deformation model (Nothnagel (2008)) is another of the new models that should be used for ICRF2. It accounts for the change in the position of the reference point of an antenna as a function of temperature relative to a specified reference temperature for each site. Specific information for each antenna (structural dimensions, expansion coefficients, reference temperature) are provided in Nothnagel (2008). A comparison of source catalogs was made with and without the thermal deformation model applied. Only small random differences are seen, up to $\sim$0.1 mas.

5 Summary of Data and Model Comparisons

Table 1 summarizes the results of the various data and model comparisons. We present the weighted means of the differences and their weighted RMS's in Right Ascension and declination, as well as the overall rotation angles between the pairs of solutions. We see that there are no systematic effects due to various data or analysis options exceeding $\sim$18 μas (WRMS) or axes rotations greater than $\sim$8 μas. This compares well with (from preliminary work) an estimated noise floor of $\sim$50 μas and an estimated axes stability of $\sim$20 μas or better for ICRF2.

References

Beasley, A. J., D. Gordon, A. B. Peck, L. Petrov, D. S. McMillan, E. B. Fomalont, C. Ma, "The VLBA Calibrator Survey-VCS1", ApJS., vol. 141, p.13-21, 2002.

Böhm, J., H. Schuh, "Vienna Mapping Functions in VLBI Analysis", Geophys Res Lett, vol. 31, L01603, doi:10.1029/2003GL018984, 2004.

Fomalont, E., L. Petrov, D. S. McMillan, D. Gordon, C. Ma, "The Second VLBA Calibrator Survey - VCS2", AJ, vol. 126 (N5), p. 2562-2566, 2003.

Kovalev, Y. Y., L. Petrov, E. Fomalont, D. Gordon, "The Fifth VLBA Calibrator Survey - VCS5", AJ, vol. 133, pp. 1236-1242, 2007.

MacMillan, D.S., C. Ma, "Atmospheric Gradients and the VLBI Terrestrial and Celestial Reference Frames", Geophys Res Lett, vol. 24, p.453-456, 1997.

Niell, A.E., "Global Mapping Functions for the Atmosphere Delay at Radio Wavelengths", J Geophys Res, vol. 101, p. 3227-3246, 1996.

Nothnagel, A. "Short Note: Conventions on Thermal Expansion Modelling of Radio Telescopes for Geodetic and Astrometric VLBI", J Geod, doi: 10.1007/s00190-008-0284-z, 2008.

Petrov, L., Y. Y. Kovalev, E. Fomalont, D. Gordon, "The Third VLBA Calibrator Survey - VCS3", AJ, vol. 129, p. 1163–1170, 2005.

Petrov, L., Y. Y. Kovalev, E. Fomalont, D. Gordon, "The Fourth VLBA Calibrator Survey - VCS4", AJ, vol. 131, pp. 1872-1879, 2006.

Petrov, L., Y. Y. Kovalev, E. Fomalont, D. Gordon, "The Sixth VLBA Calibrator Survey - VCS6", AJ, vol. 136, p. 580, 2008.

L. Petrov, J.-P. Boy, "Study of the Atmospheric Pressure Loading Signal in Very Long Baseline Interferometry Observations", J Geophys Res, vol. 109, B03405, doi:10.1029/2003JB002500, 2004.

Table 1. Summary of Data and Model Comparisons

Data/Model Comparison	$\Delta\alpha\cos\delta$		$\Delta\delta$		Rotation Angles		
	mean (μas)	wrms (μas)	mean (μas)	wrms (μas)	X (μas)	Y (μas)	Z (μas)
Start Time: 1979 vs. 1990	1	8	1	11	0	2	1
Start Time: 1979 vs. 1993	0	14	0	18	-1	5	4
Session Type: Fixed vs. Fixed+Mobile	-1	2	-1	2	0	0	-1
Session Type: Fixed vs. Fixed+Mobile+Regionals	0	5	-2	5	2	-1	-3
VCS vs. No VCS	2	17	1	18	-7	1	1
TRF vs. Baseline	-1	10	0	12	2	2	2
Gradients: a priori vs. No a priori	0	7	6	12	8	5	3
Pressure Loading: On vs. Off	0	2	0	3	2	1	0
VMF vs. NMF	-1	3	-3	5	-1	2	-1
Thermal Deformation: On vs. Off	0	0	0	1	0	0	0

Dependence of Catalogue Orientation Parameters Accuracy from Sources Set Selection

S. Kurdubov, E. Skurikhina
Institute of Applied Astronomy RAS,
191187, nab Kutuzova 10, Saint-Petersburg, Russia

Abstract. In this paper we suggest ranking method of sources sets in order to select the list of sources that better define the orientation parameters of rigid rotation transformation from one system to another. Formal errors of the transformation parameters were selected as characteristic of sources set. For the 5 catalogues IVS WG was selected special order in the sources list and obtained transformation parameters accuracy as function of the number of sources. For all catalogues that function has a minimum between 300 and 400 sources, adding the sources after the minimum leads to increasing formal errors of orientation parameters. After that we selected the common sources which placed before minimum of functions from the 5 catalogues and obtained set of 319 sources.

Keywords. Reference frames, CRF, transformation, optimization

1 Introduction

The selection of sources for determining CRF (Celestial reference Frame) catalogues is usually based on various source ranking methods, using the source individual characteristics (e.g. number of observations, position accuracy, VLBI structure). Whereas the source geometrical distribution is taken into account only to ensure a uniform sky coverage (see for example Ma et al., 1998).

Instead of other investigators, we don't use the ranking of sources. We construct a ranking parameter that can characterize the list of sources. Then we can compare not individual sources but set of them. The main advantage of our method is that it uses both criteria: the geometrical distribution of the sources and the sources position accuracy.

We try to select the set of sources that minimizes formal errors of the orientation parameters of rigid rotation transformation model calculated from this set.

2 List characteristic definition

We want to investigate a given source catalogue (RA,DE), considering another arbitrary source catalogue (ra,de). From these, we can represent the differences $dRA = RA - ra$ and $dDE = DE - de$ as follow:

$$\begin{aligned} dRA &= A1\tan(DE)\cos(RA) + \\ &\quad A2\tan(DE)\sin(RA) - A3 \\ dDE &= A1\sin(RA) + A2\cos(RA) \end{aligned}$$

where A_1, A_2, A_3 are the transformation parameters. If we select the set of common sources in the two catalogues, then we can determine the parameters $\mathbf{A} = (A1, A2, A3)$ and the formal errors $(\sigma_{A1}, \sigma_{A2}, \sigma_{A3})$ by the Least Square method:

$$\mathbf{A} = \mathbf{N}^{-1}\mathbf{b}$$

$$\sigma_{A1} = \sigma_0\mathbf{N}^{-1}[0,0]$$

$$\sigma_{A2} = \sigma_0\mathbf{N}^{-1}[1,1]$$

$$\sigma_{A3} = \sigma_0\mathbf{N}^{-1}[2,2]$$

We form normal equation matrix $\mathbf{N} = \mathbf{C^T P C}$, where $\mathbf{C} = \partial(dRA, dDE)/\partial A$ and $\mathbf{P} = \mathbf{E}$ is the unitary matrix. The diagonal elements of inverted normal matrix $\mathbf{N}^{-1}[0,0]$, $\mathbf{N}^{-1}[1,1]$, $\mathbf{N}^{-1}[2,2]$ are not affected by the differences between the two catalogues and depend only on the set of sources. For determining σ_0, we use the formal errors of the selected set of sources:

$$\sigma_0 = \frac{\sum(\sigma_{RA})^2 + \sum(\sigma_{DE})^2}{N - 3} \qquad (1)$$

Then we calculate σ_{A1}, σ_{A2}, σ_{A3} that are not affected by the differences between the two catalogues, and that depend only on the geometrical distribution of the sources in the set and on the formal errors of source coordinates.

The following standard formula is not used:

$$\hat{\sigma_0} = \frac{\sum(r_{RA})^2 + \sum(r_{DE})^2}{N-3} \qquad (2)$$

where r_{RA} and r_{DE} are the residuals after transformation, because all CRF catalogues obtained from the same data and using σ_{RA} and σ_{DE} give more adequate results.

The proper formula used here is:

$$\sigma_0 = \frac{\sum(\sigma_{RA}) + \sum(\sigma_{DE})}{N-3} \qquad (3)$$

It gives more weight to the geometrical part $\mathbf{N}^{-1}$. There is no much difference in list construction, but replacing (1) by (3) moves the position of the minimum. By using formula (1), the minimization is obtained for N=100 sources, whereas by using (3), it is obtained for N=400 sources.

The source list ranking parameter q selected is the maximum of the orientation parameters formal errors:

$$q = MAX(\sigma_{A1}, \sigma_{A2}, \sigma_{A3}).$$

3 Optimized list construction

If we want to define the best orientation of the catalogue, we need to select the set of sources that minimizes the parameter q. This will be considered as the set of "defining" sources. We take into account only sources from ICRF-ext.2 catalogue that were observed more than 10 times (i.e. during more than 10 sessions) for the catalogue gsf008a. In order to select the proper sample of sources, we use the following algorithm:

1. Triple loop over all sources, in order to select three sources that minimize q. At this step, we have an optimal set of sources for $N_{sources} = 3$.
2. Search over all remaining sources in order to minimize q for N+1 sources. Remove the sources found from the list of remaining sources, and add it to the final set.
3. Repeat step 2 for all remaining sources.

After that we have sequence of the lists that contains optimal set of sources for a given $N_{sources}$.

4 Catalogues processing

We uses two approaches for determining σ_0. First, we take global solution formal errors as the σ_{RA} and σ_{DE} in (3). By using this method, the sources that have many observations will obtain very high weight but they can have systematic motion. In order to eliminate this effect, we use another approach taking σ_{RA} and σ_{DE} from the variances of time series.

4.1 Global solution formal errors

First we use formal errors of source positions from global solution, in order to determine σ_0 with (3). The results are presented in Figures (1, 2). The coordinates and formal errors were taken from the iaa000a, mao005a, opa005a, gsf005a, usn005a catalogues.

4.2 Time series dispersion

Then we use time series variances for determining σ_0 in (3). The results are presented in Figures (1, 2). Variances were calculated by the following source position time series: iaa000b, mao006a, opa002a, gsf001a, usn000d.

4.3 Common part

Finally, from these two methods, we obtained the value MAX(σ_{A1}, σ_{A2}, σ_{A3}) as a function of the number of sources for all 5 catalogues. This gives ten graphs (Figures 2–4), each one with a minimum between 300 and 500 sources. Adding the sources after the minimum leads to increasing formal errors of orientation parameters. Therefore, we can select the common sources of all ten lists before the minimum, and then we obtain the optimal set of sources. There is 319 common sources before minimum in the "global solution sigmas case", and 280 in the "time series sigmas case". The final list with the common sources from both approaches is summarized in Table 1, and the corresponding sky distribution is plotted in Fig. (5).

References

Ma C., Arias E.F., Eubanks T.M., Fey A.L., Gontier A.-M. et al., 1998, The International Celestial Reference Frame as Realized by Very Long Baseline Interferometry, AJ, 116, 516

Table 1. Final list of 259 sources

0059+581	1508-055	1216+487	0406+121	0507+179	0003+380	1830+285	0149+218
1240+381	1124-186	0109+224	1743+173	1741-038	0202-172	1514+197	1547+507
1300+580	0342+147	1049+215	0620+389	1418+546	0010+405	2253+417	2021+614
0133+476	2318+049	1725+044	1614+051	0827+243	0823+033	0400+258	0833+585
1417+385	2335-027	1504+377	1053+704	0219+428	0601+245	0812+367	2021+317
0642+449	1219+044	0148+274	2216-038	0736+017	0039+230	2351+456	0104-408
1656+477	2329-162	1920-211	1123+264	0420+417	1502+036	0111+021	0405-123
1128+385	2214+350	1821+107	1307+121	0544+273	1936-155	1402+044	2227-088
0749+540	1022+194	0248+430	0405-385	1717+178	0554+242	1705+018	1111+149
2209+236	1144+402	1351-018	1011+250	1508+572	0201+113	1435+638	0502+049
2113+293	0048-097	1413+135	1354+195	0215+015	0237-027	0317+188	1057-797
0602+673	1045-188	1023+131	0444+634	0850+581	2149+056	0202+319	0859+470
0607-157	2144+092	1144-379	0722+145	0234+285	1557+032	1020+400	1730-130
0552+398	1236+077	1624+416	0457+024	0917+449	1929+226	1637+574	1815-553
0743+259	1357+769	0302+625	0600+177	1954+513	1616+063	1055+018	
1758+388	1519-273	1514-241	1104-445	0430+289	2008-159	1313-333	
0808+019	2029+121	1237-101	1342+663	1746+470	0426+273	1347+539	
1655+077	0458-020	1958-179	0536+145	0300+470	1633+382	0208-512	
1606+106	0829+046	1954-388	0402-362	0949+354	0537-441	0836+710	
0804+499	1255-316	0954+658	1622-297	1150+497	0146+056	1842+681	
1749+096	1406-076	0537-286	1642+690	2320+506	0754+100	1116+128	
0955+476	1226+373	0309+411	1504-166	1156+295	1432+200	1510-089	
0035+413	0955+326	2126-158	0609+607	1745+624	1546+027	0306+102	
1726+455	0727-115	1803+784	1219+285	0446+112	1342+662	2150+173	
0805+410	1334-127	0742+103	1448+762	0748+126	0920+390	1937-101	
1823+568	2319+272	1548+056	2155-152	1652+398	1417+273	1252+119	
0440+345	1459+480	1908-201	1324+224	1014+615	0119+041	0814+425	
1923+210	0821+394	1004+141	1705+456	1147+245	0945+408	1012+232	
0110+495	1751+441	0839+187	1538+149	0322+222	0454-234	1502+106	
1738+499	0707+476	0656+082	0308-611	1849+670	0657+172	0319+121	
1600+335	1738+476	0952+179	0221+067	0735+178	1732+389	0828+493	
0917+624	1639+230	1424-418	1030+074	0016+731	1030+415	1213+350	
2136+141	0229+131	1932+204	2030+547	0912+029	0123+257	0138-097	
1555+001	1145-071	0420-014	1656+053	1101+384	0239+108	1800+440	
0151+474	1215+303	1244-255	2355-106	0119+115	0745+241	0738+491	

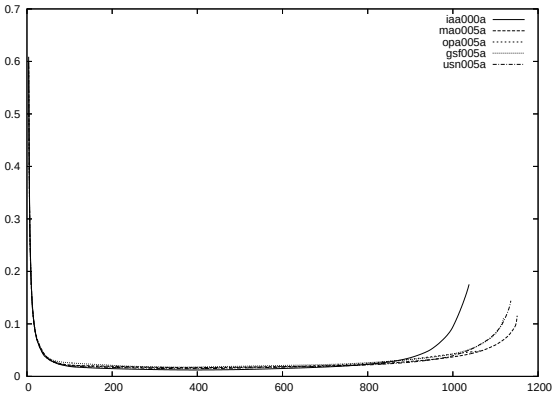

Figure 1. Normalized MAX(σ_{A1}, σ_{A2}, σ_{A3}) vs. number of sources for iaa000a, mao005a, opa005a, gsf005a, usn005a catalogues.

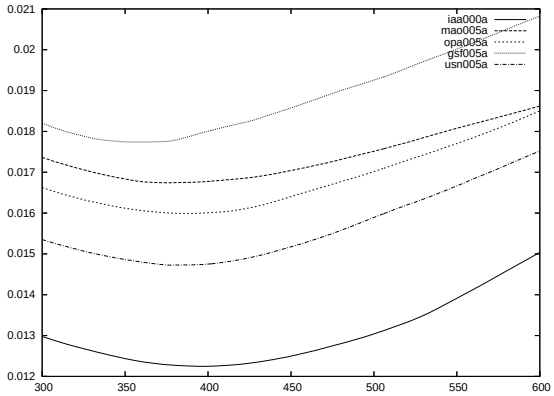

Figure 2. Normalized MAX(σ_{A1}, σ_{A2}, σ_{A3}) vs. number of sources for iaa000a, mao005a, opa005a, gsf005a, usn005a catalogues: zoom of Figure 1.

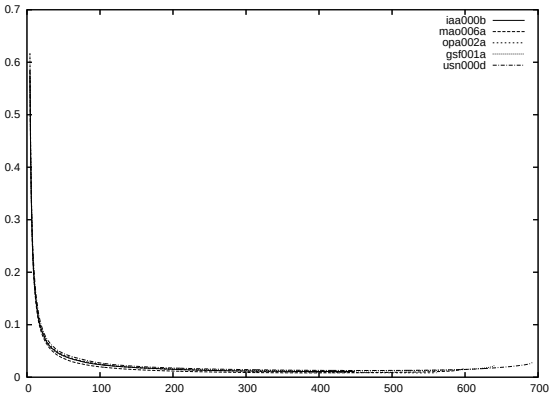

Figure 3. Normalized MAX(σ_{A1}, σ_{A2}, σ_{A3}) vs. number of sources for iaa000b, mao006a, opa002a, gsf001a, usn000d time series.

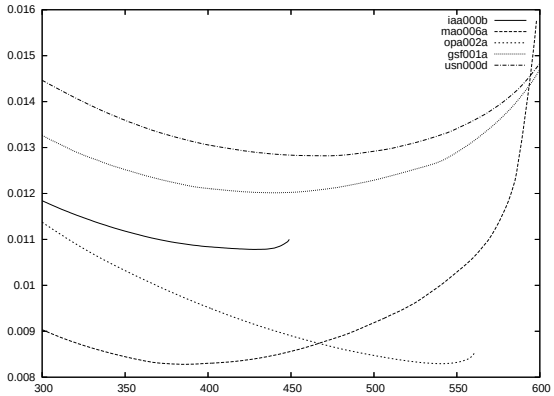

Figure 4. Normalized MAX(σ_{A1}, σ_{A2}, σ_{A3}) vs. number of sources for iaa000b, mao006a, opa002a, gsf001a, usn000d time series: zoom of Figure 3.

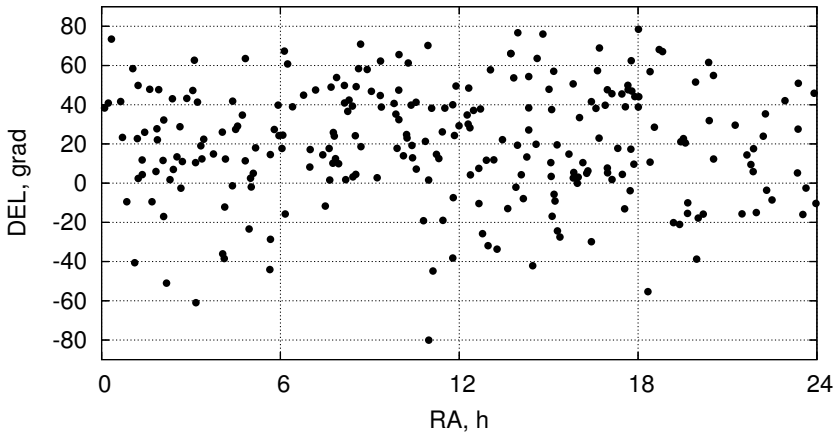

Figure 5. Final set of 259 sources.

X/Ka-band Global Astrometric Results

C. S. Jacobs, O. J. Sovers
Jet Propulsion Laboratory, California Institute of Technology,
4800 Oak Grove Dr., Pasadena, CA 91109

Abstract. In order to extend the International Celestial Reference Frame from its S/X- band (2.3/8.4 GHz) basis to a complementary frame at X/Ka-band (8.4/32 GHz), a series of X/Ka observations were acquired from 2005 to 2009 using NASA's Deep Space Network radio telescopes. We report global astrometric results from the first 41 sessions which covered right ascension over the full 24 hours and declination down to a southern limit of ≈ -45 deg. We detected 328 sources. Of these, 313 sources had at least 2 group delay measurements which were used to produce a nearly full sky catalog with median formal position uncertainties of 200 and 340 μas in $\alpha\cos(\delta)$ and δ, respectively. An external comparison of our X/Ka-band frame to a sucessor of the S/X-band ICRF shows 313 common sources with median absolute differences of 184 μas in $\Delta\alpha\cos(\delta)$ and 240 μas in $\Delta\delta$. These differences include zonal errors the largest of which are trends vs. declination. Systematic errors are due in part to the geometric weakness of using just two baselines and in part to mismodelling of troposphere and uncalibrated instrumental effects. Prospects for the future improvements are very positive with demonstrated technologies showing potential for a factor of three improvement in measurement precision.

Keywords. techniques: interferometric – catalogs – astrometry – reference systems – (galaxies:) quasars: general – radio continuum: galaxies.

1 Introduction

For almost three decades now, radio frequency work in global astrometry, geodesy, and deep space navigation has been done at S/X-band (2.3/8.4 GHz). While this work has been tremendously successful in producing 100 μas level global astrometry (e.g. Ma et al., 1998) and sub-cm geodesy, developments made over the last decade have made it possible to consider the merits of moving to a new set of dual-band frequencies. In this paper we present global astrometric results from X/Ka-band (8.4/32 GHz) observations. Complementary single-band work at 24 and 43 GHz has been done by Lanyi et al. (2008).

Moving the observing frequencies up by approximately a factor of four has several advantages. For our work in the Deep Space Network, the driver is the potential for higher telemetry data rates to and from probes in deep space. Other advantages include 1) the spatial distribution of flux becomes significantly more compact lending hope that the positions will be more stable over time, 2) Radio Frequency Interference (RFI) at S-band would be avoided, 3) ionosphere and solar plasma effects on delay are reduced by a factor of 15!

While these are very significant advantages, there are also disadvantages. The change from 2.3/8.4 GHz to 8.4/32 GHz moves one closer to the water vapor line at 22 GHz and the oxygen line at 60 GHz thereby increasing the system temperature from a few Kelvins per atmospheric thickness up to 10–15 Kelvins per atmosphere or more. Thus one becomes much more sensitive to weather. Furthermore, the sources themselves are in general weaker and many sources are resolved. Also, with the observing wavelengths shortened by a factor of 4, the coherence times are shortened so that practical integration times are a few minutes or less—even in relatively dry climates. The shorter wavelengths also imply that the antenna pointing accuracy requirements must be tightened by the same factor of 4. The combined effect of these disadvantages is to lower the system sensitivity. Fortunately, recent advances in recording technology (e.g. Whitney, 2009) make it feasible and affordable to offset

these losses in sensitivity by recording more bits. Thus while our X/Ka measurements used the same overall bit rate as previous S/X work, efforts are now underway to increase our bit rate by a factor of 4 to 8 within the next 1–2 years and by a factor of 36 within the next 3–5 years.

This paper is organized as follows. We describe the observations, modelling, and present the results. Next, we estimate the accuracy by comparing to a recent S/X celestial reference frame. This is complemented by a discussion of the error budget. Finally, we provide conclusions and anticipated directions for further research.

2 Observations and Modelling

The results presented here are based on 41 Very Long Baseline Interferometry (VLBI) observing sessions each of $\approx$ 24 hour duration done from July 2005 until January 2009 using NASA's Deep Space Stations (DSS) 25 or 26 in Goldstone, California to either DSS 34 in Tidbinbilla, Australia or DSS 54 or 55 outside Madrid, Spain to form interferometeric baselines of 10,500 and 8,400 km length, respectively.

We recorded VLBI data simultaneously at X (8.4 GHz) and Ka-band (32 GHz) sampling each band at a rate of 56 Mbps. Each band's 7 channels (each $\pm$2 MHz) spanned a bandwidth of $\approx$ 360 MHz. The data were filtered, sampled, and recorded to tape using the MKIV or Mk5 VLBI systems then correlated with either the JPL BlockII hardware (O'Connor, 1987) or SOFTC software (Lowe, 2005) correlators. Fringe fitting was done with the FIT software (Lowe, 1992). This procedure resulted in 8536 pairs of group delay and phase rate measurements covering the full 24 hours of right ascension and declinations down to -45 deg. Each observation was approximately 2 minutes in duration.

The observations were then modelled using the MODEST software (Sovers et al., 1998). A priori Earth orientation was fixed to the MHB nutation model (Mathews et al., 2002) and empirically determined UT1-UTC and Polar Motion from the Space 2006 series (Gross et al., 2007). The celestial frame was aligned to the ICRF (Ma et al., 1998) by fixing the RA and Dec of OJ 287 and the declination of CTD 20. Station locations were estimated, but velocities were fixed to decades-long S/X-band VLBI estimates.

3 Results

In all, we detected 328 extragalactic radio sources which covered the full 24 hours of RA and declinations down to $-45°$. In Figure 1 below, these sources are plotted using an Aitoff projection to show their locations on the sky. RA=0 is at the center. The ecliptic plane is shown by a dashed line and the Galactic plane is indicated as a black line shaped approximately like an Ω. The sources are coded according to their 1-σ formal declination uncertainties with the value ranges indicated in the figure's legend. Note that the declination precision decreases as one moves toward the south. This is a result of having significantly less data on the California to Australia baseline combined with the need to observe sources closer to the horizon as declination moves south thus incurring greater error from higher system temperatures and tropospheric mismodelling.

4 Accuracy and zonal errors

Experience shows that formal uncertainties tend to underestimate true errors. Thus we made an independent estimate of errors by differencing our X/Ka-band positions with those from S/X catalog GSFC-2008b-astro (Petrov, 2008). For the 313 sources in common, Figs. 2 and 3 show the weighted RMS (wRMS) differences are 203 μas in $\alpha\cos\delta$ and 279 μas in δ. The wRMS statistics are somewhat effected by outliers as shown by the median absolute deviations which are 184 and 240 μas in $\alpha\cos\delta$ and δ, respectively. Figure 4 shows $\Delta\delta$ vs. δ. Note the decreasing precision moving south.

In astrometry, it is usually much easier to measure the relative positions of nearby sources than to accurately measure sources that are separated by long arcs. In order to investigate this tendency, we calculated for both X/Ka and S/X the arclengths between all pairs of sources, binned them in 5 deg bins and then differenced the arcs. Figure 5 shows the mean arclength difference for each bin. As expected, arclengths agree better for short arcs and gradually worsen as arcs grow longer out to a mean difference of 50 μas at arcs of $\approx$ 70 deg. This is one measure of the level of zonal errors between X/Ka and S/X.

5 Error Budget

Having assessed position errors from differences with the much larger S/X data set, we now discuss the major contributions to the X/Ka measurement errors: SNR, instrumentation, and troposphere. Figure 6 shows the weighted RMS group delay vs. log10 of the Ka-band SNR. We conclude that for SNR < 15 dB, the thermal error dominates the error budget. For higher SNRs, troposphere and instrumentation errors become important. Binning of wRMS delay vs. airmass thickness shows that troposphere is not the dominant error due to the generally low SNRs just mentioned. However, the phase rates (which carry much less weight in the fit) are dominated by errors from tropospheric mismodelling, thus hinting that troposphere will become more important as our SNR improves. The last major category of errors comes from un-calibrated instrumentation. A proto-type phase calibrator has been developed for calibrating from the feed to the digitizer (Hamell et al., 2003). A test (Fig. 7) measured an approximately diurnal instrumental variation with ≈180 psec RMS. Although the data themselves can be used to partially parameterize this effect, we believe that phase calibrators will be needed to achieve accuracy of better than 200 μas in a timely manner.

6 Conclusions

The S/X-band ICRF has now been extended to the four times higher frequency of X/Ka-band (8.4/32 GHz). A total of 328 sources have been detected. For the 313 sources with sufficient quality for comparison to S/X results, we find wRMS positional agreement of 200 μas in $\alpha \cos\delta$ and 280 μas in δ. Median absolute deviations are slightly better. Zonal errors are $\approx$ 50 μas.

As positive as these results are, our X/Ka work still relies on ongoing S/X work for various geophysical models (nutation, precession, UT1−UTC). Thus it will be premature to speak of ending S/X observations for many years to come. Our current limiting errors are SNR and lack of instrumental phase calibration. We plan to address the SNR issue by increasing the recorded bit rate by a factor of 4–8. A proto-type phase calibrator has been built and operational units are being funded. If these improvements are implemented, we believe that we can achieve 200 μas or better by 2010.

Acknowledgements The research described in this paper was performed at the Jet Propulsion Laboratory of the California Institute of Technology, under a contract with the National Aeronautics and Space Administration. We appreciate the efforts of the following people in acquiring the data: Graham Baines, Leigh Cameron, Tim Gregor, Shinji Horiuchi, Cristina Garcia Miro, Esther Moll, David Rochblatt, Lyle Skjerve, Charles Snedeker, and Carleen Ward.

References

Gross R.S., 2007, Combinations of Earth Orientation Measurements: 'SPACE2006', JPL Pub. 07-5, Pasadena CA

Hamell R., Tucker B. & Calhoun M., 2003, Phase Calibration Generator, IPN Progress Report 42-154, pp. 1-14
http://tmo/progress_report/42-154/154H.pdf

Lanyi G.E., Fomalont E.B., Charlot P., Geldzahler B., Gordon D., Jacobs C.S., Ma C., Naudet C.J., Romney J., Sovers O.J. & Zhang L.D., 2008, Celestial Reference Frames at 24 and 43 GHz, AJ, submitted 21 Nov 2008

Lowe S.T., 1992, Theory of Post-BlockII VLBI Observable Extraction, JPL Pub. 92-7, Pasadena, CA

Lowe S.T., 2005, *SOFTC: A Software VLBI Correlator*, section 335 internal document, Jet Propulsion Laboratory, Pasadena, CA

Ma C., Arias E.F., Eubanks T.M., Fey A.L., Gontier A.-M., Jacobs C.S., Sovers O.J., Archinal B.A. & Charlot P., 1998, The International Celestial Reference Frame as Realized by Very Long Baseline Interferometry, AJ, 116, 1, pp. 516-546
www.journals.uchicago.edu/doi/abs/10.1086/300408

Matthews P.M., Herring T.A. & Buffet B.A., 2002, Modeling of nutation and precession: New nutation series for nonrigid Earth and insights into the Earth's interior, JGR, 107, B4, 10.1029/2001JB000390
www.agu.org/journals/jb/jb0204/2001JB000390/

O'Connor T., 1987, Introduction to the BlockII Correlator hardware, JPL internal publication, Pasadena CA

Petrov L., 2008, VLBI global solution 2008b_astro, *modified to use uninflated errors as provided by D. Gordon of NASA Goddard Space Flight Center*
http://vlbi.gsfc.nasa.gov/astro/

Sovers O.J., Fanselow J.L. & Jacobs C.S., 1998, Astrometry and Geodesy with Radio Interferometry: Experiments, Models, Results, *Rev. Mod. Phys.*, 70, 4
http://prola.aps.org/pdf/RMP/v70/i4/p1393_1

Whitney A., Romney J. & Owens K., 2009, Mark-5C VLBI Data System, this volume

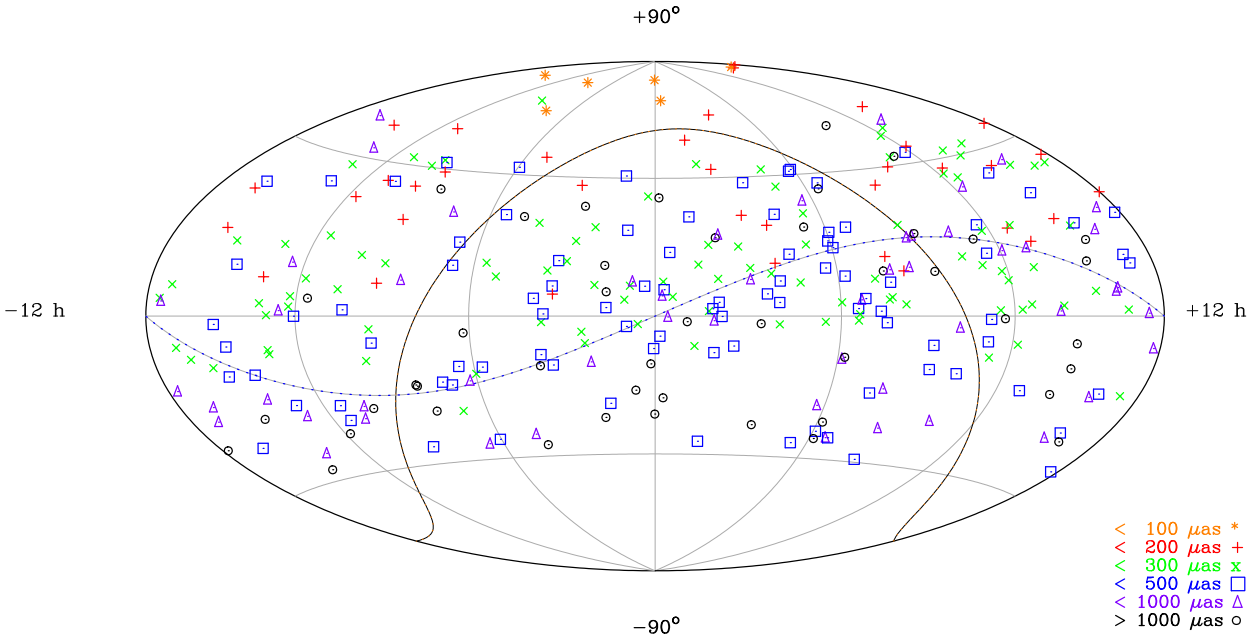

Figure 1. Distribution of 328 X/Ka-band sources detected to date. Symbols indicate 1-σ formal declination uncertainties with size bins defined in the legend at lower right. $(\alpha, \delta) = (0, 0)$ is at the center. The ecliptic plane is indicated by a dashed line. The galactic plane is indicated as a black line approximately shaped like an Ω.

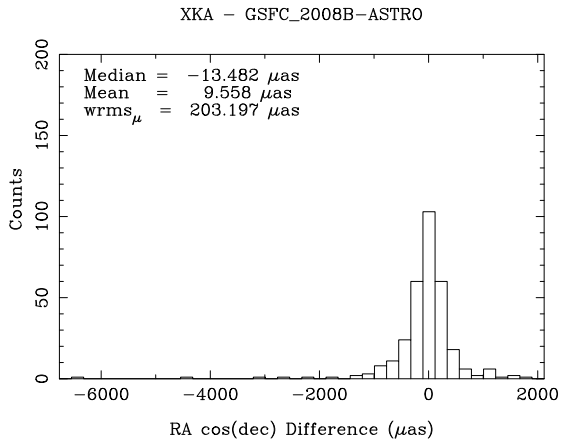

Figure 2. Histogram of $\alpha \cos\delta$ differences. WRMS scatter is 203 μas about a mean difference of 10 μas.

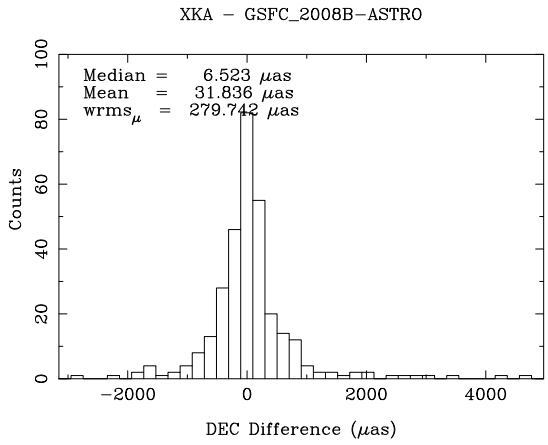

Figure 3. Histogram of δ differences. WRMS scatter is 280 μas about a mean difference of 32 μas.

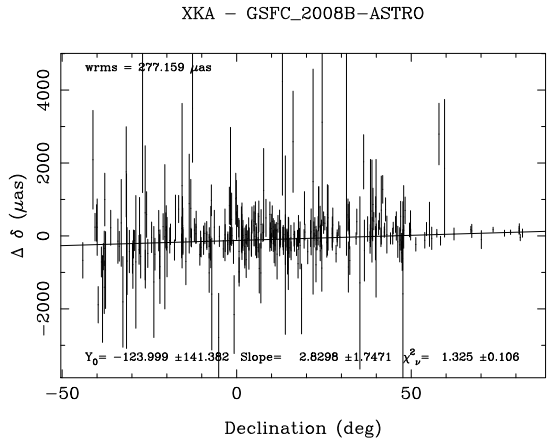

Figure 4. Declination differences (X/Ka − S/X) vs. declination. Note the decrease in precision towards the south.

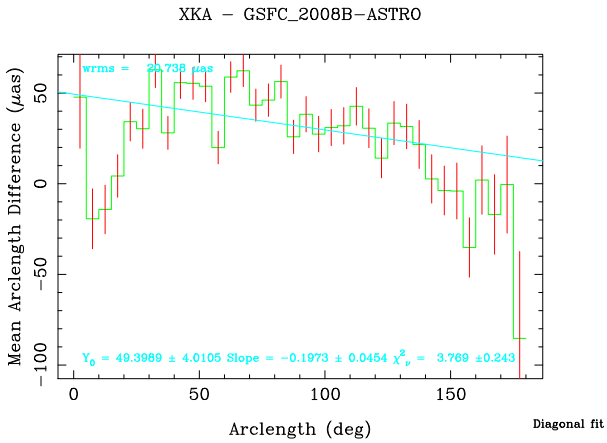

Figure 5. Arclength differences (X/Ka − S/X) vs. arclength. Zonal differences of ≈ 50 μas are seen between the X/Ka and GSFC-2008b-astro S/X catalogs.

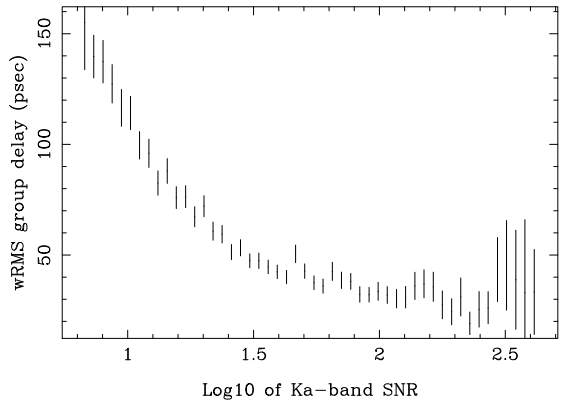

Figure 6. The wRMS residual group delay vs. the log10 of the Ka-band SNR. Note the noise floor of ≈30 psec as other error sources such as troposphere and instrumentation begin to dominate once the SNR becomes > 15 dB.

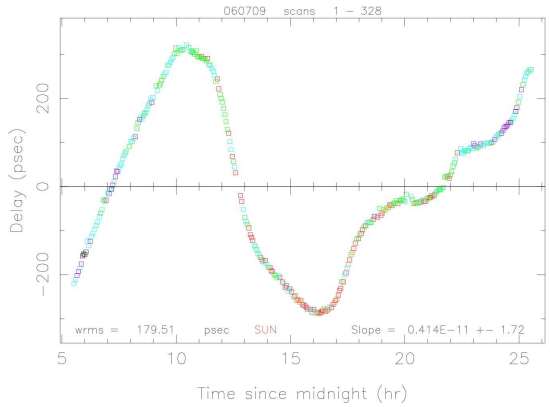

Figure 7. Ka-band proto-type phase calibrator group delays vs. time over one day. Diurnal variation is driven by thermal changes in cables and other instrumentation. Color code indicates the sun angle (in order closest to farthest: orange, red, green, cyan, purple, black).

Systematic effects in the radio source proper motion

O. Titov
Geoscience Australia, PO Box 378, Canberra, 2601, Australia

Abstract. Some models of the expanding Universe predict that the astrometric proper motion of distant radio sources embedded in space-time are non-zero as radial distance from observer to the source grows. Systematic effects due to this proper motion can even increase with distance making possible to measure them with high precision astrometric techniques like VLBI. We analyzed a large set of geodetic VLBI data spanning from 1979 till 2008 to estimate the dipole and the quadrupole harmonics in the expansion of the vector field of the proper motions of quasars in the sky. We estimated the vector spherical harmonics (three parameters for the dipole and ten for the quadrupole systematic) directly from the VLBI group delays without intermediate calculation of the individual proper motion. The estimates have been obtained separately for different redshift zones. It was shown that the dipole harmonic does not vary significantly, whereas the amplitude of the quadrupole gradually increases with the redshift. This quadrupole pattern can be interpreted either as an anisotropic Hubble expansion, or as an indication of the primordial gravitational waves in the early Universe. However, more prosaic explanations may also be possible.

Keywords. Reference frames, VLBI, apparent motion of radio sources

1 Introduction

The quasi-inertial celestial reference frame based on the accurate positions of 212 "defining" quasars is based on assumption that the physical proper motion of the radio sources are negligibly small (less than 1 μas/year) (Ma et al., 1998). However, non vanishing proper motion of distant objects in the frame of the General Relativity were predicted by Kristian and Sachs (1966). These authors showed that in the expanding Universe the proper motion of objects would increase with distance due to anisotropic expansion or the primordial gravitational waves. The corresponding systematic effect should appear in the form of second order vector spherical harmonics. The acceleration of the Solar System barycenter would cause the dipole systematic effect in the proper motion described by the first order electric type vector spherical harmonic (see, for example, Gwinn et al. 1997; Sovers 1998; Kovalevsky 2003; Kopeikin and Makarov 2006). A search for this systematic started 30 years later (Pyne et al. 1996; Gwinn et al. 1997; MacMillan 2005; Titov 2008). The search is complicated by the presence of the intrinsic motions of the radio sources themselves. Their structural change motion can reach several hundred μas/year (see Ma et al. 1998; Fey et al. 2004). Thus, the amplitude of the cosmologic effects is smaller than the random noise caused by the observational errors as well as the individual intrinsic apparent motions.

In this paper, we present the mathematical formulae used to address this problem, the most recent results obtained for the vector spherical harmonic estimates using VLBI data from 1980 to 2008, and the comparisons of the estimates made with the radio sources in different zones of redshift.

2 Vector spherical functions for the dipole and quadrupole systematics

Let us consider $\vec{F}(\alpha,\delta)$ as a vector field of a sphere described by the components of the proper motion vector ($\mu_\alpha cos\delta$, μ_δ):

$$\vec{F}(\alpha,\delta) = \mu_\alpha cos\delta \vec{e}_\alpha + \mu_\delta \vec{e}_\delta$$

where $\vec{e}_\alpha$, $\vec{e}_\delta$ are unit vectors. A vector field of spherical functions $\vec{F}(\alpha,\delta)$ can be approximated by the vector spherical functions as follows:

$$\vec{F}(\alpha,\delta) = \sum_{l=1}^{\infty} \sum_{m=-l}^{l} \left(a^E_{l,m} \vec{Y}^E_{l,m} + a^M_{l,m} \vec{Y}^M_{l,m} \right)$$

where $\vec{Y}^E_{l,m}$, $\vec{Y}^M_{l,m}$ are the "electric" and "magnetic" transverse vector spherical functions, defined respectively as:

$$\vec{Y}^E_{l,m} = \frac{1}{\sqrt{l(l+1)}} \left(\frac{\partial V_{l,m}(\alpha,\delta)}{\partial \alpha cos\delta} \vec{e}_\alpha + \frac{\partial V_{l,m}(\alpha,\delta)}{\partial \delta} \vec{e}_\delta \right)$$

$$\vec{Y}^M_{l,m} = \frac{1}{\sqrt{l(l+1)}} \left(\frac{\partial V_{l,m}(\alpha,\delta)}{\partial \delta} \vec{e}_\alpha - \frac{\partial V_{l,m}(\alpha,\delta)}{\partial \alpha cos\delta} \vec{e}_\delta \right)$$

The function $V_{l,m}(\alpha,\delta)$ is given by:

$$\begin{aligned} V_{l,m}(\alpha,\delta) &= (-1)^m \sqrt{\frac{(2l+1)(l-m)!}{4\pi(l+m)!}} \\ &\quad \times P^m_l(sin\delta)\ e^{im\alpha} \end{aligned}$$

where $P^m_l(sin\delta)$ are the associated Legendre functions.

The coefficients of expansion $a^E_{l,m}$, $a^M_{l,m}$ are estimated as follows:

$$a^E_{l,m} = \int_0^{2\pi} \int_{-\frac{\pi}{2}}^{\frac{\pi}{2}} \vec{F}(\alpha,\delta)\ \vec{Y}^{E*}_{l,m}(\alpha,\delta)\ cos\delta\ d\alpha\ d\delta$$

$$a^M_{l,m} = \int_0^{2\pi} \int_{-\frac{\pi}{2}}^{\frac{\pi}{2}} \vec{F}(\alpha,\delta)\ \vec{Y}^{M*}_{l,m}(\alpha,\delta)\ cos\delta\ d\alpha\ d\delta$$

where $*$ means a complex conjugation. This system of equations can be solved by the least squares method. In this research, the coefficients are estimated as global parameters from a large set of VLBI data.

The dipole systematic effect (secular aberration drift) in proper motion $\mu_\alpha cos\delta$, μ_δ is given by the electric-type vector spherical harmonics of the first order (Gwinn et al. 1997; Kopeikin and Makarov 2006):

$$\begin{aligned} \mu_\alpha \cos\delta &= \frac{1}{c}\ (-a^E_{1,1} \sin\alpha + a^E_{1,-1} \cos\alpha) \\ \mu_\delta &= \frac{1}{c}\ (-a^E_{1,1} \sin\delta \cos\alpha - a^E_{1,-1} \sin\delta \sin\alpha \\ &\quad + a^E_{1,0} \cos\delta) \end{aligned}$$

where c is the speed of light, and $(a^E_{1,1}, a^E_{1,-1}, a^E_{1,0})$ are the components of the vector of the secular aberration drift.

The proper motions introduced by the electric- and magnetic-type vector spherical harmonics of the second order are given by:

$$\vec{\mu}(\alpha,\delta) = \sum_{m=-2}^{2} (a^E_{2,m} \vec{Y}^E_{2,m} + a^M_{2,m} \vec{Y}^M_{2,m})$$

For instance, anisotropic expansion of the Universe makes two coefficients to be non-zero. The Hubble law for isotropic Universe $V = HR$ links the recession velocity V and distance R. In the case of anisotropic expansion, it should be replaced by:

$$\begin{aligned} V &= \left(e_{33}\ \sin^2\delta + \frac{1}{2}\ (e_{11}+e_{22})\ \cos^2\delta \right. \\ &\quad \left. + \frac{1}{2}\ (e_{11}-e_{22})\ \cos 2\alpha\ \cos^2\delta \right) \\ &= \left(H + \Delta H_3 \sin^2\delta + \frac{\Delta H_{12}}{2} \cos 2\alpha \cos^2\delta \right) R \end{aligned}$$

where the coefficients e_{11}, e_{22}, e_{33} serve as the diagonal elements of the expansion tensor, $H = \frac{1}{2}(e_{11}+e_{22})$ is the Hubble constant, and the two parameters that describe the Hubble constant anisotropy are given by:

$$\begin{aligned} \Delta H_3 &= e_{33} - \frac{1}{2}(e_{11}+e_{22}) \\ \Delta H_{12} &= e_{11} - e_{22} \end{aligned}$$

The transversal proper motion due to the anisotropic expansion are given by

$$\begin{aligned} \mu_\alpha \cos\delta &= -\frac{1}{2}(e_{11}-e_{22}) \sin 2\alpha \cos\delta \\ &= -\frac{\Delta H_{12}}{2} \sin 2\alpha \cos\delta \end{aligned}$$

$$\begin{aligned} \mu_\delta &= (e_{33} - \frac{1}{2}(e_{11}+e_{22})) \cos\delta \sin\delta \\ &\quad -\frac{1}{2}(e_{11}-e_{22}) \cos 2\alpha \sin\delta \cos\delta \\ &= \Delta H_3 \sin\delta \cos\delta - \frac{\Delta H_{12}}{2} \cos 2\alpha \sin\delta \cos\delta \end{aligned}$$

It can be shown that:

$$a^E_{2,0} = \frac{\Delta H_3}{2}$$

and

$$a^E_{2,2} = \frac{\Delta H_{12}}{4}$$

In the case of shear-free isotropic expansion of the Universe, the Hubble constant is uniform

around the sky. The diagonal elements now $e_{11} = e_{22} = e_{33}$, then $\Delta H_3 = \Delta H_{12} = a^E_{2,0} = a^E_{2,2} = 0$ and the transverse proper motion vanishes.

The effect of gravitational waves in the radio source proper motion could be detected as the both electric- or magnetic-type vector spherical harmonics. Pyne et al. (1996) and Gwinn et al. (1997) assumed that the wavelength of gravitational waves is less than the Hubble length. Under this assumption, the amplitudes of the second order harmonics should be similar for the radio sources across all range of distance. Kristian and Sachs (1966) considered arbitrary gravitational waves, and the proper motion, calculated on their approach, are proportional to the distance to a radio source, and, consequently to the redshift.

3 Data and modelling

The first and second order spherical harmonics were estimated by the least squares collocation method (Titov, 2004). The data comprises of about 4.3 million observations of group delay with different baselines and sources made in 3724 24-hour sessions between April, 1980 and September, 2008. The equatorial coordinates of more than 2000 radio sources were observed as global or "arc" parameters (see solution description below). The Earth orientation parameters, nutation offset corrections to the IAU2000 model as well as station coordinates were estimated as "arc" parameters. No-net-rotation (NNR) and no-net-translation (NNT) constraints imposed the station positions for each 24-hour session. Clock offsets, tropospheric wet delays and north-south and east-west gradients were estimated as stochastic parameters for each observational epoch. The vector spherical harmonics were treated as global parameters, similar to the approached used by MacMillan (2005).

4 Results and comparison

In the "basic" solution, all radio sources observed in geodetic and astrometric VLBI programs were considered as global parameter, except for the 102 "other" radio sources (Ma et al., 1998), treated as local or "arc" parameters. In other solutions we considered as global only the radio sources inside one of five zones of redshift as listed in Table 1.

Estimates of the secular aberration drift components are presented in Table 1. The amplitude of the effect varies in the range of 15–24 μas/year with 1σ standard error of 1–2 μas/year for different redshift zones. Figure 1 shows the dipole systematic for the "basic" solution.

The coordinates of the vector of the secular aberration drift is stable for right ascension for all solutions. Declination gradually changes from $\delta = 35^\circ$ +/- 6° for the "close" radio sources to $\delta = -9^\circ$ +/- 11° for the "distant" radio sources. The standard error for the latter case is larger due to fewer radio sources at high redshift.

We also presented another set of solutions (Table 2). The second order vector spherical harmonics were estimated along with the dipole ones. The sums of systematic (dipole and quadrupole) effects in proper motion for the "basic" solution are shown on Figure 2.

The estimates of the quadrupole effect amplitude are statistically significant (standard error is about 15–20% except for the first zone), in spite of the limited number of the reference radio sources within each redshift zone. For the most distant sources (mean z=2.6) the amplitude is unexpectedly large (58 +/- 10 μas/year), as shown on Figure 3. The dipole effect parameters in each zone of redshift are only slightly changed with respect to the similar solutions from Table 1 (within 5 μas/year in absolute values). The amplitude of the dipole effect is stable along all these zones again, whereas, the quadrupole systematic gradually increases with redshift (Figure 4). It can be concluded that the quadrupole effect might be caused by primordial gravitational waves in accordance with the early prediction by Kristian and Sachs (1966).

However, for narrow redshift zones the number of radio sources is very limited, especially at high redshift. It resulted in large correlations between first and second order vector spherical harmonics (correlation coefficients up to 0.8–0.9). More observations of distant radio sources in the southern hemisphere (under $\delta = -40^\circ$) should be undertaken in order to make more reliable conclusion.

Acknowledgements I thank David Jauncey for interesting discussion and helpful comments on this paper.

Table 1. Estimates of the vector spherical harmonics l=1 for different sets of the reference radio sources, where z - redshift; (α,δ) - positions of the vector of secular aberration drift

Range of redshift		0≤z≤0.7	0.5≤z≤1.5	All sources	1.0≤z≤3.0	1.5≤z≤3.0	z≥1.7
Number of sources		357	468	1530	542	312	287
Mean z		0.44	0.95	1.31	1.86	2.23	2.61
Electric-type	$a^E_{1,0}$	13.3 +/- 2.1	7.6 +/- 2.0	7.9 +/- 1.7	2.7 +/- 2.0	0.9 +/- 2.4	-2.5 +/- 2.8
harmonics	$a^E_{1,1}$	0.1 +/- 1.1	3.6 +/- 1.1	-1.2 +/- 0.9	0.3 +/- 1.1	0.7 +/- 1.5	10.8 +/- 2.1
(μas/year)	$a^E_{1,-1}$	-18.9 +/- 1.0	-16.9 +/- 1.0	-20.3 +/- 0.8	-15.4 +/- 1.2	-15.5 +/- 1.6	-10.7 +/- 2.0
Dipole amp. (μas/year)		23.1 +/- 1.5	18.9 +/- 1.2	21.8 +/- 1.0	15.9 +/- 1.2	15.5 +/- 1.6	15.4 +/- 2.0
α		270.6 +/- 3.3	287.8 +/- 4.2	266.6 +/- 2.6	280.3 +/- 4.8	272.6 +/- 5.8	315.3 +/- 10.7
δ		35.1+/- 5.7	23.7 +/- 6.9	21.2 +/- 5.0	9.7 +/- 7.8	3.4 +/- 9.0	-9.2 +/- 11.9

Table 2. Estimates of the vector spherical harmonics l=1,2 for different sets of the reference radio sources, where z - redshift; (α,δ) - positions of the vector of secular aberration drift for different sets of the reference radio sources.

Range of redshift		0≤z≤0.7	0.5≤z≤1.5	All sources	1.0≤z≤3.0	1.5≤z≤3.0	z≥1.7
Number of sources		357	468	1530	542	312	287
Mean z		0.44	0.95	1.31	1.86	2.23	2.61
Electric-type	$a^E_{1,0}$	12.1 +/- 3.1	0.4 +/- 3.0	6.1 +/- 3.0	-0.4 +/- 3.2	3.7 +/- 3.9	-0.4 +/- 5.5
harmonics	$a^E_{1,1}$	-2.5 +/- 1.6	-0.1 +/- 1.4	0.0 +/- 1.2	-9.2 +/- 1.7	-7.3 +/- 3.0	7.9 +/- 4.2
(μas/year)	$a^E_{1,-1}$	-17.7 +/- 1.3	-12.6 +/- 1.4	-25.6 +/- 1.1	-16.7 +/- 2.0	-17.0 +/- 3.2	-18.4 +/- 3.9
Dipole amp. (μas/year)		21.5 +/- 2.1	12.6 +/- 1.4	26.3 +/- 1.3	19.1 +/- 2.0	18.9 +/- 3.2	20.0 +/- 3.8
α		262.1 +/- 5.5	269.5 +/- 6.3	270.0 +/- 2.7	241.2 +/- 7.2	246.7 +/- 12.4	293.3 +/- 15.4
δ		34.1+/- 9.2	1.6 +/- 13.9	13.4 +/- 6.9	-1.2 +/- 9.9	3.4 +/- 14.0	-1.0 +/- 16.0
	$a^E_{2,0}$	1.2 +/- 1.9	7.1 +/- 1.7	2.5 +/- 1.5	2.9 +/- 1.9	-3.1 +/- 2.6	0.1 +/- 4.5
Electric-type	$a^E_{2,1}$	1.4 +/- 1.0	-1.7 +/- 1.0	5.2 +/- 0.7	2.0 +/- 1.7	-7.2 +/- 3.2	-5.2 +/- 3.4
harmonics	$a^E_{2,-1}$	-0.4 +/- 1.3	6.2 +/- 1.1	-1.1 +/- 0.8	9.5 +/- 1.4	7.1 +/- 2.7	0.2 +/- 3.6
(μas/year)	$a^E_{2,2}$	-3.9 +/- 0.8	2.3 +/- 0.7	1.9 +/- 0.6	7.1 +/- 0.9	10.9 +/- 1.9	42.6 +/- 3.3
	$a^E_{2,-2}$	-3.8 +/- 0.8	-4.0 +/- 0.7	-2.8 +/- 0.6	-1.0 +/- 0.9	0.7 +/- 1.9	-5.6 +/- 2.6
	$a^M_{2,0}$	-5.9 +/- 1.0	-7.6 +/- 0.8	-7.3 +/- 0.7	-12.4 +/- 1.1	-13.8 +/- 1.7	3.6 +/- 3.0
Magnetic-type	$a^M_{2,1}$	-3.8 +/- 0.9	-3.7 +/- 0.8	0.3 +/- 0.5	-14.3 +/- 1.4	-1.8 +/- 2.8	-1.5 +/- 2.8
harmonics	$a^M_{2,-1}$	-1.3 +/- 0.9	-8.2 +/- 0.8	-2.0 +/- 0.5	-4.5 +/- 1.3	2.9 +/- 2.9	3.4 +/- 2.9
(μas/year)	$a^M_{2,2}$	3.7 +/- 0.8	3.3 +/- 0.7	-0.5 +/- 0.6	1.6 +/- 0.9	2.8 +/- 2.1	14.2 +/- 3.4
	$a^M_{2,-1}$	-1.7 +/- 0.9	-1.1 +/- 0.7	2.4 +/- 0.5	2.6 +/- 0.9	12.7 +/- 1.7	36.0 +/- 2.5
Quadr. amp. (μas/year)		10.1 +/- 3.4	16.2 +/- 3.0	10.5 +/- 2.4	23.2 +/- 4.1	24.5 +/- 7.6	58.3 +/- 10.3

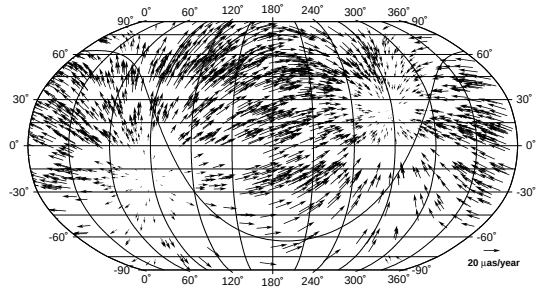

Figure 1. Dipole systematic for the "basic" solution ("all sources" in Table 1).

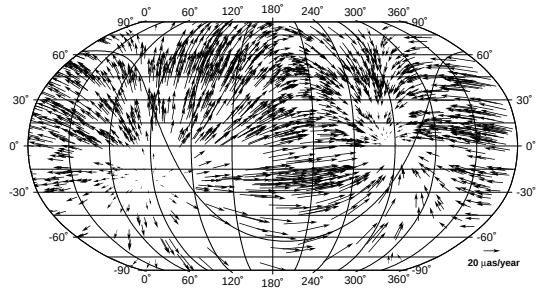

Figure 2. Dipole and quadrupole systematic for the "basic" solution ("all sources" in Table 2).

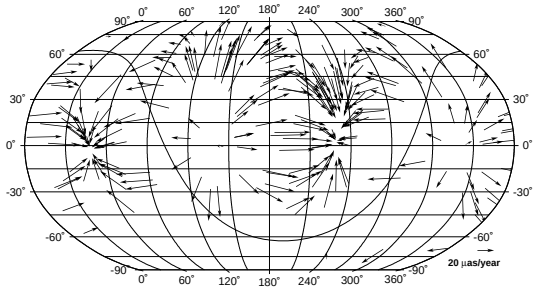

Figure 3. Quadrupole systematic for the most distance sources (last column in Table 2).

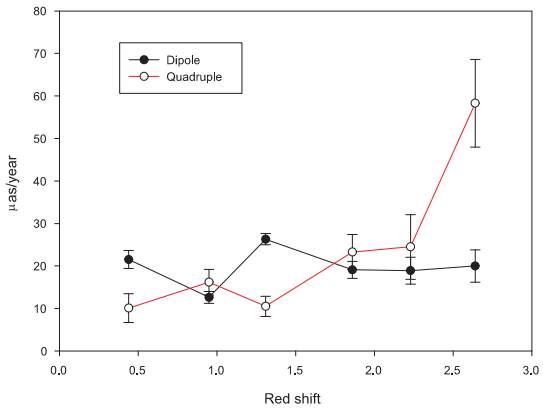

Figure 4. Amplitude of the dipole and quadrupole systematics with respect of mean redshift.

References

Fey A.L., Ma C., Arias E.F. et al., 2004, The Second Extension of the International Celestial Reference Frame: ICRF-EXT.1, AJ, 127, 3587

Gwinn C.R., Eubanks T.M., Pyne T. et al., 1997, Quasar proper motions and low-frequency gravitational waves, ApJ, 485, 87

Kovalevsky J., 2003, Aberration in proper motions, A&A, 404, 743

Kopeikin S.M. & Makarov V.V., 2006, Astrometric effects of secular aberration, AJ, 131, 1471

Kristian J. & Sachs R.K., 1966, Observations in cosmology, ApJ, 143, 379

Ma C., Arias E.F., Eubanks T.M. et al., 1998, The international celestial reference frame as realised by very long baseline interferometry, AJ, 116, 516

MacMillan D., 2005, Quasar apparent proper motions observed by geodetic VLBI networks. In: Future Directions in High Resolution Astronomy, The 10th Anniversary of the VLBA, ASP Conference Proceedings, 340, ed. J. Romney & M. Reid, 477

Pyne T., Gwinn C.R. & Birkinshaw M. et al., 1996, Gravitational Radiation and Very Long Baseline Interferometry, ApJ, 465, 566

Sovers O.J., Fanselow J.L. & Jacobs C.S., 1998, Astrometry and geodesy with radio interferometry: experiments, models, results, Rev. Mod. Phys., 70, 1393

Titov O., 2008, Proper motions of reference radio sources. In The Celestial Reference Frame for the Future, Proc. Journées 2007, ed. N. Capitaine, 16

Titov, O. 2004, Construction of a celestial coordinate reference frame from VLBI data, Astron. Rep., 48, 941

The Bordeaux VLBI Image Database

A. Collioud, P. Charlot
Université de Bordeaux, CNRS, Laboratoire d'Astrophysique de Bordeaux, 2 rue de l'Observatoire, BP 89, 33271 Floirac Cedex, France

Abstract. As part of its contribution to the International VLBI Service for Geodesy and Astrometry (IVS) and to the maintenance and improvement of the current International Celestial Reference Frame (ICRF), the VLBI group in Bordeaux produces VLBI images of extragalactic radio sources on a regular basis. These images are used to derive structure correction maps and structure indices along with visibility maps and values of source compactness which allow one to characterize the astrometric suitability of the ICRF sources. All such products are available on-line through the Bordeaux VLBI Image Database (BVID). The BVID includes more than 1500 VLBI images at 2.3 and 8.4 GHz for over 700 different sources, as well as 7500 structure correction maps and visibility maps. This dataset is constantly expanding as new VLBI experiments are processed. The Bordeaux VLBI Image Database is accessible through the following web address: http://www.obs.u-bordeaux1.fr/BVID/.

Keywords. VLBI, Reference Frames, AGN, Imaging, Databases

1 Introduction

The Very Long Baseline Interferometry (VLBI) group at the Laboratoire d'Astrophysique de Bordeaux (LAB) is involved in the International VLBI Service for Geodesy and Astrometry (IVS) (Charlot et al., 2007). In this framework, one of its contribution consists in producing VLBI images of the extragalactic radio sources that comprise the International Celestial Reference Frame (ICRF). Such images are essential for maintaining and improving the frame since the ICRF sources typically exhibit extended structures on milliarcsecond scales (Fey & Charlot, 1997, 2000), setting limits on the accuracy of astrometric source positions unless the effect of the source structure is considered.

The VLBI images produced in Bordeaux are derived from the "Research and Development with the VLBA" (RDV) sessions. These sessions, which are conducted six times a year with a VLBI network of 15 to 20 stations, are ideal for high-dynamic range imaging and for tracking source structure changes on short-time scales. Since 2007, the processing of the RDV sessions has been shared between Bordeaux and the United States Naval Observatory (USNO): the Bordeaux group processes the even-numbered sessions while the USNO processes the odd-numbered ones.

All the VLBI images produced in Bordeaux are stored in the Bordeaux VLBI image database (BVID), along with related information (source structure correction maps, structure indices, visibility maps, source compactness values). Details of the BVID content are given in Section 2. The user interface is described in Section 3. While the primary BVID goal is to contribute to the maintenance and the improvement of the ICRF, astrophysical goals are also being pursued, such as the study of superluminal motions in extragalactic radio sources.

2 BVID content

The Bordeaux VLBI Image Database (BVID) includes more than 1500 VLBI images at 2.3 and 8.4 GHz (S- and X-band, respectively) for over 700 different extragalactic radio sources (Fig. 1).

In addition to revealing source structures, these images are used to determine structure correction maps. Such maps provide the magnitude of intrinsic source structure effects in VLBI bandwidth synthesis delay measurements as a

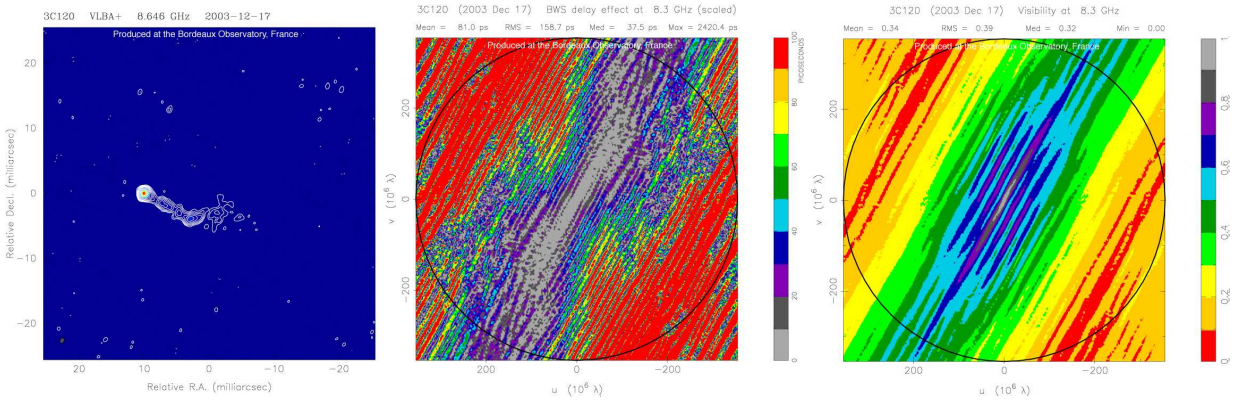

Figure 1. Excerpt from the BVID for the source 3C120 observed on December 17, 2003 at 8.4 GHz (X-band). From left to right: VLBI image, structure correction map and visibility map. The value of the structure index for this source is 4 since it has a is very extended structure.

function of interferometer resolution. From each structure correction map, a "structure index" that characterizes the astrometric suitability of the observed source (Fig. 2) is derived, as devised by Fey & Charlot (1997, 2000).

Additionally, visibility maps showing the normalized visibility as a function of interferometer resolution (Fig. 1) are also made available through the BVID. These maps serve as a basis for deriving source "compactness", a quantity that ranges from a value of 0 for fully-resolved sources to a value of 1 for point sources.

Overall, the BVID comprises more than 7500 structure correction maps and structure indices, and as many visibility maps and values of source compactness. These quantities are specificities of the BVID compared to the other VLBI image databases, such as the Radio Reference Frame Image Database (RRFID, USNO).

3 User interface

The BVID is designed as a relational database handled by the open source management system MySQL. The database is accessible and remotely queryable via a web interface available at the following web address: http://www.obs.u-bordeaux1.fr/BVID/, also including on-line help.

3.1 Query criteria

Several search criteria, organized by tabs, are available to query the database:

1. *Source name*

   Several source designations may be used: the IERS name (primary identifier), the ICRF name or any other valid SIMBAD name (Wenger et al., 2000). Shortcuts for displaying the list of all BVID sources or only the ICRF sources, as well as the list of the most popular sources, are also available in order to make the query process more user-friendly.

2. *Source coordinates*

   With this option, the search process returns all BVID sources within a specified radius, centered on a given J2000 position defined by its right ascension and declination coordinates.

3. *Observing epoch or experiment name*

   The BVID web page also provides a chronological chart to navigate through the available epochs and/or experiment names. Additional query forms may also be used for this purpose.

3.2 Query results

When a query is made using one of the above options, a web page including images and general information about the selected source is delivered to the user. Every source page is organized in the same way, with three main panels, as shown in Fig. 3.

The upper left-hand panel provides general information about the source (IERS and ICRF names, alias names, ICRF category, coordinates,

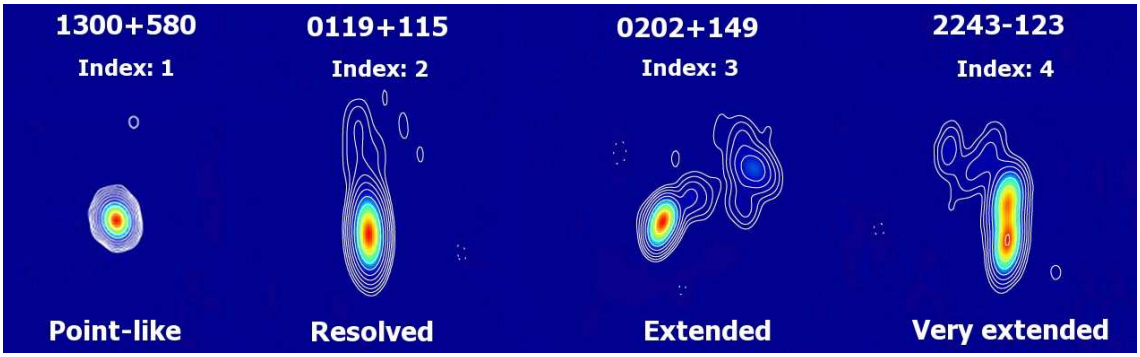

Figure 2. Illustration of the possible values of the structure index according to the complexity of the structure.

links to other databases), along with the latest total VLBI flux densities, structure indices and values of source compactness.

The upper right-hand panel displays thumbnails of the latest VLBI images, structure correction maps and visibility maps, in order to provide immediate insights into the source properties.

Finally, the lower panel provides detailed information (structure indices, values of source compactness, links to the images) for each session in which the source was observed, sorted by decreasing date.

4 Future prospects

In the future, the BVID will regularly expand as new RDV sessions are processed. It is anticipated that about 600 VLBI images, along with the corresponding structure correction maps, structure indices, visibility maps and values of source compactness, will be added each year. In addition, we plan to replace the current discrete structure indices by continuous values, in order to better trace the complexity of the sources.

On the technical side, we plan to enhance the query possibilities (multi-criteria search, file submission, etc.) and to keep on developing and improving the web interface and the associated tools. We are also considering to make available graphical displays for the structure index, source compactness and total VLBI flux data.

Acknowledgements The authors would like to thank Arnaud Caillo from the Observatoire Aquitain des Sciences de l'Univers (OASU – UMS2567) for leading the technical development of the BVID.

References

Charlot P., Bellanger A., Bourda G., Collioud A. & Baudry A., 2007, Bordeaux Observatory Analysis Center Report, International VLBI Service for Geodesy and Astrometry 2007 Annual Report, Ed. D. Behrend & K.D. Baver, NASA/TP-2008-214162, 181

Fey A. & Charlot P., 1997, VLBA Observations of Radio Reference Frame Sources. II. Astrometric Suitability Based on Observed Structure, ApJS, 111, 95

Fey A. & Charlot P., 2000, VLBA Observations of Radio Reference Frame Sources. III. Astrometric Suitability of an Additional 225 Sources, ApJS, 128, 17

Wenger M. et al., 2000, The SIMBAD astronomical database. The CDS reference database for astronomical objects, A&AS, 143, 9

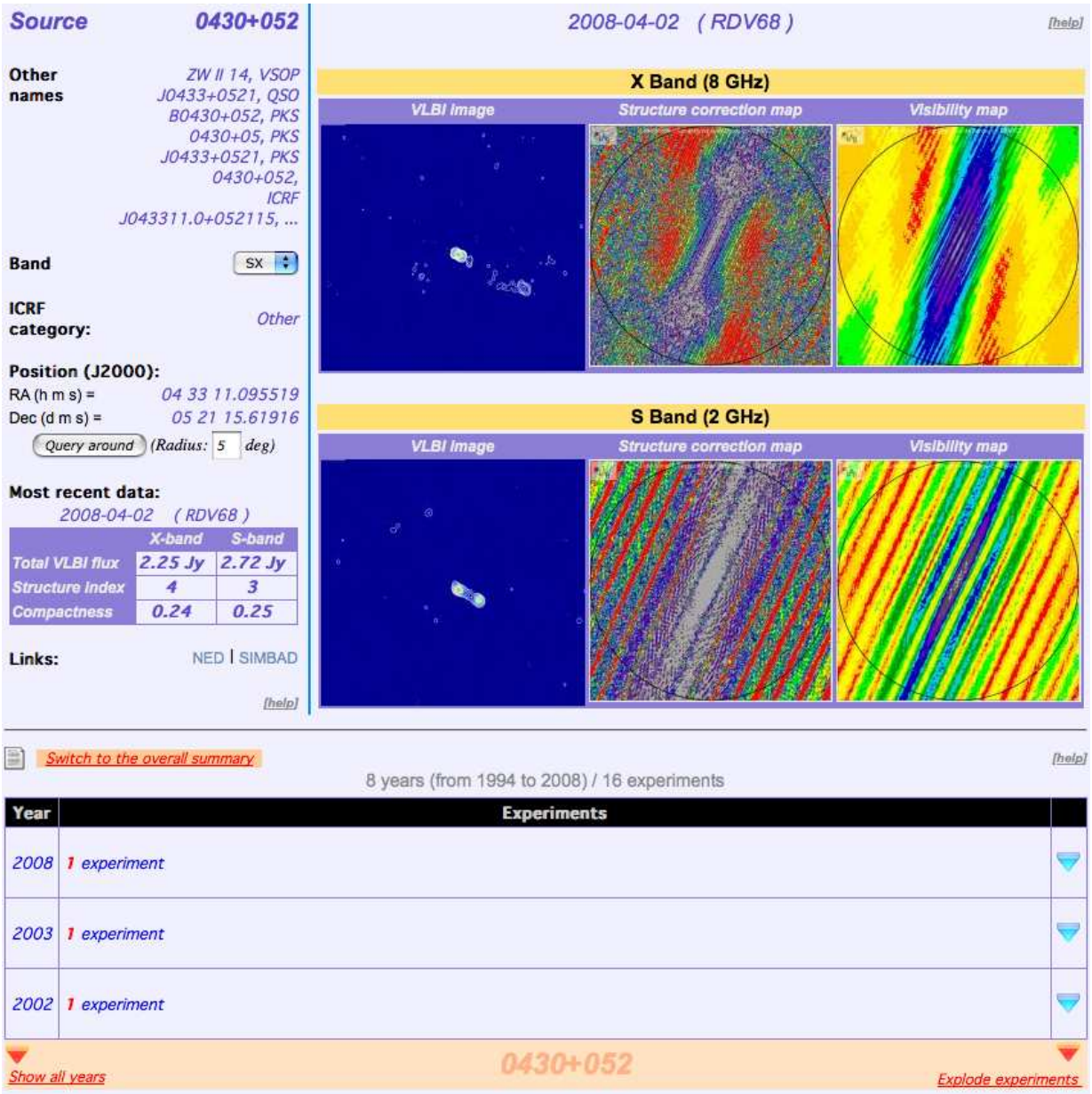

Figure 3. BVID display for the source 3C120. Source information is provided in the upper left-hand panel. Thumbnails of the latest VLBI images, structure correction maps and visibility maps are available from the upper right-hand panel, while the lower table provides details for each experiment. Switches/buttons are available to modify the display.

Scale difference between various TRF solutions

S. Kurdubov
Institute of Applied Astronomy RAS,
191187, nab Kutuzova 10, Saint-Petersburg, Russia

N. Panafidina
GFZ Potsdam, Telegrafenberg,
14473 Potsdam, Germany

Abstract. IVS Analysis Center at the Institute of Applied Astronomy (Russia) provides global VLBI solutions obtained with the software package QUASAR (Kurdubov, 2007). It was found that our terrestrial reference frame solution differs quite significantly (about 1.3 ppb for the global solution) from the ITRF2005, the reason for this behavior is not yet well understood. In this presentation we compare several different VLBI and SLR solutions in order to see a dependency of the network scale on the processing strategy and to see how the analysis options can influence solutions from two different techniques. We used VLBI daily SINEX solutions from BKG, DGFI and GSFC IVS Analysis Centers, as well as several our own test solutions obtained with different reduction models and parameter estimation modes. ASI, DGFI and GFZ weekly SINEX SLR solutions for the comparison were taken from the ILRS Analysis Centers.

Keywords. TRF, VLBI, scale, SLR

1 Introduction

Investigation of the scale differences between various analysis centers is an important task and can help to find errors in software and solve problems like rescaling ITRF2005 for SLR. Different reduction options also can lead to significant differences in scale of the obtained solutions. In our analysis, we use datum free data in SINEX format and process it in a uniform way with the Bernese GPS software (Dach et al., 2007). Thus we obtain uniform time series of station coordinates and calculate scale difference w.r.t. ITRF for each epoch. After that we perform spectral analysis for the time series of scale parameters of individual solutions.

2 SINEX files reprocessing

We use here daily VLBI solutions from several IVS Analysis Centers (ACs) on the time span 1993–2007. The solutions were re-processed with the software package Bernese starting from free daily normal equations provided online in SINEX format. The datum was defined using no-net-rotation and no-net-translation conditions w.r.t. ITRF2005, all the stations from each daily session were used for the datum definition. Scale of the network was defined by the VLBI observations. Earth rotation parameters were estimated freely using as apriori values the IERS C04 series. We used the daily free normal equations from the following IVS ACs: BKG , DGFI, GSFC, IAA. In addition to the IAA solution which is officially submitted to the IVS, we computed two other solutions for test purposes: (i) a solution with another atmospheric loading model (3D model is used for the official IVS solution and regression model is used for the test solution, which is later referred to as IAA-ALR), and (ii) a solution with no thermal deformation applied (which is reffered to as IAA-TD). For comparison reasons, we analyzed also weekly station coordinates from several ACs of the International Laser Ranging Service (ILRS). The weekly SLR solutions were also re-processed with the Bernese software package starting from weekly free normal equations. The ACs used are ASI, DGFI and GFZ. In the case of SLR observations, we need to constrain only the rotations of the network to define the datum and this was done using no-net-rotation condition w.r.t. ITRF2005 over a set of stable stations.

3 Spectral analysis of scale series

We computed Helmert transformation parameters between each daily VLBI solution and

Table 1. Mean scales for different solutions.

AC	Mean scale ppb
BKG	0.16 ± 0.02
DGFI	0.05 ± 0.02
GSFC	0.24 ± 0.02
IAA	-0.93 ± 0.02
IAA-ALR	-0.99 ± 0.03
IAA-TD	-1.00 ± 0.03
ASI SLR	-0.56 ± 0.03
DGFI SLR	0.17 ± 0.03
GFZ SLR	0.45 ± 0.03

weekly SLR solution and ITRF2005 using all the stations from the solutions with weights derived from coordinate formal errors. In further analysis only time series of scale parameter were taken into account. Obtained scale series for each individual solution considered here are shown in Figures 1–9. As one can see, all individual VLBI scale time series show similar level of scattering, although the mean values are significant only for three IAA solutions. At the same time, SLR solutions for three ACs used here show quite noticeable scale differences w.r.t. ITRF2005 which we did not expect to see.

In order to have a look at possible systematic effects present in different time series of scale, we calculated LS spectra for all 9 scale series. The mean value was extracted and 3-σ outliers were eliminated. Sampling interval was from $T = 200$ days to $T = 500$ days with the step $\Delta T = 0.5$ day.

Spectra for VLBI and SLR series are presented in Figures 10 and 11. Mean scales are shown in Table 1. There is no significant differences in spectra of IAA series and other ACs. Mean values show that different atmospheric loading modeling and thermal deformations have small impact on the mean scale and the difference w.r.t. ITRF2005 remains around 1 ppb. Comparing curves for the official IAA solution and IAA-TD solution (where no thermal deformations were applied), one can see that the annual term in scale is mainly due to antenna thermal deformations.

4 Result and Discussion

There is no significant differences in mean scale between VLBI solutions obtained with Calc/Solve software (ACs: GSFC, BKG) and solution obtained with OCCAM/DOGCS software (AC: DGFI). The IAA QUASAR software solution shows differences with the other VLBI soutions over the 1 ppb in scale. We have no explanation for the differences up to 0.6 ppb in SLR mean scales of AC with different analysis software (GeoDyn II used in ASI AC, Epos used in GFZ AC). Spectral analysis of time series of scale w.r.t. ITRF2005 show that all VLBI solutions have quite pronounced harmonics with periods about 430 days and all SLR solutions have pronounced harmonics with periods about 290 days. Also we can conclude from the spectra that the annual term in VLBI time series is mainly caused by antenna thermal deformations.

References

R. Dach, U. Hugentobler, P. FridezM. Meindl (Eds.), Bernese GPS Software, Version 5.0, Astronomical Institute, University of Bern, 2007

V.S. Gubanov, Yu.L. Rusinov, I.F. Surkis, C.Y. Shabun, S.L. Kurdubov, 2004, Project: Global Analysis of 1979–2004 VLBI Data, In: International VLBI Service for Geodesy and Astrometry 2004 General Meeting Proceedings, NASA/CP-2004-212255, pp. 315-319

S. Kurdubov, 2007, QUASAR software in IAA EOP service: Global Solution and Daily SINEX, In: Proceedings of the 18th European VLBI for Geodesy and Astrometry Working Meeting, ed. by Johannes Bohm, Andrea Pany, and Harald Schuh, GEOWISSENSCHAFTLICHE MITTEILUNGEN, Heft Nr.79, pp. 79-82

M.R. Pearlman, J.J. Degnan, J.M.Bosworth, 2002, The International Laser Ranging service, Advances in Space Research, 10.1016/S0273-1177(02)00277-6, Vol.30, No 2

L. Petrov, J.-P. Boy, 2004, Study of the atmospheric pressure loading signal in VLBI observations, Journal of Geophysical Research, 10.1029/2003JB002500, Vol. 109, No. B03405

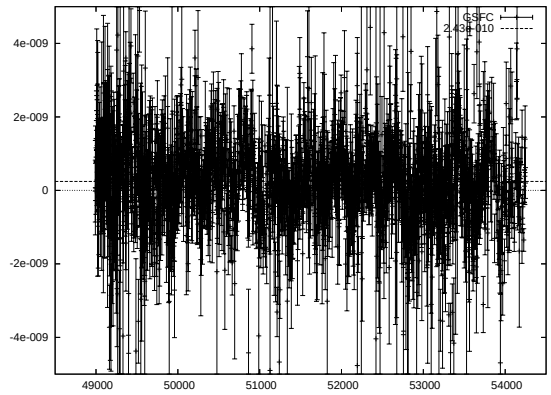

Figure 1. GSFC scale series.

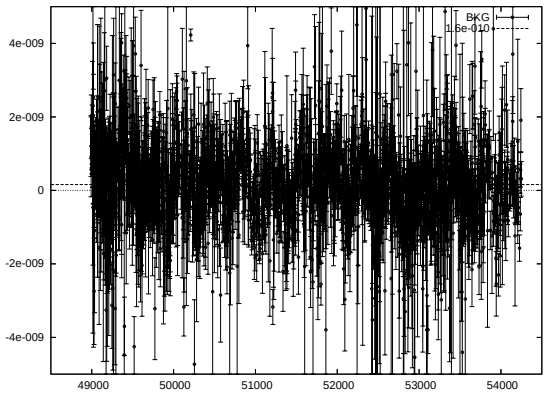

Figure 2. BKG scale series.

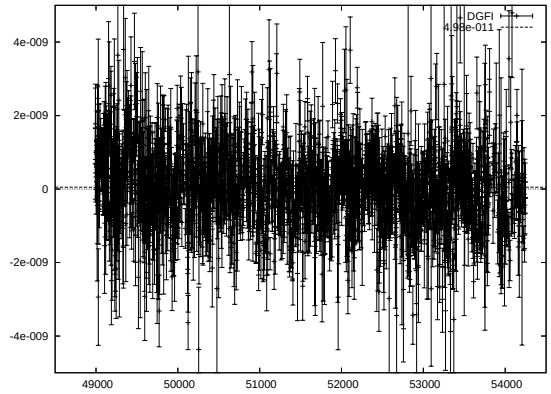

Figure 3. DGFI scale series.

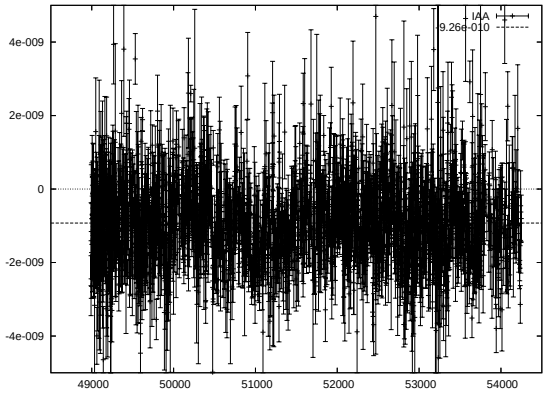

Figure 4. IAA scale series.

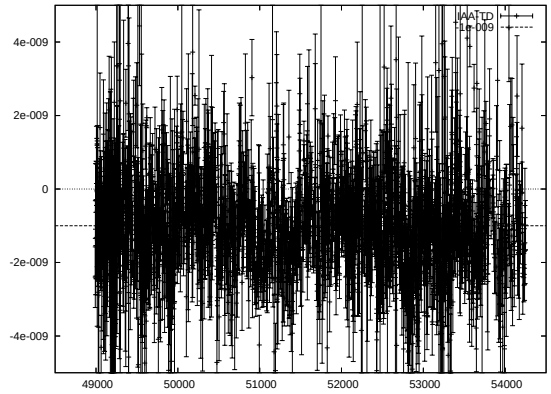

Figure 5. IAA-TD scale series (with no thermal deformations model applied).

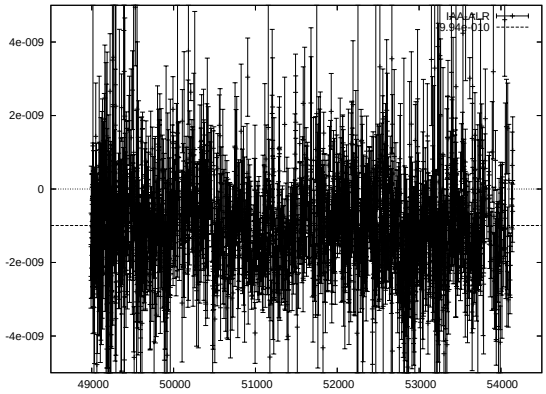

Figure 6. IAA-ALR scale series (with regression model for atmospheric loading).

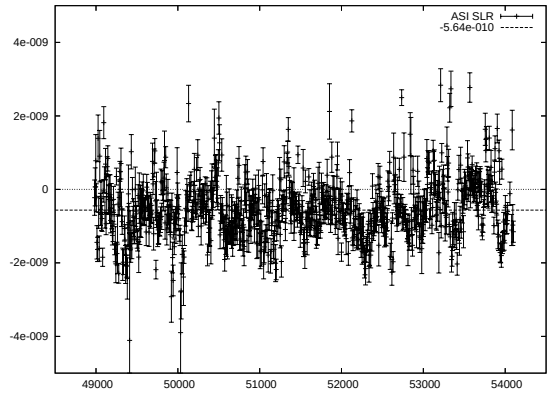

Figure 7. ASI SLR scale series.

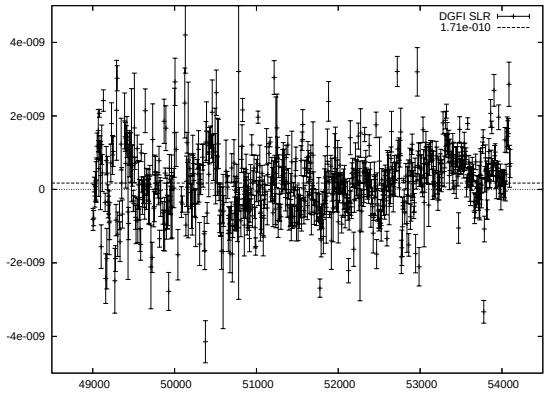

Figure 8. DGFI SLR scale series.

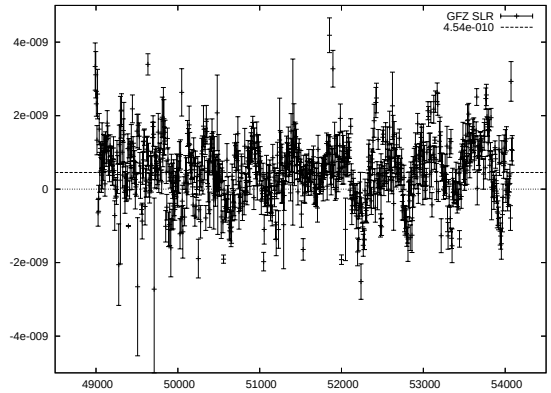

Figure 9. GFZ SLR scale series.

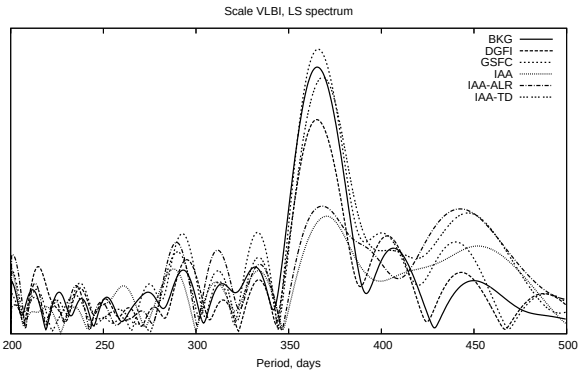

Figure 10. LS spectra of VLBI scales.

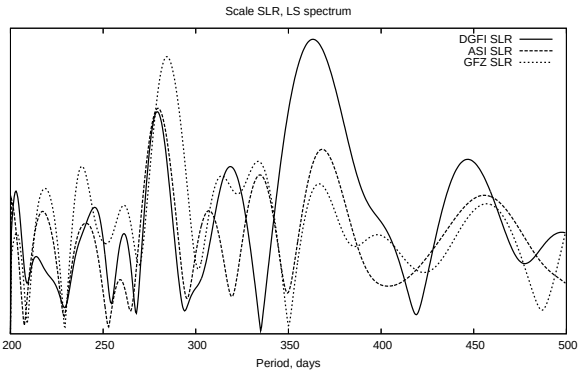

Figure 11. LS spectra of SLR scales.

On radio source selection and frame stability

S. B. Lambert, A.-M. Gontier
Département Systèmes de Référence Temps Espace (SYRTE), Observatoire de Paris, CNRS/UMR8630, Paris, France

Abstract. Geodetic products derived from VLBI analysis partly depend on an optimal maintenance of the celestial reference frame. During the analysis, this maintenance is generally done by applying a no-net rotation condition on the coordinate of a certain number of sources, that are called "defining sources", or sometimes "core" sources, and that define the system axes. In this paper, we present two selection schemes that allow one to select potential sets of defining sources that are significantly more stable and that present a much better sky coverage than the 212 defining sources provided in the first realization of the ICRF.

Keywords. Reference frames, VLBI

1 Introduction

The realization of the ideal, inertial reference system is made of a set of radio sources, that are generally regularly observed in Very Long Baseline Interferometry (VLBI) sessions. Such a set of sources defines the axes of the frame and must satisfy a number of properties. Especially, axes must be stable and non rotating with respect to the far universe. Moreover, the sky coverage must be as uniform as possible to avoid deformations and falsification of any measurement made within this frame.

The selection or the ranking of sources following their ability to be part of a frame can be done in several ways. One can choose the suitable sources following individual criteria (e.g., positional stability), or following global criteria when the source is not considered individually but together with other selected sources. In the latter case, one has to consider the stability of the frame instead of those of the sources.

In the following, we present two selection algorithms. One is based on individual criteria, the other one only on global criteria.

2 A ranking based on time series

It seems intuitive that a set of sources with time stable coordinates will result in a stable frame. A selection of these sources can be readily done using the measured standard deviations and slopes after production of coordinate time series from analysis of VLBI data. Works in this direction have been done in the recent years (Feissel-Vernier 2003, Feissel-Vernier et al. 2006).

In Lambert & Gontier (2009), we selected some 433 sources having a sufficient observational history to participate in our tests. We then considered session time series and semi-annual time series obtained by a moving average. The latter series are free from thermal noise and better reflect the "true" centroid motion. A semi-annual series with high rms is dangerous for the frame stability. As well, the value of the slope must be considered against its uncertainty to assess its significance. Finally, we tuned the selection parameters to get a reasonable number of sources and assessed the stability of the resulting frame.

The stability of a frame defined by a set of N sources can be assessed by comparing the time evolution of the global orientation of the N sources with respect to a reference set (e.g., ICRF-Ext.2 of Fey et al. 2004). If the set is stable, its orientation with respect to the reference should not change too much with time. The stability can then be quantified as the standard deviation of the orientation.

Tuning the selection parameters, we obtained interesting reference frames made of 200–270 sources with stability significantly improved by 40% with respect to the 212 defining sources

provided in the first realization of the International Celestial Reference Frame (ICRF; Ma et al. 1998) and by 20% with respect to the 247 stable sources of Feissel-Vernier et al. (2006). The best stability was obtained for a set of 262 sources (referred to as AMS sources in the following) obtained by removing by hand some sources that significantly perturbed the Z-axis stability although they passed the selection tests successfully.

3 An automated ranking algorithm

In this section, we present an automated selection scheme that ranks a list of sources in order to optimize the frame stability. It works as follows: let a set of N already ranked sources and a set of M other sources that still have to be ranked. The algorithm searches for the source among the remaining M that will optimize the stability of the frame made of $N+1$ sources. The stability of the set of size $N+1$ is evaluated on annual reference frames as explained in the previous section, by computing the standard deviation of the orientation time change with respect to a reference catalogue.

Figure 1 displays the results of the ranking. It appears that the highest stability is obtained for an optimal number of defining sources of about 400 (obtained by taking the first 400 sources of the ranking). For such a set, the mean declination is close to 0°. For comparison, the average declination of the 212 ICRF defining sources is ∼15°, the one of the AMS sources is ∼8°. A comparison of the ranking of the AMS sources against the first 262 sources of the latter reveals that they are very different. Some sources that have been classified at prominent places in AMS are now sent to the rear of the list.

However, a worthwile result concerns the sky coverage. Though the AMS list shows an average declination significantly better than the 212 ICRF defining list, most of the sources are within a band of 40° apart the equator. The poles are left empty. Though the zero-mean distribution in declination prevents from frame deformation of degree 1 (e.g., equatorial tilt), a lack of sources at the poles could produce deformations of degree 2. To avoid this, a uniform distribution with declination is necessary. Now, remember that the AMS list was built by considering "individual" stability of the sources. Consequently, sources in the southern hemisphere that

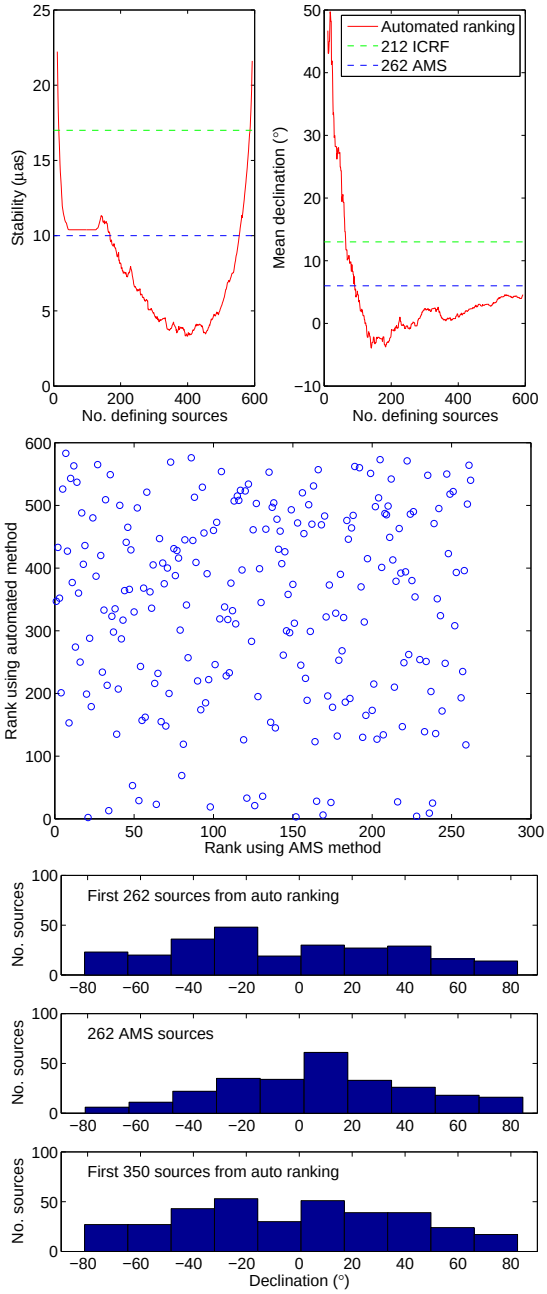

Figure 1. The left part of the upper plot shows the stability of the frame versus the number of defining sources. Its right part displays the corresponding average declination. The middle plot compares the ranks of the sources in Lambert & Gontier (2009) and in the automated ranking. The bottom plots report on the distribution of sources in declination for three subsets.

suffer from poor observational history and/or networks, were eliminated after being compared with northern sources that have large observational history with appropriate networks. The automated algorithm, based on the optimization of the "global" stability of a set of sources, never compare sources each other. During this competition for their classification, southern sources never have to directly face northern ones. Moreover, for intuitive reasons of symmetry, the algorithm naturally picks up sources in all parts of the sky, simply because taking sources in every directions optimizes the stability of the axes. As a result, the distribution of the sources versus the declination is much more uniform.

4 Concluding remarks

Optimal defining sources can be selected by several methods that lead to sets of 200–400 sources. All these sets appear to be better than the 212 ICRF defining sources in terms of stability and exhibit stabilities of the same order than the 247 stable sources of Feissel-Vernier et al. (2006). The coverage of both hemisphere is also improved.

In frame of the second realization of the ICRF (ICRF2), various ranking have been proposed (see, e.g., Kurdubov & Skurikhina 2009, who minimize the formal error of the transformation parameters; Gordon & MacMillan 2009, who base the selection on rms and χ^2 of coordinate time series). Although the source order is very different from one ranking to another, all rankings lead to similar axis stability when we run our stability tests on them. In all cases, special care should be brought to ensure a quite uniform sky coverage. In addition, other source qualifiers must also be considered like the Allan variance associated with source coordinate time series (Malkin 2008), or structure indices deduced from VLBI maps (Charlot 1990).

References

Charlot P., 1990, Radio-source structure in astrometric and geodetic very long baseline interferometry, Astron. J., 99, 1309

Feissel-Vernier M., 2003, Selecting stable extragalactic compact radio sources from the permanent astrogeodetic VLBI program, A&A, 403, 105

Feissel-Vernier M., Ma C., Gontier A.-M., Barache C., 2006, Analysis strategy issues for the maintenance of the ICRF axes, A&A, 452, 1107

Fey A. L., Ma C., Arias E. F. et al., 2004, The Second Extension of the International Celestial Reference Frame: ICRF-EXT.1, Astron. J., 127, 3785

Gordon D., D. MacMillan, 2009, Preparation for the next ICRF, this issue

Kurdubov S. L., Skurikhina E., 2009, Dependence of catalogue orientation parameter accuracy from source set selection, this issue

Lambert S. B., Gontier A.-M., 2009, On radio source selection to define a stable celestial frame, A&A, 493, 317

Malkin Z., 2008, On the accuracy assessment of celestial reference frame realizations, J. Geod., 82, 325

Ma C., Arias E. F., Eubanks T. M. et al., 1998, The International Celestial Reference Frame as realized by very long baseline interferometry, Astron. J., 116, 516

A VLBI Image Model-Fitting Pipeline Programme

M. Zhang, A. Collioud, P. Charlot
Université de Bordeaux, CNRS, Laboratoire d'Astrophysique de Bordeaux, BP89, 33271 Floirac Cedex, France

Abstract. We have developed a model-fitting pipeline programme to help extracting image model information efficiently through massive VLBI data sets. The pipeline exploits search and destroy method to find non-isolated emission peaks above a certain noise level in an image. The model parameters of interested source suspects are then passed to the image plane model-fitting programme for detailed modelling in a defined image window. The image plane fitted models are then passed to the uv plane model-fitting programme for modelling directly against visibility data. The digested outputs can be used for statistics for various purposes. The pipeline is totally programmable and scalable. Personalised modules can be easily added in. This programme has been tested with the Research and Development VLBA (RDV) geodetic multi-epoch VLBI observations. It was very successful in automatically modelling simple-structured sources. By comparing observed images and model simulated images, we can easily find out sources with complex structures which need special treats.

Keywords. VLBI, deconvolution, CLEAN, imaging, model fitting, AIPS, ObitTalk, Python

1 Introduction

Model fitting plays an important role in extracting physical information from VLBI images or visibility data. The conventional way is carried out manually with the eye guidance from CLEANed images. For larger survey or monitoring observations, the manual method will become inefficient and therefore impractical, so an automatic method is needed to achieve at least the first order result. This is not a trivial practice because without eye guidance and prior knowledge about the morphological complexity of the source structure, the machine-only processing can be erratic and many procedures are parameter-sensitive and may not always give a unique result. However, a qualified success can still be achieved with a certain source-finding algorithm on well defined source structures. In this paper, we will demonstrate our attempt in developing an image model-fitting pipeline programme to help digesting large VLBI image database. This work is an incorporation to the *Bordeaux VLBI Image Database* (BVID) project (Collioud and Charlot, 2009).

2 Methodology

Supposing the source structure is well-defined or can be decomposed into well-defined compact subcomponents, we can use a source-finding algorithm to search the subcomponents and fit the models simultaneously. The *Search and Destroy* (SAD) source-finding algorithm is available in the AIPS[1] package as well as many other calibration and mapping tasks often used in synthesis imaging. To utilise the power of AIPS tasks, we have written our pipeline programme in Python language to incorporate with the ObitTalk[2] interface to AIPS. Actually this pipeline programme frame is able to include early stage calibration and self-calibration procedures, but we mainly focus on the model-fitting part here since the majority of the data in our database have already been reduced through another standard mapping/self-calibration procedure.

In this programme, we use SAD to find out

[1]The *Astronomical Image Processing System* (AIPS) is distributed by the *National Radio Astronomy Observatory* (NRAO)

[2]The ObitTalk is part of the Obit package distributed by NRAO which offers a set of Python classes interoperable with classic AIPS (Cotton, 2008).

bright peaks and simultaneously fit them with elliptical Gaussians in the image plane above a target flux threshold. The peaks are ordered by brightness. Ideally some noise spikes can be rejected by flux threshold denial since the integrated intensity within the beam should be small enough for these spikes. We then fed the image plane model-fitting result to the *uv* model-fitting procedure as a good first guess. The fitting result in the *uv* plane is listed along with the image plane result for comparison. The deconvolution is done with task IMAGR, the image plane model-fitting is done with task SAD/JMFIT, and the *uv* plane model-fitting is done with task OMFIT. The CLEANed images and fitted models in the image plane can be sequenced, labelled and plotted into a chart for manual inspection. All control parameters are accessible from ObitTalk classes and can be determined dynamically at runtime. Some intermediary data transfer between tasks are done by parsing the formatted outputs.

3 Testing on RDV observations

We have applied our model-fitting programme on *Research and Development VLBA* (RDV) geodetic VLBI observations. Some statistics of batch-fitted parameters from this pipeline programme are shown in Fig. 1. The tested data was from RDV20 X-band global-VLBI observation. The component number was fixed to one for both image plane fitting and *uv* plane fitting. We can see the fitting results from SAD and JMFIT are very consistent, which is not surprising since SAD uses JMFIT model-fitting algorithm; differences come from different fitting window selections. The positional difference between image plane fitting and *uv* plane fitting is rather small but a noticeable excess flux distribution is obtained with *uv* plane fitting. This is physically true since the CLEAN deconvolution algorithm cannot fully recover the source flux (Zhang et al., 2007). Generally, direct model-fitting to visibility data may have the advantage to get a faithful solution over image model-fitting when CLEAN does not work well.

For compact sources or sources with well-defined structures, the programme worked out fairly well. We have illustrated our model-fitting results of selected examples of multi-component (up to 4) sources in Fig. 2. However, for extended or complicated structures the fitting may degenerate.

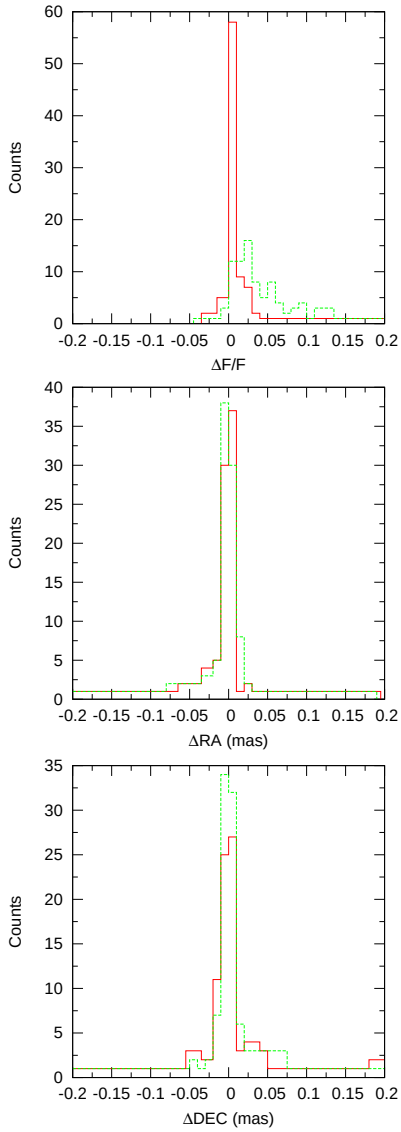

Figure 1. Distributions of the fitted parameter differences between image plane and *uv* plane approaches for 96 sources observed at X band in the RDV20 geodetic VLBI experiment. The upper panel shows differences in relative flux density, the middle and lower panels show differences in right ascension and declination, respectively. The references are taken from SAD fitted parameters. The image plane fitting is done with JMFIT and the *uv* plane fitting is done with OMFIT. The red (solid) lines are for image plane fitting, and the green (dashed) lines are for *uv* plane fitting.

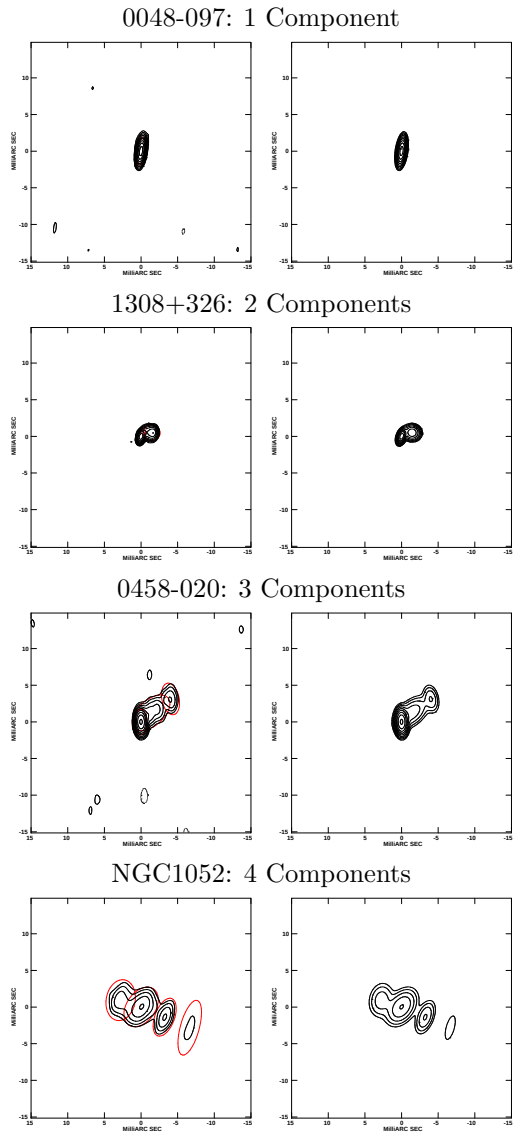

Figure 2. Successful results of automatic model-fitting for sources comprising up to four components. The left column shows the CLEANed images and the right one shows the reconstructed images from fitted models. The red elliptical lines represent the range of the first sigma of the elliptical Gaussians which have been scaled to twice the size in the figures. The contour lines start at six times the rms and increase by factors of two per interval.

For image plane model fitting, there is a compromise between the restoring beam size and the flux threshold with SAD, since a larger beam will collect more flux as well as noise spikes while a smaller beam may mottle the extended structure. Both the beam size and flux threshold selection may confuse SAD or make model-fitting difficult. An example of the effects of beam size and flux threshold selections is shown in Fig. 3 and Fig. 4. We can see that SAD could easily pick up noise spikes around when the chosen flux threshold is too low and the restoring beam size is too big; conversely the CLEANed image would be mottled and look artificial when the restoring beam size is too small. In these cases, only appropriately selected flux threshold and beam size could help SAD to fit and represent the genuine source structure to the maximum.

Some extended structures may be represented by look-alike multi-component models (see Fig. 5), but they may either not fit the image well enough or not represent physical reality. This happens, for example, when overlapping model components are generated. In many cases, such a behaviour may indicate the existence of unresolved subcomponents underneath. Because the fitting solution may not be unique, a detailed study is usually needed in these cases to fully characterise source structures.

4 Discussion

We have tested our automatic model-fitting pipeline programme with an RDV global-VLBI observation experiment. For simple-structured sources, the models can be obtained automatically with a considerable fidelity; on the other hand, for complex source structures or low-quality image or visibility data, the fitting may be erratic and need manual care. Since our Python programme utilises the ObitTalk AIPS classes, all procedures and results can be checked manually with AIPS tasks in the interactive POPS environment.

One great advantage of our Python pipeline programme is that it can fully utilise the robustness of well-tested AIPS tasks through its ObitTalk interface and save time from developing our own fitting algorithm modules. On the other hand, it also inherits some built-in limits from AIPS tasks, like the number of simultaneously-fittable components, or the precision loss in formatted output. Some adjustments can be done

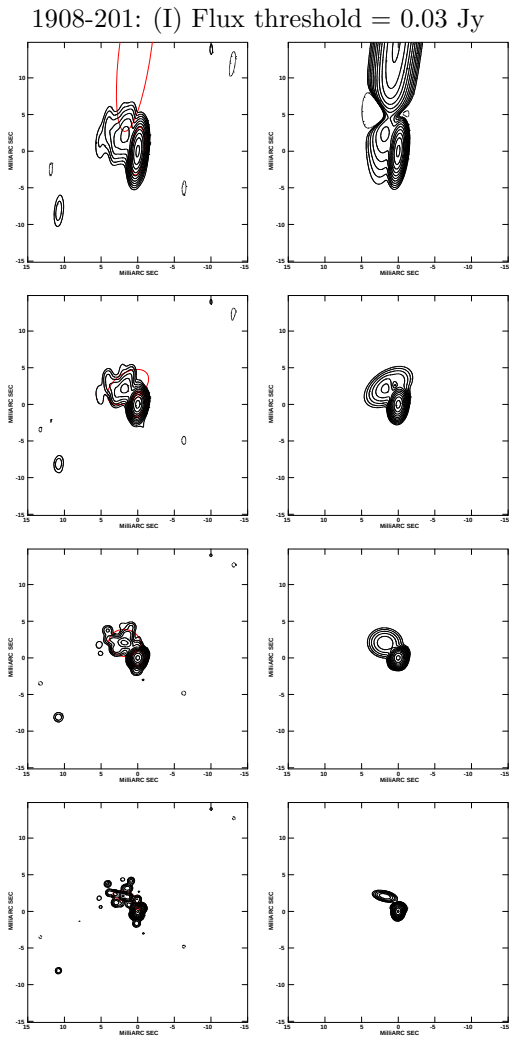

Figure 3. Compromises between restoring beam size and flux threshold with *Search and Destroy* algorithm. I: flux threshold of 0.03 Jy. The left column shows the CLEANed images and the right one shows the reconstructed images from fitted models. From top to bottom, the restoring beam sizes are chosen as 3.2×0.87 mas^2(natural), 1.6×0.9 mas^2, 0.9×0.9 mas^2 and 0.6×0.6 mas^2; the position angles are fixed at -6°. The line style and contour level settings are the same as in Fig. 2.

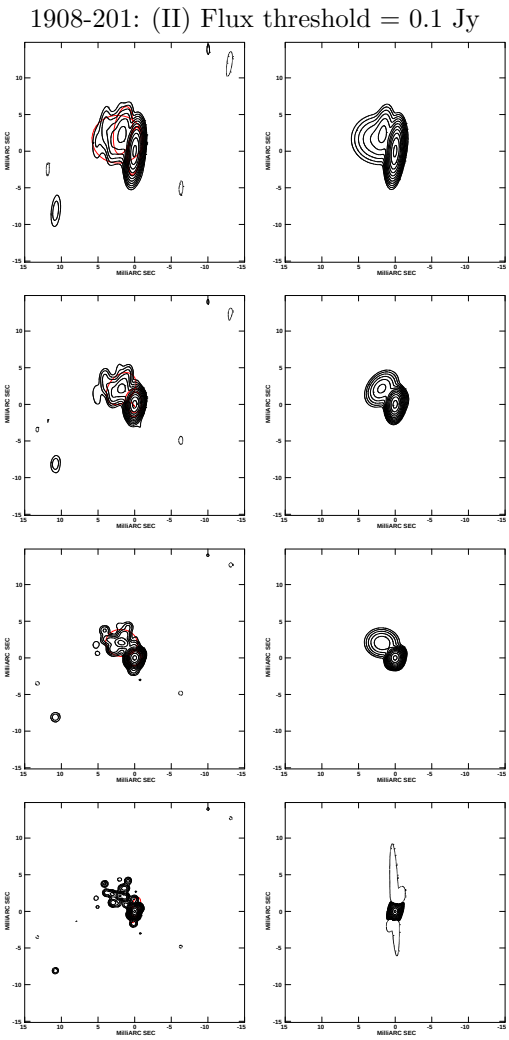

Figure 4. Compromises between restoring beam size and flux threshold with *Search and Destroy* algorithm. II: flux threshold of 0.1 Jy. The left column shows the CLEANed images and the right one shows the reconstructed images from fitted models. From top to bottom, the restoring beam sizes are chosen as 3.2×0.87 mas^2(natural), 1.6×0.9 mas^2, 0.9×0.9 mas^2 and 0.6×0.6 mas^2; the position angles are fixed at -6°. The line style and contour level settings are the same as in Fig. 2.

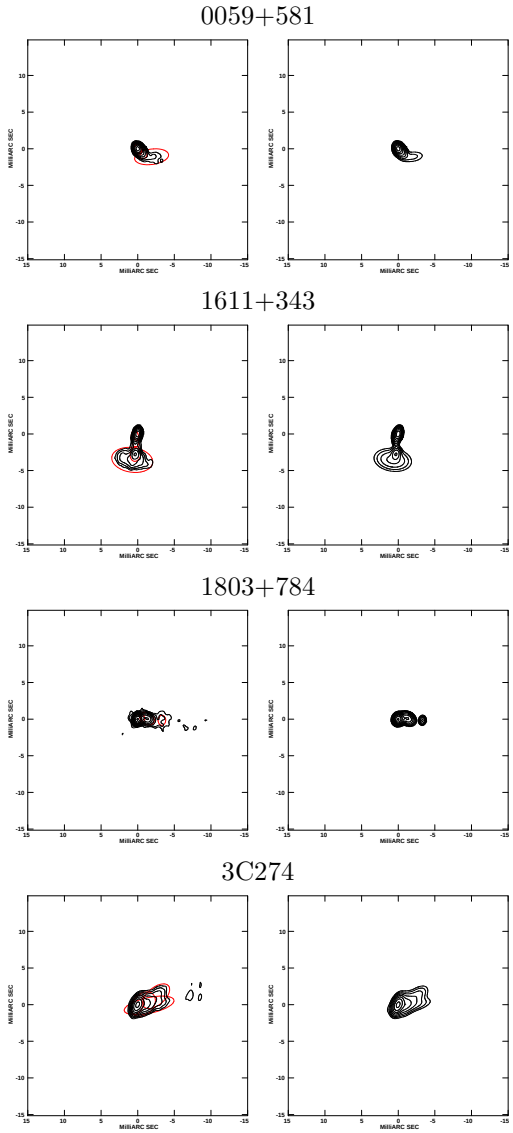

Figure 5. Confusing fitting results with extended structures. The left column shows the CLEANed images and the right one shows the reconstructed images from fitted models. The line style and contour level settings are the same as in Fig. 2.

by selecting appropriate predefined parameters. Additionally, some enhancing algorithms can be developed with our own Python modules, like multi-component redundancy checking which rejects neighbouring components that are too close to each other. There are also many Obit tasks available which can increase the data reduction power and flexibility of our pipeline programme.

Overall, our model-fitting pipeline programme has shown it can significantly improve the efficiency in mining a large VLBI database. Its high-scalability makes it easy to incorporate additional AIPS and Obit tasks or customised personal modules.

Acknowledgements M. Zhang is grateful to the CNRS (Centre National de la Recherche Scientifique) post-doctoral funding support at the Laboratoire d'Astrophysique de Bordeaux (LAB).

References

Cotton W.D., 2008, Obit: A Development Environment for Astronomical Algorithms, PASP, 120, 439

Zhang M., Jackson N., Porcas R.W. & Browne I.W.A., 2007, A search for the third lensed image in JVAS B1030+074, MNRAS, 377, 1623

Collioud A. & Charlot P., 2009, The Bordeaux VLBI Image Database, these proceedings

Multi-technique approach for deriving a VLBI signal extra-path variation model induced by gravity: the example of Medicina

P. Sarti, C. Abbondanza, M. Negusini
Istituto di Radioastronomia (IRA) - Istituto Nazionale di Astrofisica (INAF), Via P. Gobetti, 101 40129 Bologna, Italy

L. Vittuari
DISTART, Universitá di Bologna, Viale Risorgimento, 2 40136 Bologna, Italy

Abstract. During the measurement sessions gravity might induce significant deformations in large VLBI telescopes. If neglected or mismodelled, these deformations might bias the phase of the incoming signal thus corrupting the estimate of some crucial geodetic parameters (e.g. the height component of VLBI Reference Point). This paper describes a multi-technique approach implemented for measuring and quantifying the gravity-dependent deformations experienced by the 32-m diameter VLBI antenna of Medicina (Northern Italy). Such an approach integrates three different methods: Terrestrial Triangulations and Trilaterations (TTT), Laser Scanning (LS) and a Finite Element Model (FEM) of the antenna. The combination of the observations performed with these methods allows to accurately define an elevation-dependent model of the signal path variation which appears to be, for the Medicina telescope, non negligible. In the range $[0, 90]$ deg the signal path increases monotonically by almost 2 cm. The effect of such a variation has not been introduced in actual VLBI analysis yet; nevertheless this is the task we are going to pursue in the very next future.

Keywords. VLBI, Radio telescope, Gravitational Deformation, Signal Path Variation

1 Introduction

When combining space geodetic solutions of independent terrestrial reference frames, considerable discrepancies at co-located sites are often found between VLBI solutions and tie vectors (Abbondanza et al, in press). These discrepancies might be induced by specific technique-dependent biases. In this respect, VLBI, more than other space geodetic techniques, may be affected by intrinsic instrumental deformations. These can be due to *(i)* environmental effects (i.e. variations in local temperature or wind load), *(ii)* the effect of gravity acting on the antenna structure. The state-of-the-art in VLBI thermal expansion modelling can be found in Nothnagel (2008). Modelling the deformations of a VLBI antenna still remains a complex task, which has not been yet thoroughly systematised within the VLBI data processing. Since the beginning of geodetic VLBI activity, gravitational deformations have been acknowledged as one of the factors which may introduce additional biases in the estimate of fundamental geodetic parameters (Carter et al, 1980; Campbell, 1987). Gravity deforms in a differential manner the structure of a steerable antenna, thus modifying the path length travelled by the radio signal hitting the primary reflector (PR). A clear insight on how a VLBI antenna can deform can be found in Clark and Thomsen (1988). They developed a comprehensive model applied to the 22-m diameters VLBI radio telescope at Fairbanks (Alaska). The deformational effect on the antenna was quantified through a FEM. According to Clark and Thomsen (1988), the signal path variation induced by gravity (δL) can be expressed as linear combination of three terms:

$$\delta L = \alpha_R \delta R + \alpha_V \delta V + \alpha_F \delta F \qquad (1)$$

where δR is the motion of the receiver, δV is the displacement of the PR, conveniently represented by its vertex's position, δF is the focal length variation. These displacements, as well as the signal extra path, are referred to the line of sight. The three linear coefficients α_R, α_V and α_F depend on the design of the VLBI telescope. We applied a multi-technique surveying approach to the VLBI telescope of Medicina with the aim of

quantifying the effect of the three contributions to the signal path variation: *(i)* terrestrial LS was used in order to estimate the variation of the focal length of a best-fit paraboloid representing the PR; *(ii)* TTT allowed to quantify the receivers' displacement; *(iii)* a FEM of the Medicina VLBI telescope was used to quantify the vertex displacement.

2 Deformations of a VLBI telescope and impact on the RP estimation

VLBI observable is detected in the feed horn's phase centre (Electronic Point, EP). It is common practice, in VLBI data analysis, to refer the observations to the VLBI Invariant Point (IP), which is the projection of the moving axis onto that fixed. In order to do that, the distance between the EP and the IP must be known. For a VLBI telescope whose axes are not intersecting, this distance is the sum of *(i)* D_a, the projection of the axis offset onto the line of sight and *(ii)* D_b, the distance between the EP and the elevation axis. If, on one hand, the axis offset is assumed to be constant as the pointing elevation varies and what varies is its projection along the line of sight, on the other hand, due to the effects of gravitational deformations, D_b may undergo modifications depending on the pointing elevation. On the contrary, in common practice D_b is assumed to remain constant. If present, its variations may impact on the VLBI signal path and must be properly taken into account. Motions of the EP can be originated by deformations of the structure sustaining the receiver, i.e. the quadrupode and/or by a sag of the PR. Deformations of the PR must be considered as well, since they modify its shape and induce variations of the signal path length. These changes can be conveniently expressed by variations in the focal length of the best-fit paraboloid. An accurate quantification of the three terms in the equation (1) allows to determine variations of the distance D_b.

Six different surveys (2001, 2002, 2003, 2005, 2006, 2007) of the Medicina telescope were performed with the aim of determining as accurately as possible the tie vector between the VLBI IP and the GPS Antenna reference point. These tie vectors were estimated with an indirect approach: redundant observations of angles and distances between ground control points and targets applied to the telescope were acquired in order to recover the position of the IP. In this case, the IP is estimated according to geometrical/theoretical considerations, i.e. via the reconstruction of the position of the telescope rotation axes. It has been found that the estimation of the IP strictly depends on the location of targets applied to the VLBI telescope. This has been proven installing three groups of targets on different parts of the structure of the VLBI antenna: *(i)* on the top of the quadrupode (very close to the S/X receivers placed in the primary focus), *(ii)* on the edge of the dish, *(iii)* on a couple of steel rods attached to the antenna's structure very close to the elevation axis. These latter group of targets does not undergo deformations, as the antenna is steered in elevation, thus providing a more accurate estimate of the position of the elevation axis. With the indirect approach, the position of the VLBI IP is recovered following its theoretical definition, i.e. *(i)* estimating the two rotation axes of the telescope and *(ii)* projecting the elevation axis onto that fixed. It is common practice to rotate the telescope and to execute TTT at different azimuth and elevation positions on the targets applied to the antenna structure. These, during the rotations, ideally describe arcs of circles whose centres are related to the VLBI IP. Table 1 shows the Up component of the VLBI IP according to the three different groups of targets: a maximum difference by a magnitude of 1 cm has been found in the estimate of the IP height between the targets' groups I and III. Gravity deforms the antenna structure in a differential manner: targets applied to the quadrupode (Group I) and to the edge of the PR (Group II) experience higher deformations than those fixed on the steel rods (Group III). This causes the UP component of the VLBI IP to be biased. Since the targets of

Table 1. Dependency of the Up component of the VLBI IP on the targets' position applied to the telescope: **TG** in the first column indicates the Target Group; the coordinates of the Up component of the VLBI IP (second column) and their associated sigmas (third column) are expressed w.r.t a local topocentric reference frame.

TG	**UP VLBI IP (m)**	σ **(mm)**
I	17.6930	0.7
II	17.7003	0.8
III	17.7030	0.3

the Group III are free from the effect of gravitational flexure, they can be used in the computation of an accurate realization of the elevation axis. The relative displacement of the receiver and of the vertex can be referred to this latter, thus quantifying two fundamental contributions to D_b variations. Deformations of the PR must be determined as well: they intervene to modify the shape of the reflecting surface and also contribute to signal path length variation.

2.1 Receiver's displacement

While the VLBI telescope is rotated in elevation, the position of the receiver varies describing arcs of circle. In ideal conditions (i.e. in absence of deformations), the distance between the receiver and the elevation axis is constant. Nonetheless, as mentioned in section 2, gravity acting on the quadrupode may induce considerable deformations. Its effect is variable and depends on the antenna pointing elevation e: the component of the gravity force along the line of sight is a $sin(e)$ function which increases from $e = 0$ deg to its maximum at the zenith ($e = 90$ deg). In case the movement of the receiver is affected by gravity, it deviates from a circular path and the EP modifies its relative distance $d(EP, a)$ w.r.t. the elevation axis a. Therefore any receiver's displacement induced by gravity results in a variation of the incoming signal path. It is, thus, necessary to monitor $d(EP, a)$ and to determine its variations (i.e. relative radial displacement, δR) at different antenna's elevations. In case of Medicina, this was done with two independent procedures: *(i)* classical geodetic observations *via* TTT on the targets applied to the quadrupode, *(ii)* with a FEM.

2.1.1 TTT on the quadrupode

Terrestrial triangulations and trilaterations on the three targets Ia, Ib, Ic applied to the quadrupode were performed with the aim of determining $\delta R = f(e)$ in case of a receiver placed in the primary focus w.r.t an elevation axis free from gravitational-dependent biases. As mentioned in section 2, indirect approaches permit an accurate estimation of the VLBI rotation axis, providing the terrestrial measurements are minimally affected by gravitational deformations. This was ascertained for the targets of the Group III. Insights about the specific indirect approach used for recovering the VLBI IP position and the rotational axis can be found in Sarti et al (2004). For each target of the group I, the corresponding $\delta R_i(e)$ has been determined. The behaviour of the three targets' displacement is found to be similar: it tends to decrease as the elevation angle e augments, from its maximum at 5 deg to the minimum at 90 deg. The general trend can be explained considering the action of gravity on the antenna's structure: as the telescope moves from 0 to 90 deg, the component of the gravity force along the line of sight increases, thus shifting the receiver toward the elevation axis. This results in a reduction of δR, when the elevation angle e increases.

2.1.2 FEM

An analysis with a FEM of the telescope was performed with the aim of investigating the effect of gravitational deformations on the quadrupode. Three nodal points, very close to the three targets of the Group I, were identified ($R1, R2, R3$) and chosen to be representative of the deformations undergone by the quadrupode. In particular, six different models of the VLBI antenna at six elevation angles $(15, 30, 45, 60, 75, 90)$ deg were considered and used for the purpose of investigating gravitational flexure. The FEM was analysed with the ANSYS software (Hallquist, 1998): the relative displacements between the R_i and the elevation axis were computed. The agreement between the results obtained with FEM and those presented in section 2.1.1 is striking.

2.2 Vertex Motion

As the telescope is rotated in elevation, the vertex of the PR, analogously to the receiver, should ideally move on an arc of circle. Nonetheless, also in this case, gravity intervenes to deform this theoretical path: from 0 to 90 deg, the component of the force along the line of sight tends to increase, thus pulling the PR downward. This causes the vertex-to-elevation axis distance to be shortened. TTT could not be used for estimating the variation δV at different elevations, since the reticular structure of the telescope prevents from collimating targets in the vicinity of the vertex. Thus the FEM was used to derive the distances between a nodal point representative of the vertex and the elevation axis.

2.3 Deformation of the PR

The gravity force is applied on the whole surface of the PR, thus modifying its theoretical shape. In order to recover the actual shape of the PR, a LS survey was performed in September 2005 at different elevations $(90, 75, 60, 45, 30, 15)$ deg. A detailed discussion concerning the surveying approach and the results obtained can be found in Sarti et al (2009). Under the action of gravity, the PR experiences an inward folding, as the elevation decreases from 90 to 0 deg. At each elevation, the focal length of a best fit paraboloid was estimated thus proving that it smoothly increases from (10.2165 ± 0.0001) m at 15 deg to (10.2403 ± 0.0001) m at 90 deg (Sarti et al, 2009).

3 Results

According to equation 1, in order to derive δL the three terms $(\delta R, \delta V, \delta F)$ have to be combined through the corresponding α_i coefficients. With geometrical considerations Clark and Thomsen (1988) show that $\alpha_V = -1 - \alpha_R$ and $\alpha_F = 1 - \alpha_R$, where α_R can be related to the geometrical features of the PR:

$$\alpha_R = \frac{8f^2}{r_0^2} ln(1 + \frac{r_0^2}{4f^2}) - 1 \qquad (2)$$

In case of Medicina, $\alpha_R = 0.56$, $\alpha_V = -1.56$, $\alpha_F = 0.44$. In practice, these coefficients relate a displacement in the position of the receiver or the vertex and a change in focal length, all determined along the line of sight, to a change in signal path along the same direction. δL can be fit by a monotonically increasing function which ranges between 0 mm at 0 deg to a maximum of about 19 mm at 90 deg. A detailed discussion about the combination of surveying approaches, their consistency, the complete data analysis and the provision of the interpolating functions which represent the signal path variation to be applied to the VLBI observable can be found in (Sarti et al, submitted).

4 Conclusions

It is important to consider the effects of gravity on large VLBI telescopes: it has been demonstrated that, when estimating the VLBI IP with indirect approaches, gravitational deformations may induce remarkable biases (up to 1 cm), depending on the locations of targets used for recovering the elevation axis. Furthermore gravitational deformations produce significant variations of the optics of the VLBI system, thus modifying the pathlength of the signal. These variations must be investigated and accurately quantified. With this purpose, we applied a combination of three different approaches (TTT, LS and FEM), which allowed to validate results concerning the quadrupode's deformations. An elevation-dependent function of δL was determined: it quantifies the path variation to be applied to the VLBI observable in order to account for the gravitational effects. Such a variation attains the maximum value of approximately 19 mm, smoothly increasing its length from low elevation to the zenith.

References

Abbondanza C, Altamimi Z, Sarti P, Negusini M, Vittuari L (in press) Local effects of redundant terrestrial and GPS-based tie vectors in ITRF-like combinations. J Geod

Campbell J (1987) Very long baseline interferometry. In: Turner S (ed) Lecture Notes in Earth Sciences. Applied Geodesy

Carter E, Rogers AEE, Counselman CC, Shapiro II (1980) Comparison of geodetic and radio interferometric measurements of the Haystack-Westford base line vector. J Geophys Res 85:2685–2687

Clark TA, Thomsen P (1988) Deformations in VLBI antennas. Tech. rep., 100696, NASA, Greenbelt, MD

Hallquist JO (1998) LS-DYNA Theoretical Manual. Livermore Software Technology Corporation, 2876 Waverley Way, Livermore CA 94550-1740

Nothnagel A (2008) Conventions on thermal expansion modelling of radio telescopes for geodetic and astrometric VLBI. J Geod DOI 10.1007/s00190-008-0284-z

Sarti P, Sillard P, Vittuari L (2004) Surveying colocated space geodetic instruments for ITRF computation. J Geod 78(3):210–222

Sarti P, Vittuari L, Abbondanza C (2009) Laser scanner and terrestrial surveying applied to gravitational deformation monitoring of large VLBI telescopes' primary reflector. J Surv Eng http://dx.doi.org/10.1061/(ASCE)SU.1943-5428.0000008

Sarti P, Abbondanza C, Vittuari L (submitted) Gravity dependent signal path variation in a large VLBI telescope modelled with a combination of surveying methods. J Geod

An Assessment of Atmospheric Turbulence for CONT05 and CONT08

T. Nilsson* and R. Haas
Department of Radio and Space Science, Chalmers University of Technology,
Onsala Space Observatory, SE-43992 Onsala, Sweden

Abstract. We present results from the analyis of simulated VLBI data and compare these to results from the analysis of actually observed data. We use a method based upon theory of atmospheric turbulence to simulate the atmospheric delays. We concentrate on the comparison of station position repeatabilities for CONT05 and CONT08. The results show that atmospheric turbulence is the most important error source for geodetic VLBI today.

Keywords. VLBI, CONT05, CONT08, atmospheric delay, turbulence

1 Introduction

The atmosphere is one of the major error sources for geodetic Very Long Baseline Interferometry (VLBI). Especially, errors in the VLBI results are caused by the small scale fluctuations in the refractive index due to turbulence, since these are difficult to model accurately in the VLBI data analysis.

One way to investigate the errors in the VLBI results caused by e.g. atmospheric turbulence is to use simulations. For this purpose, a method for simulating wet delays in a turbulent atmosphere has been developed (Nilsson et al., 2007; Nilsson and Haas, 2008, 2009). Nilsson and Haas (2009) used this method for simulations of VLBI data for the continuous VLBI campaigns CONT05 and CONT08. When comparing the results from the analysis of the simulated data and of the actually observed data, it was concluded that atmospheric turbulence is the most important error source for geodetic VLBI today, far more important than clock errors and observation noise.

In this work we use the same simulated data as in Nilsson and Haas (2009). However, instead of looking at the results for baseline length repeatabilities as done in Nilsson and Haas (2009), we investigate the repeatabilities for the station coordinates.

2 Theory

The simulation procedure is described in detail in Nilsson et al. (2007) and Nilsson and Haas (2009), hence we only give a brief overview here.

The structure function for the fluctuations in the refractive index, n, between positions $\mathbf{r}_1$ and $\mathbf{r}_2$ is given by Treuhaft and Lanyi (1987):

$$\left\langle [n(\mathbf{r}_1) - n(\mathbf{r}_2)]^2 \right\rangle = C_n^2 \left\| \mathbf{r}_1 - \mathbf{r}_2 \right\|^{2/3} \qquad (1)$$

where C_n^2 is called the refractive index structure constant. Variations in time can be modelled by the same equation by assuming that these variations are caused by the air moving with the wind (i.e. $n(\mathbf{r}, t) = n(\mathbf{r} - \mathbf{v}(t - t_0), t_0)$, where $\mathbf{v}$ is the wind velocity and t the time). Using this structure function it is possible to calculate the covariance between two Equivalent Zenith Wet Delays (EZWD), ℓ_i and ℓ_j (i.e. slant wet delays mapped to the zenith direction):

$$\begin{aligned} C_{ij} &= \langle (\ell_i - \ell_0)\ (\ell_j - \ell_0) \rangle \\ &= \int\int \Big[\left\langle [n_i(z) - n_0(z')]^2 \right\rangle \\ &\quad + \left\langle [n_j(z) - n_0(z')]^2 \right\rangle \\ &\quad - \left\langle [n_i(z) - n_j(z')]^2 \right\rangle \\ &\quad - \left\langle [n_0(z) - n_0(z')]^2 \right\rangle \Big] \, dz dz' \end{aligned} \qquad (2)$$

*now at Institute of Geodesy and Geophysics, Technical University of Vienna, Gusshausstrasse 27-29, A-1040 Vienna, Austria

where ℓ_0 is an initial EZWD (for example the zenith wet delay at the first time epoch), and $n_i(z) = n(\mathbf{r}_i(z), t_i)$. Calculating this covariance between all observations, simulated EZWDs can be obtained by generating a series of random numbers with this covariance (can easily be done by e.g. assuming that the variations in the EZWDs are Gaussian distributed).

3 Simulated VLBI observations for CONT05 and CONT08

We used the same simulated VLBI observations for CONT05 and CONT08 as presented in Nilsson and Haas (2009). They consist of simulated atmospheric delays according to the theory described in the previous section, simulated clock errors, and white noise contributions. Here, we describe the simulations only very briefly, all details can be found in Nilsson and Haas (2009).

For the simulations of the atmospheric delays we need to know the structure constant C_n^2 and the initial EZWD ℓ_0. The value of ℓ_0 is not very important for the simulation results, hence it can for example be chosen as a typical value of the zenith wet delay. The necessary C_n^2 values can be obtained by a number of different methods, see Nilsson and Haas (2009) for details.

We applied seven different methods to determine C_n^2 that belong to three major categories:

1. Firstly, we simply assumed constant C_n^2 values for all stations. Three different cases for this constant value were tested: 10^{-15} (S-1), 10^{-14} (S-2), and 10^{-13} $\mathrm{m}^{-2/3}$ (S-3). In all three cases C_n^2 is assumed constant up to 2 km altitude and zero above.

2. Secondly, we used high resolution radiosonde data to derive station specific C_n^2 values (d'Auria et al., 1993). Unfortunately radiosonde data are not commonly available close to most VLBI station. Hence we used data from a radiosonde launch site at a similar latitude, however this may not always give accurate C_n^2. We used the method to calculate C_n^2 with two different vertical resolutions: 250 m (S-4) and 500 m (S-5).

3. Thirdly, we used zenith total delay variances estimated using GPS data collected at the particular VLBI stations (Treuhaft and Lanyi, 1987). Here we considered two cases: a constant C_n^2 up to 2 km (S-6) and a C_n^2 profile decreasing exponentially with height with a scale height of 2 km (S-7).

Table 1. Stations involved in CONT05 and CONT08, their latitude β and longitude λ in degrees, and the average number of scans observed per day, $\mathrm{N_{C05}}$ and $\mathrm{N_{C08}}$, respectively.

Station	β	λ	$\mathrm{N_{C05}}$	$\mathrm{N_{C08}}$
ALGO	45.96	−78.07	161.5	–
GILC	64.98	−147.50	448.8	–
HART	−25.89	27.69	239.4	334.2
KOKE	22.13	−159.67	406.9	657.9
MEDI	44.52	11.65	–	476.1
NYAL	78.93	11.87	366.3	532.2
ONSA	57.39	11.92	314.1	480.1
SVET	60.53	29.78	356.6	480.5
TIGO	−36.84	−73.03	173.5	360.7
TSUK	36.10	140.09	443.6	640.5
WEST	42.61	−71.49	334.9	492.9
WETT	49.14	12.88	307.4	500.9
ZELE	43.79	41.57	–	360.7

The information on when the VLBI stations observed and in what direction (azimuth and elevation) was extracted from the VLBI schedule files for the CONT05 and CONT08 campaigns and used for the simulations. Table 1 gives a short overview on the two continuous campaigns.

Clock errors were simulated as the sum of a random walk process, an integrated random walk process, and an integrated random walk process. For details on the random walk parameters see Nilsson and Haas (2009).

The observation noise was simulated as white noise with a standard deviation of 30 ps.

The each CONT-campaign, only one set of clock and white noise contributions per station was created. Then the seven different atmosphere contributions per station were used to generate the seven different simulated data sets (S-1–S-7) for the two CONT-campaigns.

4 Data analysis and results

We analyzed the simulated and the observed data sets with the CALC/SOLVE software (Ma et al., 1990) using an identical analysis strategy. Radio source positions, polar motion and the earth rotation angle were fixed to apriori values. The earth rotation rate and nutation offsets were estimated as daily parameters. Station positions were estimated for all participating stations, applying no-net-translation and no-

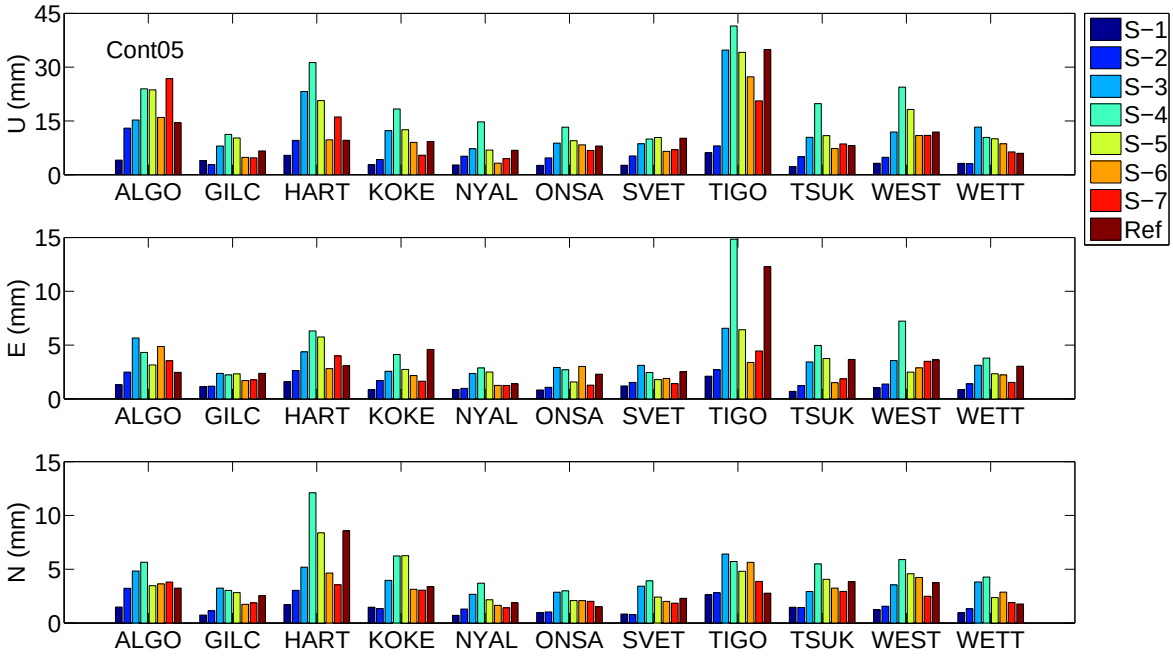

Figure 1. Repeatabilities of the topocentric Up, East, and North components of the station coordinates, from the analysis of simulated and observed CONT05 data. Shown are the results using three different constant values for C_n^2 (S-1–S-3), using C_n^2 estimated from radiosonde data (S-4 and S-5), using C_n^2 estimated from the zenith total delay variance (S-6 and S-7), and the results from the analysis of the observed data (Ref). See text for more details.

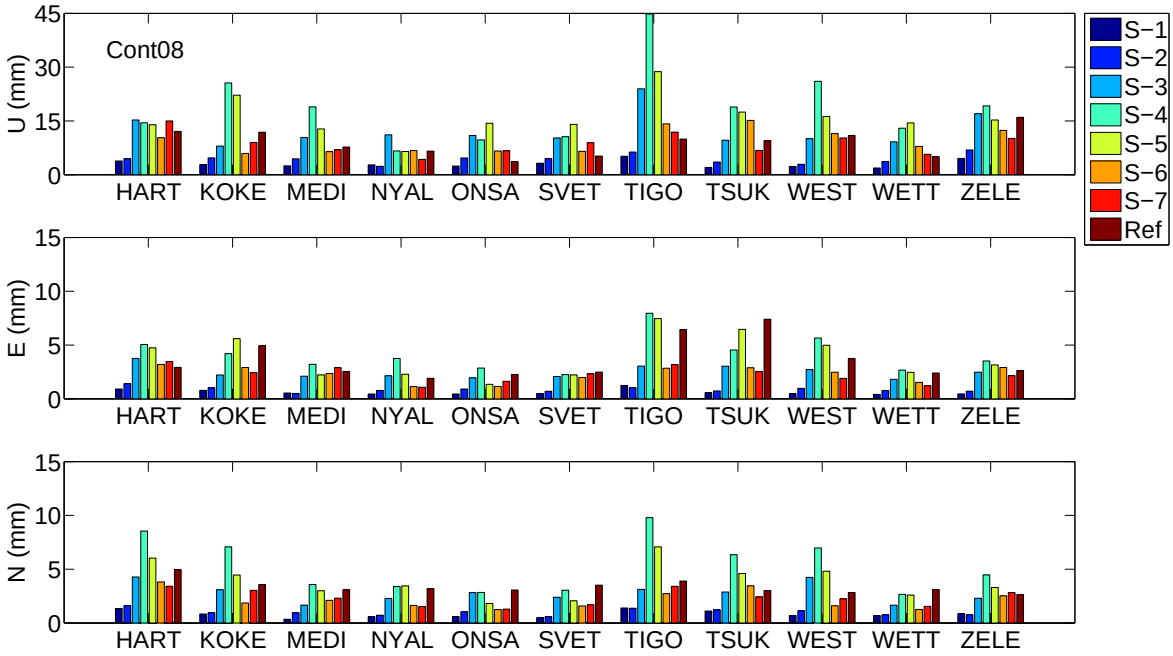

Figure 2. Repeatabilities of the topocentric Up, East, and North components of the station coordinates, from the analysis of simulated and observed CONT08 data. See caption of Fig. 1.

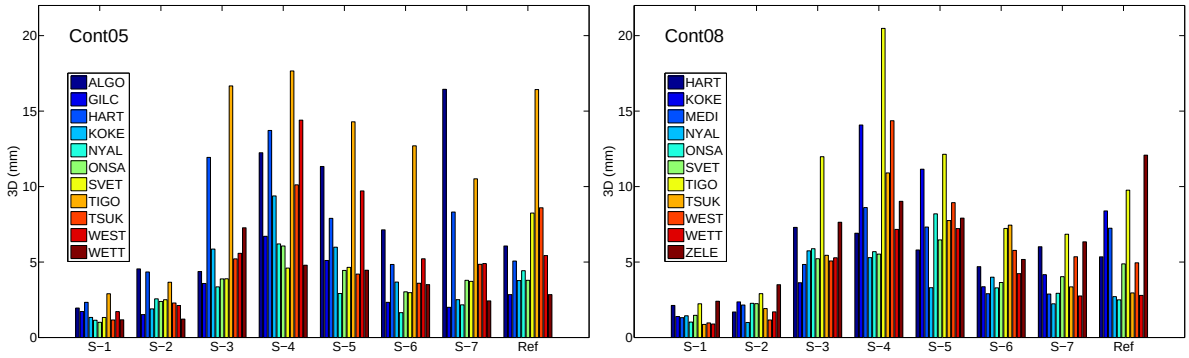

Figure 3. Repeatabilities of the three dimensional station positions grouped according to analysis for CONT05 (left) and CONT08 (right). The participating stations are shown with colored bars. Be aware that the color codes are different for CONT05 and CONT08.

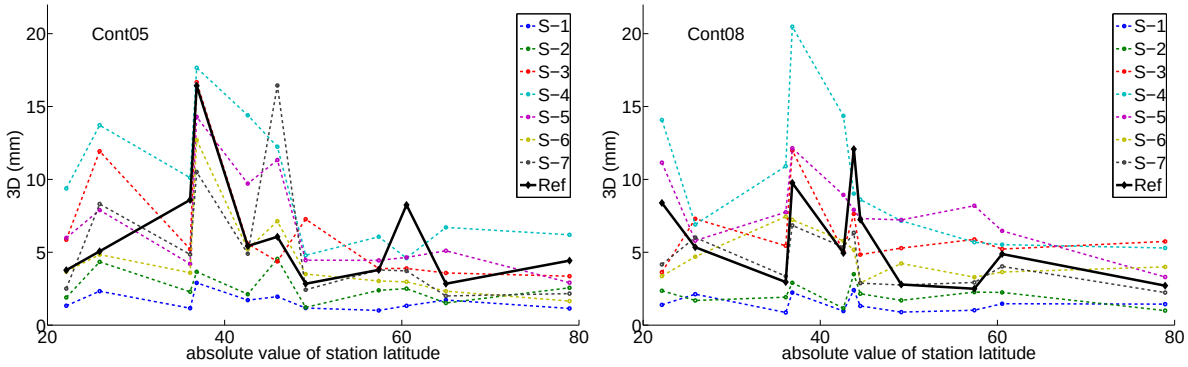

Figure 4. Repeatabilities of the three dimensional station positions versus the absolute value of station latitude for CONT05 (left) and CONT08 (right). The results of the analysis of the simulated data are shown with colored circles connected by dashed lines while the results based on the observed data are shown with black diamonds connected by a black solid line.

net-rotation conditions. Clock and atmosphere parameters were estimated as piece-wise linear functions with an interval length of 20 minutes, and horizontal gradients every 6 hours.

The repeatabilities of the resulting topocentric station coordinate are shown in Figure 1 (CONT05) and Figure 2 (CONT08), for the analysis of the simulated VLBI data sets (S-1 to S-7) and the analysis of the actually observed data (Ref). Figure 3 shows the repeatabilities of the three dimensional station position grouped according to analysis. The repeatabilities of the three dimensional station position are shown versus absolute value of station latitude in Figure 4.

We note that the repeatabilities generally are worse by a factor of about three for the vertical component than for the horizontal components, which is expected.

We can also see that stations that had relatively few observations, like ALGO, HART and TIGO in CONT05 (see Table1), generally have worse repeatabilities than stations with more observations.

If we start by looking at the results from the simulations with the same C_n^2 for all stations (S-1–S-3) we can note that the repeatabilities from the observed data mostly are in between the repeatabilities obtained from simulations S-2 ($C_n^2 = 10^{-14}$ m$^{-2/3}$) and S-3 ($C_n^2 = 10^{-13}$ m$^{-2/3}$).

For CONT08 the S-3 is agreeing rather well with the observations for low latitude stations, while it gives larger repeatabilities for high latitude stations. This is what we can expect, since C_n^2 should be higher at low latitudes where the humidity is higher. Also, C_n^2 should be higher in summer compared to winter, which explains why the observed data seem to agree better with S-3 in CONT08 (which was observed in August) compared to CONT05 (September).

We note that the repeatabilities from S-1 is much smaller than the observed repeatabilities. This shows that atmospheric turbulence is the major error source for geodetic VLBI today, since this simulation represents a case with an unrealistically stable atmosphere.

For the cases with C_n^2 estimated from radiosonde data (S-4 and S-5) we can see that the repeatabilities are generally larger compared to those from the observations. A reason for this could be that the distances between the radiosonde sites and the VLBI station are large. For example, for the stations Westford (WEST), Kokee Park (KOKE), and Tsukuba (TSUK) C_n^2 derived from radiosonde launch sites in Europe were used. We can also note that the simulations using C_n^2 obtained with a higher vertical resolution (S-4, 250 m) gives generally larger repeatabilities than for the lower resolution (S-5, 500 m). The reason is that when we use a high resolution we are more sensitive to noise in the radiosonde data.

The best agreement with the observations are obtained for the simulations using C_n^2 obtained from the variance of the zenith total delay estimated from GPS data (S-6 and S-7). Generally the agreement with the observations seems to be about the same for S-6 and S-7. The agreement seems to be relatively good for all station except for Algonquin Park (ALGO) and for TIGO in CONT05. The reason for this is unknown, altough it could somehow be a consquence of that these two station had relatively very few observations in CONT05.

5 Conclusions

The simulations indicate that atmospheric turbulence is the major error source for geodetic VLBI. The results we got here when investigating the repeatabilities for the coordinates is in agreement with the results in Nilsson and Haas (2009), where the baseline length repeatabilities were investigated.

A problem with running realistic simulations is to find appropriate values of C_n^2 for each station. Typically, C_n^2 for the VLBI stations in CONT05 and CONT08 seems to be between 10^{-14} and 10^{-13} $\mathrm{m}^{-2/3}$, with higher values for stations close to the equator. The simulations show that estimating C_n^2 from the variance of the zenith total delay gives quite realistic values that can be used in the simulations.

The method for simulating VLBI observations used here is very useful for evaluating the accuracy of geodetic VLBI, or other space geodetic techniques like Global Navigation Satellite Systems (GNSS). For example, the method is being used for simulations to investigate the accuracy of the future VLBI system, VLBI2010 (Behrend et al., 2008; Petrachenko et al., 2009).

References

Behrend, D., Böhm J., Charlot P., Clark T., Corey B., Gipson J., Haas R., Koyama Y., MacMillan D., Malkin Z., Niell A., Nilsson T., Petrachenko B., Rogers A.E.E., Tuccari G. & Wresnik J. (2008) Recent progress in the VLBI2010 development. in: Proc. IUGG XXIV General Assembly 2007, Observing our Changing Earth, IAG Symposia, 133, 833–840, Springer, doi:10.1007/978-3-540-85426-5.

d'Auria G., Marzano F.S. & Merlo U. (1993) Model for estimating the refractive-index stucture constant in clear-air intermittent turbulence. Applied Optics, 32, 2674–2680

Ma C., Sauber J.M., Bell L.J., Clark T.A., Gordon D., Himwich W.E. & Ryan J.W. (1990) Measurement of horizontal motions in alaska using very long baseline interferometry. J. Geophys. Res., 95(B13), 21 991–22 011, doi:10.1029/JB095iB13p21991

Nilsson T. & Haas R. (2008) Modeling tropospheric delays with atmospheric turbulence model. in: Proc. Fifth IVS General Meeting: Measuring the Future, A. Finkelstein and D. Behrend (eds.), 361–370

Nilsson T. & Haas R. (2009) The impact of atmospheric turbulence on geodetic VLBI, J. Geophys. Res., submitted

Nilsson T., Haas R. & Elgered G. (2007) Simulations of atmospheric path delays using turbulence models. in: Proc. 18th EVGA Working Meeting, J. Böhm, A. Pany, and H. Schuh (eds.), 175–180

Petrachenko B., Niell A., Behrend D., Corey B., Böhm J., Charlot P., Collioud A., Gipson J., Haas R., Hobiger T., Koyama Y., MacMillan D., Malkin Z., Nilsson T., Pany A., Tuccari G., Whitney A.E.E. & Wresnik J. (2009) Design aspects of the VLBI2010 system. in: IVS 2008 Annual Report, D. Behrend and K. Baver (eds.), NASA.

Treuhaft R.N. & Lanyi G.E. (1987) The effect of the dynamic wet troposphere on radio interferometric measurements. Radio Sci., 22(2), 251–265, doi:10.1029/RS022i002p00251

Modeling azimuthal asymmetries of the troposphere delay during a 14-days typhoon period in Tsukuba

A. Pany, J. Boehm, H. Schuh
Institute of Geodesy and Geophysics, Vienna University of Technology, 1040 Vienna, Austria

T. Hobiger, R. Ichikawa
National Institute of Information and Communications Technology, Tokyo, Japan

Abstract. The Monte Carlo simulations carried out within the IVS to design the next generation VLBI system, VLBI2010, have revealed that the troposphere delay is the most limiting factor in VLBI analysis. The simulation studies have shown that state-of-the-art modeling of the troposphere might be insufficient to reach VLBI2010's demanding goal of sub-mm accuracy. To exploit existing and to discover new strategies of modeling the troposphere, we computed ray-traced delays around the VLBI site in Tsukuba using KARAT, the Kashima ray-tracing tools. Tsukuba is very well suited for studies of this kind because of its rather turbulent troposphere and because it is covered by high resolution numerical weather models provided by the Japanese Meteorological Agency (JMA). For our investigations we chose a 14-days typhoon period in September 2007. The ray-traced delays are given with a resolution of 1 ° in both azimuth and elevation down to an outgoing elevation angle of 3 °. We show that the residual delays after removing the symmetric part heavily depend on how the mapping function coefficients were determined and that they exhibit systematics of higher orders that cannot be modeled with the classical gradient model only.

Keywords. troposphere delay modeling, mapping function, gradients

1 Introduction

The International Association of Geodesy's (IAG) Global Geodetic Observing System (GGOS) makes high demands on both the accuracy and reliability of the results provided by space geodetic techniques. Being the only space geodetic technique that provides the link between the celestial and terrestrial reference frame VLBI plays a vital role in GGOS. The International VLBI Service for Geodesy and Astrometry (IVS) thus began a renewal process intended to fully define, by 2010, a next generation VLBI System, capable of nearly one order of magnitude improvement in accuracy. To define the specifications of this next generation system various Monte Carlo simulations were carried out (Petrachenko et al., 2009). These simulations showed that geodetic VLBI is mainly limited due to the troposphere. In order to reach VLBI's demanding goal of sub-mm accuracy it will be necessary to further improve troposphere delay modeling.

Numerical weather models allow the computation of the refractive index field and thus a direct ray-tracing of the signals through the troposphere yielding realistic estimates of the total troposphere delay. The objective of this work was to investigate such ray-traced delays with respect to characteristical azimuthal asymmetries, test whether these can sufficiently well be modeled with gradients and explore methods for further improvements.

2 Data and Processing

2.1 The Data

The Japan Meteorological Agency (JMA) provides high resolution numerical weather models covering large parts of South-East Asia. The ray-traced delays were computed with KARAT, the Kashima ray-tracing tools (Hobiger et al., 2008) from JMA's mesoscale analysis data (MANAL) which has a horizontal resolution of about 10 km (Saito et al., 2006). The delays were computed for the VLBI site in Tsukuba for the time period from September 1 to September 14, 2007, when typhoon "Fitow"passed Japan. Tsukuba with a generally quite turbulent troposphere and a ty-

phoon passing during the data acquisition period is well suited for studies of this kind. The delays were provided with a spatial resolution of 1 ° in both azimuth and elevation and a temporal resolution of 3 hours.

2.2 Processing the Data

The delays provided by KARAT are total delays including the hydrostatic and wet symmetric and asymmetric contributions of the troposphere. In order to take a look at azimuthal asymmetries in more detail, the symmetric hydrostatic and wet parts have to be removed. The hydrostatic delay can be computed very accurately from meteorological measurements at the site. After removing the hydrostatic Vienna Mapping Function 1 (VMF1) (Böhm et al., 2006a) computed from ECMWF (European Centre for Medium-Range Weather Forecasts) data from the time series, the parameters for the wet VMF1 were determined. Similar to all mapping functions currently used in standard VLBI data processing, VMF1 is based on the continued fraction form (Marini, 1972):

$$mf(el) = \frac{1 + \frac{\mathbf{a}}{1+\frac{\mathbf{b}}{1+\mathbf{c}}}}{\sin(el) + \frac{\mathbf{a}}{\sin(el)+\frac{\mathbf{b}}{\sin(el)+\mathbf{c}}}}. \qquad (1)$$

In Equation (1), el denotes the elevation angle and **a**, **b**, and **c** are the mapping function coefficients. Theoretically, all three coefficients could be estimated in a least-squares adjustment from the ray-traced delays but in practice this is not possible due to their high correlation. For determination of VMF1 the **b**- and **c**-coefficients are thus fixed to the values of the Global Mapping Function (GMF) (Böhm et al., 2006b) and only the **a**-coefficient is estimated from the ray-traced delays. To do so there are several possibilities. Either the coefficient is determined for the lowest elevation angle, i.e. 3 °, or it is computed with a least-squares adjustment over all elevation angles from 3 ° to 90 °. In both cases the coefficient can either be estimated for each azimuth or a mean coefficient over all azimuths can be determined. The investigations show that the results for each of these approaches look different. After the determination of the wet VMF1 the symmetric wet part of the troposphere delay can be removed from the time series. The residual delays then only contain azimuthal asymmetries and mapping function errors. Figure 1 shows these residual delays for a certain time epoch (day of year 244 in 2007, 03:00 UT) in a polar contour plot where the elevation axis is scaled logarithmically. The left plot shows the residual delays for the case where the **a**-coefficient was determined at 3 ° elevation for each azimuth, the middle plot shows the residual delays for the case where a mean **a** was determined at 3 ° elevation. Comparing these two plots it can be seen that the delays look quite different. Estimating an **a**-coefficient for each azimuth will model parts of the asymmetric delay and it can be observed that the estimated **a**-coefficient is varying with azimuth. Using a mean **a** instead of the mapping function represents the mean elevation dependence and all deviations from this mean dependence will be reflected in the residual delays after removing the symmetric part. In practice, only a mean **a**-coefficient will be provided per station and time epoch and for all further investigations presented in this paper this method was applied. The right plot in Figure 1 shows residual delays where the **a**-coefficient of the wet mapping function was computed for the same station and the same time epoch but from numerical weather models of the European Centre for Medium-Range Weather Forecasts (ECMWF). These coefficients are provided by the Institute of Geodesy and Geophysics, Vienna University of Technology (http://www.hg.tuwien.ac.at/∼ecmwf1). The **a**-coefficient provided is also a mean coefficient over all azimuths. Comparing the left and the right plot in Figure 1 it can be concluded that the mapping function derived from ECMWF data, for this specific time epoch, exhibits a bias with respect to the mapping function derived from JMA data. It has to be kept in mind that what is modeled as azimuthally asymmetric delay in state-of-the-art data analysis also contains mapping function errors and is thus also dependent on which mapping function is used and on how the mapping function coefficients are determined. Figure 2 shows a comparison of the mapping functions derived from JMA data (black crosses) and ECMWF data (red circles) at 5 ° elevation. The mapping function derived from JMA data exhibits significantly more variation. One possible explanation might be the higher spatial (and temporal) resolution of the numerical weather model provided by the JMA. While the mesoscale analysis data of the JMA has a horizontal resolution of about 10 km and a temporal resolution of 3 hours, we use ECMWF data

with a spatial resolution of 2.0 ° and a temporal resolution of 6 hours. Whether the different variability is due to the different resolutions and whether it has an impact on the estimation of geodetic parameters, e.g. station position, has to be investigated in more detail.

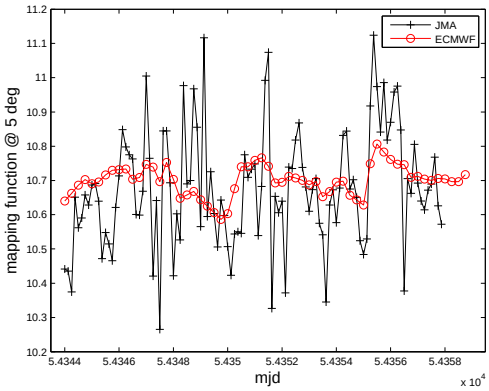

Figure 2. Mapping function at 5 ° elevation where the **a**-coefficient was once derived from JMA data (black crosses) and once from ECMWF data (red circles).

3 Modeling azimuthal asymmetries

After removing the hydrostatic and wet mapping functions different models can be fitted to the residual delays. The classical gradient model as recommended in the IERS Conventions 2003 (McCarthy and Petit, 2003) is given by

$$\Delta L_{asymm} = mf(el) \cdot \cot(el) \cdot grd \qquad (2)$$

with

$$grd = [G_N \cdot \cos(az) + G_E \cdot \sin(az)] \qquad (3)$$

where ΔL_{asymm} is the asymmetric troposphere delay, mf the wet mapping function, el the elevation angle, az the azimuth, and G_N and G_E denote North and East gradient, respectively. Figure 3 (upper left plot) presents the asymmetric part of the delay for a time epoch where there is a typical gradient systematic visible (day of year 245 in 2007, 06:00 UT). The upper right plot in Figure 3 shows post-fit residuals for the same time epoch after fitting the classical gradient model as given by Equation (2) to the residual delays in the upper left plot. As can be seen by comparing the two plots, the systematics can be modeled with gradients very well. However, this is not true for all time epochs.

Figure 3 (lower left plot) shows the asymmetric part of the delays at another time epoch (day of year 244 in 2007, 09:00 UT). The systematics present at that time epoch are no gradients but are of second order. As can be seen in the lower middle plot of Figure 3, fitting classical gradients to these delays does not yield a significant improvement. Thus second order gradients as given by Equation (2) but using Equation (4) instead of Equation (3) were applied. These second order gradients are very similar to spherical harmonic functions of degree and order 2 but have a slightly different dependence on elevation angle (Böhm and Schuh, 2001). Post-fit residuals after fitting these second order gradients to the asymmetric delays in Figure 3, lower left plot, are presented in the lower right plot of Figure 3 and show a clear improvement with respect to the post-fit residuals after applying the classical gradient model (Figure 3, middle lower plot).

$$grd = [G_N \cdot \cos(2 \cdot az) + G_E \cdot \sin(2 \cdot az)] \qquad (4)$$

The median improvement in the standard deviation of post-fit residuals is 49.8% if the classical gradient model is applied. When applying classical gradients or second order gradients only, then the classical gradients yield the smallest standard deviation of post-fit residuals in 81% of the cases. However, in the 19% of the cases where the second order gradients yield best results, the median improvement with respect to the classical gradient model is 24.5%. Applying both, classical and second order gradients, the median improvement in standard deviation of post-fit residuals is 67.4%. It has to be taken into account that in this case two more parameters have to be estimated.

4 Conclusions and Outlook

For the investigations presented in this paper only spatial structures have been considered, temporal variations of the troposphere delay have not been investigated so far. For state-of-the-art VLBI with one observation per 4 minutes approximately, temporal variations should be considered and it is planned to carry out investigations in this respect, too. However, with the much higher observation density provided by

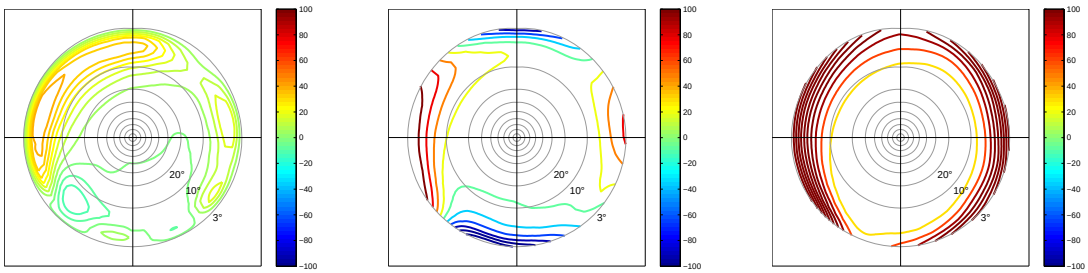

Figure 1. Residual delays [mm] after removing the hydrostatic and wet mapping functions for day of year 244 in 2007, 03:00 UT. The **b**- and **c**-coefficients of the wet Vienna Mapping Function 1 were fixed to the values of the Global Mapping Function. The **a**-coefficient was determined at 3 ° elevation for i) each azimuth from JMA data (left plot), ii) as a mean over all azimuths from JMA data (middle plot) and iii) as a mean over all azimuths from ECMWF data (right plot).

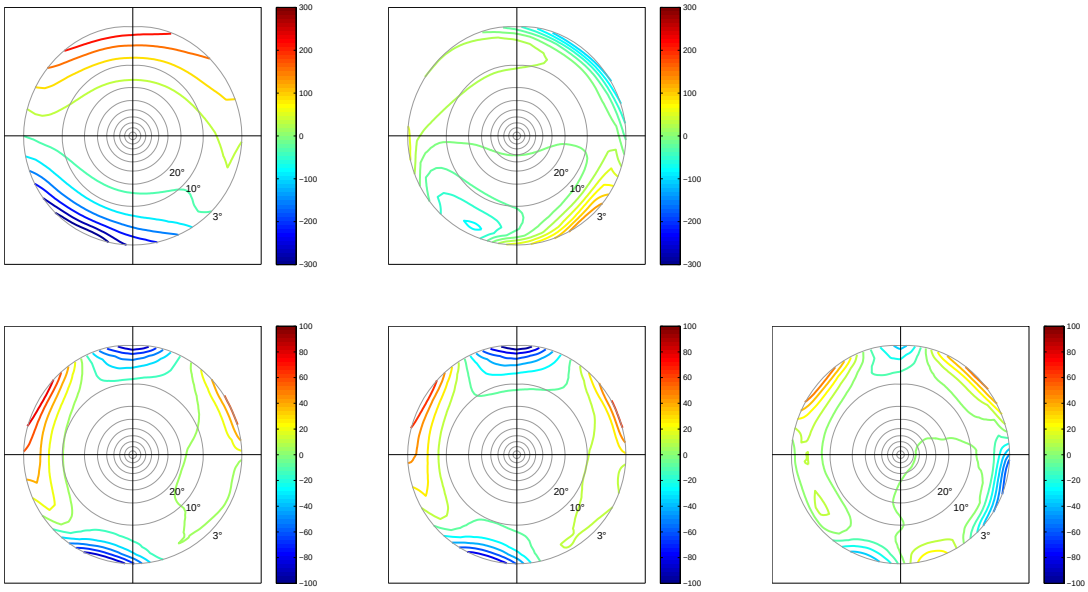

Figure 3. The upper row shows plots for day of year 245 in 2007, 06:00 UT, the lower row shows plots for day of year 244 in 2007, 09:00 UT. The left plots show the residual delays [mm] after removing the hydrostatic and wet mapping functions from the ray-traced delays. The middle plots show post-fit residuals [mm] after fitting the classical gradient model to the residual delays in the left plots. The right plot shows post-fit residuals [mm] after fitting second order gradients to the residual delays in the lower left plot.

VLBI2010 in future (∼2 observations per minute per site), accurate modeling of spatial structures in the troposphere will become increasingly important.
It can be concluded that:

- the asymmetric delay depends on the mapping function used to remove the symmetric part and on the method of how the mapping function coefficients have been determined,
- there are large gradient effects in the asymmetric delays and that the application of the gradient model in VLBI data analysis thus is indispensable, and
- that the asymmetric delays also exhibit systematics of higher orders that cannot be modeled with first order gradients only.

Other functions than the one tested here to model the systematics of higher orders will be tested and possibilities of how mapping functions might be improved by means of turbulence theory will be investigated.

Acknowledgements Andrea Pany is recipient of a DOC-fFORTE fellowship of the Austrian Academy of Sciences at the Institute of Geodesy and Geophysics, Vienna University of Technology.

References

Böhm J., B. Werl, H. Schuh, 2006a, Troposphere mapping functions for GPS and very long baseline interferometry from European Centre for Medium-Range Weather Forecasts operational analysis data, J Geophys Res, 111, B02406, doi:10.1029/2005JB003629

Böhm J., A. Niell, P. Tregoning, H. Schuh, 2006b, Global Mapping Function (GMF): A new empirical mapping function based on data from numerical weather model data, Geophysical Research Letters, Vol. 33, L07304, doi:10.1029/2005GL025546

Böhm J., H. Schuh, 2001, Spherical Harmonics as a supplement to global mapping functions and horizontal gradients. In: Behrend D., Rius A. (eds.), Proceedings of the 15th Working Meeting on European VLBI for Geodesy and Astrometry, Institut d'Estudis Espacials de Catalunya, Consejo Superior de Investigaciones, Barcelona, Spain, 143-148

Hobiger T., R. Ichikawa, T. Kondo, Y. Koyama, 2008, Fast and accurate ray-tracing algorithms for real-time space geodetic applications using numerical weather models, J Geophys Res, 113, D20302, doi: 10.1029/2008JD01053

Marini J.W., 1972, Correction of satellite tracking data for an arbitrary tropospheric profile, Radio Science, Vol. 7, 2, 223-231

McCarthy D., G. Petit, 2004, IERS Conventions 2003, Verlag des Bundesamtes für Kartographie und Geodäsie, Frankfurt am Main

Petrachenko B., A. Niell, D. Behrend, B. Corey, J. Böhm, P. Charlot, A. Collioud, J. Gipson, R. Haas, T. Hobiger, Y. Koyama, D. MacMillan, Z. Malkin, T. Nilsson, A. Pany, G. Tuccari, A. Whitney, J. Wresnik, 2009, Design Aspects of the VLBI2010 System, Progress Report of the IVS VLBI2010 Committee, in: Behrend D. & Baver K. (eds.) IVS Annual Report 2009

Saito K., T. Fujita, Y. Yamada, JI. Ishida, Y. Kumagai, K. Aranami, S. Ohmori, R. Nagasawa, S. Kumagai, C. Muroi, T. Kato, H. Eito, Y. Yamazaki, The Operational JMA Nonhydrostatic Mesoscale Model, Mon Wea Rev, 134, 1266-1298

Atmospheric VLBI: A method to validate long time series of water vapour content

G. Elgered, R. Haas, T. Nilsson
Department of Radio and Space Science, Chalmers University of Technology,
Onsala Space Observatory, SE - 439 92 Onsala, Sweden

Abstract. We assess the possibility to validate time series of the atmospheric integrated water vapour (IWV) from GPS observations using geodetic VLBI at the Onsala Space Observatory in Sweden. An overall motivation is to determine the relation—and its uncertainties—between trends in the IWV with trends in the ground temperature. We find that the frequency of VLBI experiments is too low in order to validate estimated linear trends using data acquired over a ten year period. On the other hand, the VLBI method provides an accuracy of the same order, compared to using GPS or nearby radiosonde launches for validation of the IWV on an absolute scale. Further assessments using other, as well as larger, data sets are called for.

Keywords. VLBI, atmospheric water vapour, global wetting, global warming

1 Introduction

Water vapour is an important atmospheric gas in climate models. A specific question at issue is the relation between changes in the temperature and possible corresponding changes in the integrated water vapour (IWV). Following the Clausius-Clapeyron relation, assuming conservation of relative humidity, we obtain a relation for the IWV changes due to a change in the temperature of approximately 6 [%/K] (Trenberth et al., 2003). Analyses and comparisons of trends in the temperature and the IWV using the ERA40 model do not give an accurate assessment of this relation. This is argued to be due to artifacts in the global observing system of water vapour (Bengtsson et al., 2004). Accurate observations, and especially with a high long term stability, of the IWV as well as of the temperature are therefore important.

The possibility to infer the IWV from space geodetic observations has been demonstrated, with increasing quality, during the last twenty years. First by using geodetic VLBI data (e.g. Herring et al., 1990; Heinkelmann et al., 2007) and thereafter also based on GPS (e.g. Tralli & Lichten, 1990; Elgered et al., 2005). Ground-based GPS receiver stations provide a relatively high spatial resolution and results in close to real time, at least compared to VLBI. Therefore, the IWV estimates from GPS networks are nowadays used, and their impact assessed, in assimilation into numerical models for weather prediction. The absolute accuracy, and especially the long term stability of the GPS results is of fundamental importance for applications in climate research. In order to assess the stability of the GPS results an independent, preferably a more stable and accurate, method is called for. We here investigate to what extent geodetic VLBI is an appropriate method for this task. For this purpose we use geodetic VLBI and GPS data from the Onsala Space Observatory and radiosonde data from the Göteborg-Landvetter Airport.

In Section 2 we present an overview of the results recently obtained in terms of linear trends in the IWV using data acquired with the Swedish and Finnish ground-based GPS networks from 1996 to 2006. Section 3 describes the analysis of the geodetic VLBI experiments at Onsala. In Section 4 we compare the results of the estimated IWV using VLBI, GPS, and radiosondes. Section 5 contains the conclusions.

2 GPS estimates of IWV

2.1 Summary of estimated trends

Linear trends in the IWV were recently estimated using ten years of GPS data from the

ground-based GPS networks in Sweden and Finland (Nilsson & Elgered, 2008). The trends were estimated from the IWV data using the following model:

$$V = V_0 + a_1\,t + a_2 \sin(2\pi t) + a_3 \cos(2\pi t) + a_4 \sin(4\pi t) + a_5 \cos(4\pi t) \quad (1)$$

where t is the time in years and the coefficients V_0, a_1, a_2, a_3, a_4, and a_5, are estimated using the method of least squares. The overall linear trends are identical to the estimated parameters a_1 for the different sites. These are shown in Figure 1. In general we see positive trends, except for the south-east part of Sweden.

The same type of six-parameter model is used throughout this paper to model also the ground temperatures of sites nearby the GPS receiver stations, and the equivalent zenith wet delay (ZWD) estimated from VLBI, GPS, and radiosonde data.

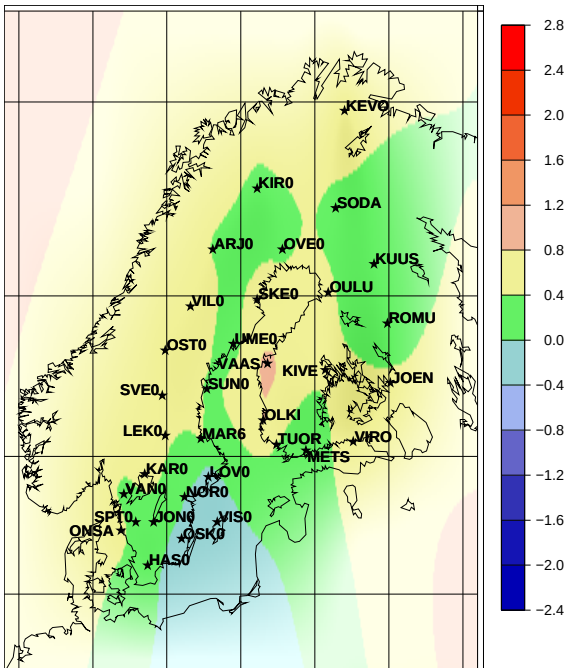

Figure 1. Estimated trends in the IWV from 1996 to 2006, from (Nilsson & Elgered, 2008).

2.2 On the relation between ground temperature and IWV

Space geodetic data offer a new and independent method compared to traditional meteorological

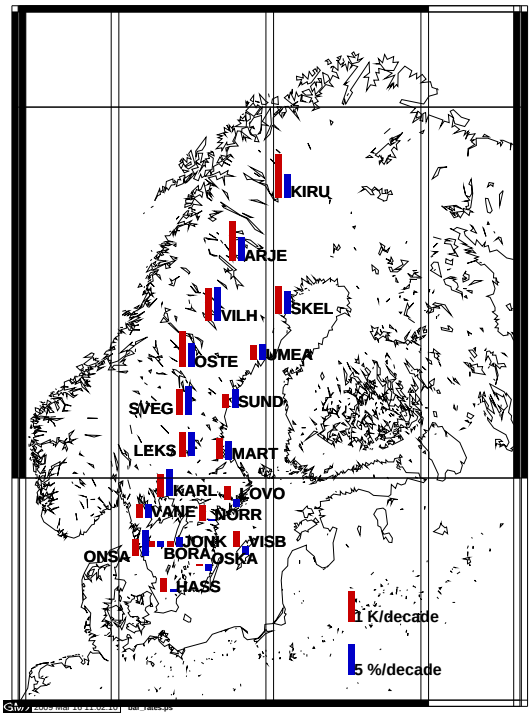

Figure 2. IWV trends from GPS sites in the Swedish GPS network and the corresponding trends in the ground temperature at nearby sites.

observations. We expect that an increase in the temperature will correspond to an increase in the IWV. We analysed monthly means of ground

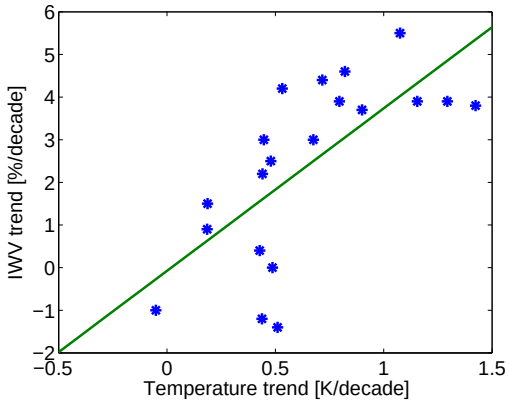

Figure 3. The relation of estimated IWV trends from GPS sites in the Swedish GPS network vs. the corresponding trends in the ground temperature at nearby sites.

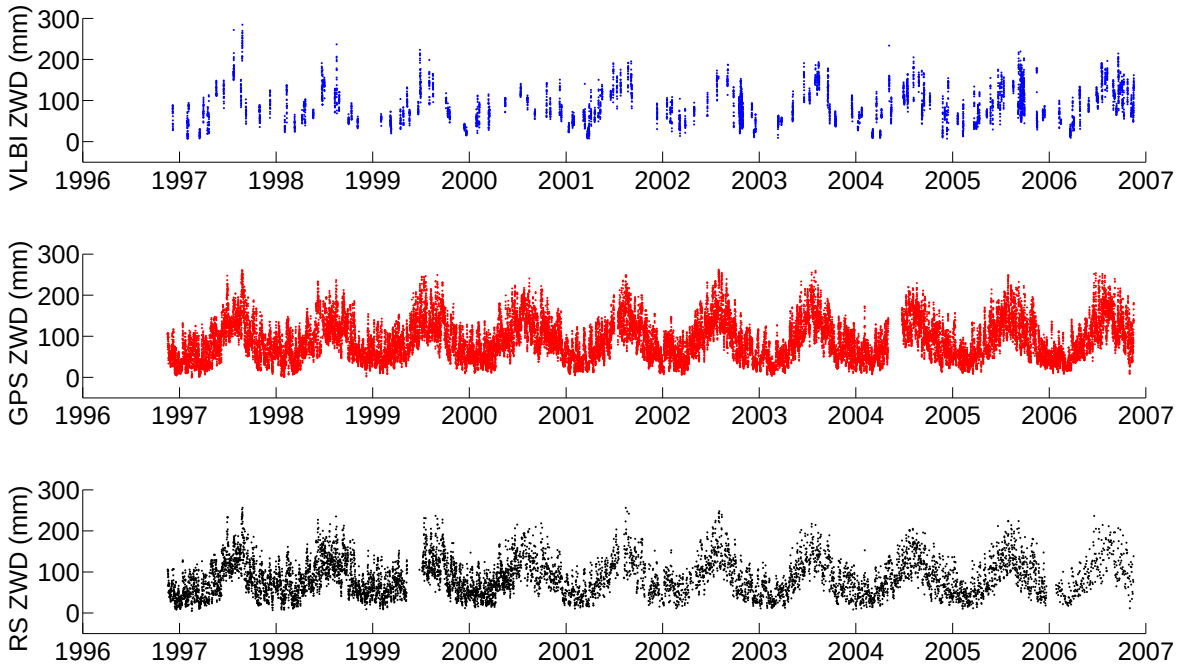

Figure 4. Time series of the equivalent zenith wet delay (ZWD) estimated from VLBI data (top), GPS data (middle), and radiosonde data (bottom).

temperatures from the observational network of the Swedish Meteorological and Hydrological Institute (SMHI) from the same ten year period as we have GPS derived IWV results. Linear trends were estimated also from these data and they are presented together with the IWV trends in the map in Figure 2.

A correlation plot between the trends is shown in Figure 3. The correlation coefficient of the data is 0.69, meaning that it has been shown that the two trends are correlated with a probability larger than 99%. It is also interesting to note that the linear slope is 3.8%/K. This indicates that the relative humidity in this area has not been conserved during the studied time period. Additional studies using different data sets are necessary in order to assess the uncertainty of this parameter.

In the remainder of this paper we will focus on the possibility to validate the IWV trend at Onsala, which is 0.58 kg/(m$^2\cdot$ decade). This corresponds to a relative trend of 4.2%/decade, and a trend in the ZWD of 3.7 mm/decade. In the following we will use ZWD time series from VLBI and radiosonde observations to represent the IWV.

3 Geodetic VLBI data analysis

We will assess the use of the ZWD estimated from VLBI data for the comparisons with the results from the other methods. The estimated time series of the ZWD originate from analyses of the global VLBI data set covering the period of interest: 17 Nov. 1996 – 16 Nov. 2006. In total 230 such 24 h long sessions included the Onsala telescope. The data were analysed with the CALC/SOLVE software (Ma et al., 1990). Radio source positions, station positions and velocities were estimated as global parameters, and earth rotation and orientation parameters as daily parameters. The necessary no-net-translation and no-net-rotation constraints were applied. Clock and atmosphere parameters were estimated as piece-wise linear functions with a 1 h resolution, and horizontal atmospheric gradients as piece-wise linear functions with a 3 h resolution. Solid earth tides, ocean loading and atmospheric loading were applied in the analysis. An elevation cutoff angle of 5 degrees was used in two different solutions, one using the NMF mapping functions (Niell, 1996), and another one using the VMF1 mapping functions (Böhm et al, 2006).

Figure 4 shows the time series of estimated ZWD from the VLBI analysis using the NMF

Table 1. Linear trends in the ZWD inferred from GPS and VLBI data from Onsala and radiosonde (RS) data from Landvetter airport.

Data source	Data points	Trend (mm/decade)
synchronizing VLBI and GPS		
VLBI (NMF)	2737	6.3 ± 0.4
VLBI (VMF1)	2737	6.6 ± 0.4
GPS	2737	9.9 ± 0.4
synchronizing VLBI and RS		
VLBI (NMF)	511	7.3 ± 0.8
VLBI (VMF1)	511	7.8 ± 0.8
RS	511	6.5 ± 0.8
synchronizing GPS and RS		
GPS	7914	5.4 ± 0.2
RS	7914	3.3 ± 0.2
synchronizing GPS(synchro2VLBI) and RS		
GPS	479	6.6 ± 0.8
RS	479	6.0 ± 0.8
unsynchronized (all) data 17 Nov. 1996 – 16 Nov. 2006		
VLBI (NMF)	5746	6.4 ± 0.3
VLBI (VMF1)	5746	6.9 ± 0.3
GPS	41104	3.7 ± 0.1
RS	8500	3.1 ± 0.2

mapping function. Also included in this figure are the GPS and the radiosonde data. It is obvious that the relatively sparse sampling of the atmosphere with VLBI means that significant periods with potentially large deviations from the ZWD model can be missed compared to the other methods. In the next section these different time series will be compared.

4 Comparison results

In order to be able to compare the estimated ZWD trends from the different methods the data shall be acquired during the same time periods. As mentioned earlier, the VLBI data have a temporal resolution of 1 h during the experiments. The GPS data have a 2 h resolution, while the radiosonde data have a 6 h (1996– mid 2000), a 12 h (mid 2000 – end of 2005), and a 24 h temporal resolution (since 2006). The trend calculations are first based on synchronized data sets and then also estimated from the complete unsynchronized data sets. All estimated trends are presented in Table 1.

We note that all the estimated ZWD trends are positive, which is consistent with earlier studies using data from Onsala but acquired during different time periods (Haas et al., 2003).

Furthermore, we note that the trends estimated using the NMF or the VMF1 mapping functions in the VLBI analyses are not significantly different.

The presented uncertainties of the trends are one standard deviation (1σ) values, assuming uncorrelated white noise deviations from the model. These shall be considered as minimum values because a temporal correlation is expected for values closer than a couple of days (Nilsson & Elgered, 2008). This is especially true for the larger data sets, where the individual data points are closer in time.

Considering that the error bars may be inflated by a factor of four, the disagreement between the different methods is reasonable. However, there are details that ought to be studied further.

For example, the trend obtained from the GPS data is significantly larger than the VLBI trend when using GPS data synchronized to VLBI experiments. On the other hand we obtain a consistent trend if the GPS data are synchronized to both the VLBI and the radiosonde data.

In order to study the accuracy of the three methods further, we calculate the root-mean-square (RMS) differences between data pairs of the different ZWD time series. These results are presented in Table 2.

Again we note that the impact of using the different mapping functions in the VLBI analyses is small. They only affect the ZWD bias, but at the level of 0.6 mm. As expected we also see the best agreement between the VLBI and the GPS results because the radiosondes are launched approximately 37 km from the Onsala site. Further conclusions are difficult to draw. The RMS differences are slightly larger for the VLBI–radiosonde calculation compared to the GPS–radiosonde result, suggesting that the GPS data are slightly more accurate, but we note that the difference is hardly significant when restricting the GPS–radiosonde comparison to the same periods as there are VLBI data available. In order to address this problem in more detail, further investigations are required based on other, as well as larger, data sets.

Table 2. RMS differences in the ZWD inferred from GPS, VLBI and radiosonde data acquired during the time period Nov. 1996–Nov. 2006.

Compared synchronized data Method 1 − Method 2	Number of data points	Mean ZWD[1] (mm)	RMS (mm)	Bias[2] (mm)
VLBI (NMF) – GPS	2737	91.3	7.5	−1.1
VLBI (VMF1) – GPS	2737	91.3	7.5	−0.5
VLBI (NMF) – radiosonde	511	86.2	11.4	−0.1
VLBI (VMF1) – radiosonde	511	86.2	11.3	+0.5
GPS – radiosonde	7914	84.6	10.2	+1.7
GPS – radiosonde (VLBI periods only)	479	85.6	10.7	+2.8

[1] The mean value is that of Method 2
[2] Method 1 − Method 2

5 Conclusions

Our preliminary analysis suggest that approximately monthly geodetic VLBI experiments do not give a sufficient temporal resolution in order to validate linear trends in the IWV estimated from ground-based GPS data at the Onsala site over a ten year period. However, when comparing the RMS differences between the ZWD from VLBI, GPS, and radiosonde data, we conclude that the VLBI data seem to be of a quality—in terms of accuracy—which is comparable to the other methods.

Acknowledgements We are grateful for the the support by Dr. Volkmar Thorandt who allowed us to perform the global VLBI data analysis on the computers of the IVS Analysis Center at the Bundesamt für Kartographie und Geodäsie (BKG) in Leipzig (Germany).

References

Bengtsson, L., S. Hagemann, & K.I. Hodges, 2004, Can climate trends be calculated from re-analysis data? J Geophys Res, 109, doi:10.1029/2004JD004536

Böhm, J., B. Werl, & H. Schuh, 2006, Troposphere mapping functions for GPS and very long baseline interferometry from European Centre for Medium-Range Weather Forecasts operational analysis data, J Geophys Res, 111, B02406, doi:10.1029/2005JB003629

Elgered, G., H.-P. Plag, H. van der Marel, S. Barlag, & J. Nash (eds.), 2005, COST 716: Exploitation of ground-based GPS for climate and numerical weather prediction applications, Final Report, European Community, EUR 21639, ISBN 92-898-0012-7

Haas R., G. Elgered, L. Gradinarsky, & J. Johansson, 2003, Assessing Long Term Trends in the Atmospheric Water Vapor Content by Combining Data From VLBI, GPS, Radiosondes and Microwave Radiometry, in: Proc. 16th Working Meeting on European VLBI for Geodesy and Astrometry, Leipzig, May 9–10, 2003, eds. W. Schwegmann and V. Thorandt, Bundesamt für Kartographie und Geodäsie, Frankfurt/Leipzig, 279–288

Heinkelmann, R., J. Böhm, H. Schuh, S. Bolotin, G. Engelhardt, D.S. MacMillan, M. Negusini, E. Skurikhina, V. Tesmer, & O. Titov, 2007, Combination of long time-series of troposphere zenith delays observed by VLBI. J Geod, 81, 483–501, doi:10.1007/s00190-007-0147-z

Herring, T.A., J.L. Davis, & I.I. Shapiro, 1990, Geodesy by radio interferometry: the application of Kalman filtering to the analysis of very-long-baseline interferometry data, J Geophys Res, 95, B8, 12561–12581

Ma, C., J.M. Sauber, L.J. Bell, T.A. Clark, D. Gordon, W.E. Himwich, & J.W. Ryan, 1990, Measurement of horizontal motions in alaska using very long baseline interferometry. J Geophys Res, 95(B13), 21 991–22 011, doi:10.1029/JB095iB13p21991

Niell A.E. (1996) Global mapping functions for the atmosphere delay at radio wavelength. J Geophys Res, 101(B2), 3227–3246

Nilsson, T. & G. Elgered, 2008, Long-term trends in the atmospheric water vapor content estimated from ground-based GPS data, J. Geophys. Res., 113, D19101, doi:10.1029/2008JD010110

Tralli, D.M., and S.M. Lichten, 1990, Stochastic estimation of tropospheric path delays in Global Positioning System geodetic measurements, Bull Geod, 64, 127–159

Trenberth K.E., A. Dai, R.M. Rasmussen & D.B. Parsons, 2003, The changing character of precipitation, Bull Amer Meteor Soc, 84 (9), 1205–1217, doi:10.1175/BAMS-84-9-1205

Recent Modeling Improvements in SOLVE Analysis

D. MacMillan, J. Gipson
NVI, Inc., NASA Goddard Space Flight Center
Greenbelt,MD, 20771 USA

Abstract. We report the results of new VLBI SOLVE data analysis options. These are: 1) modeling antenna thermal deformation, 2) elevation-dependent weighting, 3) VMF1, 4) introducing correlation between observations, 5) use of slant path tropospheric delays from numerical weather models.

Keywords. Reference frames, VLBI, Earth orientation

1 Introduction

During the last 2 years, we have investigated several improvements in modeling in SOLVE analysis. It has been known for many years that thermal deformation of antennas leads to variation of the reference point height of up to 8–10 mm depending on the antenna size and the antenna site temperature range. Thermal deformation modeling has now been incorported into SOLVE as an operational model. Over the last 10–15 years, better modeling of tropospheric delay has been developed by a number of investigators. Here we consider improved tropospheric modeling in SOLVE obtained via 1) elevation-dependent weighting, 2) better mapping functions, specifically VMF1(Vienna mapping function; Böhm et al. 2006), 3) correlations between observations, and 4) slant path tropospheric delays. In this report, we describe the new modeling options in SOLVE and show the resulting improvements in baseline length precision.

2 Antenna Thermal Deformation

The thermal deformation model, which we have implemented in SOLVE, expresses the change in position of the antenna reference point by a function of temperature relative to a specified reference temperature for each site (Nothnagel, 2008). The specific information for each antenna (structural dimensions, expansion coefficients, reference temperature) have been compiled for all IVS antennas (Nothnagel, 2008). Structural dimensions include antenna pillar and foundation heights, axis offset, height of the antenna vertex, and height of the subreflector. Each structural component of the antenna expands according to the simple model:

$$\delta L = \gamma_{exp} L (T(t) - T_{ref})$$

where L is the dimension of the component, γ_{exp} is the expansion coefficient, T(t) is the component temperature and T_{ref} is the reference temperature. For the reference site temperatures, we used the global temperature and pressure model GPT (Boehm et al., 2007). An example of an antenna that undergoes significant thermal deformation is the antenna at GILCREEK, which has a height of about 15 m and a steel expansion coefficient of about 1.2 x 10^{-5}. For an annual temperature swing of 40 K, the height will have an annual peak-to-peak variation of about 7 mm.

Using all VLBI data from 1979 to 2008, we ran a standard baseline type solution in which site position are estimated for each experiment session. Baseline length repeatabilities improved by up to 1 mm with improvement increasing with baseline length since the thermal deformation effect is primarily in the site vertical direction. Figure 1 shows this improvement. We also considered the effect of thermal expansion modeling on the TRF frame parameters. The effect was small: less than 0.25 mm in translation and rotation and only 0.013 ppb in scale. Site positions and velocities changed by less than one formal sigma. This is significant because the choice of a bad reference temperature could have biased the position estimates. Thermal deforma-

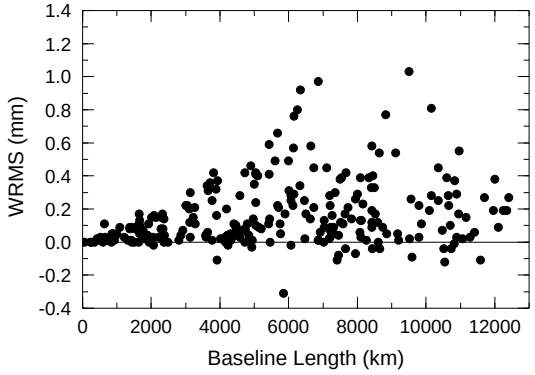

Figure 1. Improvement in baseline length repeatability when thermal deformation is modeled using all data from 1979 to 2008.

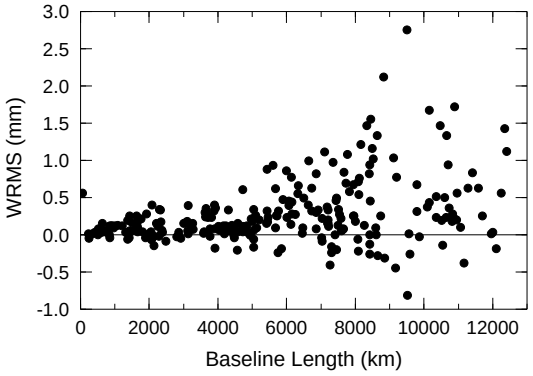

Figure 2. Improvement in baseline length repeatability with VMF1.

tion was applied in the ITRF2008 VLBI solutions and we clearly did not want to introduce biases due to the thermal effect.

3 Troposphere Modeling

3.1 VMF1

The VLBI contribution to ITRF2008 used VMF1 for the hydrostatic and wet delays (Böhm et al., 2006). The previous standard mapping functions were the Niell Mapping Functions (NMF) described in Niell (1996). VMF is derived from ray-tracing of troposphere profiles from the ECMWF data assimilation model with 6-hour temporal resolution. Both NMF and VMF1 assume azimuthal symmetry of the atmosphere around each site. In contrast to VMF1, NMF was based on radiosonde profile data from a small set of Northern Hemisphere sites. NMF is a function of site latitude, site height, and time of year. The NMF model for southern latitude sites is the same as for the northern latitudes except that the seasonal amplitudes are out of phase by a half year. To test VMF1, we ran a baseline solution for data from 1979 to 2009 and found improvement increasing with baseline length shown in Figure 2 as much as 2.5 mm.

The reference frame scale difference between NMF and VMF was 0.07 ppb. Based on elevation cutoff tests (yielding the difference in reference frame scale between solutions with 5 deg and 15 deg elevation cutoffs), this is the level of mapping function systematic error expected for NMF.

We have investigated the effect of several different troposphere modeling choices in the following section by analysing the CONT05 series of experiments. Compared to NMF, we see the reduction in length scatter in Figure 3 when VMF1 is applied.

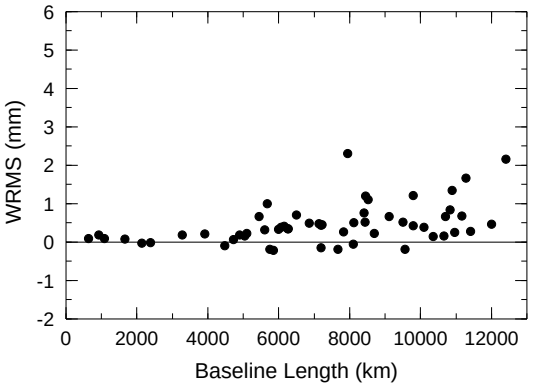

Figure 3. Improvement in baseline length repeatability with VMF1 compared to NMF for the CONT05 experiment series

3.2 Elevation Dependent Weighting

It is clear that there is mismodeling of tropospheric delay because delay residuals are greater for lower elevations. Consider the following general expression for group delay error for an observation involving station 1 and station 2:

$$\sigma_{12}^2(el_1, el_2) = \sigma_{12}^2 + \epsilon_{12}^2 + [\epsilon_1\, m(el_1)]^2 + [\epsilon_2\, m(el_2)]^2$$

where σ_{12} is the formal uncertainty of the observation, ϵ_{12} is a baseline reweighting term, and ϵ_i are site-dependent elevation-dependent noise factors.

Standard SOLVE processing adds only the

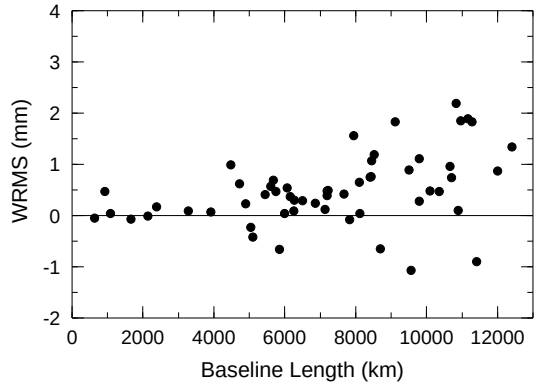

Figure 4. Improvement in baseline length repeatability with elevation-dependent weighting when compared with NMF and standard reweighting

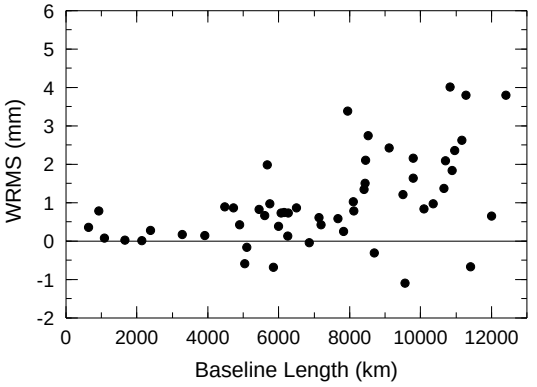

Figure 5. Improvement in baseline length repeatability with VMF1 and correlated noise when compared with NMF and standard reweighting.

baseline-dependent reweighting term calculated to make the experiment session χ^2/dof (degree of freedom) close to 1. However, even after applying this reweighting on a session basis, the χ^2/dof of estimated baseline length or position time series is 2–6 for 7 to 8 site networks (e.g. R1 and R4 sessions) and 4–20 for the 18–20 site RDV network sessions. The cause of the growth in χ^2/dof is the neglect of correlations between observations, which we discuss below. If we introduce elevation-dependent noise terms, we can account for some of the mismodeling at low elevations. Figure 4 shows the reduction in length scatter with baseline length for CONT05 sessions when elevation dependent weighting is applied instead of standard baseline-dependent weighting.

3.3 Correlated Noise

Next we consider the error for an observation on second baseline between stations 1 and 3 at the same epoch as the first observation above:

$$\sigma_{13}^2(el_1, el_3) = \sigma_{13}^2 + \epsilon_{13}^2 + [\epsilon_1\, m(el_1)]^2 + [\epsilon_3\, m(el_3)]^2$$

When two observations share the same site, the observations will be correlated since the two observations each have an elevation-dependent error contribution from the common site, which in the example above is station 1. The effect of these correlations grows as the number of stations in the network grows. To account for the correlation, we include this correlated noise term in the off-diagonal element (as well as in the on-diagonal element) of the covariance matrix between all observations (Gipson, 2007). In standard processing this matrix is diagonal and the elevation-dependent terms only appear on the diagonal. Based on CONT05 repeatability tests, the optimal average choice for ϵ_i = 6 ps. The reduction in baseline length scatter is shown in Figure 5.

3.4 GMAO

Previous approaches like VMF1 and NMF assume azimuthal independence of the refractivity field. The most advanced approach for determining the a priori tropospheric delay is to compute the slant path delay from the 3D troposphere fields. This has been done using the GEOS-5 numerical weather model from the NASA Goddard Modelling and Assimilation Office (GMAO; Petrov 2008). The spatial resolution of the model is 0.5 deg x 0.67 deg with data given every 6 hours. Figure 6 shows the improvement relative to NMF of baseline length repeatabilities for CONT05. For this case both correlated noise and GMAO were applied in the analysis. It can be seen that this analysis option yields more improvement than VMF1 applied with correlated noise in Figure 5.

4 Conclusions

In this short report, we summarized the results of tests of several new SOLVE analysis options. Modeling antenna thermal deformation clearly improves baseline length precision and accounts for part of the observed seasonal variation of site

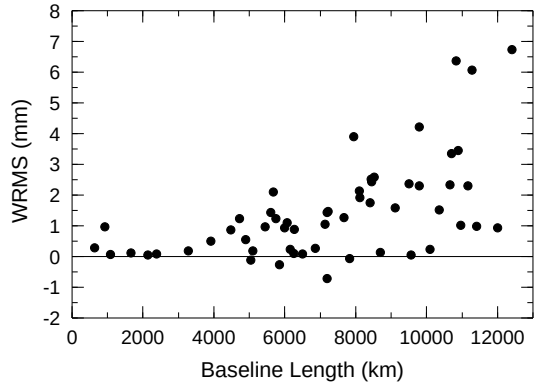

Figure 6. Improvement in baseline length repeatability with GMAO compared with NMF and standard reweighting.

vertical estimates. VMF1 is an improvement over NMF as it yields better internal precision and removes scale error of NMF. Accounting for correlations between observations on baselines reduces baseline length scatter significantly beyond the improvement with just VMF1 applied with standard reweighting. The use of slant path delay derived from a numerical weather model along with applying the correlations between observations gives the best internal precision.

References

Böhm, B. Werl, H. Schuh, Troposphere mapping functions for GPS and VLBI from ECMWF operational analysis data, J Geophys Res, vol. 111, B02406, doi:10.1029/2005JB003629, 2006.

Böhm, R. Heinkelmann, H. Schuh, Short note: a global model of pressure and temperature for geodetic applications, J Geod, doi:10.1007/s00190-007-01350-3,2007.

Gipson, J.M., "Incorporating correlation station dependent noise improves VLBI estimates," European VLBI Meeting, 2007.

Niell, A.E., "Global mapping functions for the atmospheric delay at radio wavelengths," J Geophys Res, vol. 101, no. B2, pp.3227-3246, 1996.

Nothnagel, A.,"Short Note: Conventions on thermal expansion modelling of radio telescopes for geodetic and astrometric VLBI", J Geod, doi: 10.1007/s00190-008-0284-z, 2008.

Petrov, L., "Modeling slanted path delay using numerical 4D models of the atmosphere," General Meeting, European Geophysical Union, 2008.

Measurements of the Polarization Leakage and their Effects on the Geodetic-VLBI Observables

A. Bertarini, A. Nothnagel
Institute for Geodesy and Geoinformation University of Bonn, Nussallee 17, 53115 Bonn, Germany

B. Corey
MIT Haystack Observatory, Off Route 40, Westford, MA 01886, USA

R.C. Walker
National Radio Astronomy Observatory, PO BOX O, Socorro, NM 87801, USA

W. Alef
Max Planck Institute for Radio Astronomy, Auf dem Hügel 69, 53121 Bonn, Germany

Abstract. Polarization leakage is an instrumental error that decreases the precision of geodetic and astrometric measurements. This error can be corrected in the data provided that the leakage characteristics are known. Here we report measurement of the leakage characteristics of the most commonly used geodetic stations in IVS operation and the VLBA at 2.3 GHz and 8.4 GHz.

Keywords. VLBI, polarization

1 Introduction

The aim of this project is to calculate the polarization leakage on a subset of the antennas most commonly used by the IVS and all the VLBA antennas and validate a method to remove their effects from the data. In this paper we will briefly say what polarization is and why it needs to be considered in the geodetic analysis. In the last section we will give a first glance at the measured leakage characteristic of North Liberty and Westford and a first estimate of the delay errors inferred on the baseline between North Liberty and Westford due to the leakages at the two sites.

2 Polarization Principle

Radio waves are electromagnetic fields propagating in space. Since the radio telescope feeds are sensitive only to the electric field component ($\vec{E}$) of the electromagnetic radiation, we will focus our discussion on $\vec{E}$. The electric field for a wave may be viewed as the vector sum of its components oscillating in orthogonal planes. The motion of the tip of $\vec{E}$ gives the wave's polarization state. This motion is graphically represented in figure 1. Let wave 1 be the component of $\vec{E}$ in the xz plane and wave 2 the component of $\vec{E}$ in the yz plane. If the two waves are in phase for every instant of time, as shown in Figure 1 (a), then the tip of $\vec{E}$ oscillates along a line. In this case the light is said to be linearly polarized. If there is a 90° phase shift between the two components wave 1 and wave 2, as shown in Figure 1 (b), then the tip of $\vec{E}$ describes a circle and the light is said to be circularly polarized. If the phase shift between the two waves is at an arbitrary but constant angle, then the tip of $\vec{E}$ describes an ellipse and the light is said to be elliptically polarized.

If the light comes from an incoherent emitter, the angle between the two components will change with time, therefore the tip of $\vec{E}$ will describe none of the above mentioned configuration. In this case, the polarization states of light can be measured statistically.

3 Polarization in VLBI

To determine the station and source position, VLBI uses the relative phase of the incoming electric filed at the two stations. To receive the full electric field, VLBI uses two dipoles (Thompson, Moran and Swenson, 2001). As is illustrated in Figure 2, the electric vector may have an arbitrary orientation with respect to the two dipoles

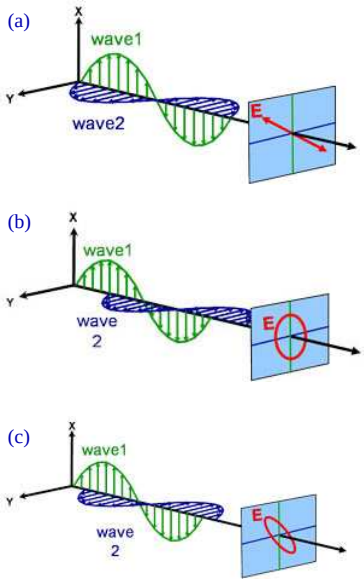

Figure 1. Motion of the electric field components along the x (wave 1 - green) and y axis (wave 2 - blue), during the propagation along the z axis and the motion of the tip of the electric vector on a fictitious screen perpendicular to the direction of the motion. The top figure (a) represents the case of linearly polarized light. The middle figure (b) represents the case of circularly polarized light. The bottom (c) figure represents the case of elliptically polarized light. Picture copyright 2009, J.A. Woollam Co., Inc, used with permission.

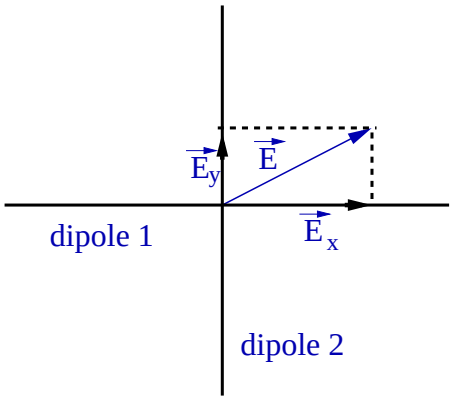

Figure 2. Incoming electric field $\vec{E}$ arriving at the two dipoles and the corresponding components of the vector along the axes of the two dipoles.

and will generally change with time.

To maximize the SNR in the cross correlation one wants to select the same polarization states at the two stations. To achieve that, every VLBI receiver has a polarizer whose task is to select these states. To avoid complications due to changes in the parallactic angle, VLBI uses circular polarization (Thompson, Moran and Swenson, 2001) and in the specific case of geodesy, only the right circular polarization (RCP) is used. The polarizers do not separate the two polarization states with perfect purity (Bertarini et al., 2008), therefore some contamination occurs from the unwanted orthogonal polarization state, which adds vectorially to the signal, corrupting the visibilites, as shown in Figure 3.

Let $E_{R,1,pure}$ be the electric field received in the right-circular (RC) polarizer output in a perfect case i.e. without any leakage coming from the left polarization at antenna 1 and $E_{R,2,pure}$ be the electric field received in the right-circular (RC) polarizer output in a perfect case i.e. without any leakage coming from the left polarization at antenna 2. In this case of perfect polarizer (i.e. perfect polarization purity) the cross-correlation product would be: $< E_{R,1,pure} E^*_{R,2,pure} >$. To connect this cross correlation to the spatial coherence function due to the astronomical source may require removal of the parallactic rotation angle from the phase of the cross correlation. Since at both stations there is most probably leakage between the polarization states, the electric field component from the RC polarizer output at antenna 1 will be:

$$E_{R,1,leak} = E_{R,1,pure} + d_1 E_{L,1,pure} \quad (1)$$

where $d_1 E_{L,1,pure}$ is the leakage term from the left circular polarization (LCP) state. d_1 is called *d*-term and quantifies the level of the leakage from the LC component into the RC component. The same happens at antenna two, and when the cross correlation is produced, there is an extra term due to the leakage, which corrupts the measurement. Assuming, for simplicity, that the parallactic angle is the same at two stations, then the cross-correlation product becomes:

$$< E_{R,1,leak} E^*_{R,2,leak} >= < E_{R,1,pure} E^*_{R,2,pure} > + d_1 d_2^* < E_{L,1,pure} E^*_{L,2,pure} > \quad (2)$$

The cross correlation for one scan is represented graphically in a real vs imaginary plane in Figure 3. The cross-correlation term due to leakage corrupts the true cross correlation leading to a measured cross correlation that differs from the true one and therefore the leakage corrupts the delay.

4 Measuring the Leakage Characteristic

In this project, we measured the polarization leakage at some geodetic VLBI stations and at the VLBA using the dualband receivers at 2.3 GHz and 8.4 GHz (the S/X receivers). The principle of the measurement is to observe an unpolarized source and ascribe any coherence found between nominally orthogonal polarization states to polarization leakage. In this section we explain how we estimated the effects of the leakages on the delay and show a sample of the results for the two stations North Liberty and Westford, chosen as examples of low leakage (North Liberty) and high leakage (Westford). Figure 4 shows the leakage amplitude and phase vs frequency at X-band (8.4 GHz) for North Liberty and Westford. The leakage for North Liberty is below 5 % in amplitude and flat in phase. The leakage for Westford is between 10 % to 15 % in amplitude and the phase turns through 360°.

To derive the visibility phase change due to the leakage, we considered an ideal visibility with 1 Jy source, 0° visibility phase, no leakage and considered a 0° parallactic angle at both stations. We then considered a measured visibility for the same conditions but including polarization leakage measured for Wesford and North Liberty (as plotted in Figure 4).

As the first step we evaluated the visibility phase change between the ideal case and the measured case within every frequency channel due to the leakage coming from the LCP. The leakage varies with frequency and so corrupts the delay. To measure the extra delay that arose from this leakage, we measured the effect of the frequency rate of change of the leakage on the multiband delay (MBD) function.

A simple way to fit approximately for the error created by the leakages in the delay follows the method used by Corey and Titus (2006). For small leakage terms, the phase error introduced by leakage at each frequency is $Im(d_1 d_2^*)$, in radians (assuming, as above, that the parallactic angle difference between the two stations

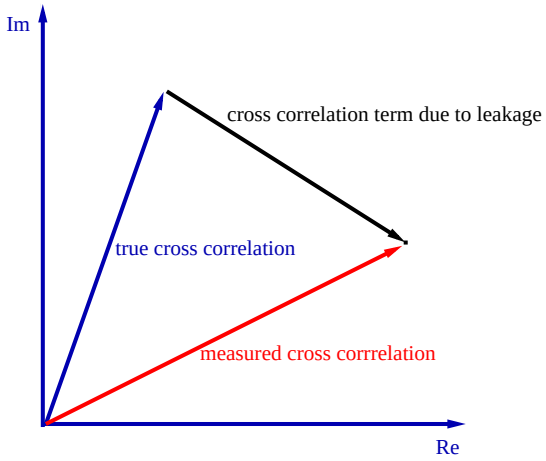

Figure 3. Plot of visibility in the real vs imaginary plane, for one scan. The vector labelled "measured cross correlation" represents the measured visibility at the correlator, which is corrupted by the polarization leakage. The vector labelled "cross correlation term due to leakage" is the leakage term. The vector labelled "true cross correlation" is the true visibility - the one that is wanted.

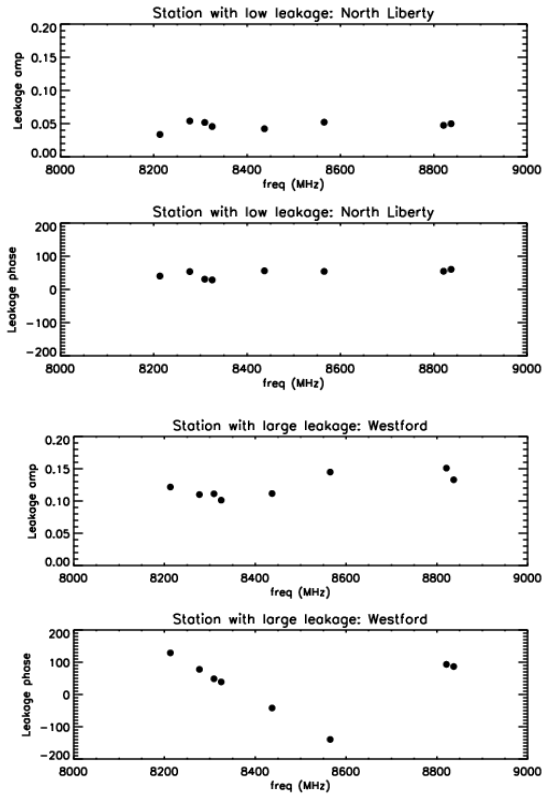

Figure 4. An example of the polarization leakage measurements between 8.2 GHz and 8.9 GHz for North Liberty (low leakage) and Westford (high leakage). Top: amplitude of the leakage vs frequency for North Liberty. Second from top: phase of the leakage vs frequency for North Liberty. Third from top: amplitude of the leakage vs frequency for Westford. Bottom: phase of the leakage vs frequency for Westford. The amplitude is in fractional voltage leakage.

is zero). The delay error is the frequency derivative of the phase error. We fit a straight line to $Im(d_1 d_2^*)$ versus frequency and the the slope gave the MBD error caused by the leakage of about 0.4 ps. It is tiny due to a fortuitous cancellation since the Wf d-term wraps through 360° over the frequency span. This translate into a path length error of 0.1 mm. Had the spanned bandwidth be 360 MHz instead of 720 MHz, so that Westford d-term rotates through 180° over the frequency spanned, then the delay error would increase to 6 ps (1.8 mm).

Since the phase change due to the leakage can vary from source to source and over time on a given source due to differential rotation between the feeds in the two antennas for different positions on the sky, it cannot be easily absorbed in a baseline clock, but the extra delay caused can be removed in d-term correction software that we will develop during the course of this PhD project. The correction should yield better baseline-length repeatability.

Acknowledgements We thank Cormac Reynolds, Ed Himwich and John Gipson for their support during the scheduling of the experiment; Alan Roy for his support during the data reduction and preparation of this presentation.

References

Thompson A. R., Moran J. M., Swenson G. W.,2001, Interferometry and Synthesis in Radio Astronomy, John Wiley & Sons, Inc. (eds.)

Bertarini A., Alef W., Corey B., Nothnagel A., Walker R. C., Effects on the Geodetic-VLBI Measurables Due to Polarization Leakage in the Receivers,2008, In: Proceedings of the Fifth IVS General Meeting, edited by A. Finkelstein and D. Behrend, ISBN 978-5-02-025332-2, 53

Corey, B., Titus, M., Antenna Cross-Polarization Characteristics at Geodetic VLBI Stations,2006, In: IVS 4th General Meeting Proceedings. Concepcion Chile. edited by D. Behrend and K. Baver K. D.

Piecewise Linear Offsets for VLBI Parameter Estimation

K. Teke, J. Boehm, H. Spicakova, A. Pany, L. Plank, H. Schuh
Institute of Geodesy and Geophysics, Vienna University of Technology, 1040 Vienna, Austria

E. Tanir
Department of Geodesy and Photogrammetry Engineering, Karadeniz Technical University, 61080, Trabzon, Turkey

Abstract. The Institute of Geodesy and Geophysics of the Vienna University of Technology is developing new software, Vienna VLBI Software, VieVS, for the analysis of Very Long Baseline Interferometry (VLBI) observations. In the parameter estimation high degrees of freedom, proper selection of estimation intervals and appropriate constraints for each parameter should be ensured. In VieVS, all parameters to be estimated are basically modelled with piecewise linear offset functions where offsets are at integer hours, integer fractions or at integer multiples of integer hours. The results of the least squares module of VieVS (*vie_lsm*) are the piecewise linear offsets of clocks, troposphere zenith wet delays, troposphere gradients, Earth orientation parameters, antenna coordinates, and others with their respective covariance matrices.

Keywords. VieVS, least squares, piecewise linear offset function, parameter estimation

1 Introduction

In the scope of creating a new VLBI analysis software called Vienna VLBI Software (VieVS) (Boehm et al., 2009), the least squares (LS) parameter estimation module has been mostly finished. The development of VieVS was not started from scratch but it is based on algorithms used in the software OCCAM (Titov et al., 2004). VieVS is designed to meet the most probable analysis related requirements of VLBI in the future, in particular the huge amount of observations compared to present sessions. Increasing the number of observations with the new VLBI system, VLBI2010, will provide enough degrees of freedom to determine the sub-daily variations of the VLBI estimates more accurately. In the least squares parameter estimation part of VieVS (*vie_lsm*) most of the estimated parameters are modelled by piecewise linear (pwl) offset functions (Boehm et al., 2009), and the required partial derivatives of the design matrix are produced by the preceding module, *vie_mod*. As exchange format between the modules Matlab "mat" files are used.

2 Least squares parameter estimation in VieVS

VLBI parameters can be estimated according to the Least Squares (LS) adjustment based on the Gauss-Markov model. The complete functional and stochastic model can be formed as:

$$\begin{bmatrix} v \\ v_c \end{bmatrix} = \begin{bmatrix} A \\ H \end{bmatrix} dx - \begin{bmatrix} l \\ h \end{bmatrix}, \quad \begin{bmatrix} P & 0 \\ 0 & P_c \end{bmatrix}, \tag{1}$$

where l is the vector of the reduced observations (observed minus computed), h is the vector of the constraint equations as pseudo observations, P is the weight matrix of the observations, P_c denotes to the weight matrix of the constraints. In Eq. (1), A is the upper block matrix of the functional model formed by presently 15 horizontally concatenated sub-matrices:

$$A = \begin{bmatrix} A_1 & A_2 & \cdots & A_{15} \end{bmatrix}, \tag{2}$$

consisting of the partial derivatives of pwl offset functions. Up to now the applied models are: pwl clock offsets (A_1), rate and quadratic terms of clock functions (A_2), pwl offsets of zenith wet delays (A_3), pwl offsets of tropospheric gradients (A_4 and A_5), pwl offsets of Earth orientation parameters (from A_6 to A_{10}), one Love number estimate per session (A_{11}), one Shida number es-

timate per session (A_{12}), and pwl offsets of antenna coordinates (from A_{13} to A_{15}). All the pwl offsets are estimated at UTC integer hours, integer fractions or at integer multiples of integer hours (Boehm et al., 2009). The length of the estimation intervals of station specific and global pwl offset parameters can be chosen between five minutes and one day. Independent from the number of clock breaks and the number of clocks where clock breaks occur, the treatment of clock breaks is handled properly by fitting clock functions for each interval defined by the clock breaks. The estimation is performed in units of centimeters and milliarcseconds. In order to avoid singularity problems of the normal equation matrix caused by an inadequate number of observations within an estimation interval, loose constraints are introduced (Kutterer, 2003).

The design matrix A_i with the partials of pwl offset functions (an example for zenith wet delays is described in Boehm et al., 2009) for a scan including three observations, three antennas, and one estimation interval (result in two unknowns for each station) is:

$$\begin{bmatrix} \frac{dL^1}{dx_{1,1}} & \frac{dL^1}{dx_{1,2}} & \frac{-dL^1}{dx_{2,1}} & \frac{-dL^1}{dx_{2,2}} & 0 & 0 \\ 0 & 0 & \frac{dL^2}{dx_{2,1}} & \frac{dL^2}{dx_{2,2}} & \frac{-dL^2}{dx_{3,1}} & \frac{-dL^2}{dx_{3,2}} \\ \frac{dL^3}{dx_{1,1}} & \frac{dL^3}{dx_{1,2}} & 0 & 0 & \frac{-dL^3}{dx_{3,1}} & \frac{-dL^3}{dx_{3,2}} \\ & & & \cdots & & \end{bmatrix}, \quad (3)$$

where $\frac{dL^k}{dx_{i,j}}$ are the partial derivatives of the delay L with respect to the offset estimates x, when k is the number of the observation, i the number of the station, and j the number of offset estimate per station. Loose constraints are introduced in order to avoid singularity (rank deficiency) of the design matrix. The constraints are applied as pseudo-observation equations:

$$x_{i+1} - x_i = 0 \pm m_{\Delta x}, \quad (4)$$

where x_i is the ith pwl offset estimate. $m_{\Delta x}$ denotes the standard deviation of the constraint which can be a function of the estimation interval and a variance rate set before processing vie_lsm. The coefficients of the standard deviations can be selected in order to derive the parameters as tightly, loosely, or "quasi-tightly" constrained. Singularity of the design matrix, which is treated properly in vie_lsm, occurs mostly when too short estimation intervals are selected before processing. The constraints Eq. (4) on the offset estimates formed in the lower block Eq. (1) of the design matrix, H, are made up as follows:

$$H = \begin{bmatrix} H_1 & 0 & \cdots & 0 \\ 0 & H_2 & \cdots & 0 \\ \vdots & \vdots & \ddots & \vdots \\ 0 & 0 & \cdots & H_{15} \end{bmatrix}, \quad (5)$$

where H_i is the sub-constrain matrix of H for the respective model, consisting of the partials of Eq. (4), simply formed by:

$$H_i = \begin{bmatrix} 1 & -1 & 0 & \cdots & 0 & 0 \\ 0 & 1 & -1 & \cdots & 0 & 0 \\ 0 & 0 & 1 & \cdots & 0 & 0 \\ \vdots & \vdots & \vdots & \ddots & \vdots & \vdots \\ 0 & 0 & 0 & \cdots & 1 & -1 \end{bmatrix}. \quad (6)$$

According to analysis requirements, any model can be excluded from the vie_lsm processing station-wise or entirely. Besides, constraints on the parameters can be omitted for each model separately or for all models.

The datum definition of the VLBI network can be provided as full-trace-minimum (No Net Translation (NNT) and No Net Rotation (NNR)) over all stations or partial trace minima can be applied for certain stations. The NNT/NNR conditions for antenna coordinates are applied according to Helmert's method as originally presented by F.R. Helmert in 1872 (Pringle and Rayner, 1971; Rao and Mitra, 1971; Pelzer, 1974; Gotthardt and Schmitt, 1978). The condition equations on the coordinate estimates (C) are added to the normal equation matrix as rows and columns:

$$C = \begin{bmatrix} 1 & 0 & 0 \\ 0 & 1 & 0 \\ 0 & 0 & 1 \\ & \cdots & \\ 0 & -z_i^{'} & y_i^{'} \\ z_i^{'} & 0 & -x_i \\ -y_i^{'} & x_i^{'} & 0 \\ & \cdots & \\ x_i^{'} & y_i^{'} & z_i^{'} \end{bmatrix}, \quad (7)$$

where $x_i^{'}, y_i^{'}, z_i^{'}$ are the a priori coordinates (translated to the geometric center of the stations and scaled) of the stations for which the

NNT/NNR conditions are introduced. The overall LS solution is done after forming the matrices:

$$dx_{total} = N_{total}^{-1}\, b_{total}, \tag{8}$$

where the vector of unknowns (dx_{total}) is

$$dx_{total} = \begin{bmatrix} dx \\ x_c \end{bmatrix}. \tag{9}$$

The normal equation matrix (N_{total}) after introducing the constraints as pseudo observations and condition equations is:

$$N_{total} = \begin{bmatrix} A^T P A + H^T P_c\, H & C^T \\ C & 0 \end{bmatrix} \tag{10}$$

and the normal equation constants (right hand side) vector (b_total) is:

$$b_{total} = \begin{bmatrix} A^T P l + H^T P_c\, h \\ b\_c \end{bmatrix}, \tag{11}$$

where b_c is the constant vector if any constants of condition equations exist. The a posteriori variance factor for the constrained normal equation system is :

$$s0_c = (v^T P v + v_c^T P_c v_c) \,/\, dof, \tag{12}$$

where dof is the degrees of freedom of the adjustment. It can easily be computed with:

$$dof = n_{obs} + n_{constr} + n_{unk}, \tag{13}$$

where n_{obs} is the number of observations, n_{constr} is the number of constraints, n_{unk} is the number of unknowns in the adjustment. The variance-covariance matrix of the unknowns of the constrained normal equation system can be computed with:

$$K_{xx} = s0_c\, N_{total}^{-1}. \tag{14}$$

Each estimated value (dx), the standard deviation of the estimate (m_{dx}), the estimation epoch in Modified Julian Date and the respective column number of the normal equation matrix, the options of the least squares parameter estimation, the normal equation matrix (N_{total}) and the vector of the right-hand side (b_{total}) for global solutions are stored in the output of the vie_lsm module in a Matlab structure array.

2.1 Future prospects

A proper outlier detection test, elevation dependent weighting of observations, and no net translation conditions for the clocks will be implemented. Pwl offsets of quasar coordinates will be estimated as well, and for specific analyses, certain stations can be excluded from the parameter estimation process, so that the respective station-wise parameters (e.g. observations, respective weights of the observations, partials and a priori values of the estimates related to these stations) will not be taken into account in the parameter estimation. Spectral analysis sub-routines of Matlab will be used for statistical analysis of the time series of the estimates produced by global solutions.

2.2 Estimation strategy

The interval for piecewise linear modelling of the parameters is usually set to values between one day and ten minutes. Due to the limited number of observations in a session, the estimation intervals should be selected accordingly. Too short estimation intervals for every parameter will cause too many unknowns which will decrease the degrees of freedom of the adjustment and may lead to several singularity problems. In order to avoid numerical problems (as e.g. rank deficiencies) and to stabilize the parameter estimation process, constraints (or pseudo-observations) have to be included in intervals with only a small number of observations. The weights of the pseudo-observations have to be chosen according to those of the real observations.

The first 24h session of CONT05 processed by the VieVS module vie_lsm showed us that Matlab has enough capacity to estimate VLBI parameters accurately with its built in functions. The elapsed time to process the first 24h CONT05 session with 6195 observations and 879 scans, ranges from 20 to 60 seconds mainly depending on the parameterization of the estimates. This time span includes loading the exchange files provided by the previous module, forming the estimation related matrices, inversion of the normal equation matrix and saving the outputs. In Figures 1, 2, and 3 some of the sub-daily estimates of VieVS are plotted for the first 24h session of CONT05.

3 Conclusions and prospects

From the investigations carried out within this study the following can be drawn:

- Piecewise linear offsets can be applied for almost all parameters of geodetic VLBI, e.g. zenith wet delays, troposphere gradients, clocks, Earth orientation parameters, antenna and quasar coordinates.
- The offsets should be determined at integer days, integer hours, or integer fractions of integer hours, respectively.
- A proper outlier detection test will be implemented.
- For specific analyses, it will be possible to exclude stations from the parameter estimation stage, with other words, the respective station-wise parameters (e.g. observations, weights of the observations, partials and apriori values of the estimates related to these stations) will not be taken into account in the *vie_lsm* module. This will provide us the flexibility of selecting particular baselines answering the needs of the analysis.
- More investigations on the magnitude of the amplitudes and respective sub-daily periods of the estimated parameters will be carried out.

Acknowledgements We are grateful to the International VLBI Service for Geodesy and Astrometry (IVS) for providing the observations. K. Teke wants to acknowledge the Scientific and Research Council of Turkey (TUBITAK) for his scholarship. Andrea Pany is recipient of a DOC-fFORTE fellowship of the Austrian Academy of Sciences at the Institute of Geodesy and Geophysics, Vienna University of Technology. Hana Spicakova is grateful to Mondi Austria Privatstiftung for financial support during her phd study at TU Vienna.

References

J. Boehm, H. Spicakova, L. Plank, K. Teke, A. Pany, J. Wresnik, S. Englich, T. Nilsson, H. Schuh, T. Hobiger, R. Ichikawa, Y. Koyama, T. Gotoh, T. Kubooka, T. Otsubo, 2009, Plans for the Vienna VLBI Software VieVS, European VLBI Service for Geodesy and Astrometry 2009, this volume.

Gotthardt E. & Schmitt G., 1978, Einfuehrung in die Ausgleichungsrechnung, Karlsruhe.

Kutterer H., 2003, The Role of Parameter Constraints in VLBI Analysis, 16th Working Meeting on European VLBI for Geodesy and Astrometry, pp. 171-179.

Pelzer, H., 1974, Zur Behandlung singulaerer Ausgleichungsaufgaben, ZfV 1974, pp: 181-194.

Pringle P.M. & Rayner A.A., 1971, Generalized Invers Matrices and Its Applications to Statistics, London.

Rao C.R. & Mitra S.K., 1971, Generalized Inverses of Matrices and Its Applications, New York.

Titov O., Tesmer V. & Boehm J., 2004, OCCAM v.6.0 Software for VLBI Data Analysis, in: Vandenberg N.R. & Baver K. (eds.) International VLBI Service for Geodesy and Astrometry 2004 General Meeting Proceedings, NASA/CP-2004-212255.

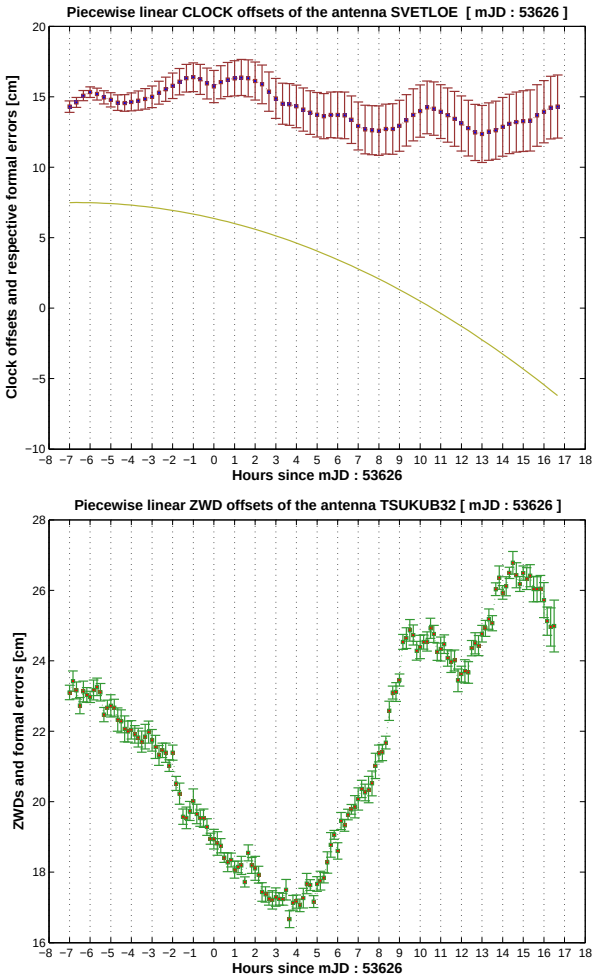

Figure 1. Parameters of clock function and pwl offset estimates of zenith wet delay.

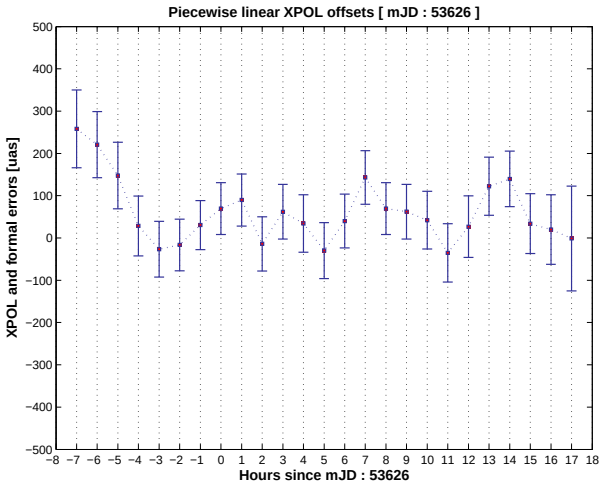

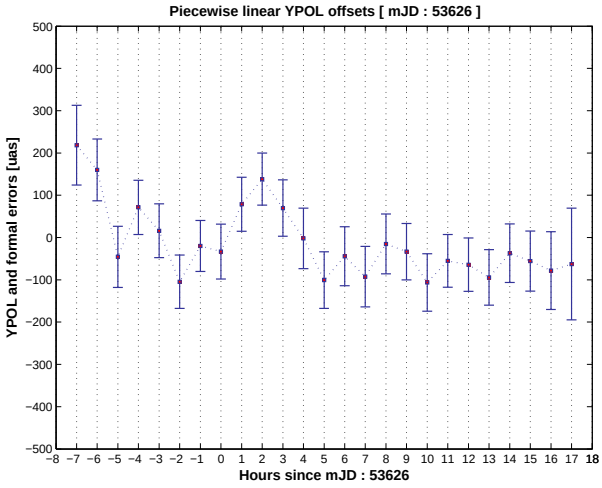

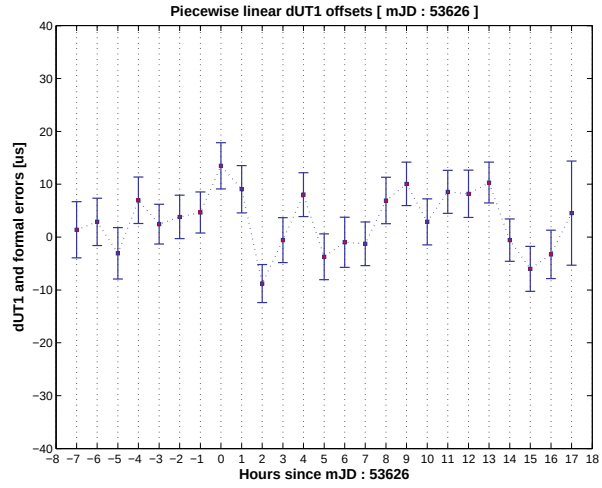

Figure 2. Sub-daily pwl offset estimates of Earth rotation parameters.

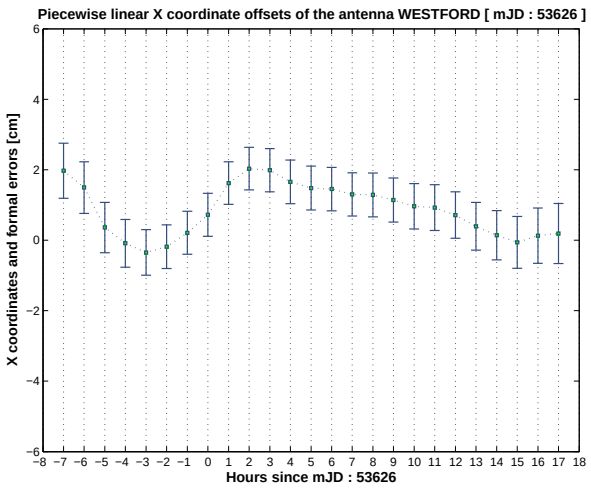

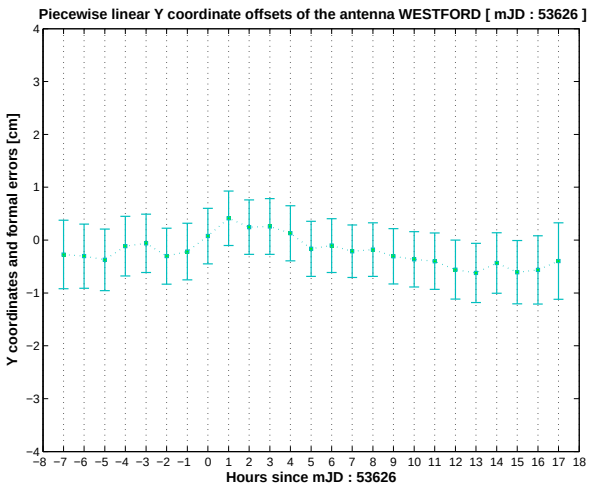

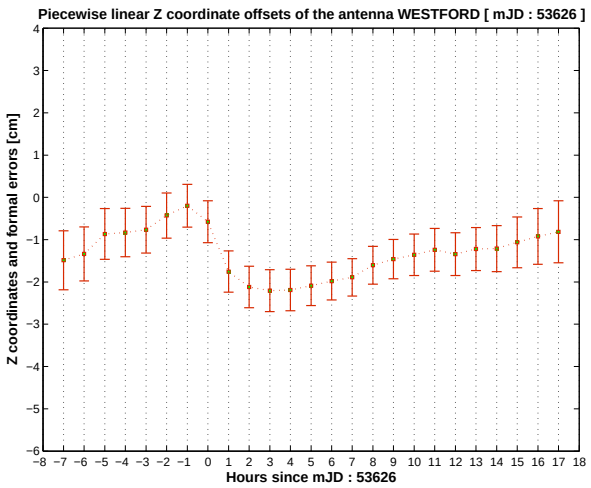

Figure 3. Sub-daily pwl offset estimates of antenna coordinates.

The Mark 5C VLBI Data System

A.R. Whitney
MIT Haystack Observatory, USA

J. Romney
NRAO, USA

K. Owens
Conduant Corporation, USA

Abstract. The Mark 5C disk-based VLBI data system is being developed as the third-generation Mark 5 disk-based system, increasing the sustained data-recording rate capability to 4 Gbps. It is built on the same basic platform as the Mark 5A, Mark 5B and Mark 5B+ systems, and will use the same 8-disk modules as earlier Mark 5 systems, though two 8-disk modules will be necessary to support the 4 Gbps rate. Unlike its earlier brethren, which use proprietary data interfaces, the Mark 5C will accept data from a standard 10 Gigabit Ethernet connection and be compatible with the emerging VLBI Data Interchange Format (VDIF). Data sources for the Mark 5C system will be based on new digital backends now being developed, specifically the DBE2/DDC in the U.S. and the dBBC in Europe, as well as others. The Mark 5C system will be adopted by NRAO as part of the VLBA sensitivity upgrade program, as well as the VLBI2010 geodetic-VLBI initiative, and will be available to the global VLBI community. Mark 5C system specification and development is supported by Haystack Observatory, NRAO and Conduant Corporation. Prototype Mark 5C systems are expected in late 2009.

Keywords. VLBI system

1 Introduction

The Mark 5C is being designed as the next-generation Mark 5 system, with a capability of recording sustained data rates to 4096 Mbps. It will use the same disk modules as the Mark 5A and Mark 5B, thus preserving existing investments in disk modules. The data interface for both recording and playback will be 10 Gigabit Ethernet, which is rapidly becoming a widely supported standard. The use of 10GigE interfaces comes with some significant implications, however. Firstly, data sources must be designed to provide data streams in a format compatible with the Mark 5C requirements. And secondly, data playback through a 10GigE interface is a good match for a rising generation of software correlators. In the interests of backwards compatibility, the Mark 5C will also support a mode which writes disk modules in Mark 5B data format which can be correlated on existing Mark 4 correlators that support Mark 5B.

The Mark 5C will be implemented using the existing Amazon StreamStor disk-interface card (used in the Mark 5B+) from Conduant Corp along with a new 10GigE-specific interface daughterboard being designed by Conduant. Unlike the Mark 5A and Mark 5B, no separate specialized I/O card will be necessary in the Mark 5C.

2 Data Sources

One major implication of the Mark 5C model is that the data source is responsible for all data time-tagging, formatting and creation of Ethernet packets. This is a departure from the VSI-H model used by the Mark 5B, which has basically only 32 parallel sample bit-streams, a clock, and 1pps tick flowing between the data source and the Mark 5B, with the Mark 5B being responsible for creating data frames with higher level time-tagging and formatting.

Fortunately, VLBI data sources capable of creating such formatted Ethernet packets are now being developed in both the U.S. and Europe as part of the development of digital downconverters and backends. Suitable 10GigE data sources to drive the Mark 5C are expected to be available sometime in the first half of 2008. The details of the data formats to be provided to the Mark 5C

are specified in a separate document "Mark 5C Data-Frame Specification". Normally, each Ethernet packet from the data source will contain sample data from only a single frequency channel, although a Mark 5B-compatible data mode is specified which will write disk modules in a format that can be re-played on a Mark 5B playback unit; this will provide the ability to process the recorded data on existing Mark 4 hardware correlators.

3 Correlation

A major shift is currently developing to move from hardware-based correlators to software-based correlators, some of which already exist. Unlike the Mark 5A and Mark 5B, the Mark 5C will have no streaming hardware playback interface. Instead, the data files will appear to the user as standard Linux files and will be read as such. We expect that the standard interface for playback to a correlator will be through a standard 10GigE interface implemented on a commercial NIC. Unlike existing hardware correlators, software correlators do not demand constant-rate streaming inputs. As such, the Mark 5C playback is well suited for interfacing to software correlators, but not well suited or intended to interface to hardware correlators.

4 General Mark 5C Characteristics

The Mark 5C will have the following characteristics:

- Mark 5C will be fully compatible with all existing Mark 5 disk modules, however some modules with older disks may limit record/playback data rates.
- At data rates above about 2 Gbps, it will be necessary to record to two 8-disk modules simultaneously, in so-called 'non-bank' mode, which is not normally used by Mark 5A or Mark 5B/5B+.
- A 10GigE interface for *receive only* will be implemented on the Amazon StreamStor disk-interface card (currently used in the Mark 5B+) by replacing the FPDP I/O daughterboard on the Amazon card with a newly designed 10GigE daughterboard. This 10GigE interface will be receive-only, optimized for sustained real-time recording of *at least* 4096 Mbps from a data source. Received Ethernet packets can be OSI Layer 2 or higher, but will only be processed by the Mark 5C at the Layer 2 level. Jumbo Ethernet packets up to 9000 bytes will be supported. The data source is required only to transmit Ethernet packets, and is not required to process any received packets.
- The entire data payload from each arriving Ethernet packet, sans a specified length of payload header (which may contain higher OSI Layer parameters or other information), will be recorded to disk. In this sense, the Mark 5C is entirely 'formatless'; i.e. all data formatting must be done by the data source. This allows each user to format the recorded data according to his/her needs.
- The Ethernet data payload may contain a user-generated 32-bit "Packet Sequence Number" (PSN), whose position within the data payload can be specified to the Mark 5C. The Mark 5C can be commanded to a "PSN monitor mode" that will parse this serial number from every packet to identify missing or out-of-order packets. Out-of-order packets, within some reasonable limits, will be restored to proper order, while the user data from each missing packet will be replaced by user-specified "fill-pattern" data. The MSB of the PSN may also be used as an 'invalid' marker to prevent recording data from a packet. If "PSN monitor mode" is disabled, data are recorded to disk in the order that packets are received; no checks are made for out-or-order or missing packets.
- Similar to the Mark 5A/B, the Mark 5C will record data as "scans", where a scan is defined as the period between starting and ending the recording of a particular observation. The duration of a scan may be from several seconds to many minutes. The host application software will maintain a directory of scans for easy identification and access. No duplicate-named scans are allowed.
- Scans will appear as normal Linux files to the host PC. Data playback on the Mark 5C will be through a 10GigE NIC interface on the host PC . A planned upgrade by Conduant of the Amazon card, which interfaces to

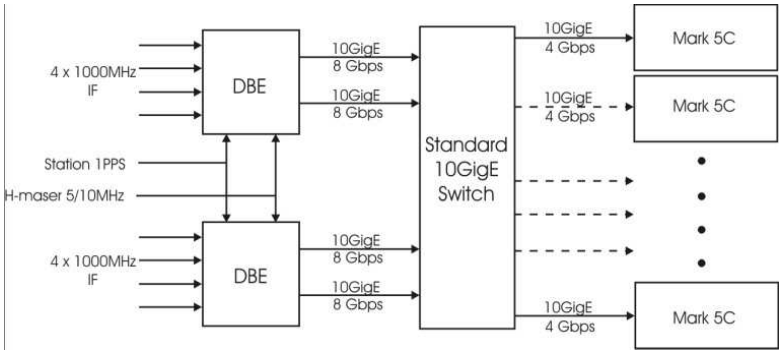

Figure 1. Generic signal-connection diagram for Mark 5C.

the PCI-X bus, will support the PCI e bus to allow substantially higher playback rates from Mark 5 disk modules.

5 Physical Connections

Because the interconnection between the data source and the Mark 5C is a standard 10 Gigabit Ether net connection, there is considerable flexibility in connection topology between data-source units and Mark 5C units. Figure 1 illustrates the general case where multiple data-source units provide data to multiple Mark 5C units through a standard Ethernet switch. The Ethernet switch allows Ethernet packets from either of the two DBE2 units to be arbitrarily routed to any of four Mark 5C units, providing an easy way to manage route data packets in an arbitrary manner, but is particularly useful to manage data-rate mismatches between individual data sources and individual Mark 5Cs. For example, an 8 Gbps packet stream from a single DBE2 could be separated into two 4 Gbps packet streams to two Mark 5C units.

6 Mark 5C Data-Frame Format

The Mark 5C itself is data-format independent and simply records Ethernet packets which are sent to it. However, most usage of the Mark 5C is expected to utilize the standardized VLBI Data Interchange Format (VDIF) specification, which is the subject of another paper in this publication.

7 Slow-disk management

Considerable experience has a shown a low, but significant, occurrences of "slow" disks, that is disks that still function to read and write, but at a reduced data rate due presumably to marginal or bad sectors on the disk. Normal RAID systems will simply slow down to accommodate such disks in a RAID array since they are not designed for real-time operation. The StreamStor disk-interface cards in the Mark 5 units are designed to re-distribute the load to normal-performing disks in the face of one or more "slow" disks in the recording array so as not to lose critical real-time data. Playback through a software correlator is generally non-critical as to playback rate, though the correlation speed may be slower than normal. If correlation speed is important, a playback mode may be invoked whereby data not received in time from slow disks will be replaced with a specified "fill pattern".

8 Upgrade path from Mark 5A, Mark 5B or Mark 5B+

The Mark 5C requires an Amazon StreamStor card ($\sim$ \$9500) plus a 10 Gigabit/sec Ethernet daughter board (\$ $\sim$3-4K); no VLBI-specific I/O board is required. Upgrade from Mark 5A or Mark 5B requires an Amazon board and 10GigE daughterboard. Upgrade from a Mark 5B+ requires only a 10GigE daughterboard.

9 Summary

The Mark 5C development is being support by Haystack Observatory, NRAO and Conduant Corporation. Prototype Mark 5C systems are expected in late 2009. Detailed specifications for the Mark 5C are available at *http://www.haystack.edu/tech/vlbi/mark5/mark5_memos* in memo number 57. Other information related to Mark 5C is also available at this URL.

DBBC.2 Backend System: status report

G. Tuccari, S. Buttaccio, G. Nicotra
Istituto di Radioastronomia, INAF, 96017 Noto (Siracusa), Italy

W. Alef, D. Graham, A. Roy, M. Wunderlich
Max Planck Institute for Radioastronomy, Auf dem Hügel 69, 53121 Bonn, Germany

A. Bertarini
Institute for Geodesy and Geoinformation University of Bonn, Nussallee 17, 53115 Bonn, Germany

A. Neidhardt
FESG TU, Arcisstrasse 21, 80333 München, Germany

R. Zeitlhoefler
Bundesamt fuer Kartographie und Geodaesie, Wettzell, Germany

Abstract. The status of the DBBC.2 project is reported. The hardware of this second version of the DBBC system is complete and a number of systems ordered by some stations have been produced. Features of the available firmware and of that under development are shown including the latest implementation. The control software of the DBBC and the Field System interface has been revised to handle the version 2 hardware. Observational tests are continuing with the progressive removal of identified problems. Finally the system deployment at the telescope is discussed.

1 Hardware

The DBBC system is an environment where more functionality of digital signal process can be realized, with very high bandwidth and high data rates. In radioastronomy its main use is as VLBI back-end.

The new class of boards developed for the DBBC in the version 2 greatly improves performance and reduce the number of elements to realize the entire functionality of a MK4 equivalent rack.

The first ADB2 board prototype production has been completed. The board offers several operation modes with de-multiplexing in two or four bus. Maximum sampling clock is 2.2 GHz, maximum signal frequency to be sampled is 3.5 GHz, 10-bit representation. A board ADB2 can feed as piggy-back element a FiLa10G, giving the possibility to place the sampling element in the receiver site, connecting the DBBC throw optical fibers.

The new processing unit Core2 board in the V5 version is now operative. The board is compatible with ADB1 and ADB2 and support a minimal equivalent of four Core1 functionality. The pcb has an number of 40 equivalent layers and all the connections for signal transfer are differential, twisted pair, matched in delay and impedance between the pads of the dice and the pins of the bus connectors. A piggy-back element can be adopted for additional functionality, like memory bank for pulsar de-dispersion, or other needs where a significant memory addition is to be adopted.

The CaT boards (Clock and Timing) are ready and used to generate the general timing to the system: the Clock board is able to generate an highly flexible number of synthesized sampling clock (e.g. 2048 MHz, 1024 MHz, etc.) values, phase locked with an external 10 MHz. Low phase-noise and very small sensitivity to temperature are main performance. The Timing board is producing 1PPS synchronization signals for all the ADB boards and the entire digital chain. Frequency selection with use of different VCOs for large range selection is programmed by use of the DBBC internal PC Set.

The FiLa10G boards realization is under way

and the first prototype of the board available and under test. It can be used as piggy-back board of any ADB2 sampler, giving the possibility to transmit and receive in the same time an high data rate of 20 Gbps + 20 Gbps. The bidirectional functionality could be required for instance when a RFI mitigation is needed to be realized in a remote position with respect to the sampling and processing site. With the typical sampling frequency of 2.048 MHz and the full 8-bit data representation, a double optical fibre set meets the full data handling requirement and Ethernet standard. Moreover the board is equipped with two additional transceiver able to operate at 1-2-4 Gbps for slower connections.

The full number of transceivers is then four and they in part or all can be used, with the possibility so to populate the board with any number of them, depending on the needed functionality. The board indeed can even support the data tx-rx of 2x2 VSI connections and in such case it can still be used as p-b element of a ADB2 or as stand-alone element. The configuration files can be also loaded by the on board stand alone flash memory. The entire triangle connectivity HSI/HSIR – VSI in/VSI out – Optical Fibres is supported. The board can support the connection with the MK5C recorder and it's ancillary in a DBBC system until MK5C is not on field.

The FiLa10G firmware is at an excellent level of development, and a test bench is progressing in MPI in parallel with the final board preparation. In the test bench is possible to verify the entire data flow from the data input as coming from samplers or from a down-converted data stream, up to the optical physical layer. The FiLa10G is necessary for MK5C connection through 10G, while DBBC.2 will is in any case usable with 2 VSI connection even at 4 Gbps. The MK5C is connected using a copper CX4, an additional board has been developed to convert CX4 to optical fiber in bidirectional way.

2 Firmware

Some elements of the already developed configurations still need to be improved. One of the main issues, the xxx.99 MHz tuning setting, is now solved and such frequencies are available.

Several groups are already working for different kind of functionalities with the DBBC programmable kit and the products are expected to be shared among the system users.

A multiband fixed tuning configuration (often called poly-phase filter) has been developed and successfully tested in Haystack. This represents the observational mode for the new geodetic VLBI2010 system. This configuration can be used also for wide band continuum astronomic observations.

3 Observation

Several test observations have been realized and the data analysis suggested modifications to the firmware. The process is still underway. The digital system use requires to optimize or to equalize the IF amplitude flatness in band: a new version of Conditioning Module was developed to optimise this aspect, but a good equalized band is expected from the receiver. Additional observation test will be realized with the three Wettzell unit. Testing is accelerated with the introduction of a DBBC.2 system even in Effelsberg and Noto for a fast evaluation time with the correlator.

A further improvement is also expected by the introduction of better in/out band filter rejection, achievable with the additional resources available in the Core2 boards.

The integration with the Field System is now under way. It is realized in a first time implementation as a collection of station commands. The system gain information in the different part of the instrument are recorded in a log that can be available under a specific FS command for calibration purposes. A second more sofisticated implementation is going to be realized by the adoption of dedicated FS commands.

4 Production

INAF created a spin-off company for the DBBC production, named HAT-Lab.

The company has an agreement with IRA-Noto Section, where laboratories are placed for a part of the production. It's under evaluation the possibility to take an other part of the production in MPI, for an initial setting phase. The production phases have been carefully defined and a certain number of operations will be realized by external companies. The full process time for a complete system, tested in laboratory, will be three months,

and in parallel more systems (4) could be built, with the initial manpower and logistic capability.

As for now the system available at the stations are: three units in Wettzell (Germany), one in Effelsberg (Germany), one in Noto (Italy), one is to be sent soon to Hobart (Australia), one to be sent soon to Yebes (Spain). A system in version 1 with only one Core board is also in Irbene (Latvia).

Starting the activity of HAT-Lab the DBBC deployment could be coordinated by EVN that plan to equipe all the stations with a DBBC unit in order to be able to observe at 4 Gbps data rate, making use of the MK5C recorder.

5 Linear to Circular and Stokes Conversion

Different projects are under development within the DBBC hardware. One is described in this section. Main aims are the conversion from linear polarization to circular polarization and the formation of Stokes parameters in the DBBC for single-dish broad-band polarimeter. The reason for requiring this is that Effelsberg and geodetic antennas are moving to broad-band feeds and extremely-broad bands are possible only with linear polarization.

It looks as VLBI is simplest with circular polarization and existing analogue polarizers are narrow band due to imperfect 90° phase shift. A possible solution is envisaged by making perfect 90° phase shift across broad bandwidth digitally (e.g. Hilbert transform).

Processing Steps in this process:
1) Receive time series from ADC at 1 Gbps
2) Measure gain and phase difference between X and Y polarizations
3) Fourier transform time series to frequency domain
4) Equalize the gain using result from (1)
5) Shift phase of one polarization by ±90° in each frequency channel
6) D-term correction (idea by Koyel Das):
6.1) Correct for leakage between X and Y
6.2) Form X − Dxy Y and Y − Dyx X outputs using an adaptive filter
6.3) Filter to adjust D to minimize the output power
7) Fourier transform back to time domain
8) Form circular polarization by summing X and phase-shifted Y
9) Send result from 8) on to existing DBBC processing stages
10) Take result from 6) and form Stokes parameters and integrate in time.

Expected result would be excellent circular polarization over wide bandwidth, zero D-terms, Stokes parameters in many channels over wide bandwidth.

MPIfR/BKG correlator report

W. Alef, H. Rottmann, D. A. Graham
Max Planck Institute for Radioastronomy, Auf dem Hügel 69, 53121 Bonn, Germany

A. Müskens
Institute for Geodesy and Geoinformation, University of Bonn, Nussallee 17, 53115 Bonn, Germany

J. Morgan
Institute of Radioastronomy – INAF, via P.Gobetti, 101, 40129 Bologna, Italy

S. J. Tingay
Curtin Institute of Radion Astronomy, GPO Box U1987, Perth, Western Australia 6845, Australia

A. T. Deller
National Radio Astronomy Observatoy, 1003 Lopezville Road, Socorro, NM 87801-0387, USA

Abstract. We report on the status of the Bonn MK IV VLBI correlator with special emphasis on geodetic correlation. The status of the successor to the MK IV correlator — the DiFX software correlator — will be discussed. The results of the first geodetic evaluation of DiFX will be presented and as well as the plans for further tests and developments of DiFX.

Keywords. Correlator, software correlator, VLBI, eVLBI, geodetic VLBI

1 Introduction

Since December 1999 the Max Planck Institute for Radioastronomy in Bonn (MPIfR), the Federal Agency for Cartography and Geodesy (BKG) and the Institute for Geodesy and Geoinformation of Bonn University jointly operate a MK IV VLBI correlator at the correlator centre of the MPIfR. It is still the workhorse for geodetic correlation and in the field of mm-VLBI. The correlator hard- and software are nearly identical to the systems at MIT Haystack Observatory, and at USNO in Washington. Data transport to the correlator is now done exclusively via disks or Internet.

The hardware correlator is now almost 10 years old and will soon be replaced by the DiFX software correlator, which is implemented on a medium sized compute cluster. A major effort at Bonn is the geodetic adaption and verification of the DiFX software.

2 MK IV correlator status

The MK IV hardware correlator has been operational for nearly 10 years. All tape drives were taken out of operation since the last EVGA meeting and have been replaced with eight Mark 5A and four Mark 5B disk playback systems. As only very few telecopes record on Mark 5B, one of those units is instead used for e-VLBI transfers, where the data is sent from the telescope to the correlator via Internet.

The correlator control has been partially upgraded from the original HP-UX systems to standard Linux PCs. As HP-UX and Linux have a different endianness (byte ordering) and are 64-bit and/or 32-bit operating systems, implementing the communication between the different tasks running on different architectures is quite demanding. While Haystack's intent is to migrate all programs to Linux, progress is rather slow.

E-VLBI data transfer to the correlator is now done on a regular basis via a dedicated 1 Gbit Internet connection via the German Academic Research Network (DFN) to the European Academic Backbone (Géant). The incoming data are initially stored on a RAID disk system. For processing with the MK IV correlator the data has to be copied to Mark 5 disk packs in a second step.

3 Geodetic correlation

Roughly 60% of the total correlation time is used for geodesy. The following types of observations

Figure 1. Picture of the MK IV correlator (left) with Mark 5As in 3 racks and 4 Mark Bs in one rack

are processed at Bonn:

R1 : about 50 experiments per year are correlated. The data base is typically ready in less than 10 days. The data from Tsukuba, Ny Ålesund and Onsala are sent to Bonn via Internet.

INT3 : Again about 50 experiments per year are correlated. The data base is typically ready in less than 7 hours! This is possible because all stations transfer the data of this 1 hour intensive observation with e-VLBI. The participating telescopes are Ny Ålesund, Wettzell, and Tsukuba.

OHIG : The OHIG series includes stations in Antarctica. It is observed about 6 times per year. It has low priority on the correlator. The data from Tsukuba and Syowa are transferred via the Internet.

Europe : The Europe series is observed about 6 times per year. It has also lower priority on the correlator. E-VLBI transfer is done for stations Metsähovi, Ny Ålesund, Onsala, and Wettzell.

T2 : Four of six T2s are correlated at Bonn per year. The data from Tsukuba, Kashima, Chichi, and Aira are sent via the Internet.

It should be noted that more manpower is needed at the correlator to handle both ways of data transfer, module shipment and e-VLBI, and a steadily increasing number of geodetic observations.

4 DiFX software correlator

The MK IV correlator should soon be replaced, as it is nearly 10 years old. It cannot correlate the future high data rates which the new digital backends to be installed in the field this year will be able to deliver. MPIfR decided about two years ago that the MK IV correlator should be replaced by the DiFX software correlator (Deller

et al., 2007), which other institutions have chosen as their future correlator, too. DiFX is open source and implements the FX technology while the MK IV is a so-called XF correlator. They differ in the order in which the Fourier transform (F) and the cross-correlation (X) are calculated. For production correlation a license from Swinburne University of Technology is required.

4.1 DiFX collaboration

The BKG financially contributed to the MK IV correlator. They are also supporting the installation and further development of the DIFX correlator for geodetic applications. A third partner is the Institute for Geodesy and Geoinformation of the University of Bonn, who have a postdoc position open for a scientist to work on the development of DiFX.

MPIfR is a member of the global DiFX developers group. Partners here are NRAO, Swinburne, ATNF, Curtin, IRA-INAF and others. Interested institutions are MIT Haystack, USNO, Metsähovi, Shanghai, and JIVE. The source code of DiFX is kept on an SVN server at ATNF. Mailing lists, a Google group and a Wiki are used for communication amongst the partners.

4.2 Hardware for the DiFX correlator

Software correlation belongs to the class of "embarrassingly parallel problems"[1]. This means it can efficiently be executed in parallel on any size computer cluster. At the end of 2008 MPIfR installed a compute cluster with 60 nodes (computers) plus two user frontends each with two quadcore processors, which gives a total of nearly 500 compute cores. Two raid systems each with 20 TB disk space can be used for storing data. Cluster interconnect is realized via 20 Gbit Infiniband and two times Gbit ethernet. At present 12 Mark 5 playback units are connected into the cluster with Gbit ethernet. It is planned to upgrade later to 10 Gbit ethernet and 16 Mark 5s. The cluster is cooled in a closed loop to save cooling energy. In the Linpack benchmark test it reaches about 4 TFlops while loading the cluster to more than 95%. The power consumption ranges from about 4 kW (cluster idle) to about 24 kW for the fully loaded cluster.

[1] http://en.wikipedia.org/wiki/Embarrassingly_parallel

Figure 2. Cluster, schematic view. From left to right: rack with 40 compute nodes; rack with 20 nodes, appliance, 2 user frontends, 20 TB raid, IB switch; rack with 20 TB raid (Picture from the Megware ClustWare®-Appliance).

4.3 Feasibility test of using DiFX for geodesy

The first installation of DiFX at the MPIfR was made by Adam Deller in 2006. He also implemented a first version of scan-based correlation. A five station geodetic observation with about 300 scans was successfully correlated resulting in 300 output files which had to be read into AIPS (Greisen, 1990).

For a first geodetic verification of DiFX about one minute of data of an astronomical VLBA observation with four frequency sub-bands (1358.49 – 1406.49 MHz) with both upper and lower sidebands was used. The observation had left and right circular polarization and was recorded with 2-bit sampling. To simplify the test the lower sideband of the first sub-band of a subset of four antennas was selected (1358.49 MHz).

The data was correlated with the MK IV and the DiFX correlators, where the MK IV should serve as a reference, as it is a well accepted geodetic correlator. Both correlators were driven from the observing schedule in VEX format. For determining the interferometer geometry the MK IV correlator uses CALC 8 while DiFX uses CALC 9. Correlation parameters

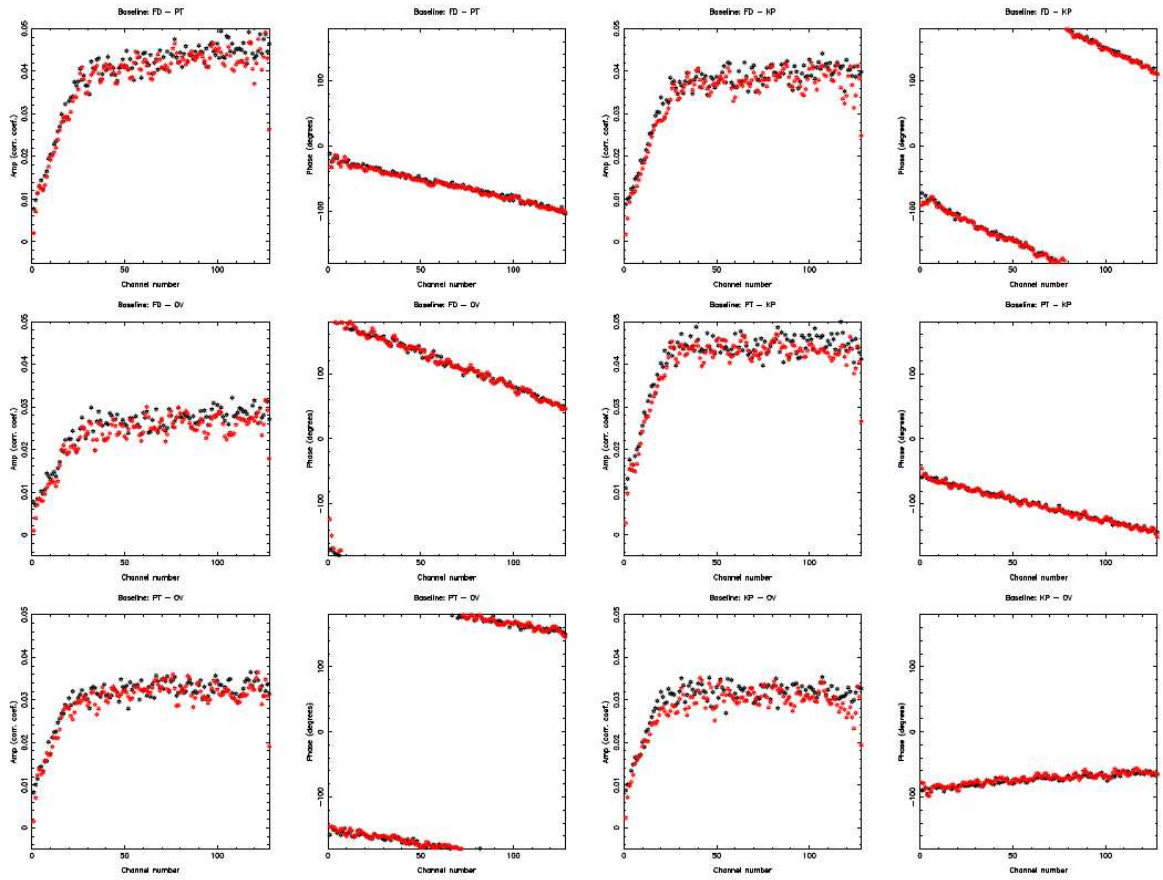

Figure 3. Comparison of the cross spectra. Red: MK IV; black: DiFX. Amplitude and phase are plotted next to each other. The phase shows an excellent agreement. The phase slope indicates a residual delay. The amplitude of the MK IV data is slightly lower than that of the DiFX correlator.

were 128 lags/channels and 2 s integration time. As DiFX cannot yet extract phase-cal signals, manual phase-cal was used for both data sets. For the MK IV data the standard post-processing was used: fringe-fitting with `fourfit` and export to AIPS with `MK4IN` (Alef and Graham, 2002). `MK4IN` stores the correlator model in the CL-table. In normal mode it adds sidebands so that had to be disabled.

DiFX was used with the same clock and clock-rate values as the MK IV correlator, except that the signs had to be reversed. The output format RPFITS was read into AIPS with `ATLOD`.

Both data sets were exported from AIPS in FITS format and then read into MIRIAD (Sault et al., 1995) where the data was plotted with `UVSPEC` and `UVPLT`.

The data had to be corrected for the differences in the delay model of the MK IV and DiFX which are quite significant. The correction on the baseline Fort Davis (FD) to Kitt Peak (KP) corresponds for instance to about 10°.

The correlated amplitudes of the two correlators agree within very few percent. The differences can be attributed to how various corrections are implemented. The mean phase differences as a function of time and frequency is well within 1σ of zero (see figures 3 and 4). For more details see Tingay et al. (2009).

4.4 Plans for further geodetic enhancements to DiFX

The next steps will be the implementation of phase-cal extraction and with somewhat lower priority a program to convert DiFX output to the standard MK IV correlator output format. The latter would enable to keep the easy and rather straightforward data reduction path that is used now, including fringe-fitting, and export

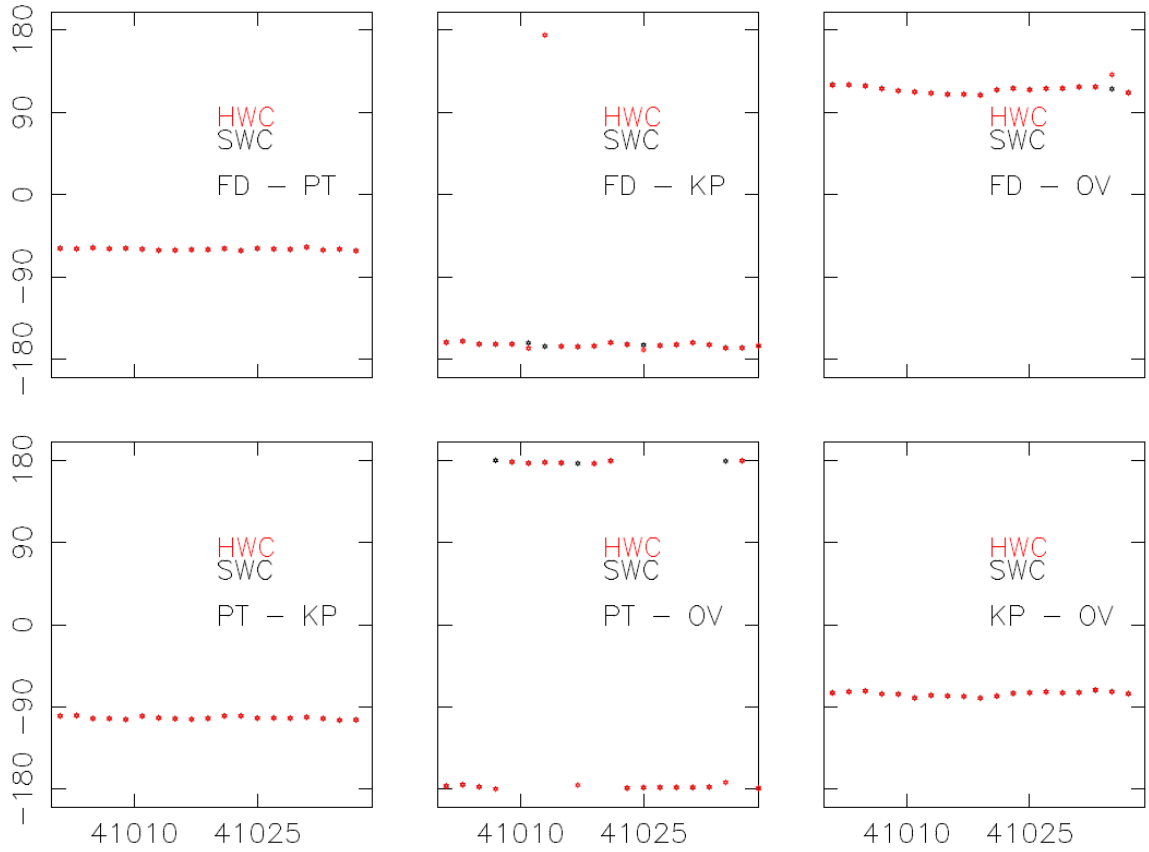

Figure 4. Phase is shown as a function of time. Red: MK IV; black: DiFX. Each dot represents 2 s of data. There is an indication that the MK IV correlated data shows some outliers, which are not seen in the data of the DiFX software correlator. Those outliers can possibly be attributed to the so-called station units of the MK IV correlator.

to CALC/SOLVE with `DBEDIT`.

When phase-cal extraction will be available we will continue with the geodetic verification in a stepwise process. It will start with a correlation of a one hour three station Intensive observation. The final test will be the correlation of a seven or eight-station 24 hour run like an R-series observation. It is envisaged that the fringe-fitting and export to CALC/SOLVE will initially be done with AIPS. Analysis centers will be asked to evaluate and compare the results of the MK IV and DiFX correlation.

References

W. Alef and D. A. Graham. The New Bonn MK IV – AIPS Data Export Path. In E. Ros, R. W. Porcas, A.. P. Lobanov, and J. A. Zensus, editors, *Proceedings of the 6th EVN Symposium*, page 31, Bonn, Germany, June 2002. MPifR.

A. T. Deller, S. J. Tingay, M. Bailes, and C. West. DiFX: A Software Correlator for Very Long Baseline Interferometry Using Multiprocessor Computing Environments. *PASP*, 119:318–336, March 2007.

E. W. Greisen. The Astronomical Image Processing System. In G. Longo and G. Sedmak, editors, *Acquisition, Processing and Archiving of Astronomical Images*, pages 125–142, 1990.

R. J. Sault, P. J. Teuben, and M. C. H. Wright. A Retrospective View of MIRIAD. In R. A. Shaw, H. E. Payne, and J. J. E. Hayes, editors, *Astronomical Data Analysis Software and Systems IV*, volume 77 of *Astronomical Society of the Pacific Conference Series*, pages 433–+, 1995.

S. J. Tingay, W. Alef, D. A. Graham, A. T. Deller. Geodetic VLBI correlation in software. I. Feasibility of using the DiFX software correlator for geodetic VLBI. Submitted to Journal of Geodesy. 2009.

e-VLBI and Other Developments at the EVN MkIV Data Processor at JIVE

R.M. Campbell, A. Szomoru
Joint Institute for VLBI in Europe, Oude Hoogeveensedijk 4, 7991 PD Dwingeloo, the Netherlands

Abstract. We review the capabilities of the European VLBI Network (EVN) Mark IV Data Processor at JIVE, briefly touching new features (recirculation) and on operations for EVN/global (astronomical) observations. The greatest strides in the past two years have come in the development of an operational real-time e-VLBI facility, increasing both the reliably sustainable data rates and the number as well as the geographical distribution of participating telescopes. The e-EVN has now observed 49 proposal-driven real-time science experiments, including 11 target-of-opportunity observations. The grid-based software correlator that forms part of the e-VLBI development is currently used operationally for processing the ftp fringe-tests in EVN sessions, and has now correlated meaningfully large data-sets in the course of validation.

Keywords. VLBI, e-VLBI, correlation

1 Current Capabilities

The EVN Mark IV Data Processor can correlate simultaneously up to 16 stations with 16 channels per station, each having a maximum sampling rate of 32 Msamples/s, for a maximum of 1024 Mbps per station with 2-bit recordings. We can currently correlate/provide: (*i*) Mark 5A or Mark 5B recordings (5B playback via 5A+); (*ii*) 1- and 2-bit sampling (possible to include stations using either within a given correlation); *iii*) full Stokes polarization output; *iv*) up to 2048 frequency points per baseline/subband/polarization, *cf.* equation 1; (*v*) full-correlator integration times down to 0.25 s; (*vi*) oversampling at 2 or 4 times the Nyquist frequency, in order to provide subband bandwidths down to 500 kHz; (*vii*) real-time e-VLBI operation; and (*viii*) multi-pass correlation for disk-recorded experiments, *e.g.,* for observations requiring enhanced spectral-resolution per subband, or those having >16 stations at any given time. Development of "native" Mark 5B playback is well underway.

The total correlator capacity can be expressed:

$$N_{\rm sta}^2 \cdot N_{\rm sb} \cdot N_{\rm pol} \cdot N_{\rm frq} \leq 131072 \cdot \mathcal{R}. \quad (1)$$

Here, $N_{\rm frq}$ is the number of frequency points per baseline/subband/polarization. $N_{\rm pol}$ is the number of polarizations in the correlation (1, 2, or 4), and $N_{\rm sb}$ is the number of distinct subbands, counting lower- and upper-sidebands from the same VC as distinct subbands. The value to use for $N_{\rm sta}$ is "granular" in multiples of 4 (*e.g.*, if you have 5–8 stations, use 8). The recirculation factor $\mathcal{R}$ is discussed in the next paragraph. Independent of equation 1, the maximum number of input channels ($N_{\rm sb} \cdot N_{\rm pol_\parallel}$) is 16, and the maximum $N_{\rm frq}$ is 2048 (a single interferometer must fit onto a single correlator board). Table 1 shows some configurations that would require the full correlatory. You can evaluate whether your experiment adheres to equation 1 interactively with the EVN calculator (via the Users' Guide on the EVN web site `www.evlbi.org`).

Recirculation time-shares correlator chips in the case that the observations don't require the correlator to operate at its maximum rate (*i.e.*, < 32 Msamples/s). This effectively increases the correlator capacity for such experiments: more lags can be processed in what otherwise would have been idle correlator-chip cycles. Recirculation would increase the right-hand side of equation 1 by a factor $\mathcal{R} = 16\,{\rm MHz}/BW_{\rm sb}$ (for Nyquist sampling), up to $\mathcal{R}_{\rm max} = 8$. However, the maximum $N_{\rm frq}$ would remain 2048, as discussed above. The principal beneficiaries of recirculation would be experiments observing below 1024 Mbps whose spectral resolution

Table 1. Examples of "maximal" correlator configurations (without recirculation).

$N_{\rm sta}$	$N_{\rm sb}$	$N_{\rm pol}$	$N_{\rm frq}$	comment
8	**1**	**1**	**2048**	EVN spectral-line
8	1	4	512	with cross-pols
9	1	1	512	gaining a $9^{\rm th}$ sta
16	**8**	**4**	**16**	Global with cross-pols
16	2	2	128	re-arranging N's
8	16	2	64	How $N_{\rm sta}$ increase can
12	7	2	64	be absorbed by $N_{\rm sb}$
16	4	2	64	(not necessarily 2^n)

would be limited by $N_{\rm sta}$ or $N_{\rm pol}$ — the EVN now has reliably > 8 stations able to observe OH- or methanol-maser emission, and interest in full-Stokes mapping of these masers is growing. Some experiments may prefer 16 MHz subbands at lower data rates (*e.g.*, extragalactic HI absorption); these would not be able to gain from recirculation.

The minimum $t_{\rm int}$ for a configuration that uses the whole correlator is 1/4 s, and some configurations that use $\leq$1/2 of the correlator can achieve $t_{\rm int} = 1/8$ s. With recirculation, the minimum $t_{\rm int}$ would be increased by a factor of $\mathcal{R}$ from its nominal value. Short integration times coupled with the spectral resolution afforded by large $N_{\rm frq}$ allow wider-field mapping via reduced bandwidth- and time-smearing in the u-v plane. The EVN calculator evaluates field-of-view limitations due to each of these smearing effects.

The standard distribution product comprises IDI FITS files (typically for further analysis in AIPS). One potential drawback to wide-field correlations (with their short $t_{\rm int}$ and large $N_{\rm frq}$) is the rapid growth of the size of the set of FITS files — reaching about 7–10 GB per correlator pass per hour of observation at our current maximum output rate. The current record for the total size of output FITS files for a single experiment stands at 1028.7 GB.

2 Operations and Data Flow

We man the correlator 80 hours per week. The reliability of the system is such that a few hours of successful output can run unattended after the end of the evening shift in necessary. The Science Operations & Support Group at JIVE provides assistance for all phases as a user's experiment — from proposing/scheduling, through correlation and review of the raw output, to analysis of the resulting FITS data. Refer to the contributions in the most recent EVN symposium (Campbell, 2009) for further details related to the pre-observation/pre-correlation steps, the post-correlation data review process, the operation and content of the EVN pipeline, and the population and use of the EVN Data Archive.

Since the previous EVGA working meeting, the new Yebes 40m antenna has begun its participation in EVN observations at K-, S/X-, and C-bands. The three KVASAR stations also participated in EVN observations for the first time in the Oct/Nov 2008 session in a series of experiments at S/X-, C-, and L-bands. Testing with the Irbene (Latvia) 32m telescope continues.

3 Real-time e-VLBI in the EVN

Real-time e-VLBI has become a proposal-driven operational mode within the EVN, with support over the past three years from the EXPReS project (`www.expres-eu.org`), funded by the EC (DG-INFSO). Technical advances in the networks, stations, and correlator have enabled routine sustained 512 Mbps observations, with some stations able to provide 1024 Mbps. Szomoru (2009) discusses specifics of the European and global connections, as well as correlator and Mark5 software modifications arising in the course of the EXPReS project. Below, we summarize important milestones over the past two years, and provide an overview of the proposal-driven science.

3.1 e-VLBI Technical Developments

At the time of the $18^{\rm th}$ EVGA Working Meeting, we had already established a 6-station e-EVN array (JbCmWbOnMcTr) running at 256 Mbps, which had observed 11 user experiments. By June 2007, we had four hours of 512 Mbps from all six stations, and all e-EVN observations have been made at $\geq$512 Mbps beginning from April 2008. Initial efforts towards accommodating 1024 Mbps observing modes, which do not fit through single Gbps fibre links, focused on packet dropping. By the end of January 2008, we could sustain 978 Mbps for over 3 hours on a 3-station array (Mc,On,Tr) by dropping packets such that all track-frame headers remained intact. However, there was no synchronization among the stations in terms of the packet drop-

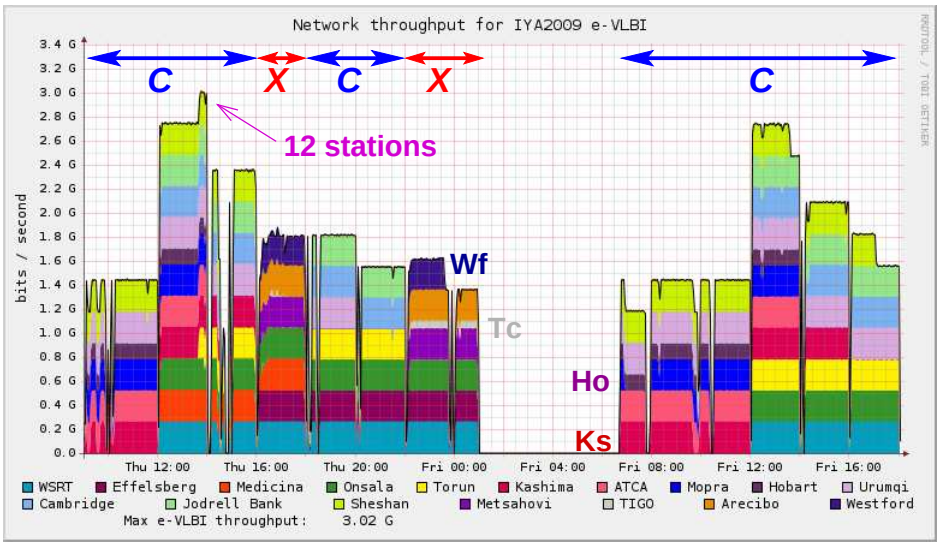

Figure 1. e-VLBI throughput into JIVE for the International Year of Astronomy Opening Ceremony, 15–16 January 2009.

ping, so effective net baseline data rates were lower. The goal in this regard remains targeting a common VEX-channel for all stations via packet dropping, leaving the other 15 entirely unaffected. In the meantime, some stations have increased their connections to 10 Gbps or have obtained a second 1 Gbps connection (we can attain 1024 Mbps in the latter case through ethernet bonding, akin to fan-out at the packet level). We had our first 1024 Mbps e-VLBI correlation without any packet dropping to three stations in November 2008, and the first such data rates in an e-EVN science observation in March 2009. Our current system can incorporate stations with different data rates in in a single correlation by providing a non-correlating fill pattern in the "unused" channels of the slower stations.

A weakness of the original e-EVN array was a lack of sensitivity. Besides the increase in the available data rate, inclusion of additional large antennas helps in this regard. The 100-m telescope at Effelsberg participated in user experiments starting in May 2008, which in itself doubled the sensitivity of the e-EVN array. Arecibo also joined the e-EVN in February 2008, limited to 128 Mbps; from September 2008, it could attain 512 Mbps in the (local) early-morning hours. For sources within its declination range, having Ar could further triple the array sensitivity and provide ∼6000 km baselines. Sheshan began regular participation in user experiments in November 2008, providing ∼8000 km baselines. The new Yebes 40m telescope adds sensitivity and u-v coverage for the higher e-EVN frequencies up to K-band.

In the late summer of 2007, we began conducting various tests involving intercontinental data transmission. During the 24$^{\text{th}}$ APAN conference in August 2007, we obtained real-time fringes on Sh–Mopra and Sh–Western-European baselines at 256 Mbps, with the data from Sh routed overland via Siberia. We also had about 10 minutes of fringes on the Mopra–Darnhall baseline (NSW, Australia to Cheshire, UK) — at 12304 km, this remains our longest real-time e-baseline to date. In October 2007, we sustained real-time fringes at 512 Mbps for over 12 hr from the wholly Australian network Parkes–Mopra–ATCA, with data arriving at JIVE along three dedicated light-paths running across the Pacific, Canada, and the Atlantic. In May 2008, we had real-time fringes on Hartebeesthoek–Arecibo and Hh–TIGO baselines at 64 and 32 Mbps, and later in the month at the Bruges TERENA Networking conference, fringes again from TIGO (including the 10840 km On–Tc baseline). The early winter 2008–9 saw a great deal of activity preparing for the International Year of Astronomy Opening Ceremony, at which we held e-VLBI demonstrations over two successive days, involving 17 stations (figures 1,2), and setting a record for the most stations simultaneously in a real-time correlation (12). In the course of preparing for and running these demonstrations,

Figure 2. Telescopes in the International Year of Astronomy Opening Ceremony, 15–16 January 2009.

we had our first real-time fringes to Urumqi, Kashima, Hobart, and Westford.

The possibility of including a second MERLIN out-station in the EVN correlation exists for recording modes that leave "unused" subbands in the Cambridge recording (*e.g.*, dual-pol, $\geq$256 Mbps), without modification to the PI's schedule. This can be processed in real-time correlation through multi-casting techniques in the JIVE switch/router, in which the incoming Cambridge signal is also routed to a second Mark5 for processing the additional "embedded" outstation. We can also use this e-VLBI technique for disk-based experiments by using two additional Mark5 units to simulate the e-VLBI transfer into the switch, in this case originating from the recorded Cambridge pack. This avoids the disk-pack copying used previously.

3.2 Real-time e-EVN Astronomy

The EVN has offered proposal-driven real-time e-VLBI observations since 2006. There have been 49 successful observations, including two planned epochs through 4 July 2009 of a target-of-opportunity (ToO) project already begun. These projects represent 21 different PIs. Thirty-eight observations have taken place since the previous EVGA working meeting (and 11 of these in the nine weeks since the "current" EVGA working meeting), including 11 ToO's and 4 triggered observations (see below).

The key distinction of a real-time e-EVN experiment is the extremely reduced latency in receiving correlation results — we can provide final FITS files within a day of the end of observations (work continues with the stations to accelerate the availability of $T_{\rm sys}$ and gain-curve information for calibration). For sources that vary on short time-scales — flaring X-ray binaries, gamma-ray bursts and other transients, just-exploded supernovae — such short-latency high-resolution VLBI results can be vital to adapting observing tactics based on the source's behavior. The increased sampling density compared to the usual thrice-annual EVN sessions also provides the potential for better monitoring of kinematics or population changes.

e-EVN observing sessions are currently scheduled for 24 hr on pre-arranged dates, about once per month. There have been a few paired dates 2–3 days apart to permit following source changes on shorter time-scales. Proposals for e-EVN observations are now submitted in the same fashion as are other EVN/global proposals at the thrice-annual deadlines, and compete for the available time with their peers based on the grades of the EVN programme committee. A new class of "triggered" proposal enables e-EVN observations of a pre-selected source when

its behavior prior to an e-EVN session shows that it has entered an interesting state. Once such a triggered proposals has been accepted, the proposing group only needs to submit a short trigger request up to 24 hr before the start of an e-EVN session to be considered for observation in that session. As always, target-of-opportunity proposals may be submitted at any time following the usual EVN procedures. The development of the high-sensitivity real-time e-EVN network seems to have spurred interest in such ToO's, to judge from their increasing frequency. The most recently observed ToO (23 June 2009) was the first e-EVN user experiment to incorporate Australian stations in its array.

4 Software Correlation at JIVE

We have been inserting ftp scans into the standard Network Monitoring Experiments during EVN sessions for some time. An automatic-ftp feature added to the Field System has been exercised since the November 2006 EVN sessions. This automatically copies a specified portion of a scan from the Mark 5 disk to a linux file and ftp's it directly to the cluster at JIVE, where the arrival of new data is detected, correlation performed, and results posted to a web page available to the stations. The ftp fringe tests themselves have been very successful in identifying problems early enough to allow stations to repair them before user experiments would have been affected.

We now process the ftp fringe tests on the software correlator we are developing as part of the EXPReS joint research activity "FABRIC" and a related project "SCARIe" funded by the Dutch national science agency. These address workflow management and correlation algorithms that can be applied to a real-time GRID-based correlator. A workflow manager application prototype, to route data to cluster computers such that the network keeps up with the incoming data, has been developed at Poznań Supercomputing and Networking Center. Thus, we can correlate data sitting on a RAID array at JIVE on a cluster in Poznań, in a fully automated fashion. We are adapting the correlator algorithms developed for observing the descent of the Huygens probe onto Titan (Pogrebenko et al., 2003) to wide-field applications. The resulting software XF correlator (SFXC) has handled the EVN ftp fringe tests since June 2007. We continue to add features with an eye towards this operational use, such as the ability to decode VLBA or Mark5B data and to correlate of 1- and 2-bit sampled data (from different stations) together at the same time.

A great deal of effort goes into optimizing the SFXC correlator. We have identified and fixed bottlenecks in the data flow, and more thorough analysis of the algorithm identified opportunities for speed-up. We wrote software to exploit fuseMk5A software from Metsähovi to stream data directly from disk packs into the correlator. Correlation of a data-set comprising 2 hours to 10 stations at 256 Mbps (four 4 MHz subbands), with cross-pols and $N_{\rm frq}$=32 now takes a couple days on a small 6-node cluster. To speed things up further, we are investigating the use of graphical processor units (GPUs) for correlation, and in a separate larger-scale larger-scale thrust in SCARIe, running on a 60-node cluster in the university of Amsterdam. We have performed some inter-correlator comparisons using the above data-set; phase agreement is quite good, and we are investigating the remaining small amplitude differences.

Acknowledgements The European VLBI Network is a joint facility of European, Chinese, South African, and other radio astronomy institutes funded by their national research councils. EXPReS is an integrated infrastructure initiative (I3) funded under the European Community's Sixth Framework Programme (FP6), contract number 026642. EVN observation of some of the user experiments mentioned herin was supported under the RadioNet programmes funded by the European Community's FP6 (RadioNet R113CT 2003 5058187) or FP7 (Advanced Radio Astronomy in Europe, 227290).

References

Campbell R.M., 2009, Recent Results from the EVN Mk IV Data Processor at JIVE, In: 9th EVN Symposium Proceedings, PoS(IX EVN Symposium)42, `pos.sissa.it/cgi-bin/reader/conf.cgi?confid=72`

Pogrebenko, S.V., L.I. Gurvits, R.M. Campbell, I.M. Avruch, J.-P. LeBreton, & C.G.M. van't Klooster, 2003, VLBI Tracking of the Huygens Probe in the Atmosphere of Titan, In: Proc. of Planetary Probe Atmospheric Entry and Descent Trajectory Analysis & Science, eds. D. Atkinson & A. Suleman, C-4.6

Szomoru A., 2009, EXPReS and the e-EVN, In: 9th EVN Symposium Proceedings, PoS(IX EVN Symposium)040, `pos.sissa.it/cgi-bin/reader/conf.cgi?confid=72`

Current status of Chinese VLBI network software correlator

Zheng Weimin, Shu Fengchun, Luo Wuchao, Yu Yun, Wang Weihua
Shanghai Astronomical Observatory, Chinese Academy of Sciences
80, Nandan Road Shanghai, 200030, P. R. China

Abstract. The Chinese VLBI network (CVN) was used to support tracking of CE-1, the first Chinese lunar probe. As the main data processor of CVN, the software correlator based on commercial PC servers had supported CE-1 more than one year. During this period, besides the routine VLBI data process task, this correlator completed some special data correlation tasks such as the orbit maneuver and the moon impact mission, because of its flexibility and reliability. The researches on the new 10-station, high speed software correlator cluster prototype were carried out to meet the CVN astronomical and geodetic requirements in the near future.

Keywords. Software correlator, VLBI, high performance computation, deep-space exploration, spacecraft tracking

1 Introduction

The Chinese VLBI network (CVN) consists of four stations (Shanghai, Yunnan, Urumchi, Beijing) and one data process center in the Shanghai Astronomical Observatory (SHAO), Shanghai, China. As the main data processor of CVN, the CVN software correlator is situated SHAO and operated by SHAO. This correlator was specially designed for CVN to support the Chinese first lunar exploration project (CE-1; Zheng et al. 2008).

CE-1 lunar probe was successfully launched at 18:05 (CST)on October 24, 2007 in the Chinese Xichang space center and impacted the moon on March 1, 2009. From October 27, 2007, CVN began to carry out the 2-stage tracking mission.

The first stage was a near real-time critical flying mission, from October 25 to November 30, 2007. In this period, CVN worked in the near real-time mode. And the data from the four stations were sent to the VLBI data center by network directly. The observation mode was 4-channel (2 S-band and 2 X-band channels) with the data rate of 16 Mbps/station. The tracking interval was 15 hours/day. At this stage, the software correlator completed the entire data processing task and the total data latency of CVN was less than 5 minutes.

The second stage was the long-term in-orbit operation mission, form November 30, 2007 to March 1, 2009. In general, CVN worked in the no-real-time mode during this period. The data were first recorded on the Mark5A hard disks, then sent to the data center by express mail. The data rate expanded to 64–128 Mbps/station to increase the precision. The tracking interval was 2 days/week. All the data sent to the center must be processed in 2 weeks. But some times, especially at the end of the second stage, when there were orbit maneuver and the moon impact experiments, CVN turned into the near real-time mode. Besides the routine VLBI data process task, the software correlator completed all the data correlation of these special experiments.

Besides the deep space exploration activities, considering the astronomical and geodetic requirements of CVN in the near future, researches on the new 10-station, high speed software correlator cluster prototype has been carried out.

2 Software correlator for CVN

2.1 Specification

The software correlator for CVN is a program running on the prevailing commercial Symmetrical Multi-Processing (SMP) PC servers. It has good portability. The former hardware platform was HP ProLiant dl585, contained 8 CPU cores and the current one (DELL PowerEdge R900)

Table 1. Specifications of the NRSC.

Architecture	FX
Station number	1∼10
IF number	1–16
Frequency channel	32∼65536/IF
Integration period	0.1∼60 seconds
Input data format	Mark5A,B
Output data format	CVN
Fringe search	2–4 stations
Speed (4 stations,2-bit)	>128 Mbps/station
Data turnover	< 3 minutes
PCAL detection	Yes

contains 16 CPU cores, or four Intel Xeon Processors (E7430, 4 Core 2.13 GHz). This correlator has the functions of near real-time correlation, fast fringe search and PCAL detection abilities (Table 1). The correlator data latency is less than 3 minutes.

The software correlator consists of the correlation module, the data preprocess module, the satellite fringe search and the PCAL abstraction module.

The software correlation module is the kernel. A harddisk array is used as the data buffer to prevent data lost in case of network congestion in the near real time mode. The data preprocess program running on the harddisk array receives data from the station MARK5 terminals firstly. After performing decoding, error correcting and synchronizing, it stores the data into a batch of standard Linux files with one minute length on the disk array. Therefore the output format is also one minute based not scan based. Other modules can access the data through the Network File System (NFS).

The satellite fringe search module is an indispensable part of the software correlator. When doing correlation, a VLBI correlator needs accurate object delay models. It is no problem when the object is an extragalactic radio source. However, when tracking a spacecraft, sometimes the prior orbit is inaccurate. To solve this problem, the satellite fringe search module is integrated in the CVN correlator system. It is able to find the onsite accurate delay and delay rate of the spacecraft automatically and reconstructing an accurate delay model for the correlation module. This is very important in special situations such as the orbit maneuver and the moon impact period. The more significant error of the orbit, the more remarkable effect will be.

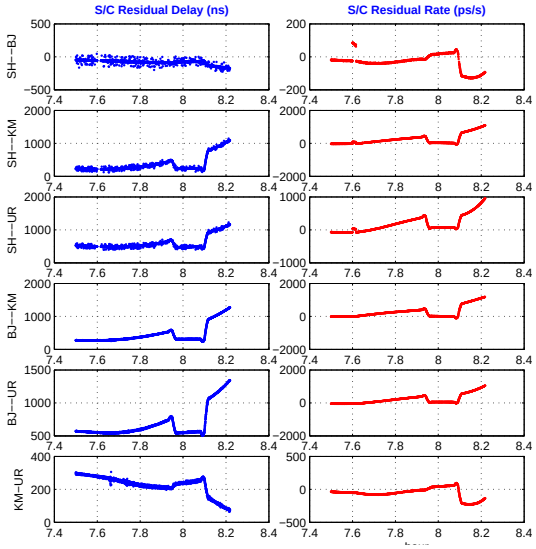

Figure 1. Delay/delay rate O-C value procedure.

2.2 Applications

Although for reliability, there are two correlators at the VLBI data center, a hardware one and a software one, the software correlator has played an irreplaceable role in the CE-1 mission. In the critical flying mission, there were 36 observations (336.55 hours). All of them were processed by the software correlator. In the long-term in-orbit operation mission, there were totally 120 observations (607.39 hours), and 434.02 hours of them were processed by the software correlator. Especially in the case of several real-time CE-1 maneuver tracking observations, only did the software correlator produce the correct results.

On March 1, 2009, CE-1 impacted on the moon surface. CVN traced the whole procedure. The last orbit control began at 7:36 (UTC), ended at 7:56. At 8:13:06, CE-1 probe hit the lunar surface at 1.64 degrees south latitude and 52.27 degrees east longitude. Fig. 1 shows the delay/delay rate O-C value of the moon impact; and the largest delay rate is up to 1600 ps/s. The unit of the horizontal abscissa is hour (UTC). This kind of data would not be correlated correctly without the fringe search module. Before the impact, there were two orbit maneuvers; the software correlator processed all the data.

Besides, the software correlator also correlated

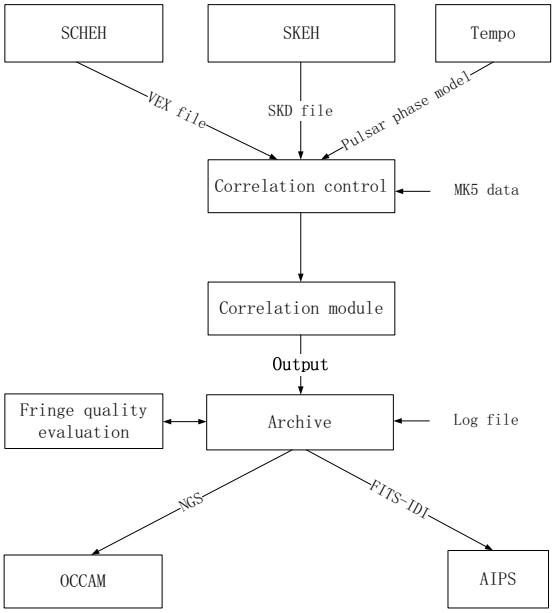

Figure 2. Structure of new CVN software correlator.

other observation data (70 hours), such as station position experiments.

More than one year's operation of CE-1 mission indicates that the software correlator is reliable, flexible, and easy to operate, as well as low-cost and high performance.

3 Current activities

After the CE-1 mission, CVN will spend more time for astronomical and geodetic observations. Nevertheless, because the software correlator of CE-1 works in a special one-minute based mode (not scan based), it does not fit the astronomical observations. On the other hand, there will be several new telescopes to join the CVN in the near future. It is apparent, that CVN need a new and powerful correlator. This correlator will deal with 10-station observations and the correlation speed is up to 512 Mbps/station. For these reason we carried out research on a 10-station software correlator prototype, which adapts Message Passing Interface (MPI) and POSIX threads. Fig. 3 indicates that this prototype correlator is actually the first Chinese Giga bit VLBI correlator (in two station situation).

On January 6, 2009, on the baseline of Shanghai-Urumqi, this prototype correlator conducted the first CVN 2-station high speed e-

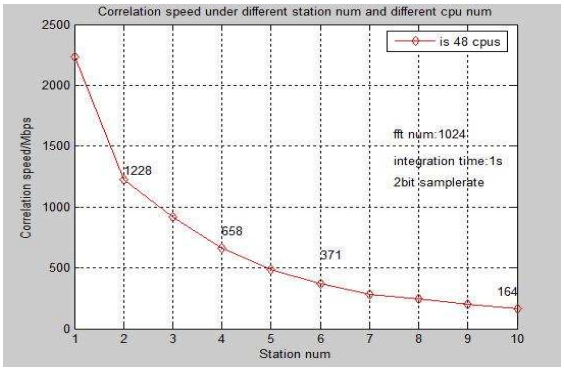

Figure 3. Speed of the prototype correlator.

VLBI (256 Mbps/station) experiment. Fig. 3 shows the speed of this prototype correlator, while the hardware platform is a small computer cluster with 3 PC servers (DELL PowerEdge R900).

Acknowledgements This work is supported by the National Natural Science Foundation of China General Program (No. 10878021) and the state 863 High Tech R&D program (2008AA12A209).

References

Zheng Weimin, Luo Wuchao, "CVN Software Correlator Development and Applications in Chinese Lunar Exploration Mission", In: Mearing the future, Proceedings of the fifth IVS gereral meeting, Nauka, 124-128, 2008

Shanghai correlation system upgrade for geodetic application

Fengchun Shu, Weimin Zheng, Xiuzhong Zhang, Zhijun Xu, Weihua Wang, Zhong Chen
Shanghai Astronomical Observatory, Chinese Academy of Sciences, Shanghai 200030, China

Abstract. Under the framework of the project Crustal Movement Observation Network of China (CMONC), 3 VLBI stations located at Shanghai, Urumqi and Kunming are defined as the fiducial stations which co-located with GPS and SLR techniques. In order to support Chinese domestic stand-alone geodetic observations with those VLBI stations, an upgrade to the correlator which was originally designed for the tracking of Chang'E-1 lunar satellite has been carried out since last year. The ongoing upgrade plan, which mainly covers the modification of correlator control system for compatibility of geodetic observing mode, the development of new software regarding format conversion and observable extraction, the implementation of MK5B playback capability, is presented in detail. Its current status and future prospect for space geodesy are also summarized.

Keywords. VLBI, cross correlation, space geodesy, terrestrial reference frames

1 Introduction

Very Long Baseline Interferometry (VLBI) is an unique and fundamental space geodetic technique which will continue to improve its product quality to meet future service requirements (Niell et al., 2006; Schlüter et al., 2007). It also has been a long effort to develop VLBI technique in China (Ye et al., 1991). Chinese VLBI Network (CVN) program was proposed as early as in the late of 1970's and always guided by Prof. Shuhua Ye. With the support of Chinese Academy of Sciences, Shanghai and Urumqi VLBI stations inaugurated in 1987 and in 1994 respectively, with each of them equipped with a 25-meter diameter radio telescope. They both are IVS (International VLBI Service for Geodesy and Astrometry) network stations, participating regularly in IVS observations. Meanwhile, SHAO (Shanghai Astronomical Observatory) is an IVS data analysis center.

In order to support the orbit measurement and scientific data downlink of Chang'E-1 lunar satellite, Beijing 50-meter telescope and Kunming 40-meter telescope were constructed in 2006, and a data processing center located in Shanghai was set up at almost the same time. As a result, CVN was enlarged with inclusion of Beijing and Kunming stations and enhanced with capability of real time tracking of near-Earth space satellites. Incorporated with the unified S-band Telemetry Tracking and Command (TT&C) system, the VLBI tracking system has been successfully applied for the tracking of the earth satellite Tance-1, the lunar satellite Smart-1 and Chang'E-1. However, such a VLBI tracking system is not fully compatible with geodetic VLBI observations due to its original design for satellite tracking.

Under the framework of the National Key Scientific Infrastructure Project Crustal Movement Observation Network of China (CMONC), the CVN upgrade plan was proposed in 2006 and approved in 2007, which purpose is to provide the primary fiducial points by performing geodetic VLBI observations monthly with independent network based on CVN. The ongoing upgrade plan, which mainly covers the modification of correlator control system for compatibility of geodetic observation mode, the development of new software regarding format conversion and observable extraction, the implementation of MK5B playback capability, is presented in detail. Its current status and future prospect for space geodesy are also summarized. The full functional geodetic VLBI observing system will be completed and put into operation at the end of 2010.

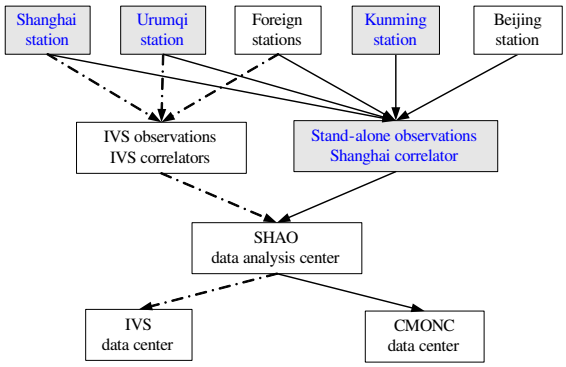

Figure 1. Block diagram of Chinese geodetic VLBI observing system with its components in grey background.

2 Overview of upgrade plan

The goal of the whole upgrade plan is to develop a full functional geodetic VLBI observing system in China, which can be operated in the stand-alone mode depending on the domestic VLBI stations and the data processing system. By performing regular geodetic VLBI observations, we will eventually precisely determine the position and velocity of stations, as well as EOP and radio sources parameters, so far contributing to the realization and maintenance of a more stable and more accurate terrestrial reference frame in Chinese mainland region or further in global scale.

Chinese geodetic VLBI observing system will include Shanghai, Urumqi, Kunming stations and Shanghai correlator system. Unfortunately, Beijing station is not included in the framework of CMONC, but its participation in the Chinese geodetic VLBI observing system is preferred. Fig. 1 shows the block diagram of Chinese geodetic VLBI observing system with its components in grey background. Shanghai and Urumqi stations participate in IVS observations routinely and send the raw data to the IVS correlators for data correlation, while the data collected in the stand alone observations will be sent to shanghai correlator to produce delay observables. SHAO data analysis center is committed to provide station coordinates and other products then place them in CMONC data center in regular intervals for dissemination to researchers and other users.

3 Shanghai correlation system

We have developed a hardware correlator and a software correlator as the main components of the VLBI tracking system of Chang'E-1 project. The hardware correlator is a 5-station FX-type correlator based on FPGA technology with a maximum data processing rate of 256 Mbps per station. The software correlator, implemented by software programs on the general commercial computers and flexible in station numbers and frequency channels, is a FX-type correlator with a maximum data rate of 80 Mbps per station for 4 stations data correlation (Zheng et al., 2007). Both correlators have special functions of multi-tone PCALs extraction and automated fringe search of satellite telemetry signals. They also can be operated in the real time mode with high speed communication networks connected to 4 Chinese VLBI stations. In 2007, the 2 correlators have been undergoing strict engineering test, and working smoothly and successfully in the test satellite tracking experiments and Chang'E-1 lunar satellite real time tracking.

In order to support domestic stand-alone geodetic observations with Chinese VLBI stations, an upgrade to the Shanghai correlator which was originally designed for the tracking of Chang'E-1 lunar satellite has been carried out since last year. The ongoing upgrade plan, which mainly covers the modification of correlator control system for compatibility of geodetic observing mode, the development of new software regarding format conversion and observable extraction, the implementation of MK5B playback capability.

The new correlator is mainly used for geodetic and astronomical application, so it will adopt a new hardware platform, but share the Mark5B data playback system with the existing satellites VLBI tracking system when the station number is greater than 5. Fig. 2 shows the hardware platform of Shanghai correlation system, which mainly includes 5 units of Mark5B data playback system, a cluster cross-correlation device linked with high-capacity disk array, an observable extraction computer, a scheduling computer, a database server and a web server.

The cross-correlation device decodes the data come from the Mark5 system, performs PCALs extraction, delay compensation, phase rotation and cross correlation. The raw output data are then in the process of data flag, fringe fit, phase

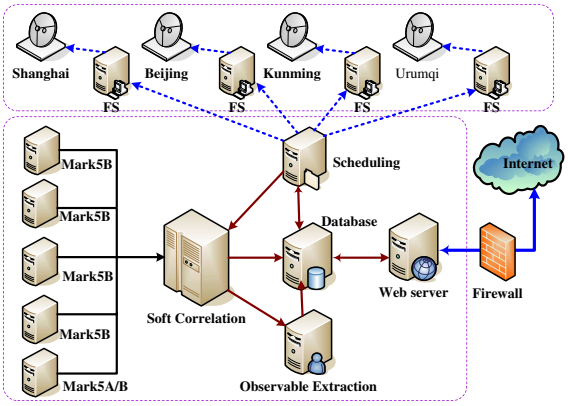

Figure 2. Hardware platform of Shanghai correlation system, with its relationship to Chinese VLBI stations.

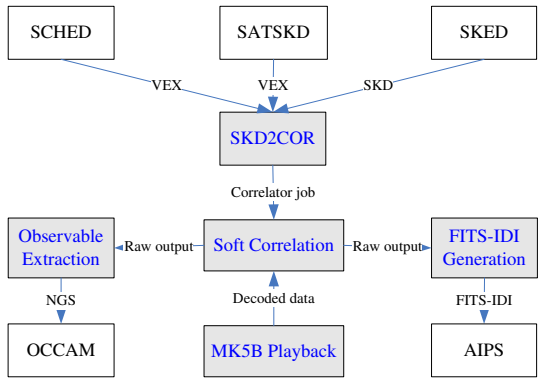

Figure 3. Software architecture of Shanghai correlation system with its components in grey background.

calibration and bandwidth synthesis for producing delay observables. Fig. 3 shows the software architecture of Shanghai correlation system. There are 5 relatively independent software modules. The SKD2COR module provides a unified interface to the correlation system for 3 different scheduling software programs (Shu et al., 2008). The FITS-IDI generation module performing data format conversion is under test now, in order that correlation output data can be read into AIPS software for astronomical application. The data playback module is being enhanced to be compatible with Mark5B data. The observable extraction module for geodetic application is also under development now.

3.1 Correlator control system

There are some drawbacks for geodetic application of the existing correlator system. One is the correlator can only handle with the scans which start at integer minute mark and last for integer minutes. In this case, the VLBI raw data and the final results after cross-correlation are all divided into segments of data with one minute long. There is a small gap between 2 consecutive minutes. The other is sub-arraying method is frequently used in geodetic VLBI schedule, but only VEX format schedule can be processed in domestic VLBI observations. Considering the software correlator is much more flexible in control logic than the hardware correlator, we have started the modification of the software correlator control system.

In the last year, the SKD2COR module has been enhanced with geodetic VLBI schedule processing capability. It also output a revised format of correlator job file with scan-based models other than one-minute based models. The control logic of the correlation module was also modified to be able to read new correlator jobs and process the data scan by scan. Thus the sub-arraying configuration is avoided and the correlator output a scan of the data continuously. This work is undergoing some tests and will be completed soon. However, the hardware correlator which processes the data of all stations simultaneously cannot operate in such a way, so its upgrade plan for geodesy is pending now.

3.2 Delay observables extraction

After the correlator producing the cross-correlation results, the observable extraction module will generate a delay observables file for geodetic VLBI data analysis software OCCAM. We hope that FITS-IDI generation module plus AIPS software can work together for generation of geodetic MK3 database used by CALC/SOLVE, but it is not guaranteed in our upgrade plan. It is also very interesting to learn the development of the new geodetic VLBI data format (Gipson, 2008; Hobiger et al., 2008). Currently we just have similar software for satellite VLBI tracking with limited functions. Compared to satellite VLBI, geodetic VLBI has additional requirements on this post-correlation software. For example, geodetic VLBI requires S/X dual band observations to calibrate iono-

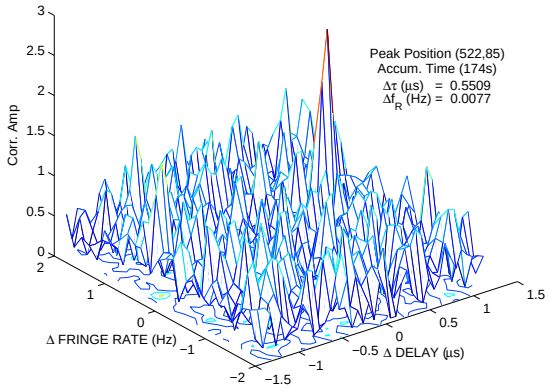

Figure 4. Cross correlation function of the source 1417+385 on the baseline Shanghai-Urumqi, with a bandwidth of 8 MHz and an integration time of 174 s.

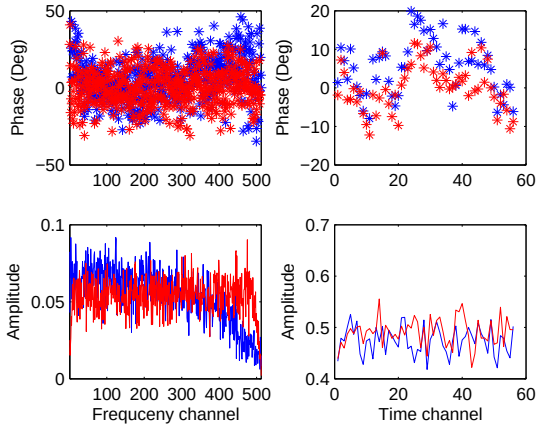

Figure 5. Cross spectrum of radio source 3C454.3 on the baseline Shanghai-Urumqi, with a bandwidth of 8 MHz and an integration time of 60 s. The blue line is analog BBC plus Mark5A data, while the red line is digital BBC plus Mark5B data. For the purpose of comparison, the delay, rate and phase residuals have been removed.

spheric effects, multi-channel per band observations for bandwidth synthesis, weak fringe detection, longer integration time for improving precision of delay observable and standard output format to be compatible with data analysis software.

Based on the experiences we obtained on satellite VLBI, we are beginning the development of the observables extraction software, including the basic functions of fringe search, phase calibration, bandwidth synthesis and observables generation. We expect the first version will be finished at the middle of 2010 for the test operation of Chinese geodetic VLBI observations.

The fringe detection of weak source with longer integration time was demonstrated using the data received by Shanghai and Urumqi stations on Jan. 22, 2009. Fig. 4 shows the cross correlation function of the radio source 1417+385 on the 2 dimensional delay and fringe rate plane with an integration time of 174 s. The fringe is almost invisible for the 60 s integration time previously adopted.

3.3 MK5B playback capability

For the Chinese VLBI network, currently there is an analog BBC with 14 channels installed at Shanghai and Urumqi stations respectively, while there is an analog BBC with 8 channels for Beijing and Kunming stations respectively. The signals from BBC are formatted by Mark4 formatter and recorded by MK5A data recording system. In the near future the analog BBC for those stations will be replaced by the digital BBC with 16 channels developed by SHAO (Zhang et al., 2008). The new digital BBC which is full compatible with traditional analog BBC had been installed in the VLBI station and under test now. It has a VSI output interface connecting with MK5B data recording system developed by Haystack Observatory (Whitney, 2007). We expect all Chinese stations will be transferred to adopt MK5B data system from the next year.

In the upgrade plan, Shanghai correlator will be equipped with 5 MK5B data system to process the data from 5 stations simultaneously. The data playback module is being modified to decode the VSI data. Currently only 4 bit-stream and 8 bit-stream data are tested.

Fig. 5 shows the phase and amplitude of cross spectrum of the radio source 3C454.3 on frequency and time domain respectively after removal of delay, rate and phase residuals. The experiment was performed with Shanghai and Urumqi stations on Feb.22, 2009. The correlator processed analog BBC plus Mark5A data labeled with blue color, and also digital BBC plus Mark5B data labeled with red color. They agree with each other, indicating Mark5B data decoding function is going well.

4 Conclusions

Chinese VLBI Network upgrade plan for geodesy and its current progress towards an operational geodetic VLBI observing system are described. The main task of the plan is to upgrade the correlation system which was originally designed for the tracking of Chang'E-1 lunar satellite. The upgrade plan has been carried out since last year. It is expected to be completed at the end of 2010 and put into operation for the geodetic application of Chinese VLBI stations.

Chinese geodetic VLBI observing system will conduct regular observations. Besides Shanghai and Urumqi stations participating in about 10 times 24-hour conventional IVS observations every year, an independent network based on domestic stations will participate in the standalone observations monthly. The correlation system is compatible with MK4 formatted MK5A data and MK5B VSI format data. The maximum station number for data correlation is 10. BBC channel number is 8 for the use of analog BBC and up to 16 for the use of digital BBC. The typical delay observable precision is about 50 ps. It will contribute to the realization and maintenance of a more stable and more accurate terrestrial reference frame in Chinese mainland region or further in global scale, and support the future deep space exploration projects of China.

Acknowledgements This work is carried out in the framework of the National Key Scientific Infrastructure Project Crustal Movement Observation Network of China, and supported by the Science & Technology Commission of Shanghai Municipality (06DZ22101).

References

Gipson J., 2008, IVS Working Group 4 on VLBI Data Structures, in IVS 2008 General Meeting, edited by Andrey Finkelstein and Dirk Behrend, pp. 143-152

Hobiger T., Koyama Y., Kondo T., 2008, MK3TOOLSCSeamless Interfaces for the Creation of VLBI Databases from Post-Correlation Output, in IVS 2008 General Meeting, edited by Andrey Finkelstein and Dirk Behrend, pp. 153-156

Niell A.E., Whitney A., Petrachenko B. et al., 2006, VLBI2010: Current and Future Requirements for Geodetic VLBI Systems, 2005 IVS Annual Report, pp. 13-40

Schlüter W., Behrend D., 2007, The International VLBI Service for Geodesy and Astrometry (IVS): current capabilities and future prospects, J Geod, Vol. 81, Nos. 6-8, pp. 379-387, June 2007

Shu F.C., Zhang X.Z., Kondo T., 2008, Development of correlator model for differential VLBI observations of satellites2008 International Conference on Microwave and Millimeter Wave Technology, ICMMT2008 Proceedings, Vol.1, p443-446, IEEE Computer Society

Whitney A., 2007, Haystack Observatory Technology Development Center, in International VLBI Service for Geodesy and Astrometry 2006 Annual Report, edited by D. Behrend and K. Baver, NASA/TP-2007-214151, 2007

Ye S.H., Wan T.S., Qian Z.H., 1991, Progress on Chinese VLBI network project, IN: Radio interferometry: Theory, techniques, and applications: Proceedings of the 131st IAU Colloquium, Socorro, NM, Oct. 8-12, 1990 (A92-56376 24-89). San Francisco, CA, Astronomical Society of the Pacific, p. 386-389

Zhang X. Z., Wei W. R., Xiang Y. et al., 2008, Progress of wideband VLBI digital system development in SHAO, in IVS 2008 General Meeting, edited by Andrey Finkelstein and Dirk Behrend, pp. 381-385

Zheng W.M., Shu F.C., Zhang D., 2007, CVN software correlator applications in deep-space exploration, in Second International Conference on Space Information Technology, edited by Cheng Wang, Shan Zhong, Jiaolong Wei, Proceedings of SPIE Vol. 6795 (SPIE, Bellingham, WA, 2007) 6795-4N

Geodetic research at IRA-INAF: recent results between a golden past and a gloomy future

M. Negusini, P. Sarti, C. Abbondanza,
Istituto di Radioastronomia (IRA)- Istituto Nazionale di Astrofisica (INAF), Via P. Gobetti, 101 40129 Bologna, Italy

Abstract. Medicina (Northern Italy) and Noto (Sicily) 32 m, AZ-EL, VLBI radio telescopes are managed by the Institute of Radioastronomy and funded by the National Institute of Astrophysics. They have been successfully performing geodetic observations since the end of the 80s. Nowadays, geodetic research is no longer an IRA institutional research activity. The finalization of the 64 m Sardinia Radio Telescope is foreseen for the second half of 2010 and, in INAF's perspectives, it will replace the two older VLBI antennas. Unfortunately, it is not meant to operate at S/X geodetic frequencies. If, on the operational side, the Italian observing activity in geodetic VLBI will shortly experience a dramatic cut (the two 32 m antennas will most probably be dismissed by the end of 2011), on the research side, IRA geodetic activity is quickly coming to an end. We focus here on the role of the two telescopes during these two decades: their importance in the Mediterranean region and within the International VLBI geodetic network. We review the most important activities carried out so far and present the most recent solutions obtained with CALC/SOLVE regarding crustal deformation.

Keywords. VLBI, Radio telescope, Medicina, Noto, SRT

1 Introduction

The Italian Consiglio Nazionale delle Ricerche (CNR) started the Italian VLBI project in mid 1970s, appointing its branch Istituto di Radioastronomia (IRA) to design a national VLBI network by planning the construction of three identical VLBI radio telescopes in different parts of Italy. The main purpose was to develop radioastronomic as well as geodetic research ensuring, at the same time, an extension of the geodetic VLBI network for geodynamics applications in the Mediterranean region. A lack of available funding led to a major reconsideration of the project: it was eventually modified withdrawing the construction of the radio telescope in Sardinia.

Medicina and Noto radio telescopes were regularly built and completed during the 80s. The first geodetic observation took place in January 1987 in Medicina (Tomasi et al., 1988) while Noto's geodetic observations began in June 1989 (Tomasi, 1993). Ever since, both telescopes have actively participated in the observations of the international VLBI network; in particular, the geodetic activities are nowadays coordinated by the International VLBI Service (see Schlueter and Behrend 2007), which has been greatly contributing in widely and uniformly promoting the scientific as well as the technological development of VLBI technique.

In the early 90s the Italian VLBI increased its potential when a geodetic 22 m VLBI telescope started its operation in Matera. Furthermore, in the same decade, the construction of the Sardinia radio Telescope (SRT) was reconsidered (Setti, 2006). By the end of 1997 IRA submitted to the Ministry of Research a first detailed executive program that was accepted, in its definitive form, only a couple of years later, in May 1999. SRT is designed as an Azimuth-Elevation (AZ-EL) 64 m dish whose technical characteristics can be found in Olmi and Grueff (2006); it should be completed and operative in the second half of 2010. Up to 2004, the Noto and Medicina observatories were funded by CNR for the specific purpose of performing astronomic and geodetic research. In 2005, after a re-organization of the Italian public research system, IRA was joined to INAF, an institution that unifies the astronomical observa-

tories locally distributed on the Italian territory and three former CNR Institutes. INAF's aims and scopes are strictly related to astronomic research and, as a result, geodetic research is considered out of the institutional activity. This statement was explicitly made by INAF's President T. Maccacaro in October 2008. Despite the efforts made in recent years, we are now facing a gloomy future for the geodetic research within IRA and a total lack of perspective. If, as a matter of fact, geodetic activities have been officially dismissed without a serious process of evaluation of the opportunities offered by the Italian geodetic VLBI infrastructure within the national and the international contexts, on the other hand, the minutes of the latest meetings of INAF's Scientific Committee depict a very uncertain future for the astronomical use of the two telescopes, too. Their operability will be reconsidered once SRT will be fully functional and it is widely agreed that SRT should replace the two VLBI telescopes within the observing activity of the astronomical VLBI networks.

2 IRA's contribution to geodetic research

Medicina and Noto telescopes are twin AZ-EL mount 32 m dish with non intersecting axis (the Medicina VLBI telescope is shown in Figure 1); according to the project's design, the offset between the fixed azimuth axis and the moving elevation axis is $O = 1.829$ m.

Since the beginning of their observing history, the two telescopes have performed both astronomic and geodetic observations. VLBI and single dish astronomic observations represent the larger amount of observing time for both telescopes. Medicina telescope participated in more than 360 geodetic experiments in the time span 1987–2008, thus performing observations in more than 16 VLBI geodetic sessions per year. The number of geodetic experiments performed at Noto observatory is lower: in the two decades 1989–2008 the telescope took part in 180 sessions, thus performing, on the average, 9 sessions per year.

The frequency operability spans the range 1.4–22 GHz for Medicina telescope and 0.3–43 GHz for Noto telescope. The two telescopes perform observations with receivers located in primary or Cassegrain focus. Insights on technical characteristics of the two telescopes can be found on the web page of IRA (`www.ira.inaf.it`). The primary reflectors are made by 240 aluminum panels supported by a reticular structure (see Figure 1). In order to counter the effect of gravity, Noto telescope's was upgraded with an active surface in 2001 (Orfei et al., 2004). The panels that form the primary reflector can be moved through electromechanical actuators. Each panel moves according to an elevation dependent correction model: values are listed in a file and represent the translations that must be applied to the panels for restoring the ideal parabolic shape of the primary mirror. A detailed survey of the primary reflectors of the two telescopes was performed in September 2005 using a laser scanner. The effect of gravity on the parabolic mirror was determined at six pointing elevations and the entire surface was scanned and was represented by point clouds containing more than 1.5 million points. A comprehensive discussion concerning the set up of the survey, the measuring approach and the collection of observations, data processing, data post processing, results and outcomes are reported in detail in Sarti et al. (2009).

Figure 1. The Medicina (Bologna) VLBI telescope: an AZ-EL 32 m steerable antenna mount whose twin telescope is located in Noto (Siracusa). In the foreground of the picture the IGS GPS antenna co-located with the VLBI telescope is visible.

Investigations on the effects of deformations

on the travelling time of signals in the near-field of the Medicina radio telescope have been gathered by studies of different components being affected by changes in gravitation. A combination of terrestrial triangulation and trilateration, laser scanner and FEM analysis was applied in order to derive an elevation-dependent correction model for the signal path traveled by the incoming radio signal. Results are summarized in a paper by Sarti et al. (submitted) recently submitted to Journal of Geodesy and currently under review.

Both telescopes have a remarkable series of tie vector's surveys. Particularly, Medicina telescope was surveyed six times with terrestrial methods (2001, 2002, 2003, 2005, 2006 and 2007) and three times with GPS technique (2000, 2003, 2006) for the purpose of estimating the tie vector between the co-located VLBI and GPS reference points. With the same purpose, Noto telescope was surveyed in 2003 and 2005 with terrestrial methods and 2003 and 2006 with GPS technique. The surveying method is based on an indirect approach (Sarti and Angermann, 2005) that combines observations acquired on targets mounted on the telescope's structure and performed rotating the antenna in elevation and azimuth (Sarti et al., 2004).

The effects generated by the introduction in the ITRF-like computation of the redundant determinations of the Medicina tie vector were tested by (Abbondanza et al., in press) using CATREF (see Altamimi et al. 2002). The residuals originated by the combination of space geodetic solutions and both terrestrial- and GPS-derived tie vectors were evaluated and used to assess the consistency of each tie vector's realization and to determine their agreement with the space geodetic observations. These residuals are potentially capable of highlighting biases that might be related to the performance of each co-located space geodetic instrument. If, on one hand, the residuals simply highlight a disagreement for a specific co-location site, on the other hand, they are the starting point for a rigorous investigation on the wide variety of causes that might originate from technique specific problems. It should be noticed that the whole process of combination of frames is characterized by the unavoidable complication of reliably coupling measurements of different nature (space geodetic and terrestrial) related to different reference points (electronic and conventional points).

IRA participated in the IVS Pilot Project on Tropospheric Parameters estimated with VLBI since its very beginning. The initial phase started in July 2002 with a regular submission of wet and total zenith delays and horizontal gradients for all IVS-R1 and IVS-R4 sessions. The solutions produced by different Analysis Centers were checked and combined together in order to identify the best analysis and combination strategy. As this phase ended, there was the transition from Pilot Project to IVS Tropospheric Products (TROP) thus ensuring a regular provision of IVS official products. Because of the importance of long time series of data and in particular of water vapour content, we estimated and submitted to the combination center long-term tropospheric parameters analyzing all the available VLBI experiments in our catalogue (see Heinkelmann et al. 2007).

3 IRA's latest solution on crust deformation in the Mediterranean

As stated in Sect. 1, investigations of crust deformation by means of VLBI technique comprised a fundamental scientific motivation towards the development of the Italian VLBI infrastructure. In the 70s, VLBI was the most promising technique for monitoring global geodetic parameters. NASA's Crustal Dynamic Project (CDP) represented the first coordinated international effort aimed at *(i)* determining the motions of the major tectonic plates, *(ii)* understanding and measuring crustal kinematic and dynamics, *(iii)* relating crustal motion with earthquakes and active fault monitoring, *(iv)* detecting and understanding the possible relations between Earth Orientation Parameters (EOP) and geodynamics and geophysical phenomena. To this respect, up to the end of the 90s, IRA has regularly produced crustal deformation solutions with VLBI technique, with a particular emphasis on the deformation patterns regarding the Mediterranean area (see Tomasi et al. 1999).

The most recent solution performed at IRA comprises all the VLBI session stored at IRA from 1987 up to 2008. The velocity estimates for the three Italian VLBI sites are given in Table 1.

The dataset is formed by more than 1000 geodetic experiments that were analyzed with CALC/SOLVE Mark-5 software. Figure (2) shows the vectors representing the estimated vertical velocities computed for the European sites.

Table 1. Estimates of *(i)* Up component of the local velocity, *(ii)* global horizontal velocity (ITRF2005), *(iii)* horizontal velocity relative to Wettzell, whose values where fixed to those of ITRF2005 and *(iv)* azimuth of the vector representing the relative horizontal velocity.

	Medicina	**Noto**	**Matera**
Vertical velocity (mm/yr)	-2.3 ± 0.1	-1.2 ± 0.1	-0.3 ± 0.1
Absolute horizontal velocity (mm/yr)	28.1 ± 0.1	28.7 ± 0.1	29.8 ± 0.1
Relative horizontal velocity (mm/yr)	3.2 ± 0.1	4.4 ± 0.1	5.0 ± 0.1
Azimuth rel. hor. vel. (deg)	47 ± 1	22 ± 2	45 ± 4

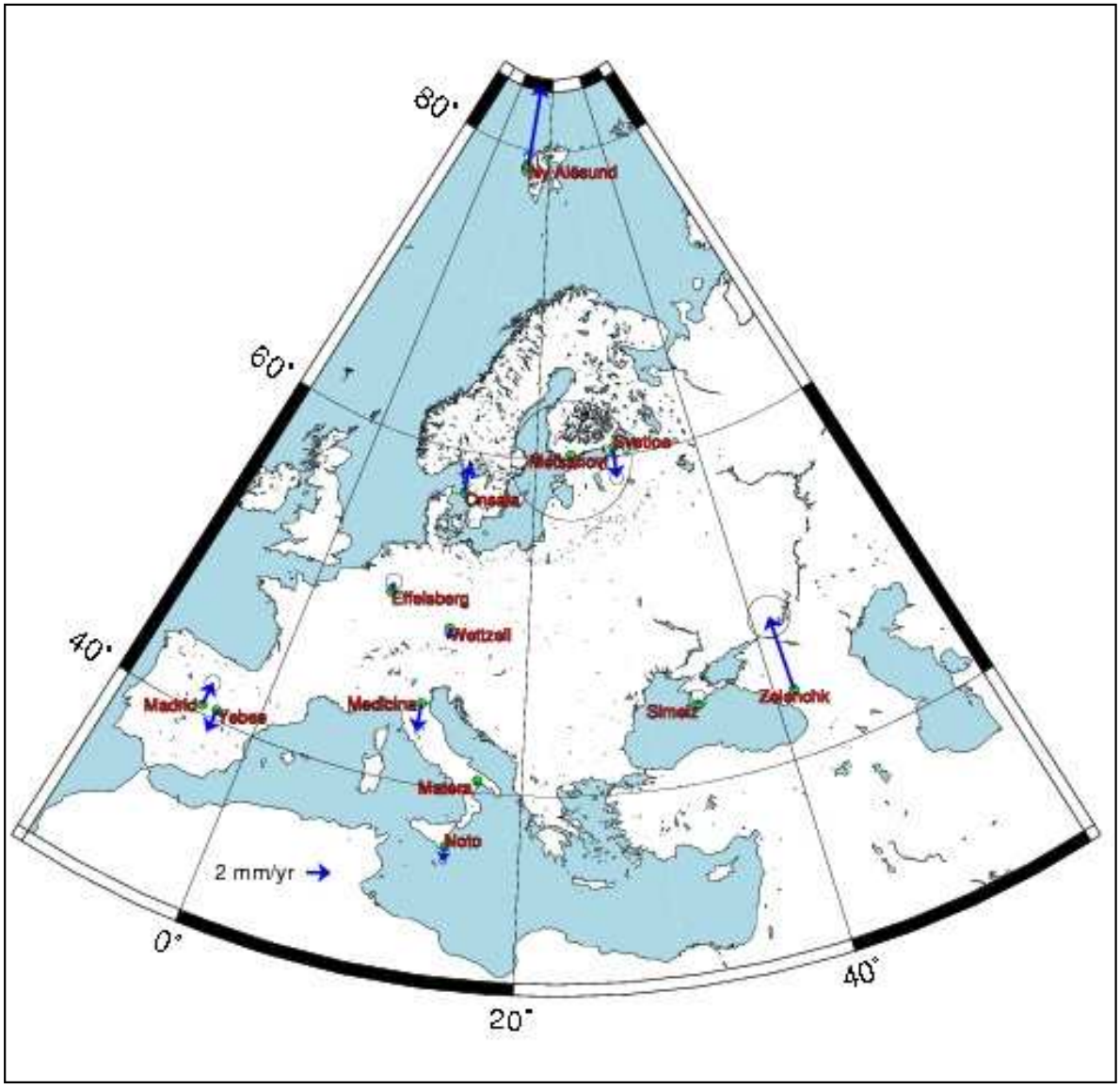

Figure 2. Representation of the Up component of the velocities for the European VLBI stations.

4 Conclusions

This paper briefly summarizes the present day situation of geodetic research at IRA and very shortly resumes its highlights and achievements. Since it was moved from CNR to INAF, IRA geodetic activity suffered from a sudden decay and is now facing a total lack of perspectives. The threat of an end in the operation of the two main Italian radioastronomical sites represent a miserable eventuality not only for geodesy and astronomy. The evolution of our planet is strictly connected to reliable long time series of records: they are fundamental in depicting and understanding complex phenomena which, to a varying extent, combine and contribute to the evolution of our planet Earth. In this respect, the sites of Medicina and Noto have accurately observed for more than two decades phenomena such as e.g. the evolution of the crust kinematic, the rotation of the Earth and its response to global phenomena, the presence and variability of water vapour in the atmosphere and have greatly contributed in boosting technological development as well as accuracy in the estimate of geodetic parameters.

References

Abbondanza C, Altamimi Z, Sarti P, Negusini M, Vittuari L (in press) Local effects of redundant terrestrial and GPS-based tie vectors in ITRF-like combinations. J Geod

Altamimi Z, Sillard P, Boucher C (2002) ITRF2000: A new release of the International Terrestrial Reference Frame for Earth science applications. J Geophys Res 107:B10, 2114–2133

Heinkelmann R, Boehm J, Schuh H, Bolotin S, Engelhardt G, MacMillan D, Negusini M, Skurikhina E, Tesmer V, Titov O (2007) Combination of long time series of troposphere zenith delays observed by vlbi. J Geod 81(6-8):483–501

Olmi L, Grueff G (2006) SRT: design and technical specifications. In: Brand J, Mack KH, Prandoni I (eds) Mem. S.A.It. Suppl., vol 10, pp 19–24

Orfei A, Morsiani M, Zacchiroli G, Maccaferri G, Roda J, Fiocchi F (2004) An active surface for large reflector antennas. IEEE Antennas and Propagation Magazine 46(4):11–19

Sarti P, Angermann D (2005) Terrestrial Data Analysis and SINEX Generation . IERS Tech Note 33:118–127

Sarti P, Sillard P, Vittuari L (2004) Surveying colocated space geodetic instruments for ITRF computation. J Geod 78(3):210–222

Sarti P, Vittuari L, Abbondanza C (2009) Laser scanner and terrestrial surveying applied to gravitational deformation monitoring of large VLBI telescopes' primary reflector. J Surv Eng http://dx.doi.org/10.1061/(ASCE)SU.1943-5428.0000008

Sarti P, Abbondanza C, Vittuari L (submitted) Gravity dependent signal path variation in a large VLBI telescope modelled with a combination of surveying methods. J Geod

Schlueter W, Behrend D (2007) The international vlbi service for geodesy and astrometry (ivs): current capabilities and future prospects. J Geod 81(6-8):379–387

Setti G (2006) Synthetic history of the SRT project. In: Brand J, Mack KH, Prandoni I (eds) Mem. S.A.It. Suppl., vol 10, pp 15–18

Tomasi P (1993) Noto station status report. In: Campbell J, Nothnagel A (eds) Proc. IX Working Meeting European VLBI for Geodesy and Astrometry, vol 81, pp 11–12, Bonn, Germany, September 30-October 1, 1993

Tomasi P, Mantovani F, Ambrosini R, Bombonati A, Grueff G, Nothnagel A, Schuh A (1988) The first geodetic VLBI experiment with the Bologna radio telescope. Il Nuovo Cimento 11(2):205–208, DOI: 10.1007/BF02561732

Tomasi P, Rioja MJ, Sarti P (1999) The European VLBI Network activity in geodesy: crustal deformation in Europe. New A R 43(8-10):603–607, DOI: 10.1016/S1387-6473(99)00062-7

The 2008 Local-tie Survey at the Onsala Space Observatory

M. Lösler,
Geodetic Institute of the University of Karlsruhe (TH),
DE-76128 Karlsruhe, Germany

R. Haas
Department of Radio and Space Science, Chalmers University of Technology,
Onsala Space Observatory, SE-439 92 Onsala, Sweden

Abstract. We describe an innovative approach to perform a local-tie survey at a fundamental geodetic station. The work was performed in September 2008 at the Onsala Space Observatory and used a laser tracker as survey instrument. Both the reference point of the radio telescope used for geodetic VLBI and the local tie between the latter and the reference point for GNSS measurements were determined. The application of the laser tracker allowed fast survey work and resulted in accurate coordinates with complete covariance information in a local true cartesian coordinate system. This project is highly relevant for the Global Geodetic Observing System (GGOS).

Keywords. Reference point, local-tie, VLBI, GNSS, GGOS, laser tracker

1 Introduction

The Global Geodetic Observing System (GGOS) of the International Association for Geodesy (IAG) aims at a combination and integration of observations and results of the various geodetic techniques in order to support the monitoring of the Earth system and global change research (Rummel et al., 2005). Fundamental geodetic stations that host co-located equipment for different geodetic space techniques, e.g. Very Long Baseline Interferometry (VLBI) and Global Navigation Satellite Systems (GNSS), play a key role for the GGOS. A meaningful combination and integration can only be achieved if the local-ties at these fundamental stations are know accurately. The local-ties are the coordinate differences between the reference points of the geodetic space techniques. The requirements for the reference points are that they are known with an accuracy of better than 1 mm (Niell et al., 2006) and that the full covariance information is available. For the GGOS even a continuous terrestrial monitoring of the local-ties at an accuracy of 0.1 mm is desirable (Plag and Pearlman, 2008).

Usually, local-tie surveys at fundamental stations are performed every couple of years. One of the main reasons for this low repeat frequency is that the local-tie survey work usually is a difficult and time consuming engineering task. Furthermore, did survey work often also mean a considerable downtime for the geodetic space techniques, which is undesirable of course. Traditionally is the local-tie survey often a mixture of direction and distance measurements with tachymeters and height differences from levelling work. Often the local-tie information is incomplete, i.e. the covariance matrix is not complete.

The increased requirements on local-tie information call for new strategies and approaches. In this work we describe an innovative and promising new approach that makes use of a laser tracker as the survey instrument.

2 Laser tracker measurements

Laser trackers instruments are widely used for high accuracy survey work in industry. They can be operated both in absolute and interferometric mode and require retro reflectors, e.g. corner cube reflectors, to reflect the laser beam.

For our project we used an instrument of type Leica LTD840. According to Leica is the 2σ absolute coordinate accuracy that is achievable with this instrument on the order of ± 10 ppm for distances up to 35 m. This includes both the uncertainty of the angular measurements (2 axis) and the absolute (or interferometric) distance measurements. The instrument has a rotating head that emits and receives a laser beam. Its rotation around two perpendicular axes is re-

Figure 1. The laser tracker in its standard operation mode where the tracker head can move ±235° in azimuth and ±45° in elevation.

stricted to ±235° and ±45° and usually the instrument is used with an orientation so that these axes are the primary and secondary axis, respectively (see Fig. 1). However, it is neither possible nor necessary to orient the instrument with one axis parallel to the local plumb line. The instrument's orientation is always derived with transformations based on overdetermined measurements in a network.

3 Determination of the VLBI reference point

The 20m radio telescope at the Onsala Space Observatory is of azimuth-elevation type and is enclosed by a protective radome that prevents any direct observation of the telescope structure from the outside. The telescope reference point does not exist as a material point and is the intersection of the right-angle projection from the elevation-axis onto the azimuth-axis. Neither of the two axes can be observed directly. However, it is possible to mount targets on the telescope structure, in particular on the elevation cabin that is movable both in azimuth and elevation.

The particular situation at Onsala complicates any survey work for reference point determination. A local network of geodetic markers exists outside the radome. Through windows and doors in the radome building this outer geodetic network can be connected to three markers in the concrete floor of the radome building. The three markers are placed symmetrically around the telescope tower and can be connected to five survey pillars that are located on the radome foundation. The radome foundation is a ca. 3 m heigh concrete wall with diameter of about 18 m and surrounds the telescope tower in about 7 m distance to it. The telescope elevation axis is at about 14 m height with respect to the floor of the radome building. Further details on the network of markers and pillars inside the radome building and the outside network of ground markers are described by Haas and Eschelbach (2005).

Due to the geometrical situation it was not possible to use the laser tracker in its standard operation mode (secondary axis with ±45° opening angle) from any point in the radome building to observe any target close to the elevation axis. We therefore constructed an adapter to mount the instrument horizontally on the survey pillars on the radome wall (see Fig. 2), so that the telescope elevation cabin could easily be reached with the laser beam due to the ±235° opening angle of the primary axis. In this orientation the laser beam could also reach targets on at least three other survey pillars on the radome wall and targets on all three ground markers in the radome floor, due to the ±45° opening angle of the secondary axis.

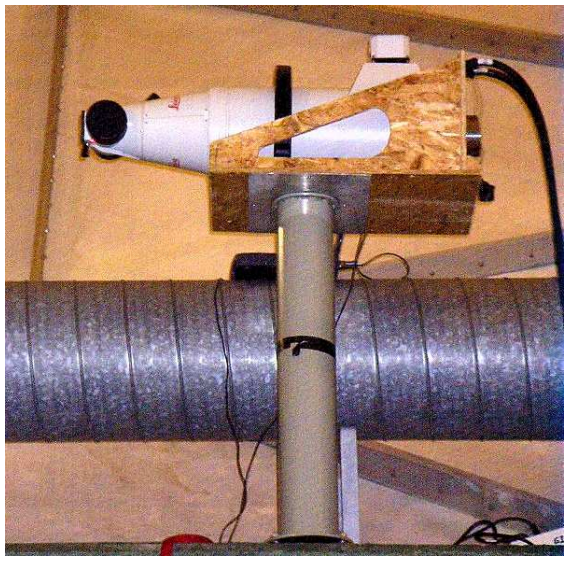

Figure 2. Laser tracker on a survey pillar on the radome wall. The tracker head can now move ±235° in elevation and ±45° in azimuth and thus targets close to the telescope elevation axis can be reached.

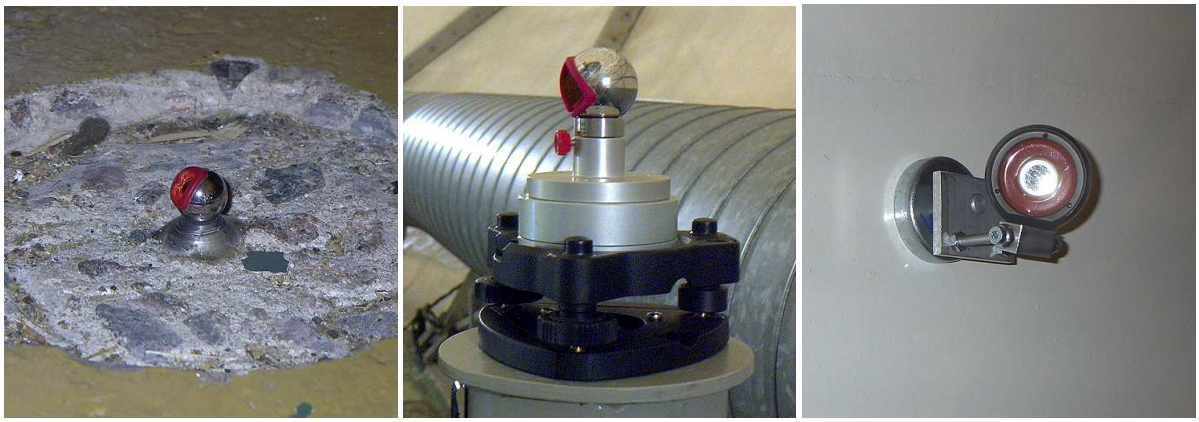

Figure 3. Three different types of retro reflectors used for the survey work: Left: 0.5" CCR used on ground markers; Middle: 1.5" CCR used on the survey pillars; Right: CER used on the telescope elevation cabin.

Three different types of retro reflector were used for the survey work (see Fig. 3). On the ground markers we used 0.5" corner cube reflectors (CCRs), on the survey pillars 1.5" CCRs, and on the telescope elevation cabin cat eye reflectors (CETs). The latter were mounted with magnets and have an opening angle of 60°, while the CCRs have an opening angle of only 30°.

Measurements were performed from each point of the small network inside the radome building to all other visible points in this network. Two CETs were attached with magnets on each side of the telescope elevation cabin symmetrically at about 1 m distance from the elevation axis. They were observed from each survey pillar at different azimuth and elevation positions of the telescope. A series of tracker measurements was performed in each azimuth position while running the telescope up and down in elevation. Two measurement campaigns were observed with the CETs mounted in two different constellations on the elevation cabin. In total the telescope was positioned in 10 different azimuth positions and in 18 different elevation positions per azimuth position, resulting in 720 coordinated points (Lösler, 2009a).

During the laser tracker measurements the tilt of the instrument was monitored by a levelling device Nivel210. A long-term monitoring of the instrument tilt over 48 hours revealed that the survey pillars were slightly tilting with time when the laser tracker was mounted. However, since the actual tracker measurements did not take more time than about 30 minutes per standpoint, were the tilt changes during this short measurement period negligible. Short term tilt changes due to the movement of the laser head were also detectable, but small in magnitude and negligible, too. Further details on the survey work are given in e.g. Lösler (2009a) and Lösler and Eschelbach (2009).

The analysis of the data was done with two different approaches, performing a one-step analysis with an advanced model (Lösler and Hennes, 2008; Lösler, 2009b), and performing a two-step analysis with constrained circle-fitting (Eschelbach and Haas, 2003). Besides the actual coordinates of the telescope reference point, also the offset between the azimuth and elevation axis and axis tilt parameters were part of the model. The results of the two different approaches agree very well, better than 0.05 mm for the three coordinate components and the axis offset. The advanced one-step analysis has the big advantage that the whole covariance information is available while the two-step circle-fitting approach applies a reduced stochastic model and neglects correlations between various parameters.

4 Local-tie determination

To determine the local-tie between the VLBI and GNSS reference points, additionally a traverse was measured. The network inside the radome building could be connected to the outside network of ground markers by observations through windows in the radome building. Due to dry weather conditions the laser tracker could be used out-doors (see Fig. 4). For the traverse, small tripods equipped with 1.5" CCRs were placed on the bed rock (see Fig. 5), and a 0.5" CCR could be placed directly on the refer-

Figure 4. The laser tracker outdoors during the measurement of the traverse between the radio telescope enclosed by the white radome in the background and the GNSS monument in the foreground.

Figure 5. A small tripod equipped with a 1.5" CCR, placed on the bedrock for the traverse measurements.

ence point of the GNSS monument (see Fig. 6).

The advanced analysis model (Lösler and Hennes, 2008) was extended to allow a one-step network analysis that included both the VLBI and GNSS reference points. The analysis gave results in a local true cartesian system since the laser tracker was not oriented with respect to the local plumb line.

The results for the coordinates of the VLBI and GNSS reference points in the local cartesian

Figure 6. The 0.5" CCR on the reference point of the GNSS monument.

Table 1. Coordinates of the VLBI and GNSS reference points and their standard deviations in the local true cartesian coordinate system.

	X	Y	Z
VLBI	90.12325 m	35.94974 m	22.75947 m
	± 0.10 mm	± 0.10 mm	± 0.08 mm
GNSS	12.75551 m	23.39043 m	9.06529 m
	± 0.21 mm	± 0.25 mm	± 0.27 mm

coordinate system are given in Table 1 and the corresponding complete covariance information in Table 2.

A direct comparison with the results derived by Eschelbach and Haas (2003) is not possible on the level of coordinates, since the two local networks differ slightly from each other. However, coordinate system invariant results can be com-

Table 2. Fully populated covariance matrix for the VLBI and GNSS reference points in the local true cartesian system. The order of elements left to right and top to down is X_{VLBI}, Y_{VLBI}, Z_{VLBI} X_{GNSS}, Y_{GNSS}, Z_{GNSS}, and the units are 10^{-9} m^2.

10.34	1.73	1.53	−2.71	0.37	−0.44
	9.52	−0.79	0.17	−1.69	−3.34
		7.22	−0.35	1.12	5.85
			45.82	2.88	−12.96
				60.30	38.42
					72.97

Table 3. Distance d between the VLBI and GNSS reference points and axis offset e of the VLBI radio telescope for two epochs.

epoch	d (m)	e (mm)
2002	79.5685	−6.0
2008	79.5678	−6.2

pared. These are the distance d between the two reference points and the axis offset e of the radio telescope. Table 3 compares these two results for the two epochs. A statistical hypothesis test showed that no statistically significant deformation between the two epochs can be detected.

5 Conclusions and outlook

The 2008 local-tie survey at Onsala was very successful. From our experience we can draw important conclusions both for local-tie surveys at geodetic fundamental stations in general and the Onsala Space Observatory in particular.

The application of a laser tracker allows to derive the local-tie results in a local true cartesian system. Levelling observations are not necessary and the local-tie results are not influenced by the plumb line of the local gravity field. The local-tie results in the local true cartesian system can easily be related to a global cartesian system, e.g. the International Terrestrial Reference Frame (ITRF; Altamimi et al. 2007).

The use of a laser tracker provides highly accurate local-tie results on the sub-mm level.

Using a laser tracker allows fast survey work and short station downtime.

The advanced analysis approach (Lösler and Hennes, 2008) gives the complete covariance information that is required for the ITRF.

For the Onsala Space Observatory we can conclude that the local-tie between the VLBI and GNSS reference points is stable, comparing the 2002 and 2008 results. The local-tie information is now available with the complete covariance information required for ITRF combinations. We also could confirm the previously derived axes offset of 6 mm (Eschelbach and Haas, 2003; Haas and Eschelbach, 2005).

Acknowledgements Michael Lösler was supported by DFG-project `HE5213_2-1`. We thank Hexagon Metrology Nordic AB, Göteborg, for providing the laser tracker.

References

Altamimi Z., Collilieux X., Legrand J., Garayt B. & Boucher C. (2007) ITRF2005: A new release of the International Terrestrial Reference Frame based on time series of station positions and Earth Orientation Parameters. J. Geophys. Res., 112, B09401, doi:10.1029/2007JB004949

Eschelbach C. & Haas R. (2003). The IVS-Reference Point at Onsala – High End Solution for a Real 3D-Determination. In: Proc. 16th Working Meeting on European VLBI for Geodesy and Astrometry, edited by W. Schwegmann and V. Thorandt, Bundesamt für Kartographie und Geodäsie, Frankfurt/Leipzig, 109–118.

Haas R. & Eschelbach C. (2005). The 2002 Local Tie at the Onsala Space Observatory. In: Proc. IERS Workshop on site co-location, edited by B. Richter, W. Schwegmann and W.R. Dick, IERS Technical Note, **33**, Verlag des Bundesamts für Kartographie und Geodäsie, 55–63

Lösler M. & Hennes M. (2008). An innovative mathematical solution for a time-efficient IVS reference point determination. In: Proc. FIG2008 – Measuring the changes, `http://www.fig.net/commission6/lisbon_2008/papers/pas07/pas07_02_losler_mc029.pdf`

Lösler M. (2009a). Bestimmung des lokalen Verbindungsvektors zwischen IVS- und IGS-Referenzrahmen am Raumobservatorium Onsala (Schweden), Allgemeine Vermessungs-Nachrichten (in press)

Lösler M. (2009b) A new mathematical model for reference point determination of an azimuth-elevation type radio telescope. Journal of Surveying Engineering (in press)

Lösler M. & Eschelbach C. (2009) Evolution and obtained expertise in reference point determination at the GIK. Proc. 19th Working Meeting on European VLBI for Geodesy and Astrometry, Bordeaux, this issue

Niell A., Whitney A., Petrachenko B., Schlüter W., Vandenberg N., Hase H., Koyama Y., Ma C., Schuh H. & Tuccari G. (2006) VLBI2010: Current and Future Requirements for Geodetic VLBI Systems. in: IVS Annual Report 2005, edited by D. Behrend and K. Baver, NASA/TP-2006-214136, 13–40

Plag H.P. & Pearlman M. (2008) The Global Geodetic Observing System. Meeting the requirements of a global society on a changing planet in 2020. The reference document (v0.18beta)

Rummel R., Rothacher M. & Beutler G., 2005, Integrated Global Geodetic Observing System (IGGOS) – science rationale, J Geodyn, 40, 357–362

IVS' contribution to ITRF2008 - Status & Results

S. Böckmann, T.Artz, A. Nothnagel
Institute of Geodesy and Geoinformation, University Bonn, Nußallee 17, D-53115 Bonn, Germany

Abstract. In late 2008, the IERS ITRF product center issued a call for contributions to the next realisation of the ITRS, the ITRF2008. Until now (March 2009), four IVS Analysis Centres provided their solutions to the official IVS contribution to the ITRF2008. The input to the combination process are sets of datum-free normal equations in SINEX format containing coefficients for station positions and EOP. All contributions are completely reprocessed from 1979 till 2008 following homogeneous analysis options according to the IERS Conventions 2003 and VLBI-specific constants such as axis offsets and reference temperatures. In this paper, the status of the IVS' contribution to ITRF2008 is given and some preliminary results of the contributions are presented.

Keywords. Combination, reference frame, VLBI, station coordinates, Earth orientation

1 Introduction

Like for the last realisation of the International Terrestrial Reference System (ITRS), the ITRF2005, the combination of VLBI, GPS, SLR and DORIS observations is based on weekly or session-wise equation systems including station positions and daily Earth Orientation Parameters (EOPs) with their full variance-covariance information. This combination strategy allows for a rigorous combination of the TRF and EOP time series to improve the consistency and accuracy of the major IERS (International Earth Rotation and Reference System Service) products (Rothacher, 2003). For the ITRF2008 one input per technique was requested that should be the result of an intra-technique combination done by the corresponding services of the International Association of Geodesy (IAG), i.e. from the International VLBI Service for Geodesy and Astrometry (IVS), from the International GNSS Service (IGS), from the International Laser Ranging Service (ILRS) and from the International DORIS Service (IDS).

In case of IVS, different analysis centres (ACs) analyse geodetic VLBI observations with different software packages and provide their contributions as datum-free normal equation systems of each single VLBI observing session with a duration of 24 h in SINEX format. The VLBI combination of the individual contributions mainly consists of a stacking of the normal equation systems. Details of the combination are described in Vennebusch et al. (2007).

The intra-technique combination requires an assessment of the quality and consistency of the individual contributions used as input for the combined solution. Systematic differences have to be detected and removed before the combination. In the first part of this paper, we aim at assessing the agreement of the individual contributions at this stage and detecting possible systematic differences. In the second part, the quality of a preliminary IVS combined series is investigated by comparisons with ITRF2005.

2 Solution Setup

Generally, all ACs calculate their solution with models and strategies selected to the best of their knowledge. In case of the contribution to ITRF2008, requirements were set up by the IVS Analysis Coordinator for consistency reasons. The ACs have been asked to apply all models which are defined by the IERS Conventions 2003 (McCarthy and Petit, 2004), like the Solid Earth tide and the Pole tide model, or the thermal expansion model defined by the IVS Data Analysis Conventions (Nothnagel, 2008). Further-

more, the same ocean loading model (FES2004; Letellier 2004) and the same tropospheric mapping function (VMF1; Boehm et al. 2006) have been used by all contributing ACs. For consistency reasons with the contributions of other techniques no atmospheric pressure loading has been applied. Nevertheless, the contributions have several differences in their solution setup. The following list gives an overview over the remaining analyst's specific options:

- the outlier detection,
- the weighting of the observations,
- the temporal resolution of troposphere parameters and gradients,
- the handling of constraints for clock and troposphere parameters,
- the interpolation scheme to map daily a priori EOP values to the observation epoch,
- the a priori gradients,
- the estimation of baseline-dependent clocks
- the celestial reference frame

3 Results

Until March 15th 2009, four out of nine IVS ACs, namely BKG (Federal Agency for Cartography and Geodesy), DGFI (German Geodetic Research Institute), GSFC (Goddard Space Flight Center), and OPA (Paris Observatory), submitted their contributions to the IVS Analysis Coordinators' office. Altogether 4592 different VLBI sessions have been analysed by these 4 ACs. In the following, some preliminary results derived from these contributions are discussed. To get comparable results only those sessions are used in the comparisons which are analysed by all ACs.

3.1 Internal comparisons

For each contribution, station position time series, TRFs and long term EOP series are computed separately and compared to preliminary combined station position time series, a combined TRF and combined long term EOP series in order to detect remaining systematic differences.

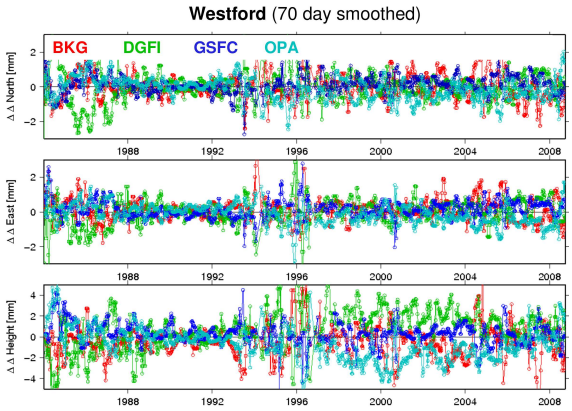

Figure 1. Differences of each individual solution w.r.t. the preliminary combined solution (smoothed with a 70-day median filter) for Westford.

Figure 1 displays the median smoothed station position differences between each individual series and the preliminary combined series for the station Westford between 1984 and 2008 exemplary. For the horizontal components the different solutions agree at the level of less than ±2 mm. However, it is immediately obvious that the level of scatter differ at certain periods of time. These variations coincide with changes in the network constellations. For example, since NyÅlesund started to participate in the observing network in 1993, the differences in the height components between the solutions reach up to ±4 mm.

An overview over the TRF heights of each individual solution with respect to the preliminary combined TRF at the epoch 2000 is given in Fig. 2. Generally, the internal agreement over all stations is in the range of 1 mm and 2 mm. Nevertheless, there are some stations with height offsets of more than 5 mm. It turned out that for most of these stations (Svetloe, Ohiggins, Medicina, NyÅlesund, Shanghai) the ACs used different antenna axis offsets in their analyses. Furthermore, there are two stations, HRAS at Fort Davis and 85-3 NRAO (Green Bank), which had observed many years ago. The extrapolation with the rate from the observation epoch to the epoch 2000 leads to bigger uncertainties of the height estimates. Comparing these results with the differences displayed in Fig. 1 for the Westford height component, it can be assumed that the bigger differences since 1993 are related to the different antenna axis offsets used for NyÅlesund.

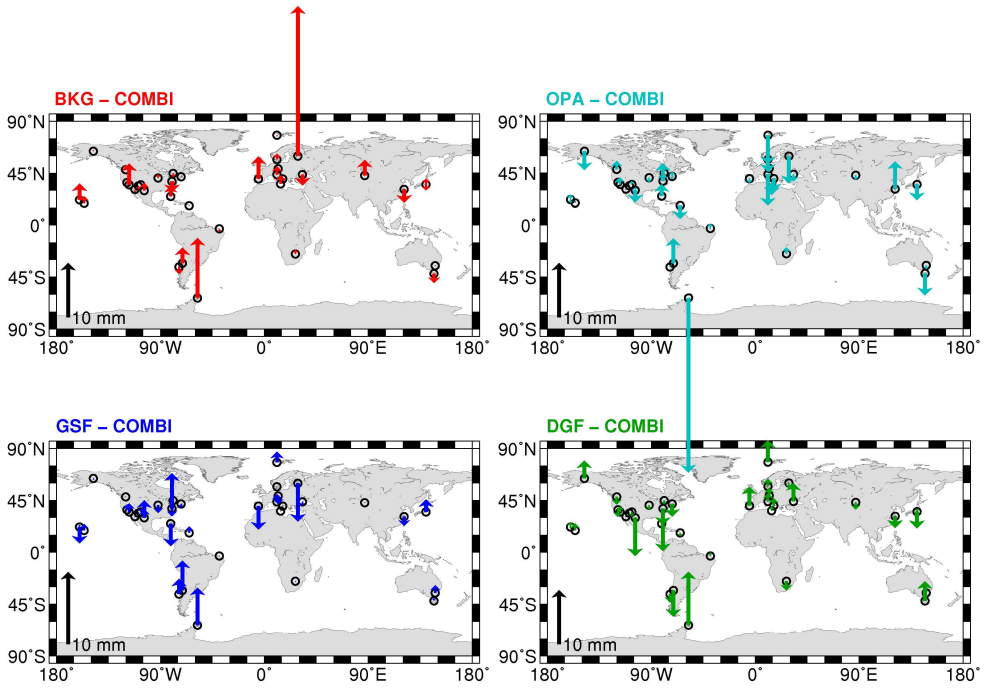

Figure 2. TRF height differences between each individual and the preliminary combined solution at the epoch 2000.

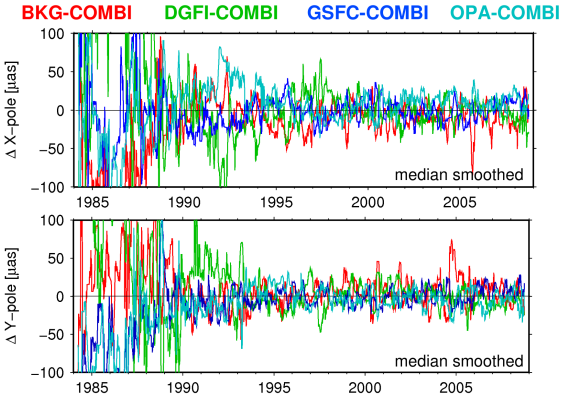

Figure 3. Daily polar motion estimates of each individual solution compared to the preliminary combined solution, upper plot: X-Pole component, lower plot: Y-Pole component.

Like for the station positions, long term EOP series computed from each individual contribution are compared to the preliminary combined EOP series. For polar motion and dUT1 the individual series agree very well, in terms of weighted RMS the agreement is less than 50 μas and 4 μs, respectively (cf. Fig. 3). Analysing the comparison for the LOD component in Fig. 4 visually, clear systematic variations appear in the differences. Further investigations confirmed that these variations are mainly caused by different high-frequency EOP models. Small systematic variations remain in the differences due to different interpolation schemes of the daily a priori EOPs to the observation epoch. The comparison of the nutation offsets in obliquity show a very small, but significant rate of 3 μas/year between the DGFI contribution computed with the software package OCCAM (Titov et al., 2004) and the contributions analysed with the software package Calc/Solve (Petrov, 2006) (c.f. Fig. 5). It is assumed that these differences might be caused by an error in the OCCAM adjustment (pers. communication Oleg Titov).

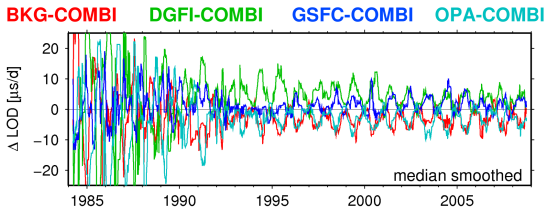

Figure 4. Daily LOD estimates of each individual solution compared to the preliminary combined solution.

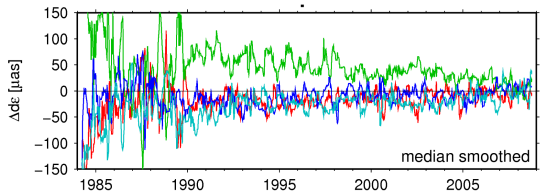

Figure 5. Daily nutation offsets in obliquity ($d\varepsilon$) of each individual solution compared to the preliminary combined solution.

3.2 External comparisons

To measure the accuracy of the preliminary IVS combined contribution to ITRF2008, the combined TRF is compared to ITRF2005 and the scale temporal behaviour with respect to ITRF2005 is evaluated.

The results of the TRF heights of the combined VLBI TRF solution w.r.t. the ITRF2005 are displayed in Fig. 6 for all stations participating in more than 30 sessions. A clear systematic behaviour in the signs is visible, which are related to a different selection of the mean pole within the pole tide model used for both TRF solutions. For the IVS contribution to ITRF2005 the mean pole was defined as $X_0 = Y_0 = 0$, the new contribution uses a linear mean pole as recommended in the IERS Conventions 2003. This effect is well known and causes systematic differences in the height component up to 5 mm (Böckmann et al., 2007). Furthermore, some larger differences are visible at stations with observations many years ago. The differences of the horizontal components between both TRF solutions are at the level of about 3 mm in terms of WRMS over all stations. The velocity differences average 0.5 mm/year.

The scale factors presented by Altamimi et al. (2007) calculated from the IVS contribution to

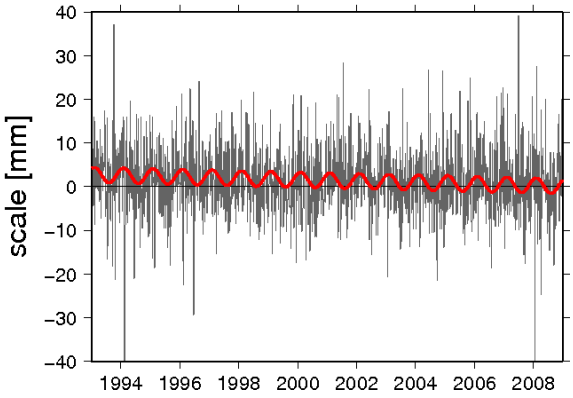

Figure 7. Helmert transformation scale parameters for each VLBI session.

ITRF2005 showed a clear annual signal with an amplitude of 2.7 mm w.r.t. its own cumulative solution. It was expected that the better part of this signal was due to the non-correction of the thermal expansion of the radio telescopes. This is confirmed by our preliminary results. The scale factors between the preliminary combined VLBI including thermal expansion and the ITRF2005 polyhedron are shown in Fig. 7. Comparing both series the annual amplitude of the scale is reduced by 1 mm. It is expected that, a further reduction of the annual signal can be reached by corrections of atmospheric pressure loading. Tesmer et al. (2006) showed that the amplitude of the annual signals in height is generally reduced by up to 0.7 mm due to atmospheric loading corrections.

4 Summary and Outlook

The internal comparisons of the station positions already show a good agreement for most of the stations. Most of the TRF height differences are less than 2 mm. However, for some stations, significant height offsets are detected due to different antenna axis offsets. The comparisons for the EOP have shown that the internal agreement for polar motion is less than 50 μas. The use of different high-frequency EOP models resulted in significant systematic variations in the LOD component of up to 10 μs/d. Differences between OCCAM and Calc/Solve solutions in the nutation offsets in obliquity are assumed to be due to an error in the OCCAM software package. The external comparisons show systematic height offsets w.r.t. ITRF2005 due to a different

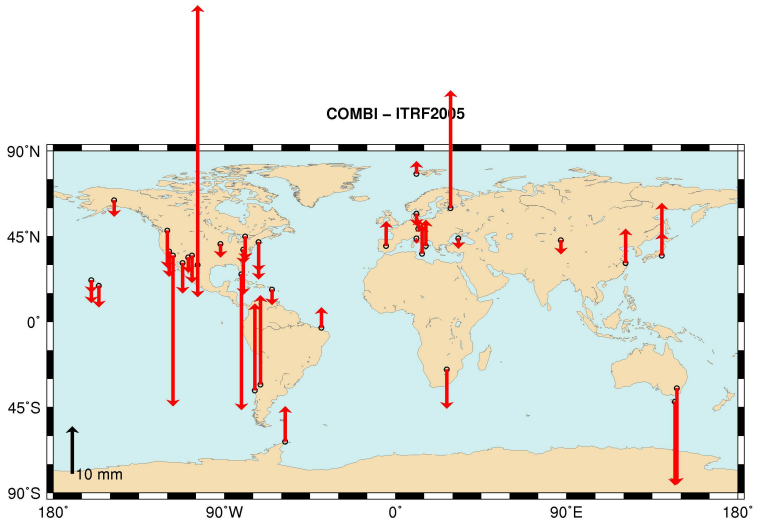

Figure 6. TRF height differences between the preliminary combined solution and the ITRF2005 at the epoch 2000.

mean pole in the pole tide model used. Annual variations in scale are reduced by about 1 mm due to the correction for thermal expansion of the radio telescopes.

For the final contribution to the ITRF2008 all VLBI input solutions will be reprocessed with the official IVS table for antenna axis offsets and the same high-frequency EOP model according to the IERS Conventions 2003. Furthermore, the nutation parameters will be pre-reduced from the DGFI contribution before the combination step.

Acknowledgements The authors would like to thank the IVS Analysis Centers for their strong efforts to provide their solutions for the combination.

References

Z. Altamimi, X. Collilieux, J. Legrand, B. Garayt, and C. Boucher. ITRF2005: A new release of the International Terrestrial Reference Frame based on time series of station positions and Earth Orientation Parameters. *J. Geophys. Res.*, 112:9401–9420, sep 2007. doi: 10.1029/2007JB004949.

S. Böckmann, T. Artz, A. Nothnagel, and V. Tesmer. Comparison and combination of consistent VLBI solution. In *Proceedings of the 18th European VLBI for Geodesy and Astrometry Working Meeting, Geowissenschaftliche Mitteilungen*, volume 79, pages 82–87, 2007.

J. Boehm, B. Werl, and H. Schuh. Troposphere mapping functions for GPS and very long baseline interferometry from European Centre for Medium-Range Weather Forecasts operational analysis data. *J. Geophys. Res.*, 111:B02406, 2006. doi: 10.1029/2005JB003629.

T. Letellier. *Etude des ondes de marée sur les plateaux continentaux*. PhD thesis, Université de Toulouse III, Ecole Doctorale des Sciences de l'Univers, de l'Environnement et de l'Espace, 2004.

D. McCarthy and G. Petit. IERS Conventions (2003). *IERS Tech. Note 32*, 2004. Verl. Bundesa. Kart., Frankfurt.

A. Nothnagel. Conventions on thermal expansion modelling of radio telescopes for geodetic and astrometric vlbi. *J. Geodesy*, 2008. doi: 10.1007/s00190-008-0284-z.

L. Petrov. Mark V VLBI Analysis Software Calc/Solve. 2006. http://gemini.gsfc.nasa.gov/solve.

M. Rothacher. Towards a rigorous combination of space geodetic techniques. In B. Richter, W. Schwegmann, and W. R. Dick, editors, *Proceedings of the IERS Workshop on Combination Research and Global Geophysical Fluids*, IERS Technical Note No. 30, pages 7–18. Verl. Bundesa. Kart., Frankfurt, 2003.

V. Tesmer, J. Boehm, R. Heinkelmann, and H. Schuh. Impact of Analysis Options on the TRF, CRF and Position Time Series Estimated from VLBI. In *International VLBI Service for Geodesy and Astrometry 2006 General Meeting Proceedings*, pages 243–251, 2006.

O. Titov, V. Tesmer, and J. Boehm. Occam v6.0 software for VLBI data analysis. In N. R. Vandenberg and K. D. Baver, editors, *International VLBI Service for Geodesy and Astrometry 2004 General Meeting Proceedings*, pages 267–271, NASA/CP-2004-212255, NASA, Greenbelt, 2004.

M. Vennebusch, S. Böckmann, and A. Nothnagel. The contribution of Very Long Baseline Interferometry to ITRF2005. *J. Geodesy*, 81:553–564, jun 2007. doi: 10.1007/s00190-006-0117-x.

Monitoring UT1 using both VLBI and GPS estimates

D. Gambis and C. Bizouard
IERS Earth Orientation Center, Observatoire de Paris, CNRS/UMR8630
61 avenue de l'Observatoire, Paris, France

Abstract. The objective of the paper is to describe the improvements performed at the IERS EOP Product Center to derive an optimal combined series of UT1 based on results derived from both VLBI and GPS techniques. VLBI, as the only technique referring to a non rotating celestial reference frame is the main contributor to UT1. Alternatively, satellite techniques (like GPS) which are realizing their celestial frame through the orbit determination do not allow determining an accurate UT1; because of mis-modelling of various perturbations, the orbit is affected by long-term systematic variations. Nevertheless, LOD derived with a good accuracy can be used for improving UT1 when calibrated by VLBI data.

Keywords. Earth orientation, combinations, VLBI, GPS

1 Introduction

Earth Orientation Parameters (EOP) describe the orientation of the Earth with respect to a non rotating reference frame. One of the parameter, Universal Time UT1 represents the rotation of the Earth around its axis. Until the 1970's, UT1 was exclusively monitored by astrometric techniques based on optical instruments like photozenithal tubes (PZT), meridian refractors and astrolabes. In the 1970's the emergence of Lunar Laser Ranging (LLR) allowed to determine UT0. In 1985, its accuracy was in the range of 0.400 ms. Meanwhile VLBI technique was emerging and determined UT1 with an accuracy at least ten times better than LLR (see Table 1). Thanks to technique and data processing improvements, as well as models developments, UT1 accuracy has dramatically increased. It is now in the range of 4–5 μas. Densification of UT1 on a daily basis is made using the intensive session programs with however a lesser accuracy of about 15 μs. Figures 1 and 2 give the statistics for various VLBI solutions with respect to the combined 05C04 solution (Gambis, 2004; Bizouard and Gambis, 2009). These statistics are part of the C04 solution currently derived (http://hpiers.obspm.fr/eop-pc/products/combined/verif.html). The increasing requirement to have a regular and accurate UT1 is however at present not fully satisfied using VLBI estimates. UT1 derived from the intensive sessions are sometimes erroneous, 50 to 100 μs offsets are possible. At some epochs close to the New Year, gaps of sometimes 4 to 5 days exist in the daily data. The interpolated values of the C04 are thus unconstrained by observations and can diverge from real UT1 as much as 100 μs. Another blemish is the time delay availability of the UT1 of one week back which prevents the accurate real time UT1 determination required for operational orbit determinations. GPS technique rely on the computation of satellite orbits. The celestial frame realized through satellite orbit determination is not referred to a stable non rotating or quasi inertial reference frame as it is for VLBI technique. The satellite orbit determination realizing the celestial frame is perturbed by systematic errors which consequently affect the long term stability of the derived UT parameter. GPS technique can nevertheless determine daily LOD estimates of which values are slightly biased. To use correctly LOD(GPS) in a UT determination, this time depending bias has to be modelled or computed. In the next sections, we present the way LOD(GPS) can be used for UT1 computation when calibrated by UT1 derived from VLBI. The data we used in the analyses are for UT1: IVS combined solution with a time resolution of 3–4 days (accuracy 5–8 μas),

Table 1. Contribution of astro-geodetic techniques to the determination of UT1 and LOD.

Technique	Since	EOP	Time resolution	Accuracy
ASTROMETRY	1899	UT1	5 days	1 ms
LLR	1969	UT0	1 day	0.4 ms
SLR	1976	LOD	3 days	200 μs
VLBI	1981	UT1 Standard	3-4 days	5 μs
	1981	UT1 Intensive	1 day	15 μs
	1981	LOD	3-4 days	15 μs
GPS	1993	LOD	1 day	10 μs

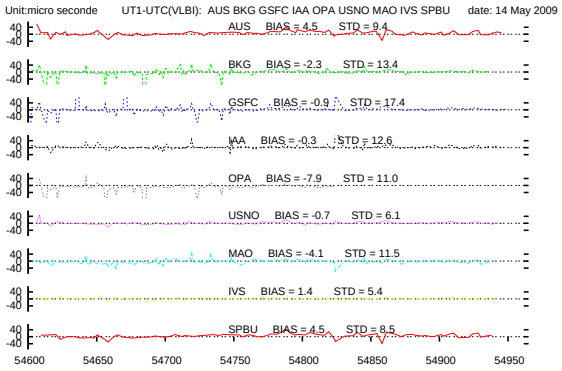

Figure 1. Statistics (biases and WRMS) of the standard individual analysis center solutions and the IVS combined with respect to the O5C04 solution.

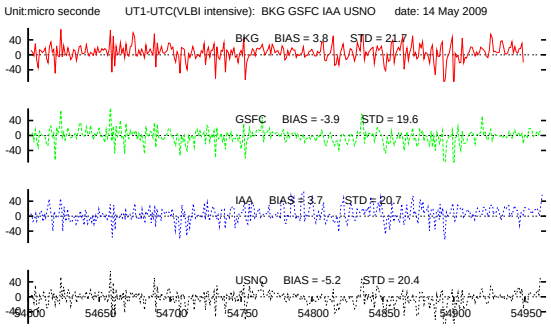

Figure 2. Statistics (biases and WRMS) of the intensive individual analysis center solutions and the IVS combined with respect to the O5C04 solution.

and daily intensive sessions (accuracy 15–20 μs); for LOD: IGS00P3 combined solution given daily with an accuracy of 10 μs.

2 Use of Length of Day (LOD) estimates derived from GPS technique

2.1 Current approach

On time scales of a couple of weeks, the propagation of errors in the orbit are limited. That allows to use the high-frequency signal contained in the GPS UT determination for densification of UT1 (Gambis et al, 1993; Ray et al., 1995). High frequency GPS LOD estimates calibrated by VLBI are integrated in the 05C04 solution. This additional contribution is of main importance for UT1 densification in particular when intensive VLBI data are missing. This happened several times in a few years. As an example, between end 2007 and beginning 2008, 6 days were missing for the IVS standard sessions and 5 days for the IVS intensive sessions. The use of this series UT(GPS) allows the densification of the series (Figure 3). When using this latter series in the C04 combination (Figure 4), the solution we get is more consistent than the C04 combined without this UT(GPS) when VLBI is missing.

2.2 Method of combined smoothing

An alternative approach is based on the simultaneous combination of UT1 and its rate LOD using the so-called method of "Combined Smoothing" (Vondrak and Gambis, 1999; Vondrak and Cepek, 2000). It is a generalization of Vondrak smoothing (Vondrak, 1969, 1977). The method assumes that two relatively smooth curves are available:

- The first one fitting well to VLBI UT1 estimates;
- The second one fitting well to GPS LOD estimates.

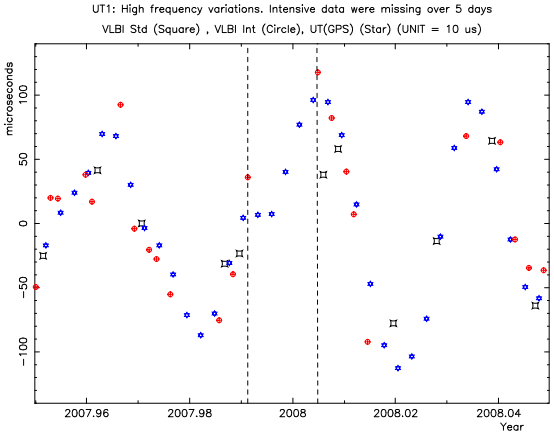

Figure 3. UT1-UTC high frequency variations. Around the end of 2008, VLBI standard and intensive are missing over 5–6 days. UT based on the integration of LOD(GPS) can then be used to densify the UT1 series.

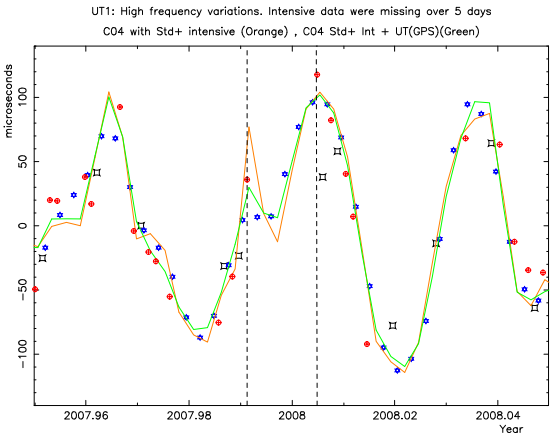

Figure 4. UT1-UTC. The contribution of UT(GPS) in the combination improves the consistency of the C04 combined series. Improvement of the C04 appears due to the contribution of UT(GPS) (Green line).

Both curves are tied by the constraint that LOD is the first derivative of UT1 LOD=$-d(UT1-TAI)$/dt with t in days. The optimal solution is obtained when minimizing an expression taking into account the two conditions for two adapted smoothing parameters. These parameters were determined after a series of simulations. The estimation of the improvement obtained by the use of GPS LOD estimates is not straightforward since no "ideal" or "Truth" series exists for comparison. To discriminate quality between EOP time series, various authors suggested to use for comparison an external series based on atmospheric excitations of the Earth's axial angular momentum variations (Kouba and Vondrak, 2005). The tests we made showed that no significant improvement appears and the discrimination of series cannot be done such a way. The justification we assume comes likely from the fact that AAM (Atmospheric Angular Momentum) data are partly derived from models. That prevents its use to discriminate between UT1 series. Comparisons with an external UT1 combined series like the Bulletin A of the Rapid/prediction Service at USNO (http://maia.usno.navy.mil/) or SPACE solution performed at JPL (Gross, 2006) can alternatively give a gross evaluation of the quality of the series. Figure 5 shows the comparison of various combined UT1 series with the external Final Bulletin A series. It appears that the contribution of GPS LOD either by the direct integration of LOD(GPS) or when applying the Combined Smoothing leads to a small improvement of a few μs in the WRMS compared to the solution which does not incorporate any LOD(GPS) data. It is also striking that the improvement of the solution is only a few μs when the IVS intensive sessions are included in the combination.

3 Conclusion

As an inertial technique, VLBI is unique in determining UT1. The C04 combination now takes into account the IVS combined solution derived from both standard and intensive sessions. However, gaps in the data and erroneous estimates deteriorate the quality of the combination and its consistency. The increasing accuracy of LOD(GPS) estimates can be employed in the combination. Two methods, i.e. the current one based on the integration of LOD(GPS) calibrated by VLBI and the Combined Smoothing approach, give similar results and allow the densification of the combined C04 series as well as the improvement of its internal consistency.

References

Bizouard C. & Gambis D., 2009, the combined solution C04 for Earth Orientation Parameters, recent improvements, Springer Verlag series, Series International Association of Geodesy Symposia,

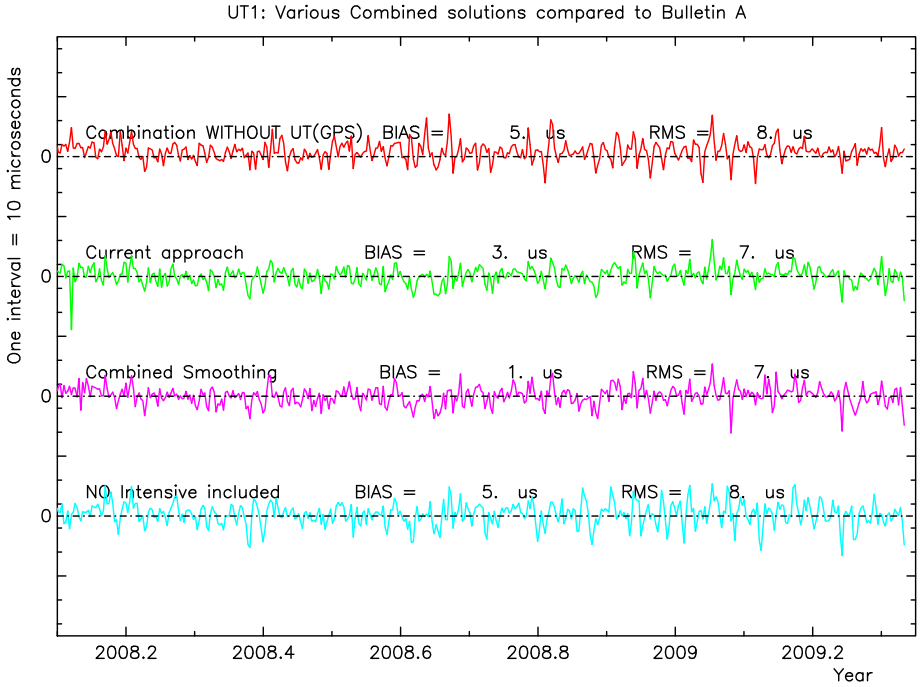

Figure 5. Comparison of different UT1 combined series. It appears that the contribution of GPS LOD, either by the direct integration of LOD(GPS) (referred as Current approach) or when applying the Combined Smoothing, leads to a small improvement of one μs in the WRMS compared to the solution which does not incorporate any LOD(GPS) data (upper line). We can notice that if we do not include tha IVS intensive sessions in the UT1 combination, the final solution is not significantly degraded.

Vol. 134, Hermann (Ed.), 330 p., ISBN: 978-3-642-00859-7

Gambis D., Essaifi N., Eisop E. & Feissel M., 1993, Universal Time derived from VLBI, SLR and GPS, IERS Technical Note 16, Dickey and Feissel (eds), Observatoire de Paris ,IV15-20.

Gambis D., 2004, Monitoring Earth orientation using space-geodetic techniques: state-of-the-art and prospective, J. of Geodesy, Volume 78, Issue 4-5, pp. 295-303, doi 10.1007/s00190-0040394-1.

Gross R.S., 2006, Combinations of Earth orientation measurements: SPACE2005, COMB2005, and POLE2005, Jet Propulsion Laboratory Publ. 06-3, 26 pp., Pasadena, California

Kouba J. & Vondrak J., 2005, Comparison of length of day with oceanic and atmospheric angular momentum series, J of Geod., Volume 79, Issue 4-5, pp. 256-268

Ray J.M., Carter W.E. & Robertson D.S., 1995, Assessment of the accuracy of daily UT1 determinations by very long baseline interferometry, JGR, vol. 100, no. B5, pp 8193-8200, may 10

Vondrak J., 1969, A contribution to the problem of smoothing observational data, Bull. Astron. Inst. Czechosl. 20: 349-355

Vondrak J., 1977, Problem of smoothing observational data II, Bull. Astron. Inst. Czechosl. 28: 84-89

Vondrak J. & Gambis D., 1999, Accuracy of Earth orientation parameters obtained by different techniques in different frequency windows, in: Soffel M., Capitaine N. (eds.) Journes 1999 Systmes de rfrence spatio-temporels and IX. Lohrmann Colloquium, Observatoire de Paris, 206-213.

Vondrak J. & Cepek A., 2000, Combined smoothing method and its use in combining Earth orientation parameters measured by space techniques, Astron. Astrophys. Suppl. Ser. 147, 347-359

CONT08 - First Results and High Frequency Earth Rotation

T. Artz, S. Böckmann, A. Nothnagel
Institut für Geodäsie und Geoinformation der Universität Bonn, Nußallee 17, D-53115 Bonn, Germany

Abstract. First results from the most recent continuous VLBI campaign (CONT08) are shown. CONT08 took place in August 2008. One of the scientific goals was the generation of high precision Earth Orientation Parameters (EOP) with sub-daily resolution. A general quality assessment of CONT08 is performed investigating station position variations and daily EOP. In addition, high-resolution Earth rotation time series are generated in a way that ensures consistency over the whole time span. Here, we demonstrate the effect of a modified scheduling procedure concerning (in-)consistency of sub-daily EOP at session borders. Results of prior continuous campaigns have differed significantly from each other in amplitude and phase of the spectral components. Thus, we also compare the CONT08 amplitude spectra with results from CONT02 and CONT05.

1 Introduction

The International VLBI Service for Geodesy and Astrometry (IVS) conducts continuous VLBI observations of up to 14 days duration (CONT) in irregular intervals. In contrast to the routine 24 h VLBI observations, which are performed two or three times per week, those CONT-campaigns are around-the-clock observations over several days. The last three CONT campaigns carried out in 2002, 2005 and 2008 took place over fortnightly time-spans. CONT-sessions should always demonstrate the highest available accuracy that can be achieved by VLBI observations. Additionally, one of the main scientific goals is the generation and interpretation of highly resolved Earth Orientation Parameters (EOP) due to the continuity of the campaign.

Most recently, CONT08 took place in 2008 from August 12–26 with individual sessions being

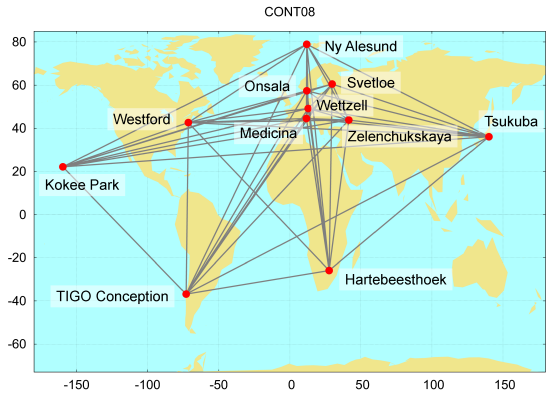

Figure 1. CONT08 observing network.

set up for 0 h to 24 h UTC each. The observing network was arranged by 11 globally distributed VLBI telescopes (see Fig. 1). The network has a strong European part since the stations in North-America at Fairbanks and Algonquin Park (that were part of prior continuous campaigns) were powered off and replaced by Medicina and Zelenchukskaya.

There are several changes in the scheduling of CONT08 with respect to prior continuous campaigns. The keypoint is the necessity of system checks that have to be performed on a daily basis. For CONT08 these have been decoupled in view on the observing sites. Prior to CONT08, the system checks were performed in the last $\approx$ 30 min of each session for all stations. Now, subsequent 2 h slots for each site have been planned for each session with exception of the first one. In those slots, the 30 min system checks should be performed (see Table 1). In reality, this idea has been fullfilled. Moreover, some stations performed system checks so quickly that nearly no gaps are visible in the observations.

Table 1. Time slots for system checks during CONT08 (http://ivscc.gsfc.nasa.gov/program/cont08/cont08-notes.txt).

Station	Weekends [UT]	Weekdays [UT]
Hr	13-15	12-14
Kk	00-02	18-20
Mc	15-17	06-08
Ny	17-19	10-12
On	11-13	08-10
Sv	05-07	04-06
Tc	21-23	16-18
Ts	07-09	00-02
Wf	19-21	14-16
Wz	07-09	18-20
Zc	09-11	02-04

Focussing on the observations themselves, one can state that each session has an overall number of 9 000 to 11 000 observations. This is a great increase w.r.t. CONT02 (mean: 3 000) and CONT05 (mean: 6 000) due to a raise of the recording rate and, thus, shorter scan lengths. The variation between the individual sessions mainly depends on station problems. TIGO/Conception missed 3 sessions and had several interruptions of up to 6 h. Zelenchukskaya is absent in one session because of lost disks. Furthermore, post fit residuals of observations with Zelenchukskaya show bi-modal patterns suggesting the existence of sub-ambiguities. Since these could not be fixed, the observations affected have been eliminated from the solution.

In this paper, first results of the analysis of CONT08 observations are given with a special focus on the estimation of sub-daily EOP. In particular, the impact of the modified scheduling on the estimates is evaluated. Furthermore, CONT-campaigns of 2002, 2005 and 2008 are compared on the basis of station position estimates and the frequency representation of polar motion.

2 Solution Description

Three different solutions have been performed for the analysis of CONT08 as well as of CONT02 and of CONT05:

1. Solution for session-wise station position estimates. The datum defect has been solved by NNR/NNT conditions w.r.t. ITRF2005 over the whole set of stations.

2. EOP solution with daily estimates of polar motion, ΔUT1 and their rates as well as nutation offsets.

3. EOP solution with hourly PM and ΔUT1 parameterized as continuous-piece-wise-linear-functions (CPWLF). Nutation parameters are fixed to a priori values estimated in a separate solution.

In solutions 2 and 3, the station positions are estimated only once for the middle epoch of the fortnightly time-span to de-correlate the estimates as shown by Artz et al. (2007).

All of these solutions have in common the same modelling and parameterization of nuisance parameters (clocks and atmospheres). Source positions are fixed to ICRF and its extensions. Station clocks are estimated w.r.t. Kokee Park clock by a 2^{nd} order polynomial with additional clock parameters modelled by 60 min CPWLF. Troposphere parameters are estimated as CPWLF, too. The zenith wet delay is parameterized with a temporal resolution of 20 min and gradients in 12 h intervals.

For all of these solutions a priori EOP are taken from USNO finals [1]. Nutation is modelled by IAU2000A (McCarthy and Petit, 2004) plus additional corrections from a global VLBI solution. Ocean loading is modelled according to FES2004 (Letellier et al., 2004), furthermore, thermal expansion of the radio telescopes (Nothnagel, 2008) and atmospheric pressure loading (Petrov and Boy, 2004) have been applied.

The solutions presented here are all run in a two step procedure. First, the data is processed by the VLBI analysis software Calc/Solve (Petrov, 2008) and the normal equation system (NEQ) is exported. In a second step the NEQ is solved with a Perl backend to Calc/Solve. To ensure the continuity of the campaign and to stabilize parameters at the session borders, a modified solution strategy is used. The NEQ are built up for each single session. Clock parameters are treated as session parameter, thus, they have been reduced from each individual session NEQ. Finally, the individual NEQ are added to a single one for the complete campaign by adding elements of parameters of the same type and the same epoch. Thereby, parameters at the session borders are stabilized and estimated only once (Artz et al., 2007).

[1] ftp://maia.usno.navy.mil/ser7/finals.daily

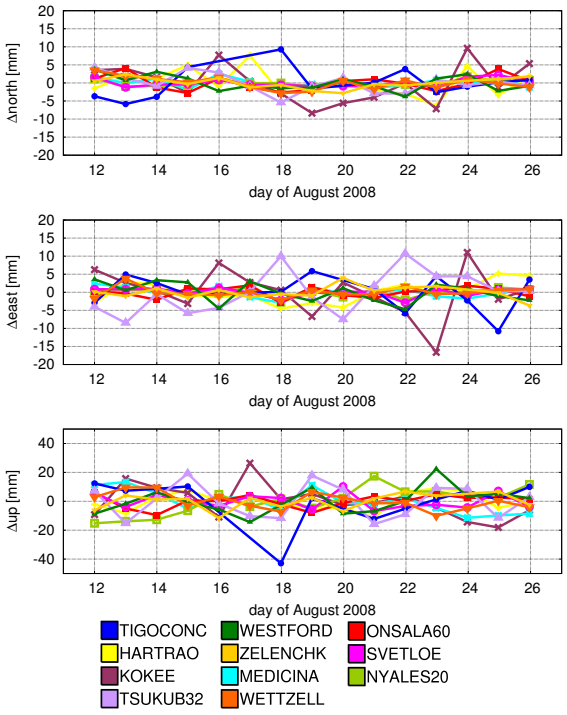

Figure 2. Differences of the individual session estimates to the campaign mean in CONT08.

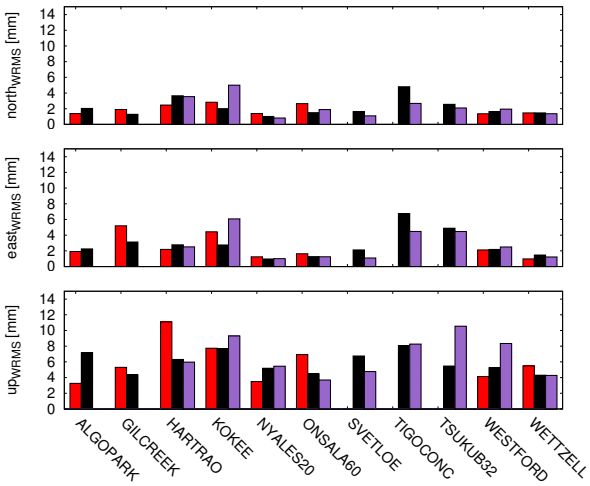

Figure 3. Station position repeatabilities for each campaign. The datum definition has been applied by NNR/NNT conditions over all stations in CONT02 (red) and over all stations but Kokee Park and Tsukuba in CONT05 (black) and CONT08 (purple). The two stations that were active in CONT08, only, (Medicina and Zelenchukskaya) are excluded from this figure.

3 Quality Assessment

On the basis of solutions 1 and 2, an assessment of the quality of CONT08 can be achieved. On the one hand, station position estimates will be compared within the campaign. On the other hand, the repeatabilities are compared to those in CONT02 and CONT05. Furthermore, an external validation is performed on the basis of daily EOP. These are compared to those estimated from GPS observations.

The differences of the individual station position estimates and the campaign mean are quite homogeneous (Fig. 2). Most of them are below 10 mm for the horizontal and 20 mm for the up component. Only the variability of the east component of Kokee Park and Tsukuba is large compared to the other sites. Nevertheless, the impact on the estimation of other parameters is not big e.g. excluding these sites from the datum definition has nearly no impact on the other station positions. The bigger deviations of TIGO/Conception in the session of August 18^{th} can be explained by the minor contribution to this session. Here, TIGO had only a few hours of observations due to some station problems and, thus, the error bars of these estimates are huge. As a consequence, there is no big impact on the estimation of other parameters as well.

In general, the station position estimates are as stable as those of the prior campaigns. Figure 3 shows the station position repeatabilities for CONT02, CONT05 and CONT08. Only observing sites that were in at least two campaigns are displayed.

Most of the repeatabilities in CONT08 are of comparable size as in the prior campaigns or even better. Only the repeatabilities of Kokee Park, Tsukuba and Westford have become worse. The main cause can be seen in the switch-off of the telescopes at Fairbanks and Algonquin Park reducing the geometric links between these sites. As a general consequence, it can be stated that the CONT08 network was not that well distributed over the Earth as it was in CONT05.

Calculating the WRMS of the daily EOP differences between the VLBI estimates and external EOP series leads to an insight in the quality of the EOP from a continuous campaign. These WRMS differences are shown in Fig 4, where the official combined EOP series of the International GNSS Service [2] has been used for polar motion.

[2] ftp://igscb.jpl.nasa.gov/pub/product/igs00p03.erp.Z

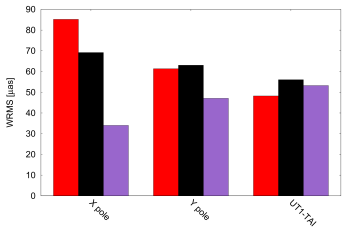

Figure 4. EOP repeatabilities for each campaign. The WRMS values are calculated w.r.t. IGS EOP series for polar motion and USNO finals for ΔUT1.

For ΔUT1 the USNO finals have been used to calculate the EOP repeatabilities. The differences have been detrended to eliminate the impact of differences in the underlying terrestrial reference frame. The UT1 variations from the three continuous VLBI campaigns agree with the reference series at the same level, whereas the CONT08 polar motion agrees much better with the IGS time series than those from CONT02 or CONT05.

4 Sub-daily Earth Rotation

The estimation of EOP with a sub-daily resolution from CONT campaigns is of great interest. Hourly EOP estimates over a time-span of two weeks provide the opportunity to analyze the characteristics of the EOP in the frequency domain.

Furthermore, the time series of hourly EOP shows the effects of the modified scheduling used in CONT08. Figure 5 displays the X pole differences w.r.t. the IGS time series for CONT05 and CONT08 from a solution where each session is analyzed independently. There are huge outliers in the CONT05 time series at the session borders. Those are due to the lack of observations in the last ≈ 30 min of each 24 h block where the system checks were performed. Such outliers are not visible in the CONT08 time series. For CONT08 the scheduling was changed in a way that the observations are really continuous as described in Sec. 1. Thus, the estimates in the last interval of each individual session are already stabilized through this type of scheduling.

In addition to the scheduling, the modified solution strategy of stacking the normal equations helps to further improve the sub-daily EOP estimates. Here, parameters at the session boundaries are estimated using observations from the

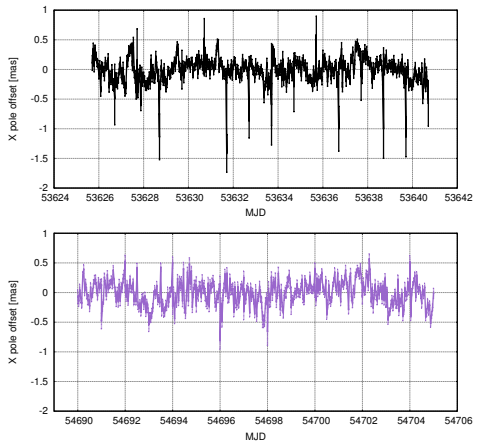

Figure 5. X pole differences to IGS with a hourly resolution from CONT05 (upper plot) and CONT08 (lower plot) from an independent solution.

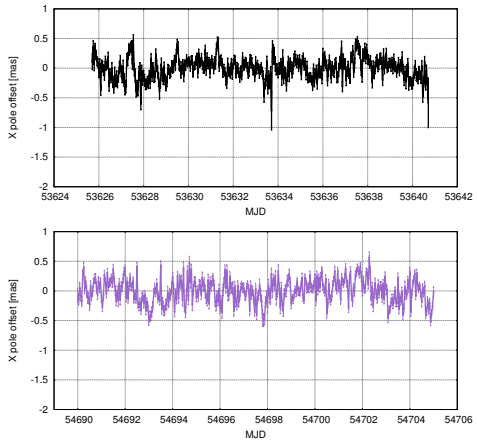

Figure 6. X pole differences to IGS with a hourly resolution from CONT05 (upper plot) and CONT08 (lower plot) where the modified solution strategy has been applied.

last interval of the first session and the first interval of the second session and so on. The resulting time series are shown in Fig. 6. Nearly all of the outliers in CONT05 are eliminated or at least minimized by the modified stacking approach. A minor improvement can be seen for CONT08 as well.

In the spectral domain several authors have reported about a retrograde ter-diurnal signal in the CONT02 Polar Motion data (e.g. Haas and Wünsch 2006). This signal is visible in our analysis, too, as it is shown in Fig. 7. However, there is no such signal present in the other cam-

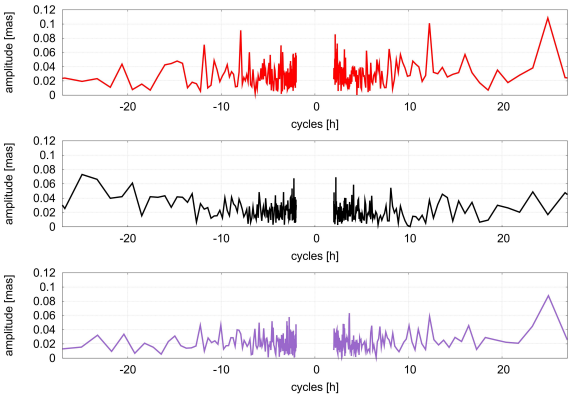

Figure 7. Polar Motion spectra from CONT-campaigns.

paigns. To derive the spectra, total EOP series are reduced by the IERS sub-daily tidal model (McCarthy and Petit, 2004). The reason for this phenomena is still an open issue and under investigation. Subsequently, those values have been detrended by CPWLF with a resolution of one day. Afterwards, a FFT of the residuals has been calculated. Some peaks can be seen at the diurnal and semi-diurnal bands. The prograde diurnal and semi-diurnal as well as the semi-diurnal retrograde signal can be interpreted as inconsistency between the IERS sub-daily tidal model and the VLBI observations. The remaining retrograde diurnal signal is due to mismodelling of nutation. Nutation is fixed to a priori values for the estimation of sub-daily EOP, thus, some of the remaining signal appears as a near diurnal retrograde term.

In the ΔUT spectra no significant variations besides the diurnal and semi-diurnal bands can be seen. There is a small irregular variation at a period of 6h in the CONT05 data only.

5 Conclusions

CONT08 serves as a high quality continuous data-set from VLBI observations. The variations of the station position estimates is quite homogeneous besides some bigger variations in the east component of Kokee Park and Tsukuba.

The modified scheduling improves the estimation of parameters with a sub-daily resolution as shown for the hourly EOP estimates. Not only EOP but all parameters with a sub-daily resolution as zenith wet delay or clock parameters benefit from this procedure.

The sub-daily EOP estimates match the GPS series quite well for all campaigns. The derived spectra for polar motion are inhomogeneous. The peaks at the well known tidal bands with periods around 12h and 24h vary. Furthermore, the retrograde ter-diurnal term is present in CONT02 polar motion but not in CONT05 or CONT08. For variations in ΔUT, no significant irregular variations could be found.

References

T. Artz, S. Böckmann, A. Nothnagel, and V. Tesmer. ERP time series with daily and sub-daily resolution determined from CONT05. In J. Böhm, A. Pany, and H. Schuh, editors, *Proceedings of the 18th Workshop Meeting on European VLBI for Geodesy and Astrometry*, volume 79 of *Geowissenschaftliche Mitteilungen, Schriftenreihe Vermessung und Geoinformation der TU Wien*, pages 69–74. TU Wien, 2007.

R. Haas and J. Wünsch. Sub-diurnal earth rotation variations from the VLBI CONT02 campaign. *J. Geodyn.*, 41:94–99, 2006.

T. Letellier, F. Lyard, and F. Lefevre (2004), The new global tidal solution: FES2004, *Proceeding of the Ocean Surface Topography Science Team Meeting, St. Petersburg, Florida*

D. D. McCarthy and G. Petit. *IERS Conventions (2003).* IERS Conventions (2003). Dennis D. McCarthy and Gérard Petit (eds.), International Earth Rotation and Reference Systems Service (IERS). IERS Technical Note, No. 32, Frankfurt am Main, Germany: Verlag des Bundesamtes für Kartographie und Geodäsie, ISBN 3-89888-884-3, 2004, 127 pp., 2004.

A. Nothnagel. Conventions on thermal expansion modelling of radio telescopes for geodetic and astrometric VLBI. *J. Geodesy*, 2008. doi: 10.1007/s00190-008-0284-z.

L. Petrov. Mark-5 vlbi analysis software calc/solve. Web document http://gemini.gsfc.nasa.gov/solve/, 07 2008.

L. Petrov and J.-P. Boy. Study of the atmospheric pressure loading signal in very long baseline interferometry observations. *Journal of Geophysical Research (Solid Earth)*, 109:3405–+, Mar. 2004. doi: 10.1029/2003JB002500.

Evolution and obtained expertise in reference point determination at the GIK

M. Lösler, C. Eschelbach
Geodetic Institute of the University of Karlsruhe (TH), 76128 Karlsruhe, Germany

Abstract. The International Terrestrial Reference System (ITRS) is realized by geodetic space techniques, which are linked by local ties at the observation stations. Therefore, reliability and high accuracy are the main requirements for the determination of the different reference points in the corresponding local reference frame. At the Geodetic Institute of the University of Karlsruhe several scientific studies have been carried out to determine the reference point of radio telescopes at different observation stations and with different calculation models. Starting in 2002 the IVS reference point at Onsala Space Observatory was determined by 3D-circle fits with error propagation using full covariance information, which is custom procedure nowadays. In 2008 a completely new mathematical model was established able to fulfill future requirements as for example minimizing downtime of the telescope. Geodetic measurements with a tacheometer, respectively a lasertracker, at the Fundamentalstation Wettzell and the Onsala Space Observatory, yielded a good verification of the model. This contribution shows the evolution and obtained expertise in reference point determination at the Geodetic Institute of the University of Karlsruhe by comparing the results of different campaigns at the Onsala Space Observatory.

Keywords. Reference point, VLBI, local tie, mathematical model, radio telescope, surveying

1 Introduction

The main objective of the two campaigns at the Onsala Space Observatory was the determination of the IVS reference point of the 20-m radio telescope which is surrounded by a radome. But the mathematical models differ and, therefore, the strategies for the performance of the terrestrial geodetic measurements were different as well. Nevertheless the campaigns base on equal requirements. The reference point of a VLBI telescope of azimuth-elevation type is defined as the intersection of azimuth axis and elevation axis or if they do not intersect the point on the azimuth axis which is nearest to the elevation axis. This implies its independence of any orientation of the telescope and its inaccessibility. Furthermore, the 20-m telescope at Onsala is surrounded by a radome, which limits the operating range for the measurement equipment. The radome wall is equipped with five steel pillars to be used as observation points for the measurements up to the telescope.

2 Campaign 2002

2.1 Measurements

The two reference points were connected by the measurement of marked points inside and outside the radome. The determination of the coordinates was separated in the horizontal and the vertical component. Therefore, the measurements included horizontal angles and horizontal distances from a Leica TCR1102 and a Leica T2002 and height differences from a Zeiss DINI10. Due to bad accessibility the height components of the steel pillars on the radome wall were calculated by trigonometric measurements. The IGS-reference point (Fig. 1) was appended from two net points.

The measurements to the telescope cabin, which result in the coordinates of the IVS-reference point, were carried out twice. In the first epoch four target markers were stuck at the two sides of the telescope cabin, in the second epoch the end points of the elevation axis itself were signalised by magnetic target markers (Fig. 2). These telescope points were observed in different telescope positions from two of the five observation pillars without distance measurements simultaneously. The telescope was moved in discrete steps of 10° in elevation at 15 different azimuth positions.

Figure 1. IGS-reference point (right) in the IGS-monument (left).

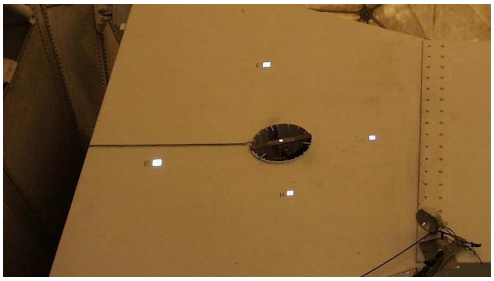

Figure 2. Target markers (2002) at the telescope cabin and at the endpoint of the elevation axis.

2.2 Reference point determination

The coordinates of the net points were determined by the software $Netz2D$ and $HEIDI$, programs of the Geodetic Institute (GIK) of the University of Karlsruhe (TH) (Fig. 3). A free network adjustment was chosen to avoid stress in the network and still allow a transformation in superior coordinate systems. The standard deviations of the coordinates of the IGS-reference point were $\hat{\sigma}_{IGS} = [0.2\,0.2\,0.6]^T_{mm}$.

The determination of the IVS-reference point based on the coordinates of the target markers at different telescope positions delivered from a 3D-network adjustment by $Netz3D$ (from the GIK). $Netz3D$ also supplies the full covariance matrix of the coordinates which was used for the following calculations. 3D-circe fits combined with restrictions deduced from the telescope structure yielded the coordinates of the endpoints of the elevation axis. The mathematical model is shown in Equations (1) and (2) and was calculated as a Gauß-Helmert-model:

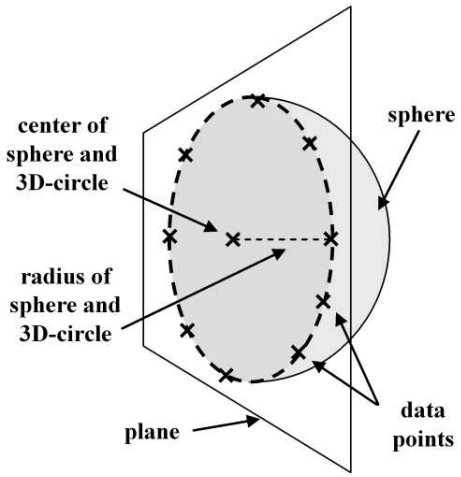

Figure 4. Schematic description of the 3D-circle fit.

Table 1. Standard deviations of the coordinates of the IVS-reference point (2002).

	X [m]	Y [m]	Z [m]
Epoch 1	0.0001	0.0001	0.0001
Epoch 2	0.0001	0.0001	0.0003

$$f_i^1 = \left(\widetilde{X}_i - X_0\right)^2 + \left(\widetilde{Y}_i - Y_0\right)^2 + \left(\widetilde{Z}_i - Z_0\right)^2 \quad (1)$$

$$f_i^2 = A_0\widetilde{X}_i + B_0\widetilde{Y}_i + C_0\widetilde{Z}_i - 1 = 0 \quad (2)$$

The coordinates $\left[\widetilde{X}_i\,\widetilde{Y}_i\,\widetilde{Z}_i\right]^T$ are the observed parameters. The unknown parameters consist of the centre of the circle $[X_0\,Y_0\,Z_0]^T$, the radius R_0 and the parameters A_0, B_0 and C_0 of the plane the circle lies in Figure 4. The coordinates of the centres of the elevation circles again form 3D-circles which centre on the IVS-reference point. A detailed description of the model is given in Eschelbach (2002). The second epoch additionally provided the axis offset with $e = -0.0060 \pm 0.0003m$. Table 1 shows the standard deviations of the IVS-reference point.

3 Campaign 2008

3.1 Measurements

In 2008 the second campaign was carried out. A Leica Lasertracker LTD840 was used instead of

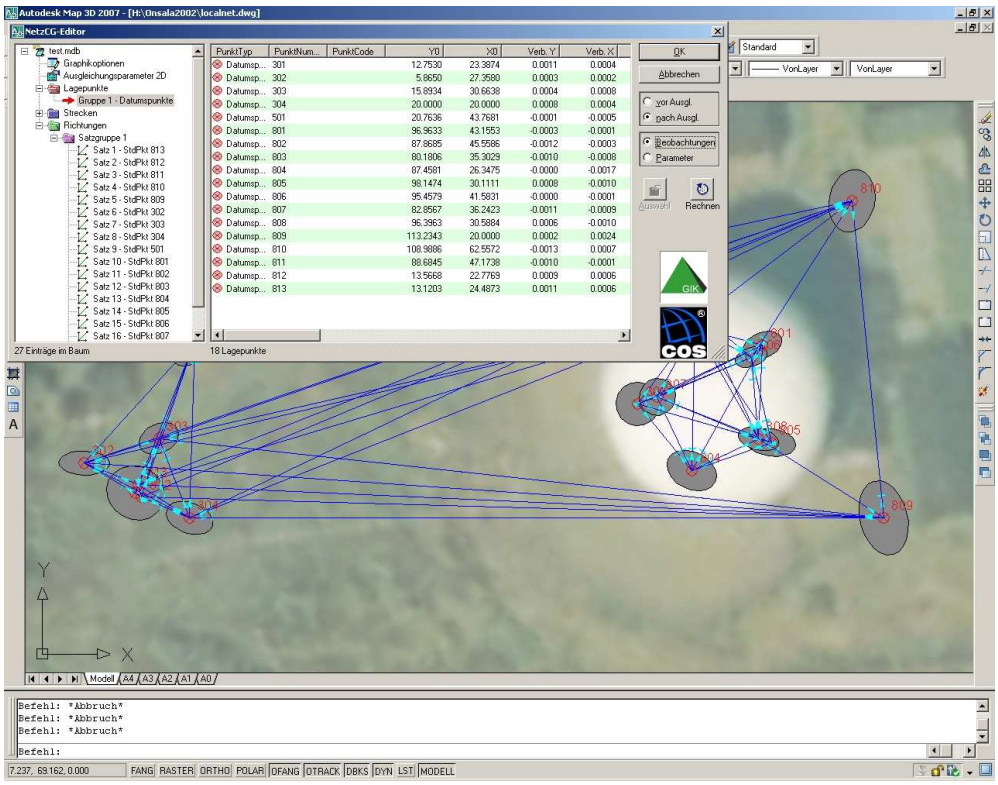

Figure 3. Observation network after net estimation (Aerial picture by Microsoft Visual Earth).

the two theodolites. In principle a lasertracker is similar to a tacheometer, but there are three main differences. A lasertracker operates with an interferometer, which limits its range but raises accuracy. It only works with automated target tracing and recognition and measurements do not refer to the plumb line. As a polar measuring system, furthermore, the two angles, which are necessary for 3D-coordinates, are measured with two angle encoders. The schematic description is given in Figure 5. An emitted laser beam is deflected on a multiaxial rotatable mirror in the head of the lasertracker and is reflected at a mirrored target. The reflected laser beam is split into two signals. One leads to a position sensitive device, which controls the head to follow the target, the other one leads to the distance measurement device. For static targets the accuracy given by the manufacturer is 10 ppm (2σ) in 40-m range of operation, which is also limited by the opening angle of about $\pm 235°$ for the horizontal and $\pm 45°$ for the vertical angle (Leica, 2001). Moving objects are measured with an accuracy of 20–40 ppm (2σ) in the same operation area.

At first the local network was measured with the LTD840. The local coordinate system of 2002 could not be used, because the lasertracker provides better accuracies than achieved in 2002 and moreover two of the five steel pillars had been replaced and have not measured yet. The measurements yielded the coordinates of the five pillars, three marked points in the radome basement, six marked points outside the radome and the IGS-reference point itself. The IVS-reference point is an immaterial point inside the telescope structure and can not be measured directly, therefore, so-called Cat-Eye-Reflectors with an opening angle of $\pm 60°$ were attached to the telescope cabin (Fig. 6). This large opening angle is necessary, so that the laser beam will not be disrupted immediately while the telescope is moved around the elevation axis. To fully utilize the cramped confines inside the radome the lasertracker was mounted on the pillars in a tilt of 90° to the plumb line. This setup was possible, because the lasertracker works without referring to the plumb line anyway, and provided coordinates of 720 points resulting from 5 different azimuth positions and 18 different elevation positions (see Lösler, 2009a; Lösler and Haas, 2009).

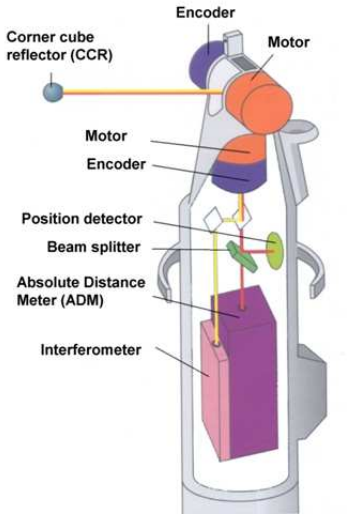

Figure 5. Schematic description of the Leica Lasertracker LTD840 (Leica, 2001).

Figure 6. Cat Eye Reflectors at the telescope cabin.

3.2 Reference point determination

The coordinates of the points inside and outside the radome were calculated from the lasertracker data by a free 3D-network adjustment using the author's program. The accuracies of the coordinates resulted in $\hat{\sigma}_{IGS} = 0.3$ mm for each component and the full covariance matrix was available after the net estimation, which provided error propagation for the subsequent determination of the IVS-reference point. The mathematical model of the determination was redeveloped and derives the coordinates of the reference point from dependencies between the local coordinate system and the coordinate system of the telescope (Fig. 7). Equation (3) describes these dependencies between the two coordinate systems mathematically and considers the axis offset $Ecc = [0\, e\, 0]^T$ and possible inclinations of the axes by estimating the angles of rotation α, β and γ.

$$P_{Obs} = P_R + R_x(\beta)\, R_y(\alpha)\, R_z(A + O_A) \ldots \quad (3)$$
$$R_y(\gamma)\,(Ecc + R_x(E + O_E)\, P_{Tel})$$

A detailed description of the derivation is given in Lösler and Hennes (2008) and Lösler (2009b), in addition robust solutions for a non-linear system of equations (Gauß-Helmert-Modell) are mentioned. The model was first verified using measurement data from the Fundamentalstation Wettzell (Lösler, 2008). Unlike the traditional circle fit the new model does not require predefined telescope positions, which allows real-time measurement. Now the observation parameters are the coordinates of the points at the telescope cabin and the corresponding antenna orientation angles. The stochastical model (see Equation (4)) consists of the covariance matrix of the coordinates of the telescope points derived from the net estimation extended with the uncertainties of the antenna orientation angles A (azimuth) and E (elevation).

$$C_{ll} = \begin{bmatrix} \sigma^2_{X_1} & \sigma_{X_1Y_1} & \sigma_{X_1Z_1} & 0 & 0 & \sigma_{X_1X_2} & \cdots \\ \sigma_{Y_1X_1} & \sigma^2_{Y_1} & \sigma_{Y_1Z_1} & 0 & 0 & \sigma_{Y_1X_2} & \cdots \\ \sigma_{Z_1X_1} & \sigma_{Z_1Y_1} & \sigma^2_{Z_1} & 0 & 0 & \sigma_{Z_1X_2} & \cdots \\ 0 & 0 & 0 & \sigma^2_{A_1} & 0 & 0 & \cdots \\ 0 & 0 & 0 & 0 & \sigma^2_{E_1} & 0 & \cdots \\ \sigma_{X_2X_1} & \sigma_{X_2Y_1} & \sigma_{X_2Z_1} & 0 & 0 & \sigma^2_{X_2} & \cdots \\ \vdots & \vdots & \vdots & \vdots & \vdots & \vdots & \ddots \end{bmatrix} \quad (4)$$

The estimation of the IVS-reference point yielded a standard deviation of $\hat{\sigma}_{IVS} = 0.1$ mm for each coordinate. The axis offset was significantly identified with $e = -0.0062 \pm 0.0001$ m.

4 Comparison of the results

The comparison of results of the two campaigns has to be exempted from any influence of the geodetic data. Due to the slightly different net structure the coordinates of the reference points themselves do not reveal any conclusion about the stability of the local tie vector. Instead the length of the local tie vector and the axis offset are free from influences of the geodetic data

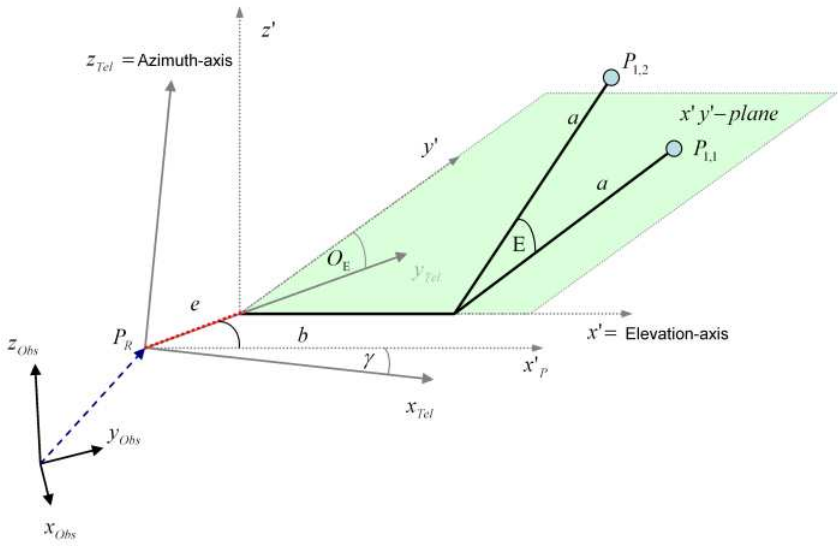

Figure 7. Dependencies between the local coordinate system and the coordinate system of the telescope.

Table 2. Comparison of the rersults

	2002 [m]	2008 [m]	Difference [m]
e	-0.0060	-0.0062	0.0002
d	79.5685	79.5678	-0.0007

and can be compared directly. The results in Table 2 are taken from Haas and Eschelbach (2003) and Lösler (2009a), respectively. A statistical hypothesis test detects significant deformations by choosing no deformation as the null hypothesis and the significance level to be $\alpha = 0.1\%$.

$$H_0 : T = \frac{(d_{2002} - d_{2008})^2}{\hat{\sigma}^2_{d_{2002}} + \hat{\sigma}^2_{d_{2088}}} = 5.4 \sim F_{1-\alpha,1,\infty} \quad (5)$$

If the T-value (in Equation (5)) exceeds the critical value $K_\alpha = 11.6$ of the *Fisher*-statistic the null hypothesis would have to be rejected and the deformation would be highly significant. The results do not show any statistically significant deformation.

5 Comparison of the strategies

The two campaigns in 2002 and 2008 achieved similar results and accuracies, but differ in a few points but basic ones. The biggest disadvantage of modelling the reference point determination by circle fits is the necessity of predefined movements of the antenna, which can only be carried out during long observation breaks of the telescope. Instead the new model can handle diffuse telescope positions but affords azimuth and elevation angles of the antenna. Furthermore, in 2002 the points at the telescope cabin were measured simultaneously from two observation pillars by two theodolites in combination with target markers without measuring distances. In 2008 the polar measurement system lasertracker with automated target tracing in combination with Cat Eye Reflectors was used, which could be replaced in the near future by a total station with the same operational opportunities but only with a slightly lower accuracy. Therefore, any disadvantages of the installation of the lasertracker can be evaded. In summary the new mathematical model in combination with modern surveying instruments is a successful evolution in IVS-reference point determination and represents an automatable measurement strategy for telescopes of azimuth-elevation type while the downtime of the telescopes is reduced or even avoided.

Acknowledgements This research has been supported by Deutsche Forschungsgemeinschaft (DFG), HE5213/2-1.

References

Eschelbach C., 2002, Determination of the IVS-reference point at the Onsala Space Observatory

in a local reference frame, Geodetic Institute of the University of Karlsruhe

Haas R., Eschelbach C., 2003, The 2002 Local Tie Survey at the Onsala Space Observatory, Proceedings of the IERS Workshop on site co-location, Matera, Italy, 23 - 24 October 2003

Leica, 2001, Axyz Trainingshandbuch für Tracker, Leica Geosystems AG, Unterentfelden

Lösler M., 2008, Reference point determination with a new mathematical model at the 20 m VLBI radio telescope in Wettzell, J. App. Geod 2, p.233-238.

Lösler M., 2009a, Bestimmung des lokalen Verbindungsvektors zwischen IVS- und IGS-Referenzrahmen am Raumobservatorium Onsala (Schweden), AVN (in press)

Lösler M., 2009b, A new mathematical model for reference point determination of an azimuth-elevation type radio telescope, J. Surv. Eng. (in press)

Lösler M., Haas R., 2009, The 2008 local-tie determination at the Onsala Space Observatory, Proceedings of the EVGA European VLBI for Geodesy and Astrometry, France, Bordeaux 23.-24. March 2009

Lösler M., Hennes M., 2008, An innovative mathematical solution for a time-efficient IVS reference point determination, Proceedings of the FIG2008 Measuring the changes, Portugal, Lisabon 12.-15. May 2008

Analyses on the Time Series of the Radio Telescope Coordinates of the IVS-R1 and -R4 Sessions

E. Tanir
Dept. of Geodesy and Photogrammetry Eng., Karadeniz Tech. University, Trabzon, Turkey

V. Tornatore
Politecnico di Milano, DIIAR, Sezione Rilevamento, Piazza Leonardo da Vinci 32, 20133 Milano, Italy

K. Teke
Institute of Geodesy and Geophysics, Vienna University of Technology, 1040 Vienna, Austria

Abstract. In this study, we investigate the coordinate time series of the radio telescopes which regularly take part in IVS-R1 and -R4 sessions. Firstly, we determine the linear trend (velocity vectors of the antenna coordinates) due to e.g. plate tectonics. The trends of the coordinate time series are estimated by Least Squares (LS), fitting the coefficients of a linear regression function. After removing the linear trend from the series, sinusoidal variations of the series, if they exist, are determined by estimating the amplitudes and phase of the Fourier series based on the frequency of the maximum power spectral density in the respective spectra plot (periodogram). In order to sample the data, evenly linear interpolation is used. The spectral density of the data is produced by Fast Fourier Transform (FFT). For most of the investigated radio telescope time series, harmonic variations are not found. The significant periods of the up components ranges from $\approx$ 50 to $\approx$ 450 days and differ for each antenna. The amplitudes of the detected variations are small, in ranges between 0.4–0.1 mm. Many geophysical models had been applied to the data (daily sinex normal equations of VLBI sessions were provided by Deutsches Geodatisches Forschungsinstitut; DGFI) except the models of atmosphere loading and thermal deformation.

Keywords. VLBI radio telescope coordinate time series, harmonic analysis, IVS -R1 and -R4 sessions.

1 Introduction

Several studies have been performed in the last ten years to individuate harmonic site position variations by VLBI (Titov and Yakovleva, 1999; Petrov and Ma, 2003; Tesmer et al., 2007). All these studies detected annual signals in VLBI baseline length time series and also a semiannual signature has been determined on some baselines. A more complete study has been published by Collilieux et al. (2007) comparing ITRF2005 input data that come from VLBI, GPS, and SLR. In this work, on co-located sites, the GPS height annual signal has been confirmed by VLBI and SLR measurements, however no significant signal at lower periods has been confirmed neither by VLBI nor by SLR.

With in this study we start to investigate on these inconsistencies using IVS-R1 and -R4 experiments that have a high density of sessions respect to other standard VLBI experiments. On the whole, 17 radio telescope sites which have continuously taken part in most of the IVS-R1 and -R4 daily sessions from the beginning of 1994 to the end of 2008 are included in our study. The a priori coordinates of these VLBI stations provided from Deutsches Geodatisches Forschungsinstitut (DGFI), estimated by introducing No Net Rotation (NNR) and No Net Translation (NNT) conditions with the ITRF2000 coordinates of 25 globally distributed VLBI antennas. The corrections to the apriori coordinates are estimated with LS adjustment from the daily sinex normal equations (minimum constrained) of IVS-R1 and -R4 sessions.

2 VLBI radio telescope coordinate time series analysis

After the estimate of the adjusted coordinates of the antennas at their respective time epochs,

coordinate time series of each antenna are produced. The determination and removal of the yearly trends (velocities) from the radio telescope coordinates is carried out by LS fit to the linear function:

$$X_t - X_{mean} = a_1(t - t_1) + \epsilon_t \,, \qquad (1)$$

where X_{mean} is the yearly mean value of the coordinate series, a_1 is the trend (velocity vector, cartesian components) of the year (estimated values) and ϵ_t are the residuals. If a parameter is to be judged as statistically different from zero, and thus significant, the computed T value (the test statistic) must be greater than $t_{1-\alpha,f}$, where $1-\alpha$ is the level of confidence and f is the degrees of freedom. Simply stated, the test statistic is:

$$T = \frac{|parameter|}{S} \,, \qquad (2)$$

where S is the standard deviation of the parameter (Wolf and Ghilani, 1997). Offsets (yearly mean values of the coordinate series) and statistically significant yearly trends are removed from the time series of the antenna coordinates. The residual parts (ϵ_t) of the coordinates are then transformed to the local topocentric coordinates as follows:

$$\begin{bmatrix} North \\ East \\ Up \end{bmatrix} = \Omega * \begin{bmatrix} \epsilon_{X(t)} \\ \epsilon_{Y(t)} \\ \epsilon_{Z(t)} \end{bmatrix} \,, \qquad (3)$$

with

$$\Omega = \begin{bmatrix} -sin\varphi\, cos\lambda & -sin\varphi\, sin\lambda & cos\varphi \\ -sin\lambda & cos\lambda & 0 \\ cos\varphi cos\lambda & cos\varphi sin\lambda & sin\varphi \end{bmatrix} \,, \qquad (4)$$

where φ is the latitude and λ is the longitude of the station. The related co-variances of the station coordinates are transformed to local topocentric system as follows:

$$Q_{NEU} = \begin{bmatrix} q_{NN} & q_{NE} & q_{NU} \\ q_{NE} & q_{EE} & q_{EU} \\ q_{NU} & q_{EU} & q_{UU} \end{bmatrix} = \Omega\, Q_x\, \Omega^T \,. \qquad (5)$$

The resulted series in the local topocentric system are analysed by means of detecting cyclicities (harmonics). This single spectral analysis approach, known as auto spectral analysis (autospectrum, or periodogram), is based on the detection of the maximum power and respective frequency. The procedure is carried out iteratively eliminating the maximum amplitude up to reaching noise floor (Schuh, 1981).

In case a time series contains a periodic sinusoidal component with a known wavelength (frequency) the model will be:

$$X_t = \sum_{p=1}^{k} R_p cos(\omega_p t + \phi_p) + Z_t \,, \qquad (6)$$

where ω is called the frequency, R is the amplitude, ϕ is the phase and Z_t denotes a stationary series. Since $cos(\omega+\phi) = cos\omega\, cos\phi - sin\omega\, sin\phi$, Eq. (6) can be expressed as:

$$X_t = \sum_{p=1}^{k} (a_p cos\omega_p t - b_p sin\omega_p t) + Z_t \,, \qquad (7)$$

where $a_p = R_p cos\varphi_p$ and $b_p = -R_p sin\phi_p$. The amplitude and phase of the variation ($p^{th} harmonic$) are:

$$\begin{aligned} R_p &= \sqrt{a_p^2 + b_p^2} \\ \phi_p &= tan^{-1}(-b_p/a_p) \end{aligned} \qquad (8)$$

If we are interested in variation at low frequency of 1 cycle per year, then we should have at least 1 year's data in which case the lowest frequency we can fit is at 1 cycle per year. In other words, the lowest frequency covers the longest time period over the data. The Nyquist frequency is the highest frequency for which we can get meaningful information from a set of data. The Fourier series representation of the data is normally evaluated at the frequencies of $\omega_p = 2\pi p/N$ provided from the fundamental $(2\pi/N)$ frequency by multiplying the integers $p = 1, 2, ..., N/2$, called as harmonics (Chatfield, 2004; Trauth, 2007). The procedures that is done to analyse the coordinate time series of VLBI radio telescope coordinates are itemized below:

- The normal equation matrices' sinex files of the sessions IVS-R1 and -R4 are downloaded from the DGFI database. The corrections to the antennas' a priori ITRF2000 coordinates are estimated at their session time epochs with LS (step 1).
- Firstly, yearly mean values of the coordinate series are removed (see Eq. (1)). Then, the yearly linear trends (velocities) of each antenna are estimated (see Eq. (1)) with

LS. All the significant (see Eq. (2)) linear trends from the series are removed resulting in the stationary series (the series without any trend). The residual stationary series with their covariance matrices are transformed to local topocentric coordinate system (see Eq. (3) and (4)) (North, East, and Up) (step 2).

- In order to produce the data evenly distributed a linear interpolation is introduced to the real data (as to make use of FFT to plot spectral density of the series). By the linear interpolation the same number of artificial data with the real data which are all in the range of the real data are produced (step 3).
- The maximum power of the spectral density and its frequency is computed with FFT (step 4).
- The coefficients of the Fourier series (see Eq. (7)) are estimated with LS based on the frequency of the maximum power (step 5).
- The amplitude and phase of the first largest cycle are calculated (see Eq. (8)) with these coefficients of the Fourier series (step 6).
- In case the amplitude is larger then 0.1 mm then the harmonic effect is removed from the respective series then the iteration procedure from step 4 is repeated again for the same series (step 7).
- In case the estimated amplitude is smaller then 0.1 mm the loop is finished for this series (step 8).
- The same procedure is applied for the north, east and up components of each antenna (step 9).

3 Results of the analysis

Table 1 shows a comparision between our estimates of yearly significant velocities from the IVS-R1 and -R4 sessions and retrieved velocities from the combined solution of the Terrestrial Reference Frame (TRF) of International Earth Rotation and Reference Systems Service (IERS), ITRF2000 at epoch 1997.0, in local topocentric coordinates. The series are unevenly spaced. Averages of the sampling intervals are used for producing the Nyquist frequencies. To form evenly spaced data linear interpolation is applied. For the unevenly spaced data it seems to be impossible to prevent artefacts and spurious effects on the interpolation results. The power spectral density of the time series is computed by FFT and plotted e.g. for the Wettzell antenna coordinate series of the up component given in Figure 2. The coefficients of Fourier series (a_p and b_p) given in Eq. (7) are estimated with least squares according to the period of the maximum power produced by the power spectral density plots. With the coefficients of the Fourier series amplitude and phase of the maximum harmonic variation (spectra) is computed with Eq. (8). Iteratively, cyclicities are removed from the data, based on the frequency of maximum power (Schuh, 1981). The iterations are stopped when the amplitudes are found out below the value of 0.1 mm. Harmonic behaviour of the up component of the Wettzell antenna from 1994.01 is shown in Figure 1. Significant harmonics (amplitude, phase, and period) of the VLBI antenna coordinates are given in Table 2.

4 Conclusions and prospects

After removing the linear trend from the series, sinusoidal variations of the series are determined by estimating the amplitudes and phase of the Fourier series based on the frequency of the maximum power spectral density in the respective spectra plot (autospectrum). The significant periods of the up components ranges from ≈ 50 to ≈ 450 days and differ for each antenna. The amplitudes of the detected variations are small, in ranges between 0.4–0.1 mm (Table 2). The retrieved data (daily sinex normal equations of VLBI sessions) provided by DGFI has already been modeled as a priori by certain geophysical models (e.g. troposphere, solid Earth tide, ocean loading, and pole tide) except atmosphere loading and thermal deformation. This may be caused by the artefacts of the data interpolation carried out linearly or the data itself because of the un-modeled geophysical parts of the a priori coordinates derived.

Acknowledgements We are grateful to the International VLBI Service for Geodesy and Astrometry (IVS) for providing the observations. Special thanks to Prof. Dr. Harald Schuh for his reviews on the paper. K. Teke wants to acknowledge the Scientific and Research Council of Turkey (TUBITAK) for his scholarship.

References

Chatfield C., 2004, The Analysis of Time Series An Introduction, Sixth Edition, Chapman & Hall/Crc, Washington, D.C, pp.121-146.

Collilieux X., Altamimi Z., Coulot D., Ray J., Sillard P., 2007 Comparison of very long baseline interferommetry, GPS, and satellite laser ranging height residuals from ITRF2005 using spectral and correlation methods. J. Geophys. Res. 112(B12403): 1-18.

Petrov L. and Ma C., 2003, Study of harmonic site position variations determined by very long baseline interferometry, J. Geophys. Res., 108(B4), 2190, doi:10.1029/2002JB001801.

Schuh H., 1981, Zur Spektralanalyse von Erdrotationsschwankungen, Sonderdruck aus: Die Arbeiten des Sonderforschungsbereiches 78 Satellitengeodaesie der Technichen Universitaet Muenchen im Jahre 1980, Heft Nr. 41, Muenchen 1981, pp. 176-193.

Tesmer V., Boehm J., Heinkelmann R., and Schuh H. (2007), Effect of different tropospheric mapping functions on the TRF, CRF and position time-series estimated from VLBI, J. Geod., 81, 409 421, doi:10.1007/s00190-006-0126-9.

Titov O. and Yakovleva H., 1999, Seasonal variation in radial components of VLBI stations, Astron. Astrophys. Trans., 18, 593 606.

Trauth H.M., 2007, MATLAB Recipes for Earth Sciences, 2nd Edition, Springer-Verlag Berlin Heidelberg, pp. 83-131.

Wolf R.P. and Ghilani D.C., 1997, Adjustment Computations, John Wiley & Sons, Inc., pp. 353-354, Newyork.

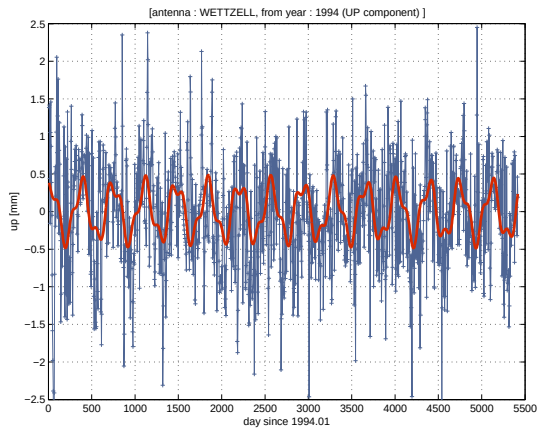

Figure 1. Harmonic behaviour of the antenna Wettzell; up component from 1994.01

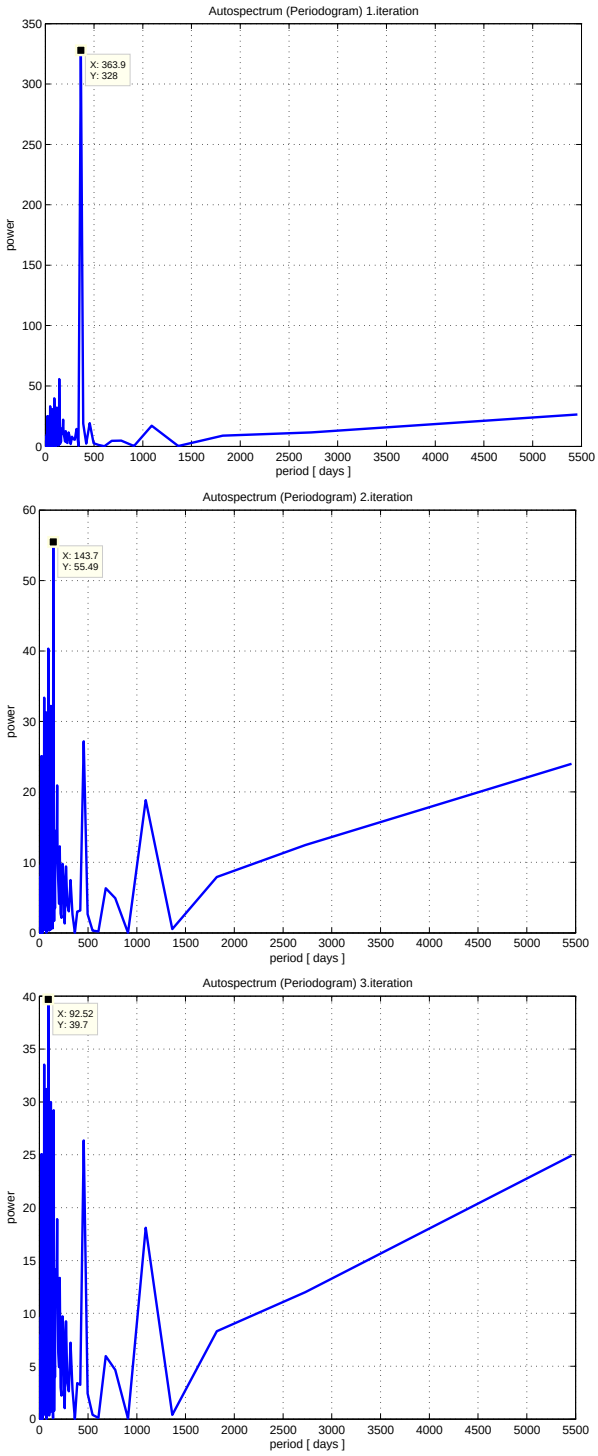

Figure 2. Spectra plot of the time series of the up component of the antenna Wettzell for the first three iterations.

Table 1. The velocity vectors derived from ITRF2000 at epoch 1997.0 and IVS-R1 and -R4 Sessions.

	ITRF2000			IVS-R1 and -R4		
	v_{north} (cm)	v_{east} (cm)	v_{up} (cm)	v_{north} (cm)	v_{east} (cm)	v_{up} (cm)
Algopark	0.13	-1.66	0.23	0.17 (2005)	-1.61 (2005)	0.23 (2002)
Fortaleza	1.21	-0.43	0.09	1.16 (2008)	-0.48 (2008)	0.11 (2006)
Kokee	3.24	-6.24	-0.08	3.29 (2008)	-6.46 (1995)	-0.09 (2007)
Matera	1.81	2.37	-0.10	1.81 (2003)	2.36 (2003)	-0.11 (2003)
Wettzell	1.44	2.03	-0.09	1.37 (2008)	2.02 (2008)	-0.07 (2008)

Table 2. Significant harmonics of the antenna coordinates.

	Up			East				North			
Iteration	Amp. (mm)	Phase (°)	Per. (days)	Iter.	Amp.	Phase	Per.	Iter.	Amp.	Phase	Per.
Algopark (time interval: 2002.01–2006.53, number of data: 262)											
1	0.21	59.4	411.2	1	0.30	−4.76	205.6	1	0.21	−1.1	234.9
2	0.25	72.9	328.9	–	–	–	–	2	0.17	−25.9	31.0
Fortaleza (time interval: 1990.02–2008.9, number of data: 525)											
–	–	–	–	1	0.13	−37.2	325.8	1	0.12	−24.3	155.8
Kokee (time interval: 1994.01–2008.9, number of data: 1129)											
1	0.17	−50.2	454.5	–	–	–	–	–	–	–	–
Nyales20 (time interval: 1996.03–2008.9, number of data: 723)											
1	0.16	6.05	196.4	–	–	–	–	–	–	–	–
Westford (time interval: 2002.0–2008.9, number of data: 417)											
1	0.25	−19.1	360.9	1	0.21	76.9	210.6	1	0.66	−41.9	360.9
2	0.21	13.8	148.6	–	–	–	–	2	0.43	−27.4	2526.9
3	0.16	76.7	84.2	–	–	–	–	3	0.25	−30.5	93.6
4	0.12	72.2	126.3	–	–	–	–	–	–	–	–
5	0.11	−48.7	53.8	–	–	–	–	–	–	–	–
Wettzell (time interval: 1994.0–2008.9, number of data: 1353)											
1	0.35	−45.2	363.9	1	0.18	−53.1	1819.6	1	0.24	−36.6	5458.9
2	0.13	54.9	143.7	2	0.14	−33.7	341.2	–	–	–	–
3	0.04	20.0	92.5	3	0.13	72.8	779.8	–	–	–	–
–	–	–	–	4	0.12	41.0	1364.7	–	–	–	–

Status of the Twin Telescope Wettzell Project

H. Hase, R. Dassing, G. Kronschnabl, T. Klügel, C. Plötz
Bundesamt für Kartographie und Geodäsie
Geodätisches Observatorium Wettzell, Sackenrieder Str. 25, D-93444 Bad Kötzting, Germany

A. Neidhardt, P. Lauber, R. Kilger
Forschungseinrichtung Satellitengeodäsie, Technische Universität München
Geodätisches Observatorium Wettzell, Sackenrieder Str. 25, D-93444 Bad Kötzting, Germany

Abstract. The Twin Telescope Wettzell Project (TTW) is a rigorous realization of the VLBI2010 vision of the International VLBI Service. The project execution takes place in the period of 2008-2011. The status report includes background information how the product specification of the IVS translated via the IVS Vision VLBI2010 into the TTW project. Some of the technical characteristics of the new instruments and the actions taken for the realization of the TTW are presented.

Keywords. TTW, twin telescope, ring focus, VLBI2010, IVS, Wettzell

1 Introduction

The *International VLBI Service for Geodesy and Astrometry* (IVS) was founded in 1999. Since then the geodetic and astrometric VLBI became an official international service within the *International Association of Geodesy* (IAG) and the *International Astronomical Union* (IAU). The IVS Directing Board created in 2001 its Working Group 2 to define "Product Specifications and Observing Programmes". The IVS-WG2 Report (Schuh et al. 2002) had been presented in 2002, concluding the future demands of the service products. Several products, like station coordinates, episodic events, Earth rotation velocity, rotational pole position, nutational parameters as well as geophysical properties of the ionosphere and troposphere demand a continuous 7 days per week observation.

The global VLBI network infrastructure is not yet prepared to accomodate a continuous service, although several a fortnight long continuous observation programmes had been successfully executed in 2002, 2005, 2008. The experience gained by previous so called CONT experiment series and the desire to incorporate upcoming new technologies into the VLBI process lead to the creation of the IVS Working Group 3 "VLBI 2010" in September 2003. The IVS WG3 "examined current and future requirements for VLBI geodetic systems, including all components from antenna to analysis, and produce a report with recommendations for a new generation of systems". The final report had been presented in 2005 (Niell et al. 2005). The recommendations of the IVS-WG3 had been constraint not only by the outcome of the IVS-WG2 product specification but also on the requirements of the Global Geodetic Observing System (GGOS) project of the IAG and the science driven geodetic goals outlined in the NASA Solid Earth Science Working Group Report (SESWG). The envisaged goals are:

- 1 mm measurement accuracy on global baselines,
- continuous measurements for time series of station positions and Earth orientation parameters,
- turnaround time to initial geodetic results of less than 24 hours.

2 The Wettzell 20 m Radio Telescope

Since 1983 Wettzell is participating with its 20 m radio telescope in geodetic VLBI measurements. At the time of its construction it was the first radio telescope which design criterias considered geodetic aspects, such as the possibility to measure the materialized invariant point in the intersection of the azimuth/elevation axis with respect to a geodetic local survey network. One end of the geodetic baseline measured by VLBI

Figure 1. Geodetic Observatory Wettzell. In the foreground the 20 m radio telescope. In the backyard the acquired plot of land for the Twin Telescope Wettzell Project.

methods could therefore be easily tied with the national, respectively the continental, geodetic reference network.

Even with the existence of Global Navigation Satellite Systems of today the issue of connecting different geodetic space techniques by a local geodetic survey remained as an essential task for the production of the terrestrial reference frames by the *International Earth Rotation and Reference System Service* (IERS).

According to the statistics of the IVS (IVS-Webpage) the Wettzell 20 m radio telescope has been so far the most frequent scheduled VLBI station of the IVS network. With more than 130 observation days (24h) plus the daily Intensive series (INT1, INT2, INT3) troughout the years the Wettzell radio telescope is operating at its technical limits and is serving for more than 25 years.

Given the IVS-initiative VLBI2010 and concerns about the age and observation load of the 20 m radio telescope led the VLBI group of the Geodetic Observatory Wettzell to the creation of the Twin Telescope Wettzell Project as a midterm replacement.

3 Twin Telescope Wettzell - TTW

The Twin Telescope Wettzell Project (TTW) started in 2006 with a careful analysis of the IVS-WG3 VLBI2010 vision and the product catalog of IVS-WG2 in mind. In conclusion a few characteristics made clear that a new type of radio telescopes needed to be constructed. The stringent requirements are:

- Radio telescopes are needed as long term geodetic monuments. With respect to the challenges of GGOS to establish an observing system which will achieve on the global scale accuracies better of 1 mm for the position error and 1 mm/year for the site velocity error the construction of the radio telescope itself should guarantee and maintain the stability of the invariant point as reference during lifetime of the instrument (20 years for TTW).
- Continuous observations of Earth orientation parameters contradict with necessary maintenance cycles of the radio telescope. Maintenance moments or days are necessary to refresh the cryogenic cooling system, to maintain the mechanical parts of the radio telescope, to perform system checks and pointing tests. If any geodetic observatory shall provide observational data continuously to the IVS, then more than one radio telescope is needed at one site. Therefore it was decided to construct two identical radio telescopes featuring the VLBI2010 goals. This concept of twin radio telescopes enables new observation modes, when no maintenance has to be performed. Both radio telescopes can be used simultaneously at one source ("array mode") to increase the sensitivity. If both radio telescopes point to different sources then different subnets are tied at the same time. If the source change will be scheduled, while the other radio telescope is still tracking a source, then the "continuous" observation gets a new content, because one of the twin radio telescopes always hooks at a source. Hence continuous interferogrammes of Earth rotation can be realized by VLBI and compared with those of laser gyroscopes.
- The 1 mm accuracy can be achieved only with more observations per time unit (Petrachenko et al. 2008). Likewise GNSS antennas observe simultaneously at different directions and achieve therefore a good geometric stability for the position determination, VLBI suffers the handicap utilizing radio telescopes with a strong directivity. In order to make VLBI as omnidirectional as possible the approach is to make the radio telescopes much faster. Instead of 8–12 observations per hour it is suggested to approach with 30 s slew-track cycles per source

up to 120 observations per hour (10 times more). With respect to the necessary signal to noise ratio at the correlator output, the suggested diameter of 12 m and kinematic parameters of $6-12^o/s$ for both axes were specified. These parameters take into account that the necessary integration time to detect the radio source and the dimensions of the radio telescope (aperture diameter, accelerating masses) needed to be compromised.

- Reduced susceptibility to external interference challenges the entire IVS network. The commercial exploitation of the microwave spectrum does unfortunately not exclude the radio window of the electromagnetic spectrum. Geodetic VLBI uses since more than three decades the S-band spectrum at $2.2-2.35$ GHz and the X-band spectrum at $8.1-8.9$ GHz. The lower S-band frequencies are increasingly effected by radio frequency interference. Hence in the future it will be more and more difficult for the IVS to continue observing as before. This situation is one reason for the IVS to suggest the development and implementation of so called wideband feeds which cover ideally the radio window of $2-18$ GHz. If the radio telescope can be equipped with such a wideband feed, then unpolluted spectra can be used and correlated for VLBI. In addition a wider spectrum enables a better phase connection among the correlated spectral channels. Using then the phase delay instead of the group delay in the analysis of VLBI observation, will result in higher accuracy - as demanded. The fact of favourizing wideband feeds has a direct impact to the radio telescope optics. Wideband feeds have a larger opening angle. For this reason the optics of suitable radio telescopes are much different with respect to the existing VLBI radio telescopes which limits the possibility to upgrade the old once. Hence new optimized constructions will be necessary at several existing radio telescope sites, when wideband observations after a period of transition will become the IVS standard.

Based on those documents a technical specification for the new radio telescopes was finished in 2007 (Dassing R. et al. 2007). The technical specification of the Twin Telescope Wettzell was used for an open bidding. From five interested companies only two German companies had been able to fulfill the technical specifications. By the end of 2007 the company Vertex Antennentechnik GmbH in Duisburg was contracted by the Bundesamt für Kartographie und Geodäsie for the Twin Telescope Wettzell Project. The execution time was set to the period 2008–2011.

4 The first project year, 2008

4.1 Construction of the radio telescopes

The Kick-Off Meeting took place in January 2008 at Wettzell. The participants agreed on a time schedule which fixed the design review to December 2008. Based on the contracted offer several simulations had to be made in order to proof the concept of the twin radio telescopes and to optimize constructive parameters.

The offered design contains the following characteristics:

- Number of identical radio telescopes: 2
- Main reflector size: 13.2 m
- Mount: elevation over azimuth (identical to ALMA)
- Kinematics: Velocity: Az $12^o/s$, El $6^o/s$, Acceleration: Az, El $3^o/s^2$
- Optics: Axially displaced ellipse reflector or ring focus
- Subreflector with hexapod mount
- Path length error: < 0.3 mm
- 3D reference point: < 1 mm (accessible and measurable with respect to a local survey network)
- Life time: > 20 years

Compared to the characteristics of existing radio telescopes for VLBI, the characteristics of VLBI2010 going beyond the state-of-the-art in radio telescope constructions. One difficult criteria is the reliable continuous frequent movement during lifetime. The accumulated movements in the period of more than 25 years of the 20 m Wettzell radio telescope shall be reached within less than 1.5 years given the envisaged VLBI2010 observation schedules with continuous

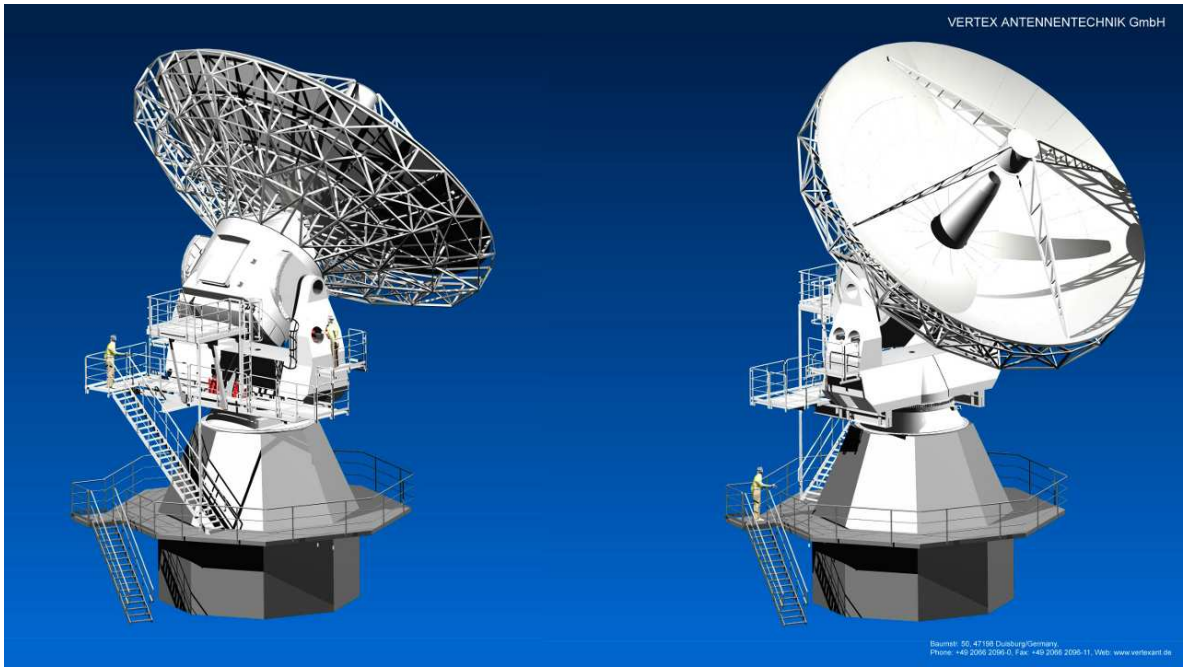

Figure 2. Simulated view of the twin telescope. The radio telescopes use a primary ring focus and a secondary point focus. The subreflector is very close to the wideband feed, which has a half opening angle of about 65^o.

30 s slew/track cycles. This observation load combined with 3-times higher acceleration and 4-times higher velocities means an enormous increase of mechanical stress which the construction will have to withstand.

Another important mechanical parameter is the specification of the path length error to be < 0.3 mm. The radio telescope must be very stiff in order to be robust against varying gravitational loads (due to elevation) and environmental forces (wind, snow, rain, hail, ice). A small path length error is specially important for VLBI, as the quality of time delay and phase delay measurements are directly influenced by it. This specification can be achieved with an optimized construction and a moveable subreflector which is mounted on a hexapod in order to compensate for tiny remaining deformations of the main reflector.

The optics of the radio telescope are based on the concept of an axially displaced ellipse reflector. The vertex of the rotating parabel defining the surface of the main reflector is shifted about 0.72 m from the line of sight. Therefore the primary focus becomes a ring structure if the parabel rotates with this offset. This is called ring focus design. Consequently the shape of the subreflector must bring the primary focal ring into a secondary focal point. This is achieved by a rotating ellipse, which secondary focus intersects with the line of sight as rotational axis.

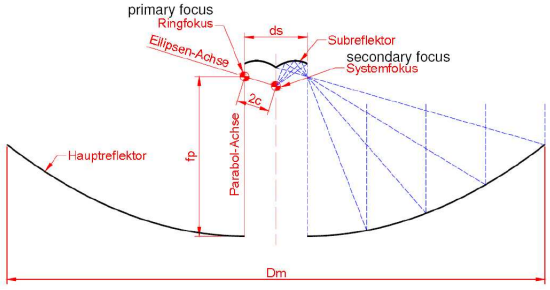

Figure 3. The optics of the Twin Telescope Wettzell. The parabel is shifted apart by the distance of ds. Therefore the subreflector in the central part does not shadow the illumination of the main reflector.

The advantages of the ring focus optics are threefold:

- The subreflector does not shadow the main reflector. Only the supports of the subreflector are going to shadow small areas of the subreflector.
- The feed horn can be positioned close to the subreflector as needed for wideband feeds.

- The shape of of the subreflector minimizes backward reflection towards the feed horn (in contrast to a usual Cassegrain optics).

- Rays from the main reflector rim illuminate the pointed vertex of the subreflector, while rays from the central area illuminate the subreflector rim. The provoked electrical field within the feed is dominated by the outer main reflector surface, which has more reflecting surface than the central area. Therefore the ring focus optics optimize the feed illumination and a high effenciency above 70% seems to be feasible.

In summary: The TTW radio telescope design for geodetic VLBI is a rigorous attempt to realize the aims of VLBI2010. The VLBI2010 specifications request a new design of radio telescopes meeting these challenging criterias.

4.2 Preparation for the constructions at Wettzell

The twin telescope needs additional and suitable space at the Geodetic Observatory Wettzell. Therefore an adjacent plot of land to the Observatory was acquired during 2007. In order to find the best locations at the new land for a solid foundation which is stable to the millimeter level during the coming two decades (lifetime of TTW) a profound soil analisis was made during 2008. A total number of more than 15 drillings down to a depths of 16 m gave a clue about the underground situation. Based on this analysis the final positions for the two radio telescopes and the operation building could be defined.

One of the telescopes will be setup close to the gravity meter house of the Geodetic Observatory. As the constructions might have an impact to the long standing observation series, a new gravity meter house closer to the "quiet" area of Wettzell next to the laser gyroscope was built. It is planned to continue with measurements of gravity at both sites and study the impact of the TTW. If the TTW will have an intollerable impact to the gravity measurements, then the observation might be discontinued at the old gravity site.

Figure 4. Drilling cores of three drillings ($0-16$ m) indicating stable rocky underground to define one radio telescope location. Each box corresponds to one meter depth from surface (most upper box) to -16 m (bottom box).

5 The second project year, 2009

5.1 Construction of the radio telescopes

After the design review by the end of 2008, first telescope parts will be manufactured during 2009. An open item was the front end for the TTW. The reason for this is the non-existence of an appropiate feed horn which covers the spectral range $2-18$ GHz and has one focal point for any frequency. The decision on the future feeds the IVS depends also on the future observation modes which are planned to be executed. The IVS organized with the local staff of the Geodetic Observatory Wettzell a *Workshop on Future Radio Frequencies and Feeds* on March 18-20, 2009. This workshop came up with a recommendation which was adopted at the IVS-Directing Board meeting in Bordeaux on March 23, 2009. The content of the recommendation is:

- *The initial implementation of the VLBI2010 system needs to be capable of observing the broadband range of 2.2 to 14 GHz.*

- *The VLBI2010 system needs to be capable of S/X operation.*

- *The antenna should allow for a possible future inclusion of Ka-band (32 GHz) operation.*

- *The complete end-to-end operation of the VLBI2010 system should be demonstrated in*

a campaign in early 2012. As many antennas as possible should participate.

- *A plan should be established for the transition from the legacy S/X system to the VLBI2010 broadband delay system. Such a transition plan can be beneficial for obtaining future funding and will support a timely changeover.*

Based on these recommendations the TTW project group is specifying now the feed and receiver parts. Two concurrent feed designs are currently under discussion (FRFF 2009): A proposed variation of the Eleven-feed of Prof. Per-Simon Kildal from Chalmers University in Gothemburg, offering the one continuous spectral band from 2.2–14 GHz. A prototype is under development and will be tested during 2009. A cooled version will be developed in 2010. As an alternative a triple band feed is proposed by Mirad AG in Switzerland. This proposal will cover an extended S-band (~ 2 GHz) and X-band ($\sim 8-9$ GHz) plus a third Ka-band (~ 32 GHz). Both development options will be tailored to the given geometrical constraints of the telescope optics and later be considered for implementation.

5.2 Constructions at Wettzell

For 2009 it is scheduled to start with the preparation of the construction area. Infrastructure (electricity, communication, water, etc.) has to be layed to the new property. The concrete fundaments for the radio telescopes and the concrete towers should be constructed during 2009. It is planned to complete the towers in 2010. Therefore the platforms for constructing the main reflector must be prepared as well as the underground to host a heavy crane when the moment of reflector installation comes. The operations building shall be part of the constructions which are planned also to begin in 2009.

6 Conclusion

The Twin Telescope Wettzell Project is an ongoing project, scheduled for the period 2008-2011. It is a first rigorous attempt to realize the aspects of the VLBI2010 vision of the IVS. It involves new optics for VLBI radiotelescopes which are crucial for the use of new wideband feeds operating in the spectrum of at least $2.2-14$ GHz. The radio telescopes will be constructed of a long lasting geodetic monument capable to resist continuous (7/24) very fast movements minimizing the slewing from source to source. The construction needs to be extremely stiff to minimize deformations and to enable phase delay observations. The sum of these criterias cannot be addressed with an upgrade of an existing radio telescope - it makes a new construction necessary.

Acknowledgements The authors are grateful to Dr. Wolfgang Schlüter, former Director of the Geodetic Observatory Wettzell, who setup the TTW-Project successfully before he entered the second phase (liberation of duties) of his early retirement programme in August 2008.

References

Schuh H., Charlot P., Hase H., Himwich E., Kingham K., Klatt C., Ma C., Malkin Z., Niell A., Nothnagel A., Schlüter W., Takashima K., Vandenberg N., 2003, IVS Working Group 2 for Product Specification and Observing Programs, Final Report, http://ivscc.gsfc.nasa.gov/about/wg/wg2/IVS_WG2_report_130202-letter.pdf

Niell A., Whitney A., Petrachenko B., Schlüter W., Vandenberg N., Hase H., Koyama Y., Ma C., Schuh H., Tuccari G., 2005, VLBI2010 - A Vision for Geodetic VLBI, Current and Future Requirements for Geodetic VLBI Systems, http://ivscc.gsfc.nasa.gov/about/wg/wg3/IVS_WG3_report_050916.pdf

IVS-Webpage, http://ivscc.gsfc.nasa.gov/program/search-master-form.html#usage

Dassing R., Hase H., Kilger R., Kronschnabl G., Lauber P., Schlüter W., Schwarz W., 2007, Technical Specification for the Design, Manufacturing and Construction of the Twin-Telescope Wettzell (TTW), Geodätisches Observatorium Wettzell, (unpublished)

Petrachenko B., Boehm J., MacMillan D., Pany A., Searle T., Wresnik J., 2008, VLBI2010 Antenna Slew Rate Study, Proceedings of the 5^{th} IVS General Meeting, St. Petersburg

Contributions to the IVS Workshop on Future Radio Frequencies and Feeds, 2009, Wettzell, Germany, http://www.fs.wettzell.de/veranstaltungen/vlbi/frff2009/frff2009.html

An Atlantic Network of Geodynamical and Space Stations (Project RAEGE)

J. Gómez-González, F. Colomer
Instituto Geográfico Nacional (IGN), Calle General Ibañez de Ibero 3, E-28003 Madrid, Spain

J.A. López-Fernández
Instituto Geográfico Nacional (IGN), Cerro de la Palera s/n, 19141, Yebes, Spain

Abstract. Project RAEGE ("Red Atlántica de Estaciones Geodinámicas y Espaciales") intends to set up a Spanish-Portuguese network of four Geodetic Fundamental Stations in Yebes (1), Canary Islands (1), and Açores Islands (2), as part of the developments needed for the IVS VLBI2010 scenario. It is envisaged that each Geodetic Fundamental Station will be equipped with one radiotelescope of VLBI2010 specifications (at least 12-m diameter, able to operate up to 40 GHz, fast slewing speed), one superconducting gravimeter, one permanent GNSS station and, at least at the Yebes site, one SLR facility. The National Geographical Institute of Spain (IGN) has experience in VLBI, being member of the European VLBI Network since 1993, and participating in geodetic VLBI campaigns with the 14-m radiotelescope in Yebes since 1995. A new 40-m radiotelescope has been built and recently put in operation, already participating in IVS campaigns. Infrastructure for the new stations in Yebes and Canary Islands are available. An agreement between IGN and the Portuguese Geographical Institute (IGP) and the Regional Government at Açores ensures that the RAEGE project can become a reality by 2012.

Keywords. IVS, VLBI2010, VLBI, Network, Plate Tectonics, Reference frames, Earth orientation

1 Introduction

The IVS Working Group #3 (VLBI2010) has defined the specifications of the new observing systems in order to achieve 1 mm accuracy for positions, and 0.1 mm/yr accuracy for station velocities: small (12-m) antennas, slew speeds larger than 7.5°/s, recording rates of 8–16 Gbps, and new feeds to allow observations in the range 2–18 GHz (see IVS WG3 website). Several scientific institutes are working to build new geodetic VLBI sites with these characteristics in Germany, Australia/New Zealand, South Korea, USA, and others are considering their options in Norway, Saudi Arabia, India, and Turkey (Schuh & Behrend, 2008).

2 Location of the RAEGE stations

RAEGE comprises the construction of four Geodetic Fundamental Stations including radio telescopes that fulfill the characteristics of the next generation VLBI system (dubbed VLBI2010) being developed under the auspices of the International VLBI Service for Geodesy and Astrometry (IVS). The four RAEGE stations will be located in the Atlantic region (Fig. 1): one in mainland Spain at Yebes, one on the Canary Islands (Spain), and two on different islands (and different tectonic plates, Fig. 2) of the Açores islands (Portugal).

The strategic location of these four stations will allow the monitoring of crustal dynamics of three tectonic plates: Eurasian (Yebes), African (Lanzarote and Santa María), and American (Flores). Together with the Wettzell antennas and others (like the new antenna planned in Fairbanks, Alaska), also plate rotation will be measured (for which at least two antennas per plate are needed).

3 RAEGE equipment

In order to fulfill the requirements of the IVS VLBI2010 vision, three or more geodetic techniques need to be colocated at each Geodetic Fundamental Station. Therefore, at each of the four sites a new antenna of the characteristics described by the VLBI2010 specifications will be

Figure 1. Location of the RAEGE stations.

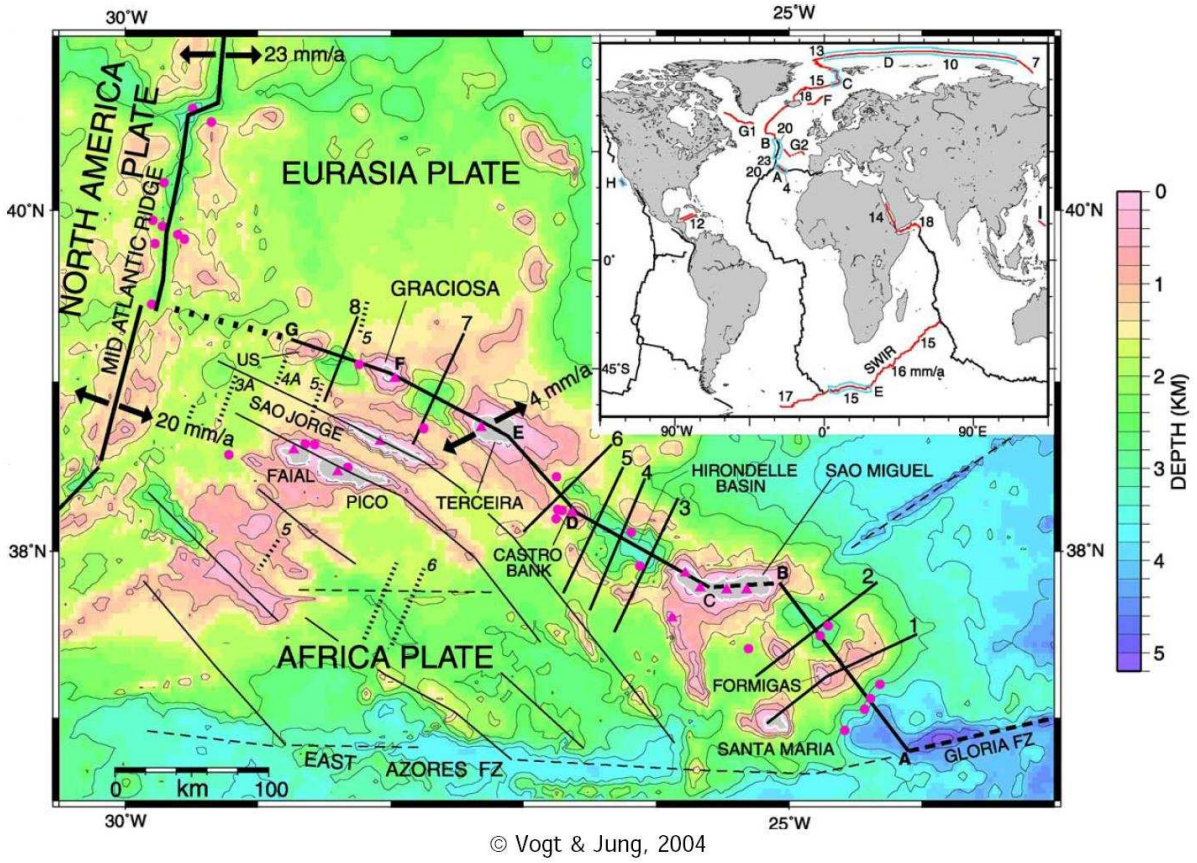

Figure 2. Plate tectonics in the Açores region.

Figure 3. Possible placement of the geodetic instruments at the RAEGE station in Yebes (Spain).

built: 12–15 m parabollic antenna, capable of observing in the 2–18 GHz frequency range (and indeed up to 40 GHz in order to be a useful astronomical instrument), very fast slew velocities (up to 12°/sec), etc. These are the characteristics of the Twin-Telescope Wettzell (TTW) project, described in Hase et al. (2008).

Moreover, a GNSS permanent receiver (GPS, Galileo, etc.) will be installed at each site, and appropriate local-tie measurements between the VLBI antenna and the GNSS receiver will be performed regularly.

A superconducting gravimeter will be installed. Initially, a SLR system will be installed in Yebes; other could be installed also in the other RAEGE stations in the future.

4 Summary

The construction and operation of the RAEGE network, as currently envisioned, will constitute a leading-edge scientific and technical contribution to the global VLBI2010 efforts. VLBI2010 itself will entail a qualitative improvement of the geodetic VLBI technique and of the capability to conduct scientific research in the coming years in fields such as Earth orientation and crustal dynamics.

From a technological point of view, RAEGE will employ the most modern instrumentation for the VLBI2010-type radio telescopes as well as the other equipment (e.g., superconducting gravimeters and GNSS receivers and antennas). The construction and installation of this instrumentation can surely be realized, as the IGN holds appropriate laboratories and workshops, and has skilled technical staff (at Yebes Observatory) in the respective techniques.

The placement of the future RAEGE stations (Yebes, Açores, and Canary Islands) is of great value for geodynamical studies both for its geographical and its tectonic distribution (Eurasian, African, and American plates).

The international scientific communities of astronomy, geodesy, and geophysics (in particular those of Spain and Portugal) will benefit from the RAEGE project. Spanish and Portuguese engineers will have the additional benefit of performing technical developments in the fields of mechanics, electronics, computers, and telecommunications, while the instruments and equipment of the RAEGE project are being constructed, installed, and put into operation.

Acknowledgements We are grateful to Luisa Magalhães (Secretaria Regional da Ciência, Tecnologia e

Equipamentos, Direcção de Serviços de Cartografia e Informação Geográfica, Regional Government of Açores) and Joao Carlos Nunes (Geosciences Departament, Açores University) for their enthusiasm and help in the development of the RAEGE project in Portugal.

References

IVS WG3 website on the VLBI2010 project: `http://ivscc.gsfc.nasa.gov/about/wg/wg3/index.html`

Schuh H., Behrend D., 2008, IVS plans and perspectives, The 5th IVS General Meeting Proceedings, p. 3-7

Hase H., Dassing R., Kronschnabl G., et al. 2008, Twin Telescope Wettzell: a VLBI2010 Radio Telescope Project, The 5th IVS General Meeting Proceedings, p. 109-113

A concept for remote control of VLBI-telescopes and first experiences at Wettzell

A. Neidhardt, M. Ettl, R. Zeitlhöfler: FESG, TUM, Geodätisches Observatorium Wettzell, Sackenrieder Str. 25, D-93444 Bad Kötzting, Germany

C. Plötz, M. Mühlbauer, R. Dassing, H. Hase: BKG, Geodätisches Observatorium Wettzell, Sackenrieder Str. 25, D-93444 Bad Kötzting, Germany

S. Sobarzo, C. Herrera: UdeC, Camino Einstein Km 2,5., Casilla 4036, Correo 3, Concepción, Chile

W. Alef, H. Rottmann: MPIfR, Auf dem Hügel 69, 53121 Bonn, Germany

E. Himwich: NASA/GSFC, Greenbelt, MD 20771, USA

Abstract. The requirements for VLBI systems are increasing: higher observation density schedules, real-time access for changing schedules, more automation of observations and remote control of complete sites are being planned. To support these changes new additional software components are required. The addition of (semi-) autonomous, remote accessible control features, which are becoming a reality now will provide needed support by offering reliable, safe, and modular structures from the high-level controlling layers down to the basic equipment interaction elements. An extension to the current NASA Field System (FS) with remotely accessible, autonomous process cells is being developed at the Wettzell Geodetic Observatory. It uses the specially designed middleware generator "idl2rpc.pl", developed at Wettzell, to generate the remote C++- interfaces for communication issues. A new modern graphical user interface in combination with an initial programmatic interface to the FS, both developed as extensions, demonstrate the capability for controlling radio telescopes remotely. The first successful remote control tests, with operators present, during regular experiments with the telescopes at O'Higgins, Concepción and Wettzell have demonstrated that this approach works well in the global communication network.

Keywords. VLBI, field system, automation, remote control, e-control, idl2rpc, middleware

1 Introduction

Personnel staff from the Geodetic Observatory Wettzell operate not only the 20 meter radio telescope at Wettzell. In cooperation with other institutes they also run the 9 meter radio telescope at the German Antarctic Receiving Station (GARS) O'Higgins, Antarctica and the 6 meter radio telescope of the Transportable Integrated Geodetic Observatory (TIGO) Concepción, Chile for geodetic VLBI experiments. Because of the remote locations especially in case of the telescope in the Antarctica and because of the increasing requirements for such observations, e.g. relating to the number of experiments, a first concept was developed, to control sites remotely. This is also an appropriate starting point for the control modes of the new VLBI2010 TWIN radio telescope at Wettzell.

The current equipment at VLBI radio telescopes is controlled by the NASA Field System (FS) software package, which is a very stable, well known and well supported package. But the current realisation of the FS has some deficits according to that new possibilities of remote control and remote attendance. Already existing tools to forward mouse, keyboard and video signals are also suboptimal, because they don't allow monitoring of the internet connection itself. This is especially important for safety issues at a site to facilitate safety actions when no responsible observer is connected anymore. Therefore it is necessary to extend the given controlling mechanism by a Ethernet based, safe and stable remote communication. Since most of the new devices controlled by the field system are also connected via ethernet mechanisms the new concept also includes ideas to standardize such individual communication needs. Together it offers the appropriate elements for remote control as a new VLBI observation mode, possibly named "e-control".

2 The layers of e-control

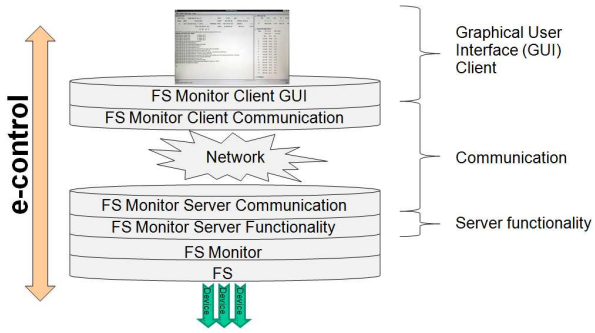

Figure 1. The complete e-control stack.

The given remote control design realises a classic client-server-model on the basis of a communication with Transmission Control Protocol over Internet Protocol (TCP/IP) or User Datagram Protocol over Internet Protocol (UDP/IP). In such a client-server-model a service requesting client starts the communication and sends an order request via message communication to a service offering server. At the server side the order is processed and an answer message is returned to the client (Singhal et al., 1994). The client-server-based complete stack for e-control from user interaction via remote procedure call communication to the FS interaction is shown in Fig. 1.

One of the main drivers in the given design is a consequent separation of control, communication and presentation logic. The complete arithmetic and workflow control logic reside in the server, defined as device control code. It is an autonomous working process which interacts with the remote controlled device (here at this level, the FS). The communication code independently connects the server to the outer world for requesting clients. And the clients are only used to realize an user interface with a presentation of the server processed elements.

2.1 The communication middleware with remote procedure calls

In classic communication networks each client server interaction is programmed individually during the software development process. This proprietary approach makes it more difficult to set up a remote control and to include or adapt new properties of remote usable devices. Another more modern attempt reduces the efforts of communication programming by defining a standardized way for the transmission of so called remote procedure calls (RPC). RPCs are comparable to local calls of procedures (functions) in a structured program but realized as control and data flows over a communication network to allow a standardized interaction between a requesting client and a service offering server (Singhal et al., 1994). The client just calls a procedure or function without the concrete knowledge of the processing location and an additional RPC communication layer realizes the transfer between the client and the remote processing server. The derived answer follows the same way vice versa to the client, so that the procedure call seems as local (see Fig. 2).

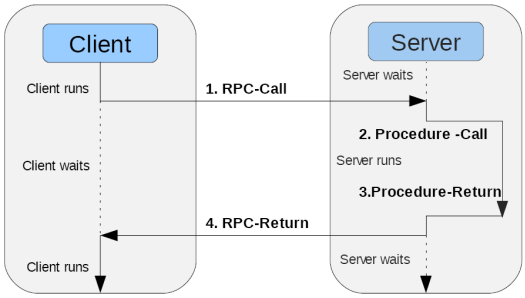

Figure 2. Sketch of the remote procedure call client-server-model (Saxonia Systems, 2007).

To reduce the programming effort the complete communication layer within this model is created by a special RPC generator which reads an interface definition file and produces all of the necessary modules. They can directly be used in the application code. So the application programmer has only to think about his application specific code and not about the lower-level data transfer parts. Modern networking techniques know several realizations of the RPC because this communication method is also the basis for the distribution platforms of modern web services. These distribution platforms are also known as distributed systems. A distributed system consists of several independent computers (processors), which are connected together to solve a collective task in a cooperative way. During the processing time they don't share mem-

ory, clocks or other hardware and just communicate information while transferring messages via a computer network (Singhal et al., 1994 and Puder et al., 2001).

For the planned remote control of the FS, basic and compact realizations are more flexible and reliable than huge, sophisticated, additional communication packages, which are also in most cases commercially offered. Several basic RPC-realisations are well known over years. In the given context the Open Network Computing Remote Procedure Call (ONC RPC) is a preferred communication technique because it is available in each Linux operating system as standard and has been well tested since the year 1988. To generate the actual communication code units of RPC in the programming language C, the generator "rpcgen" is used which is also part of the Linux operating system. The generated code also includes the platform independent conversion of procedure parameter data using the External Data Representation (XDR; Stevens, 1992).

To update these interface paradigms for modern object oriented implementations an additional C++ layer over the C coded communication was added and to include more sophisticated communication control mechanisms a new, very straight forward code generator "idl2rpc.pl" is used. This code generator is based on a script written in Perl language containing C++/C code templates. The templates are filled using remote function definitions written in a specific Interface Definition Language (IDL) as a high level description of a remote interface. This definition looks similar to C function headers, so that it is easily understandable. The generator converts the IDL description into standard RPC equivalent code already supported by the Linux operating system. Several C++ adaptor classes for the C written RPC communication are created as well as necessary modules for threads to use in parallel tasks and with semaphores to protect critical sections. In only a few steps the complete communication is generated (see Fig. 3). For the application developer only a few files are important to edit while the rest automatically realize the communication.

With this approach the application programmer doesn't have to consider communication concerns and can concentrate on the actual application tasks. But he should use the possibilities on server side like threaded periodic loop activities, etc., to realize independent servers which always keep stable states. The servers can be located wherever they are needed to realize the structures of a distributed system. For reliability each server contains something like a watchdog process which always restarts it after an unexpected crash. In addition to that an automatic safety device (ASD) is implemented which expects periodic requests from responsible clients. If this "alive"-signal is not detected, the server can activate a specific routine which leads the system into a stable and safe state again (Neidhardt, 2009).

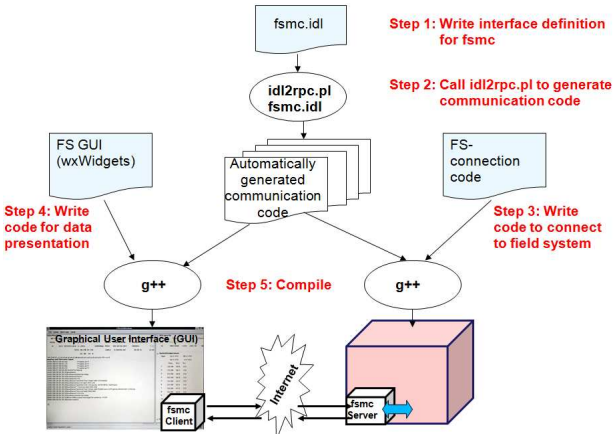

Figure 3. The generation process using the code generator "idl2rpc.pl".

In case of the FS an additional client-server-communication is defined using the new idl2rpc.pl. In the first implementation it consists only of a few methods returning the local information output as string arrays to the remote requesting client. The client can also send a string command to the server. The server itself is the main part of the proposed extension to the FS.

2.2 The field system extension as a remote accessible, autonomous process cell

The server skeleton is created automatically and is completed with functions to communicate to the existing FS. Therefore an additional C-written adapter (FS monitor) allows the connection to the FS via shared memory access. The commands are injected into FS using the supported injection methods. To smooth the communication behaviour the server uses threads to separate between the asynchronous remote

procedure calls and the contact with the FS. Semaphore protected variables allow the handling of critical sections when both tasks work in parallel with the same variable values.

Overall the created server acts completely autonomously. It can be used to check system status information independently and can decide what to do to keep stable and safe states. Such controlling utilities can be defined as autonomous process cells. The generated watchdog process keeps it alive and the automatic safety device allows to register if a responsible client is connected. After a breakdown of the communication to the client the server can operate completely autonomous until a critical situation (e.g. increase of wind speed to a level which is critical for the telescope) forces it to run into a safe state. In combination with additional monitoring information around the site (meteorology, power supply, air conditioning status, etc.) that compact server extends the FS for a reliable remote control.

2.3 The field system client as a remote graphical user interface

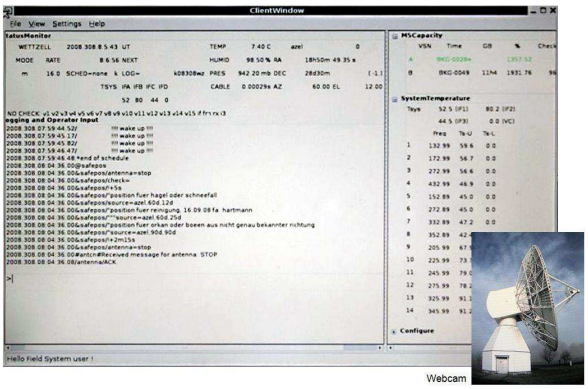

Figure 4. The graphical user interface on the basis of wxWidgets.

On the other end of the remote control the operator interacts with the system. For that it is possible to use different and parallel user interface clients. Because of the consequent separation of control and presentation logic the client can be realized in different ways. So it is possible to implement command line clients as well as high sophisticated web applications or graphical user interfaces. This permits management of devices remotely via browser, command line and/or graphical user interface.

For a first general realization all servers can have a rudimentary command line control. In addition to that it is useful to offer a graphical user interface. For the described FS extension wxWidgets is the prefered way to do this. It is a C++ based open source framework for platform independent developments of graphical user interfaces (Smart et al., 2005). Although the current RPC generator only supports Linux systems (32 and 64 Bit), the graphical user interface is modular enough to support different platforms like Windows, Linux, OSX and others. In terms of the proposed FS extension a new graphical user interface was created using the wxWidgets framework for its realisation (see Fig. 4). To keep usage similar, the display elements are organized to be like those of the current local interface to the FS.

2.4 Safety and security

To protect humans and the system itself safety and security concepts are in development in addition to the inline safety functionality of the generated communication. Safety hereby means the local protection against local error states or critical situations, possible for automatically moving hardware. For the basis of an autonomous and stable software application, the programmer should follow previously defined design rules. For example, at Wettzell the developed elements follow the Wettzell design rules, which describe how code must be structured, documented, commented and what is allowed. But no software is good enough to have no bugs. So an additional, modular and multi-layered system monitoring hardware is in production which should check all of the important system states, like temperatures, weather conditions, safety switches and so on, parallely to the FS. This hardware is realized with standard equipment on a robust, well known architecture and supports several individual, vendor independent sensor devices. It is created with open source products in combination with Linux operating systems (also with a minimal installation) and implements internally also the “idl2rpc.pl” created communication system. So it is an additional parallel monitoring system for safety reasons, also used for emergency issues.

Security however means the protection of the

system from not allowed activities done by foreign attackers or users without the sufficient right policies. All of the communication activities are based on simple socket communications with TCP/IP or UDP/IP with fixable ports on which the additional RPC layer is established. To bring in an additional level of security the Secure Shell (SSH) tunneling methods can be used to build up an access protection. SSH hereby allows several authentication possibilities like passwords, passphrases and key files or combinations of them. For the internal correct access for operator actions it is planned to realize an authentication (registration of a user with username and password) and authorization (personification of a user for a specific remote procedure with dedicated rights) similar to what is already implemented in other projects at Wettzell (Neidhardt, 2006). This should allow a first attempt of safe and secure remote control from almost any place.

3 Remote control tests

To prove the functionality of the remote control and the general character of the implementations as well, several tests were initiated to run the radio telescopes operated by Wettzell with the described software. Several 24 hour and 1 hour intensive experiments were successfully run by remote control also at the very remote site O'Higgins. These tests will be extended and will lead to routine remote operation of VLBI experiments at Wettzell.

4 Summary

Overall the described method allows the development of distributed systems consisting of several independent servers which act completely autonomously. It extends given structures to have a remote control possibility and splits complex systems up into several manageable units interacting together with a general, standardized but also flexible communication method. The concept can also be used to update the internal structures of the FS to connect it to a future network of controllable instruments. It offers a possibility to add devices like the new Digital Baseband Converters (DBBC) with standardized and stable methods to the FS.

The described software concept is a product of a long development done by several developers at Wettzell. The result is an option for upcoming Fundamental Stations with several different colocated measuring systems like radio telescopes and laser ranging systems to realize remotely controllable, autonomous subsystems on a basis of a stable, flexible and general communication platform. It can be used to reduce development time for highly available systems especially along the goals of the Global Geodetic Observing System (GGOS). New observing strategies proposed in VLBI2010 can be realised also with very remote stations. But nevertheless there are always some situations which cannot be controlled and handled by such an automated system (like power failures where e.g. the laser telescope dome is not closed automatically), so that responsible, well educated engineers at the sites should always be the final instance of automation.

References

Neidhardt, Alexander: Verbesserung des Datenmanagements in inhomogenen Rechnernetzen geodätischer Messeinrichtungen auf der Basis von Middleware und Dateisystemen am Beispiel der Fundamentalstation Wettzell. Dissertation, Mitteilungen des Bundesamtes für Kartographie und Geodäsie, Nr. 37, Bonifatius GmbH 2006

Neidhardt, Alexander: Manual for the remote procedure call generator "idl2rpc.pl". Geodetic Observatory Wettzell 2009 (latest version)

Singhal, Mukesh; Shivaratri, Niranjan G.: Advanced Concepts in Operating Systems. McGraw-Hill, Inc. 1994

Puder, Arno; Römer, Kay: Middleware für verteilte Systeme. 1. Auflage. dpunkt-Verlag GmbH Heidelberg 2001

Saxonia Systems: Remote Procedure Call, http://www.linuxfibel.de/rpc.htm, Download 2007-04-23

Smart, Julian; Hock, Kevin; Csomor, Stefan: Cross-Platform GUI Programming with wxWidgets. Prentice Hall International 2005

Stevens, Richard W.: Programmieren von UNIX-Netzen. Grundlagen, Programmierung, Anwendung. Prentice-Hall International, Inc. London 1992

VLBI2010 Project for Geodesy and Astrometry

A.E. Niell
MIT Haystack Observatory, USA
for the VLBI2010 Committee and the Broadband Development Team

Abstract. Efforts are underway to define the next generation geodetic VLBI system and to demonstrate that the required concepts can be implemented. Numerical simulations have been used to define the system requirements, and proof-of concept versions of the required instrumentation have been built and are being tested.
Keywords. VLBI, VLBI2010

1 Introduction

Very Long Baseline Interferometry (VLBI), Satellite Laser Ranging, GPS, and DORIS measure the shape of the Earth and its orientation in space. VLBI provides the Celestial Reference Frame as defined by the extragalactic radio objects that are the source of the observed radio emission, the orientation of the spin axis in inertial space, and time. VLBI also contributes significantly to determining the scale of the Earth's size.

Due to the requirement for greater accuracy and to the declining operational capability of aging antennas, a new geodetic VLBI network is needed. The desirable properties of that network have been established by the VLBI2010 Committee, which was established as Working Group 3 (WG3) within the International VLBI Service (IVS). Based on the recommendations of this group, a proof-of-concept demonstration is being implemented using two antennas of the current geodetic VLBI network. Prototype instrumentation has been mounted on these antennas, and initial observations have been made to evaluate the new concepts.

Since a primary limitation to the accuracy of geodetic VLBI is the variable nature of the neutral atmosphere, the goal of greater accuracy will be addressed by making much more frequent observations around the visible sky with each antenna.

The next-generation system will consist of a) much faster slewing antennas and b) data acquisition systems that accept signals in four bands chosen to be at the optimal frequencies in the range from the current S-band up to approximately 14 GHz.

In this paper the work of the VLBI2010 working group and the results to date of the proof-of-concept demonstration are described. A more complete report of the working groups progress up to the end of 2008 can be found in Petrachenko et al. (2009).

2 Recommendations of the VLBI2010 Committee

The goals to be fulfilled by the next generation geodetic VLBI system are:

- 1-mm position accuracy on global scales
- continuous measurements for time series of station positions and Earth orientation parameters
- turnaround time to initial geodetic results of less than 24 hours

To evaluate proposed hardware configurations, observing scenarios, and analysis models, a large number of Monte Carlo simulations was run by the simulation team using several geodetic VLBI analysis packages. For these simulations the parameters varied were the number of antenna sites in a network (8, 16, 24, or 32), the type of schedule, the stochastic properties of both the atmosphere and the frequency standards, and the amount of white noise affecting the delay observable. The figure of merit used to

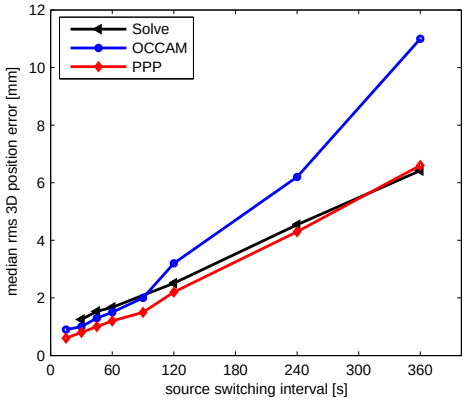

Figure 1. Median of the rms 3D position errors for uniform sky schedules with regular source-switching intervals ranging from 15 seconds to 360 seconds. The delay noise was 4 ps per baseline observation; the clock Allen Standard Deviation was 1×10^{-14} at 50 minutes; and the turbulence parameters were modeled for the latitude of the sites (see Appendix A of Petrachenko et al., 2009).

compare the results was the median of the RMSs of the three-dimensional positions for the sites in the network. The RMS is taken over each set of twenty-five simulations for a given set of parameters for a 24-hour schedule.

A major conclusion from the simulations is that the median RMS position error decreases almost linearly with the source-switching interval (Figure 1). This is attributed to improved estimation of the atmosphere delay as the atmosphere is sampled more frequently in more different directions. If the switching times needed for 1 mm RMS are related to antenna slew rates and accelerations, rates of approximately 12°/second in azimuth and 4°/second in elevation are needed for a standard az/el antenna. However, to achieve 1.5 mm RMS the numbers are relaxed to about 5°/second in azimuth and 1.5°/second in elevation, a much more modest requirement.

In general it is less expensive to achieve high slew rates the smaller the antenna, but sufficient sensitivity must be attained to detect a large number of radio sources (∼100) in the short times (∼5 seconds) allowed for scans in the fast-switching schedules. The simulations showed that for a data rate of 8 Gbits per second, which is achievable with recent advances in VLBI technology, an antenna of 12 m diameter would satisfy the requirements. In order to obtain the target delay precision of 4 psec per observation, a new approach was proposed. Instead of the two-band S/X operation, four bands will be observed spanning the frequency range from ∼2 GHz to ∼14 GHz to be able to resolve the phase delay. To distinguish from the S/X group delay used now, the technique is known as broadband delay. The current S- and X-band would be included in order to overlap with the existing systems. This is needed to provide continuity of the reference frames.

The simulations demonstrated that the imprecision in modeling the temporal and spatial variations in the atmosphere delay continues to be the limiting error source. Thus it is important to continue research into better ways to model the atmosphere. Another recommendation from the Committee was to reduce systematic errors by improving electronic calibration, improving or measuring antenna deformation, and correcting the observed phases by modeling radio source structure based on the observations. For the network configuration a minimum of sixteen globally distributed VLBI2010 antennas is recommended.

Much greater detail is provided in the progress report (Petrachenko et al., 2009).

3 The proof-of-concept demonstration

A key new element of VLBI2010 is the broadband delay. In order to demonstrate that the concept is feasible, all of the components of the broadband delay system have been implemented on two antennas, the 18-m antenna at the Haystack Observatory in Westford, Massachusetts, and the 5-m MV-3 antenna at the NASA Goddard Space Flight Center in Maryland, a baseline of 597 km. The combined effective collecting area of these two antennas is somewhat less than that of two 12 m antennas but should be sufficient to validate the concept.

To receive the multiple bands required by the broadband delay technique, the proof-of-concept system uses a commercially available feed that covers the range ∼2 GHz to ∼18 GHz in two linear polarizations. To eliminate unacceptable ohmic losses at higher frequencies, the feed is cooled to approximately 20 K in a cryogenic Dewar. Following the feed in the Dewar are, for each polarization, a high-pass filter, a directional coupler, and a low noise amplifier. As part of the

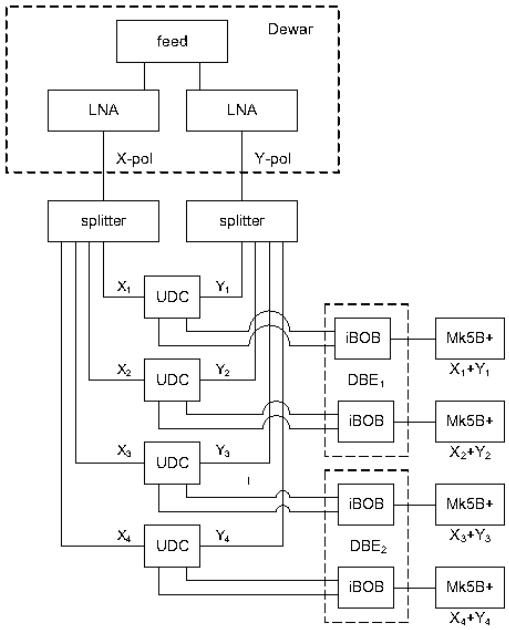

Figure 2. Diagram of the main components of the broadband delay data acquisition chains from feed through data recorder.

VLBI2010 effort a new phase calibration generator has been developed (Rogers, 2008) that utilizes digital components rather than the tunnel diode used for the Mark IV version. The output is injected through a directional coupler in each path. The rail spacing is currently 5 MHz, although 10 MHz spacing is also being considered. Injection of a noise diode signal for amplitude calibration is planned.

See Figure 2 for an overview of the system.

The radio frequency (RF) signal for each polarization is carried from the Dewar to the control room on a separate optical fiber. In the control room each RF polarization channel is divided into four branches. The two polarizations from each branch are then frequency converted in an UpDown Converter (UDC) and filtered to give a 512 MHz band, digitized in a Digital Back End (DBE), and recorded as a pair. Four UDCs, DBEs, and Mark5B+ recorders are required for the four bands. Half of the data from each polarization are recorded as two bit samples at a data rate of 2 Gbits/second per band.

The use of a broadband feed, rather than the concentric dual frequency S/X feed, introduces several challenges. One consequence of being broadband is that any feed will intrinsically produce only linear polarization. This is not a fundamental problem, and full sensitivity will be obtained by cross-correlating all four polarization products. It is likely that this would be required for circular polarization as well to obtain the highest phase delay precision in the face of not-perfect polarization properties. Two other properties of the feed are the beamwidth and the phase center location. It is desirable that the feed has the same beamwidth at all frequencies in order to illuminate the sub-reflector or reflector equally, and that the phase center be independent of frequency in order to obtain the maximum sensitivity at all frequencies. Several research projects to achieve these characteristics are underway, but in the meantime a commercial feed is being used. One consequence of phase center variation is demonstrated in Figure 3 which shows the relative cross-correlation amplitude at four bands in both polarizations as the focus was varied at Westford. For subsequent observations a setting of +1.5 was used. A similar test has not been made for MV-3.

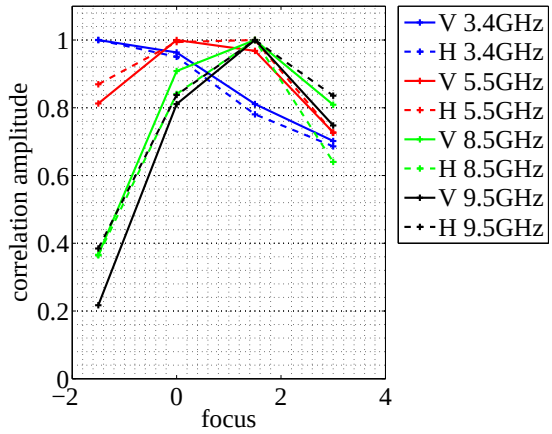

Figure 3. Amplitudes normalized to maximum value. The focus value for maximum sensitivity moves to more positive values as the frequency increase.

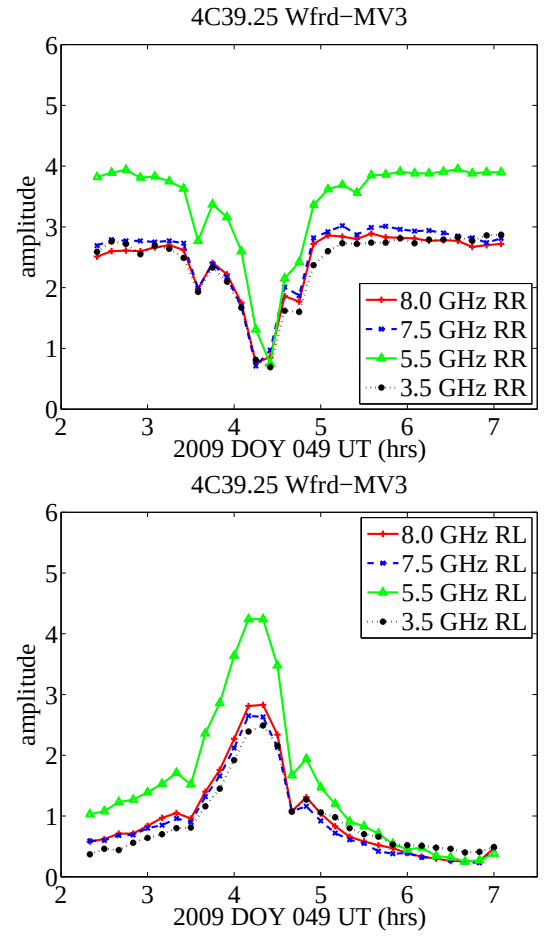

Figure 4. Amplitudes for a) parallel and b) orthogonal polarization products.

The effect of using linear polarizations was explored by observing the source 4C39.25, which passes north of MV-3 and south of Westford, resulting in a rotation of the differential parallactic angle of almost 180°, passing from parallel to anti-parallel and back to parallel. The amplitudes for initially parallel and orthogonal polarizations (R corresponds to locally horizontal polarization at low elevation; L corresponds to locally vertical polarization) are shown in Figure 4. The minima at approximately 3.5 UT and 4.7 UT correspond to the time during which first Westford then MV-3 were partially off-source due to azimuth rotation when the source went through transit. The minimum at 4.3 UT, which occurs when the equivalent feed polarizations are at 90°, does not go to zero both because the scan is an average over ten minutes and because the feed polarization purity is not 100%.

4 Plans

There are still significant challenges to verify that accurate phase delays can be obtained from this type of system. Phase cal must be included to demonstrate that phase can be connected across the four bands for all scans, and the corrected phase delays must be shown to be equivalent for the two senses of polarization. In future observations the ability to utilize lower signal-to-noise observations will be explored, and geodetic-type observations will be attempted.

Acknowledgements

The Broadband Development Team:

- MIT Haystack Observatory
  - Chris Beaudoin
  - Brian Corey
  - Alan Hinton
  - Arthur Niell
  - Mike Poirier
  - Alan Rogers
  - Dan Smythe
  - Jason SooHoo
  - Mike Titus
  - Bruce Whittier
- HTSI, Inc
  - Irv Diegel
  - Mark Evangelista

- ▷ Skip Gordon
- ▷ Jay Redmond

- GSFC/NVI
  - ▷ Tom Clark
  - ▷ Ed Himwich
  - ▷ Chuck Kodak

The VLBI2010 Committee:

- Natural Resources Canada, Canada
  - ▷ Bill Petrachenko (Chair)
- Haystack Observatory, Massachusetts Institute of Technology, USA
  - ▷ Brian Corey
  - ▷ Arthur Niell
  - ▷ Alan Whitney
- NVI, Inc./Goddard Space Flight Center, USA
  - ▷ Dirk Behrend
  - ▷ John Gipson
  - ▷ Dan MacMillan
- Institute of Geodesy and Geophysics, University of Technology, Vienna, Austria
  - ▷ Johannes Böhm
  - ▷ Andrea Pany
  - ▷ Jörg Wresnik
- Bordeaux Observatory, France
  - ▷ Patrick Charlot
  - ▷ Arnaud Collioud
- Onsala Space Observatory, Chalmers University of Technology, Sweden
  - ▷ Rüdiger Haas
  - ▷ Tobias Nilsson
- Kashima Space Research Center, NICT, Japan
  - ▷ Thomas Hobiger
  - ▷ Yasuhiro Koyama
- Pulkovo Observatory, Russia
  - ▷ Zinovy Malkin
- Radio Astronomy Institute, Italian National Astrophysical Institute, Italy
  - ▷ Gino Tuccari

Special Thanks

The authors give special thanks to Sandy Weinreb and Hamdi Mani of Caltech for the design of the Dewar, feed, and amplifier system and for their generous advice.

References

Petrachenko et al., 2009, Design Aspects of the VLBI2010 System: Progress Report of the IVS VLBI2010 Committee, April 17, 2009 (ftp://ivscc.gsfc.nasa.gov/pub/misc/V2C/PR-V2C_090417.pdf)

Rogers, A.E.E., 2008, Haystack Observatory Mark5 Memo 75, 14 July, 2008 (http://www.haystack.mit.edu/tech/vlbi/mark5/memo.html)

VLBI2010 simulations at IGG Vienna

J. Wresnik, J. Boehm, A. Pany, H. Schuh
Institute of Geodesy and Geophysics, Vienna University of Technology, 1040 Vienna, Austria

Abstract. The Institute of Geodesy and Geophysics (IGG), Vienna University of Technology, participates in the VLBI2010 Committee (V2C) simulation group with Monte Carlo simulations. The simulator produces artificial group delays by modeling the stochastic processes caused by station clocks, wet troposphere, and additional system errors. The clocks are simulated with a random walk plus integrated random walk, zenith wet delays are derived from a turbulence model, and system errors are represented by white noise. The Monte Carlo simulator is implemented in a modified version of the software package OCCAM and the Kalman Filter approach of OCCAM is applied. Various schedules assuming antennas with different slew speeds (from 1.5°/s to 12°/s in azimuth and 0.7°/s to 3.1°/s in elevation) are compared w.r.t. rms values of station position residuals. The investigation shows that antennas faster than 6°/s in azimuth and 2.1°/s in elevation are definitely needed to achieve the ambitious goals described above. Different scheduling strategies, such as using observation schedules with uniform sky coverage, are also tested.

Keywords. VLBI, VLBI2010, Monte Carlo simulation

1 Introduction

The goals of the next generation VLBI system, VLBI2010, are to achieve 1 mm position accuracy over a 24-hour observing session and to carry out continuous observations, i.e. observing seven days per week. Initial results shall be delivered within 24 hours after taking the data. These goals require a completely new technical and conceptual design of VLBI measurements on which the VLBI2010 Committee (V2C) has worked in the last three years. At the Institute of Geodesy and Geophysics (IGG), Vienna University of Technology, different simulations are performed to evaluate new observing strategies and schedules, to improve the modeling of troposphere refraction and clocks, to find the best antenna design and to optimize the network geometry. Therefore the VLBI analysis software package OCCAM (Titov et al., 2004) was adapted to be used after a sequence of other software programs. First the observations are scheduled with SKED (Vandenberg, 1999) and transformed to NGS format to be read in for further analysis.

The main part of the simulation studies is a so-called Monte Carlo simulator which creates the artificial observations based on realistic properties of the zenith wet delays and clocks. The observed group delay minus computed group delay $(o-c)$ can be described as follows:

$$o-c = (zwd_2 \cdot mfw_2\,(e_2) + cl_2) - (zwd_1 \cdot mfw_1\,(e_1) + cl_1) + wn_{bsl} \quad (1)$$

In Equation (1), $zwd_{1,2}$ are simulated zenith wet delays based on the turbulence model (Nilsson et al., 2007), $cl_{1,2}$ are simulated clock values modeled as a random walk plus integrated random walk (Boehm et al., 2007) at stations 1 and 2, and $mfw_{1,2}(e_{1,2})$ are the wet mapping functions for the elevation angle $e_{1,2}$ which are assumed to be error-free in our studies. For each baseline observation an additional white noise wn_{bsl} is added to model the instrumental errors of stations 1 and 2. The Monte Carlo simulator, implemented in OCCAM, imports zenith wet delay values from the turbulence model, creates clock values for each station and epoch, and adds white noise for each observation. The performance and evaluation of the Monte Carlo simulator, which was mainly done with the comparison to real data from the CONT05 continuous

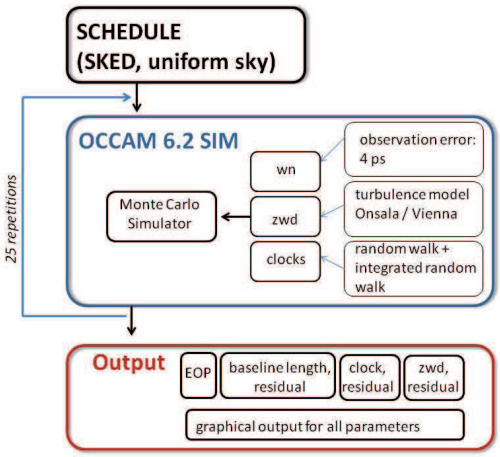

Figure 1. Schematic workflow of a Monte Carlo simulation.

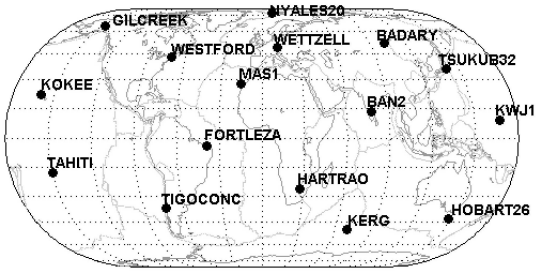

Figure 2. 16-station VLBI2010 test network.

Table 1. Total number of observations for different antenna slew speeds in azimuth and elevation for a 16 station network. The right column shows the median values of the rms of the 3D station positions for the various schedules.

slew speed az [°/s]	slew speed el [°/s]	nr. of obs.	median rms 3D st. pos. [mm]
1.5	0.7	59 392	2.6
3.0	0.7	83 149	1.7
4.5	2.1	134 134	1.5
6.0	2.1	159 088	1.4
12.0	3.5	173 831	1.1

VLBI campaign, are described in Wresnik et al. (2009a). Figure 1 shows the schematic workflow of a Monte Carlo simulation.

The following criteria can be used to evaluate the potential of the VLBI system: baseline length repeatabilities, the root mean square (rms) of the 3D station position residuals, formal errors and standard deviations of the Earth Orientation Parameters (EOP), and the standard deviation between the simulated stochastic processes (troposphere delays, clocks) and their estimates. In this paper, we are focussing on the rms of the 3D station positions to evaluate and compare different observing strategies and scenarios.

2 Slew speeds and scheduling strategies

One of the main goals of the simulations is to obtain information about antenna specifications for the new VLBI2010 system by testing different slew speeds and to develop the perfect scheduling strategie for VLBI2010. Therefore the 16 station network was used (Figure 2) which was agreed by the upon within the V2C.

For testing different slew speeds, in the range from 1.5°/s to 12°/s in azimuth and from 0.7°/s to 3.1°/s in elevation, schedules for the analysis were produced by J. Gipson (NASA/GSFC, Greenbelt, USA) using the software package SKED. To get a sufficiently dense schedule, about 100 of 230 radio sources were taken from a recently compiled list of geodetic sources, and the on-source time was reduced to a maximum of 5 to 10 seconds. The total number of observations for the different schedules are summarized in Table 1. For the Monte Carlo simulations, the zenith wet delays are simulated using the turbulence model, the clocks are simulated with an Allan standard deviation (ASD) of $1{\cdot}10^{-14}$@50 min, and the measurement white noise is simulated using a 4 ps 1-sigma Gaussian random variable. The very small white noise corresponds to that one predicted for the new VLBI2010 antenna and receiving systems.

Comparing the median of the rms of the 3D station position (Table 1), the schedule performance improves steadily from the 1.5°/s in azimuth and 0.7°/s elevation to the 12.0°/s in azimuth and 3.5°/s in elevation.

Another scheduling strategy is to achieve uniform sky coverage at each station, which is essential to de-correlate zenith wet delays, clock parameters, and station heights. This was realized by a source-based scheduling, which means that the scheduler selects e.g. one pair of radio sources, which are located on opposite parts of the sky, from the catalogue without regarding

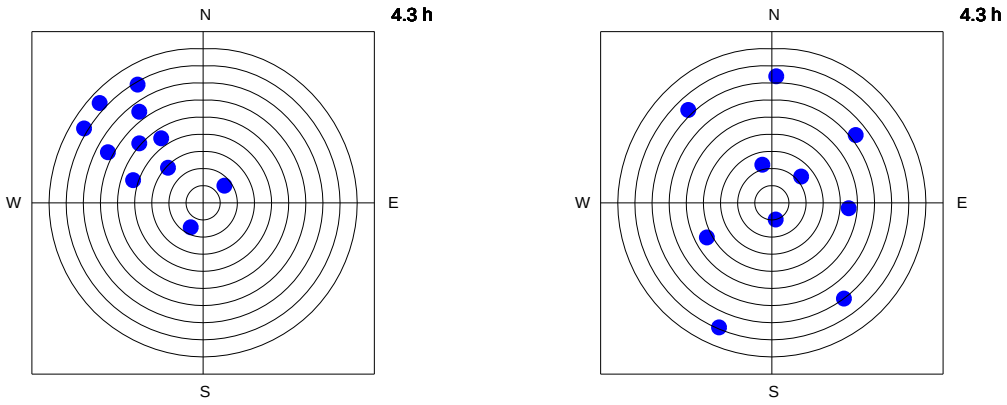

Figure 3. Sky coverage of 6 minutes at station Fortaleza for different scheduling strategies. Left plot: schedule created with the automatic scheduling software SKED, where the observations are often clustered. Right plot: a uniform sky schedule created with a source dependent scheduling strategy, where the observations are well destributed.

their direct impact on individual stations. This strategy requires different sub-nets throughout the session in order to optimize geometry and number of observations. Thus, all possible baselines of the network are observed. In the following, the switching interval between the observed sources was set to a minimum of 15 s and a maximum of 120 s and the uniform sky coverage was achieved for time intervals of 3 min to 12 min. An example of the comparison of the different scheduling strategies is shown in Figure 3, where we can see clearly that for the schedule created with the automatic scheduling software SKED, the observations are clustered compared to the uniform sky approach.

Table 2 shows the settings for switching intervals, time intervals for uniform sky coverage, the slew speeds that are needed to realize the schedule, the number of observations of the schedule, and the medians of the rms values of the 3D station position. The uniform sky schedules were generated by Tony Searle (Natural Resources Canada; NRC).

To be able to compare between different scheduling strategies with different slew speeds, the same approach for simulating the zenith wet delays, clocks, and the measurement white noise as for the slew speed tests was used. The median values of the rms of the 3D station positions show a steady improvement with shortening the switching interval. But shorter than 30 s switching interval, which is similar to the specifications of one antenna of the Wettzell twin telescope, to 15 s switching interval, which implies very unrealistic antenna specifications, there is hardly any difference in the rms values of the 3D station position (see Table 2).

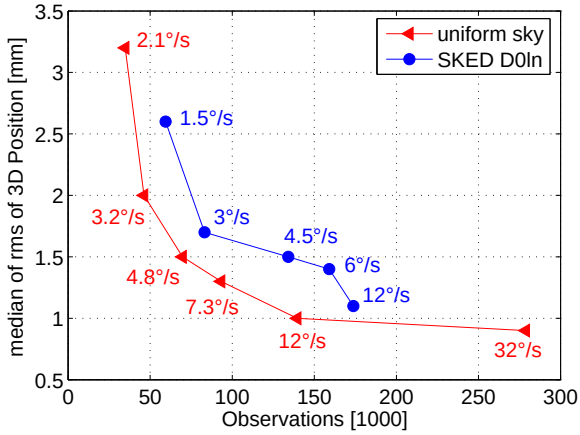

Figure 4. Median of the rms of the 3D station position for the uniform sky (red triangles) and the SKED scheduled (blue circles) sessions against numbers of observations.

The comparison between the different scheduling strategies plotted in Figure 4 shows that up to slew speeds of 12°/s both scheduling strategies follow an improvement of $\sqrt{n}$, where n is the number of observations. The uniform sky approach needs faster antennas to get the same number of observations within 24 hours than the schedule done with SKED. But obversely the uniform sky schedules profit from the uniform distribution of the observations, so that the 1 mm level for the 3D rms of the station position is

Table 2. Switching intervals for the uniform sky coverage schedules. The right column shows the median values of 3D station positions for the various schedules.

switching interval [s]	uniform coverage [min]	slew speed az [°/s]	slew speed el [°/s]	nr. of obs	median 3D st. pos. [mm]
120	12	2.1	0.6	34 806	3.2
90	12	3.2	0.8	46 244	2.0
60	12	4.8	1.1	69 708	1.5
45	9	7.3	1.8	93 231	1.3
30	6	12	3.2	139 564	1.0
15	3	32	8	278 830	0.9

reached with less observations than the SKED schedule. This is a big advantage of the uniform sky schedules.

3 Conclusions and prospects

For the IVS VLBI2010 Committee, simulation studies are of very high interest because decisions about the next generation VLBI system will be mainly based on these results. Therefore, the Monte Carlo simulator has to be able to reproduce real observations (Wresnik et al., 2009a). Since zenith wet delays have the largest impact on the simulation results, they have to be simulated as realistically as possible. Thus, applying a turbulence model, which is assumed to yield the most realistic description of the stochastic properties of troposphere up to date, is an important part of these Monte Carlo simulations. The use of the turbulence model for the Monte Carlo simulation is described in Wresnik (2009b) in detail. The determination of optimal slew speeds for the VLBI2010 antennas was a very critical issue for the VLBI2010 Committee. The comparisons between the uniform sky and the schedule produced with SKED show that there is a need for fast antennas. With respect to the median of the 3D station position, the uniform sky schedules show a better performance including less observations than the SKED schedules. This is due to the better geometry achieved with the uniform sky approach. The median value of the rms of 3D station position for the uniform sky schedule with 30 s switching interval (equivalent to the antenna specifications of the Wettzell twin telescope) are at the 1 mm level, which is the defined goal of the VLBI2010 Committee. Considerable improvements can be expected with the use of twin telescopes, i.e. two identical antennas at each site.

Acknowledgements The authors would like to thank the Austrian Science Fund (FWF) for supporting this work (P18404-N10). Andrea Pany is recipient of a DOC-fFORTE fellowship of the Austrian Academy of Sciences at the Institute of Geodesy and Geophysics, Vienna University of Technology.

References

Boehm J., J. Wresnik, and A. Pany, Simulation of wet zenith delays and clocks, IVS Memorandum 2006-013v03, http://ivscc.gsfc.nasa.gov/publications/memos (2007)

Nilsson, T., R. Haas, and G. Elgered, Simulations of atmospheric path delays using turbulence models, In: J. Boehm , A. Pany, H. Schuh (eds.): Proceedings of the 18th European VLBI for Geodesy and Astrometry Working Meeting, Vienna, Austria, 175-180 (2007)

Petrachenko, B., J. Boehm, D. MacMillan, A. Niell, A. Pany, A. Searle, and J. Wresnik, VLBI2010 Antenna Slew Rate Study, In: Measuring the future, Proceedings of the 5th IVS General Meeting, A. Finkelstein, D. Behrend (eds.), 410-415 (2008)

Titov, O., V. Tesmer, and J. Boehm, OCCAM v. 6.0 software for VLBI data analysis, In: NR. Vandenberg, KD. Baver (eds.): Proceedings of the third IVS General Meeting, Ottawa, Canada, 267-271 (2004)

Vandenberg, N., Interactive/Automatic Scheduling Program, Program Reference Manual, NASA/Goddard Space Flight Center, NVI, Inc., (1999)

Wresnik, J., J. Boehm, A. Pany, and H. Schuh, Towards a new VLBI system for geodesy and astrometry, Advances in Geosciences, AOGS 2007, in print (2009a)

Wresnik, J., Simulationen für die neue Generation von VLBI-Systemen, Geowissenschaftliche Mitteilungen, Schriftenreihe der Studienrichtung Vermessung und Geoinformation, Technische Universitaet Wien, Nr. 85 (2009b)

Considerations on the observation of GNSS-signals with the VLBI2010 system

V. Tornatore
Politecnico di Milano, DIIAR, Sezione Rilevamento, Piazza Leonardo da Vinci 32, I-20133 Milano, Italy

R. Haas
Department of Radio and Space Science, Chalmers University of Technology,
Onsala Space Observatory, SE-439 92 Onsala, Sweden

Abstract. One interesting aspect for the development of the VLBI2010 system would be to have the possibility to observe Global Navigation Satellite System (GNSS) signals. This might allow to improve the integration and combination of these techniques, which is an important aspect for the Global Geodetic Observing System (GGOS) of the International Association for Geodesy (IAG). We present calculations for different GNSS systems and VLBI radio telescope sensitivities to assess the expected signal strength. We present L-band observations of GNSS signals and attempts to receive GNSS signals with present day S-band systems. Finally, we give a rough estimation on the expected precision of the VLBI delays and the positions of the GNSS satellites.

Keywords. Reference frames, geodetic VLBI, GNSS, GGOS

1 Introduction

The geodetic VLBI technique is currently in a renewal phase and the next generation geodetic VLBI system, called VLBI2010 (Niell et al., 2006), is envisaged. A report on VLBI2010 design aspects has recently been published (Petrachenko et al., 2009) and it is to be expected that the new system will be built-up within the next years. Several projects worldwide to construct new geodetic VLBI telescopes have been started, e.g. Hase et al. (2008), Titov et al. (2008).

Also the GNSS technology is evolving rapidly, see e.g. Hein et al. (2007).

The IIR(M)-20 satellite of the U.S. Global Positioning System (GPS/Navstar GPS) was launched in March 2009, and started successfully to transmit the third civil GPS signal (L5).

There are plans to complete the Russian GLObal NAvigation Satellite System (GLONASS) to become a full constellation of 24 satellites by 2010, to improve the system performance, to implement new signals, and to encourage the worldwide GLONASS use by promoting GNSS Compatibility and Interoperability.

Two satellites of the European Galileo system, Giove-A and Giove-B (GIOVE stands for Galileo In-Orbit Validation Element), have started to transmit signals in 2006 and 2008, respectively, for the European Space Agency (ESA) to test technology in orbit for the Galileo system.

A second modernized satellite (Beidou 2) of the Chinese Compass system was launched in April 2009. The complete Compass satellite constellation will consist of approximately 30 vehicles. The first phase of the project will cover mainly the Chinese territory, but in the future global coverage is envisaged.

While the evolution and renewal of the VLBI and GNSS systems are very promising developments to improve the accuracy of the individual techniques and the results that can be derived from them, another important aspect is the combined and integrated use of these techniques. The International Association for Geodesy (IAG) strives toward a Global Geodetic Observing System (GGOS) that combines and integrates all geodetic space techniques (Rummel et al., 2005).

Presently the combination of different geodetic space techniques is based on so-called local ties at co-location stations. A local-tie (LT) is the three-dimensional coordinate differences between the reference points of two different co-located geodetic space techniques, derived from local terrestrial geodetic surveys carried out at these stations. The LTs are very important for the construction of the international terrestrial reference frame (Altamimi et al., 2007), but there are still problems today that reduce the potential

of multi-technique combinations:

• Generally, the local terrestrial surveys to derive LTs are quite difficult engineering tasks, are labour intensive and time consuming.

• Statistical information, in particular the variance-covariance matrix, is sometimes not available.

• Some of the existing LTs are quite dubious and do by far not fit to the space geodetic results (Thaller et al., 2007).

To improve in particular the combination of VLBI and GNSS, the observation of GNSS satellites by geodetic VLBI appears to be of interest (Tornatore et al., 2008). The idea to observe artificial radio sources with VLBI is not new and has been successfully realized previously in various satellite and space-craft project, see e.g. Kawano et al. (2006), Zhang et al. (2006). An integration and direct comparison of VLBI and GNSS and their different realizations of the terrestrial reference system (TRF) could be possible when GNSS signals are observed using the same optics as the VLBI signals (including gravitational and thermal deformations). These observations could give the opportunity to achieve a "co-location in space", meaning to combine the kinematic VLBI reference frame of natural celestial radio sources and the dynamical GNSS reference frames of satellite orbits. The GNSS satellite positions could be expressed with respect to the background natural radio sources. Furthermore, the connection of the VLBI TRF to the earth's gravity field could be improved.

2 GNSS L-band signal strength

To evaluate the possibility to observe GNSS L-band signals with geodetic VLBI we first calculated the expected signal strength at a single radio telecope. We used information on GPS, GLONASS and Galileo as summarized in Hofmann-Wellenhof et al. (2008) and calculated the expected signal flux density at the earth surface under worst conditions, both expressed in units dBW/m^2 and Jansky. Worst case conditions means that we assumed low elevation observations (5 degrees) and an atmospheric attenuation of 2 dB.

We calculated the expected received signal strength for two different example radio telescopes. These example telescopes have an aperture efficiency of 0.6 and diameters of 20 m and 10 m, respectively, and correspond roughly to today's typical geodetic VLBI telescope (20 m) and a possible future VLBI2010 telescope (10 m). For our calculations we disregarded all possible signal amplification behind the feed horn. Table 1 shows the corresponding results.

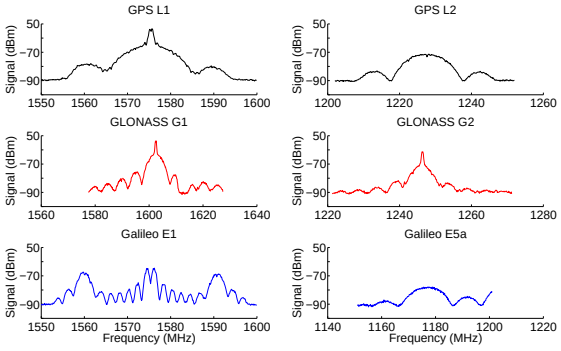

Figure 1. Examples of GNSS-signal reception with the L-band system on the Onsala 25m radio telescope. Shown are spectra for a GPS, GLONASS and Galileo satellite.

It becomes clear from Table 1 that the GNSS-signals have a much stronger signal strength than the natural radio sources that are normally observed with geodetic VLBI (usually only flux densities of a couple of Jansky). It should thus be easily possible to detect the GNSS-signals with L-band receiving systems on radio telescopes. Due to the strong signal strength it might even be necessary to attenuate the signals in order to avoid saturation or even damage of the instrumentation. The GNSS satellites move relatively slow by ca. 0.5° per minute only, so that the satellite tracking should not be a problem for any existing or planned geodetic VLBI telescope.

As a proof, observations of GNSS signals were performed with the L-band receiving system on the Onsala 25m radio telescope. Figure 1 shows examples of the obtained spectra for a GPS, a GLONASS and a Galileo satellite. Signals with strenght in the range of −90 to −50 dBm were observed and prove the expectations.

3 Tests to receive L-band signals with present S-band systems

The plans for the future VLBI2010 systems involve broadband observations over at least 2–14 GHz, but do not covered GNSS signals.

One option to make GNSS signal observations possible with VLBI2010 would of course be to extend the VLBI2010 frequency range downward

Table 1. Overview of some characteristics of three GNSS. Shown are the names of the navigation signals, their center frequencies f_c, the corresponding bandwidth B, the minimum flux density F at the earth surface assuming satellite observation at 5 degrees elevation, expressed both in dBW/m^2 and in Jansky, and finally the received powers P_{r-10m} and P_{r-20m}, assuming a radio telescope with aperture efficiency of η=0.6 and a diameter of 10 m and 20 m, respectively.

System	Signal	f_c (MHz)	B (MHz)	F (dBW/m^2)	(Jy)	P_{r-10m} (dBm)	P_{r-20m} (dBm)
GPS	L1 (C/A)	1575.42	2.046	–159.5	∼6000	–101.8	–91.8
	L1 (P)		20.460	–162.4	∼300	–104.7	–94.7
	L2 (C/A)	1227.60	2.460	–161.0	∼4000	–103.3	–93.3
	L2 (P)		20.460	–159.4	∼600	–101.7	–91.7
GLONASS	G1 (C/A)	1602.00	1.022	–164.0	∼4000	–106.3	–96.3
	G1 (P)		10.220	–164.0	∼400	–106.3	–96.3
	G2 (C/A)	1246.00	1.022	–170.0	∼1000	–112.3	–112.3
	G2 (P)		10.220	–170.0	∼100	–112.3	–112.3
Galileo	E1	1575.420	32.000	–159.0	∼400	–101.3	–91.3
	E5	1191.795	51.150	–157.0	∼400	–99.3	–89.3
	E6	1278.750	40.920	–157.0	∼500	–99.3	–89.3

so that L-band is included. However, this means a re-design of the proposed feed prototypes and might cause problems due for example to necessary changes in the feed dimensions.

Another option might be to try to receive the L-band signals anyway, although the VLBI2010 feed horns will not be designed for L-band. The feed horns will still have some sensitivity for lower frequency ranges, in particular since L-band is so close to S-band, and this sensitivity might be enough for the strong GNSS signals.

We considered to test the latter idea with the existing S-band systems at the Italian radio telescopes Medicina, Matera and Noto, and at the Onsala 20m radio telescope, and thus inspected the corresponding S-band systems in detail.

The Medicina and Noto S-band systems are very similar. Here the S-band horns could receive L-band signals, however with an attenuation of about 20 dB, and the low noise amplifier (LNA) used for the S-band also could work for L-band. However, there are filters in the signal path that will not let pass the L-band signal after the down conversion with the local oscillator frequency. Thus, some hardware changes would be necessary, which is not that easy in particular due to the prime focus installation at these stations. The situation at Matera is similar, and also there it would be necessary to remove filters in the signal path.

At Onsala the transition from a circular to a rectangular waveguide directly after the S-band horn has a sharp cutoff at a frequency of 1690 MHz. Thus, no L-band signals at all will pass into the S-band signal path after the horn. There is additionally a filter that excludes L-band.

So there are hardware restrictions at all four sites that make it impossible to observe L-band signals with the current S-band systems.

However, at Onsala we were able to modify the S-band system for test purposes. We exchanged the filter in the signal path to make possible that L-band signals can propagate in the signal path. We used a signal generator and inserted an artificial signal at frequency 1575 MHz with signal strength −80 dBm via the phasecal cable into

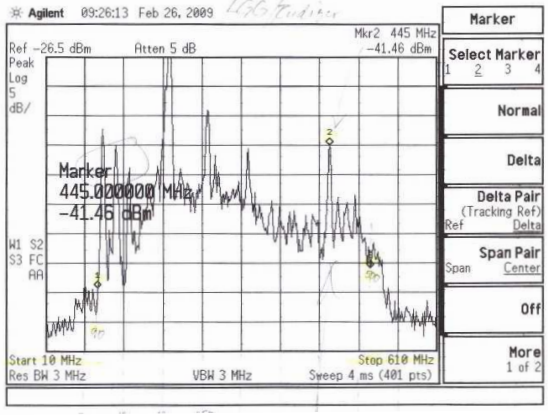

Figure 2. Spectrum of the S-band IF-signal in the control room of the Onsala 20m radio telescope. An artificial signal at RF frequency 1575 MHz (GPS L1) with 80 dBm signals strength was fed in at the input to the S-band receiver via the phasecal cable. This artificial signal is clearly visible in the spectrum at IF frequency 445 MHz (Marker 2).

the S-band system. This signal went through the whole signal path, was down-converted with the local oscillator frequency 2020 MHz, and finally observed with a spectrum analyzer in the control room at the expected IF frequency of 445 MHz, see Figure 2.

This proves that today's S-band systems in principle can observe the strong GNSS signals in L-band. However, some hardware modifications are necessary, in particular filters in the signal path need to be replaced, and in some cases it is even necessary to exchange waveguides.

4 Expected precision of VLBI group delay observations of GNSS signals

The expected precision of a VLBI group delay observation can be calculated as follows (Rogers, 1970; Clark et al., 1985):

$$\sigma_\tau = \frac{2k}{F} \cdot \sqrt{\frac{T_1 \cdot T_2}{A_{e1} \cdot A_{e2} \cdot 2 \cdot B \cdot t_i}} \cdot \frac{1}{2\pi \cdot \eta \cdot f_{rms}} \quad (1)$$

Here, k is Boltzmann's constant, F the flux density of the signal, T_1 and T_2 the system temperatures of the two radio telescopes, A_{e1} and A_{e2} their effective aperture areas, B the recorded bandwidth, t_i the integration time, η the correlation efficiency factor, and f_{rms} the rms-spanned bandwidth of the bandwidth synthesis technique. Assuming a flux density F of 300 Jy for a GNSS signal (see Table 1), telescopes of 10 m diameter, aperture efficiency of 0.6 and system temperatures of 150 K, an integration time of 1 s, a correlation efficiency factor of 0.8, and a bandwidth synthesis with 6 frequency channels of width 2 MHz distributed within 10 MHz (e.g. GPS L1 (P)), the corresponding group delay precision becomes about 28 ps, or roughly 8 mm.

This indicates that is should be possible to determine groups delays for GNSS signals with a precision on the order of 1 cm or better. It could be done with both L-band frequencies, e.g. GPS L2 and L1, so that the two delays can be used to calculate the ionospheric correction.

This VLBI delay corresponds to a difference in range between the satellite and the two receiving stations, see Figure 3. The actual observing geometry, e.g. the nadir angles to the receiving stations as seen from the satellite, determine the uncertainties in the coordinate system of the orbiting satellite (radial, along-track, cross-track).

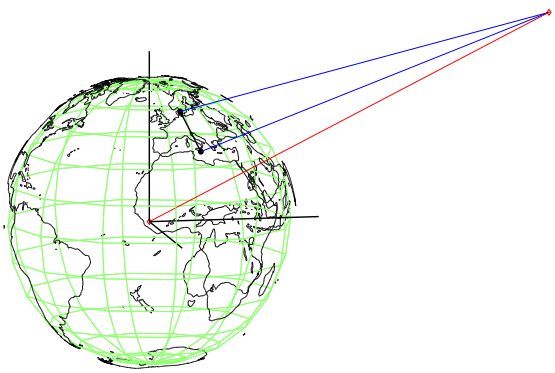

Figure 3. Schematic view of VLBI observations of a GNSS satellite for the example of the baseline Onsala-Noto. The delay (range difference) is measured in the triangle indicated by the blue lines that connect the satellite and the receiving stations.

5 Conclusions and outlook

GNSS L-band signals could in principle be observed with the today's S-band systems, but some modifications would be necessary at most stations. Appropriate filters would need to be installed, and solutions to equalize the signal strength would need to be developed.

The observation of strong L-band signals could be included in the plans for the VLBI2010 system. It seems not impossible that the future VLBI2010 feed horns may be used to observe L-band signals. However, solutions with separate L-band systems to avoid dispersion effect in waveguides and unpredictable phase-changes caused in the receiver, might be preferable. In any case it might be worthwhile to consider such possibilities when establishing new radio telescopes for VLBI2010, or for example the new Sardinia Radio Telescope (SRT).

For the future more work needs to be done and it seems necessary:

- to include SatTrack (Moya Espinosa and Haas, 2007) in the next official VLBI Field System (FS) distribution. (SatTrack allows tracking of satellites directly from the FS),
- to establish the most suitable VLBI observing mode for GNSS signals (geodetic, phase referencing, astronomical),
- to consider the effect of the Phase Centre Variation (PCV) of the GNSS satellite antennas,
- to develop special VLBI observing strategies and schedules,
- to extend the correlator model for finite

distance radio sources (Sekido and Fukushima, 2006) to be applicable for earth orbiting satellites, too, and implement it in a correlator,

• to extend the present VLBI data processing software to include GNSS orbit determination,

• to derive the expected final accuracy of the GNSS orbits that might be obtained from VLBI observations.

Acknowledgements The authors wish to thank the staff at the stations considered in this work and many colleagues for their hints and discussions.

References

Altamimi Z., Collilieux X., Legrand J., Garayt B. & Boucher C. (2007) ITRF2005: A new release of the International Terrestrial Reference Frame based on time series of station positions and Earth Orientation Parameters. J. Geophys. Res., 112, B09401, doi:10.1029/2007JB004949

Clark T.A., Corey B., Davis J., Elgered G., Herring T.A., Hinteregger H.F., Knight C.A., Levine J.I., Lundqvist G., Ma C., Nesman E.F., Phillips R.B., Rogers A.E.E., Rönnäng B., Ryan J.W., Schupler B.R., Shaffer D.B., Shapiro I.I., Vandenberg N.R., Webber J.C. & Whitney A.R. (1985) Precision Geodesy Using the Mark-lll Very-Long- Baseline Interferometer System. IEEE Trans. Geosci. Remote Sens., GE-23:4, 438–449

Hase H., Dassing R., Kronschnabl G., Schlüter W., Schwarz W., Kilger R., Lauber P., Neidhardt A., Pausch K. & Göldi W. (2008) Twin Telescope Wettzell: a VLBI2010 Radio Telescope Project. In: IVS 2008 General Meeting Proceedings "Measuring the Future", edited by A. Finkelstein and D. Behrend, 109–113

Hein G.W., Rodriguez J.A.A., Pany T., Eissfeller B. & Hartl P. (2007) Envisioning a Future GNSS System of System. Inside GNSS, 2(1), 58–67.

Hofmann-Wellenhof B., Lichtenegger H. & Wasle E. (2008) GNSS – Global Navigation Satellite Systems GPS,GLONASS, Galileo, and more. Springer-Verlag, Wien, ISBN: 978-3-211-73012-6, 516 p.

Kawano N., Hanada H. & Matsumoto K. (2006) International VLBI Tracking of SELENE. in: IVS 2006 General Meeting Proceedings, edited by D. Behrend and K. Baver, NASA/CP-2006-214140, 47–61

Moya Espinosa M. & Haas R. (2007) SATTRACK – A Satellite Tracking Module for the VLBI Field System. In: Proc. 18th European VLBI for Geodesy and Astrometry Working Meeting, edited by J. Böhm, A. Pany, and H. Schuh, Geowissenschaftliche Mitteilungen, Schriftenreihe der Studienrichtung Vermessung und Geoinformation, Technische Universität Wien, 79, 53–58

Niell A., Whitney A., Petrachenko B., Schlüter W., Vandenberg N., Hase H., Koyama Y., Ma C., Schuh H. & Tuccari G. (2006) VLBI2010: Current and Future Requirements for Geodetic VLBI Systems. in: IVS Annual Report 2005, edited by D. Behrend and K. Baver, NASA/TP-2006-214136, 13–40

Petrachenko B., Niell A., Behrend D., Corey B., Böhm J., Charlot P., Collioud A., Gipson J., Haas R., Hobiger T., Koyama Y., MacMillan D., Malkin Z., Nilsson T., Pany A., Tuccari G., Whitney A. & Wresnik J. (2009) Design Aspects of the VLBI2010 System – Progress Report of the IVS VLBI2010 Committee. available on the IVS webpage `ftp://ivscc.gsfc.nasa.gov/pub/misc/V2C/PR-V2C_090417.pdf`

Rogers A.E.E. (1970) Very long baseline interferometry with large effective bandwidth for phase-delay measurements. Radio Science, 5(10), 1239–1247

Sekido, M. & T. Fukushima (2006) A VLBI Model for a Radio Source at Finite Distance. J. Geod., 80:137–149

Thaller D., Krügel M., Rothacher M., Tesmer V., Schmid R. & Angermann D. (2007) Combined Earth orientation parameters based on homogeneous and continuous VLBI and GPS data. J. Geod., 81:529–541

Titov O., Gulyaev S., Lovell J. & Dickey J. (2008) Australian New Zealand Geodetic VLBI Network Project In: IVS 2008 General Meeting Proceedings "Measuring the Future", edited by A. Finkelstein and D. Behrend, 114–118

Tornatore V., Tuccari G. & Wei E. (2008) First considerations on the feasibility of GNSS observations by the VLBI technique. In: IVS 2008 General Meeting Proceedings "Measuring the Future", edited by A. Finkelstein and D. Behrend, 439–444

Zhang, X. & Team of the Chinese VLBI Network (2006) Spacecraft Tracking with the Chinese VLBI Network. In: IVS 2006 General Meeting Proceedings, edited by D. Behrend and K. Baver, NASA/CP-2006-214140, 52–55

Rummel R., Rothacher M. & Beutler G. (2005) Integrated Global Geodetic Observing System (IGGOS) – science rationale. J. Geodyn., 40, 357–362

VLBI Data Interchange Format

A.R. Whitney
MIT Haystack Observatory, USA

M. Kettenis
Joint Institute for VLBI in Europe, The Netherlands

C. Phillips
CSIRO/ATNF, Australia

M. Sekido
NICT, Japan

Abstract. One important outcome of the 7th International e-VLBI Workshop in Shanghai in June 2008 was the creation of a task force to study and recommend a universal VLBI data format that is suitable for both on-the-wire e-VLBI data transfer, as well as direct disk storage. This task force, called the VLBI Data Interchange Format (VDIF) Task Force, is envisioned as the first part of a two part effort, the second of which will address standardization of e-VLBI data-transmission-protocols. The formation of the VDIF Task Force was prompted particularly by increased e-VLBI activity and the difficulties encountered when data arrive at a correlator in different formats from various instruments in various parts of the world. The task force has proposed a streaming packetized data format that may be used for real-time and non-real-time e-VLBI, as well as direct disk storage. The data may contain multiple channels of time-sampled data with an arbitrary number of channels, arbitrary # bits/sample up to 32, "real" or "complex" data; data rates in excess of 100 Gbps are supported. Each data packet is completely self-identifying via a short header, and data may be decoded without reference to any external information. The VDIF task force has completed its work and submitted its final report to the VLBI community for review and approval.
Keywords. VLBI, data format

1 Introduction

The VLBI Standard Interface (VSI) specifications, developed in the early 2000s and designated VSI-H and VSI-S, and are aimed primarily at recording and playback systems, specify standards for a hardware/electrical VLBI data interface and a software control interface, respectively. These VSI specifications intentionally *do not address the format of the transported data*.

In recent years, a number of new VLBI data-acquisition and capture systems have appeared, along with increasing need to interchange data on a global scale, including real-time and near-real-time transfer via high-speed network, as well as by standard disk-file transfer. These types of data transfers have been increasingly plagued by the lack of an internationally agreed data format, often requiring *ad hoc* format conversions that require both programming effort and computing/storage resources. Recognizing this problem, a so-called VSI-E ("E" for "e-VLBI") specification, based on standard RTP/RTCP network protocol, was first proposed and implemented in 2003–2004, which specified both data formats and data-transport mechanisms for real-time e-VLBI data transfer. Though VSI-E was comprehensive, it was never formally ratified by the larger VLBI community. Its adoption was further hampered by its complexity, and it has been largely abandoned.

The VLBI Data Interface Specification (VDIF) has a somewhat different goal from VSI-E, specifying only a *standardized transport-independent VLBI data-interchange format that is suitable for all types of VLBI data transfer, including real-time and near-real-time e-VLBI, as well as disk-file storage*. The VDIF specification, unlike VSI-E, explicitly makes no attempt to define an on-the-wire data-transport protocol, which is expected to be the subject of a subsequent specification document. The combination of VDIF, along with this follow-on

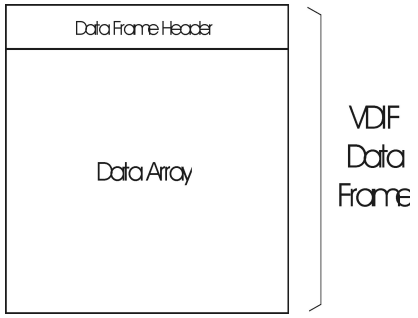

Figure 1. VDIF Data Frame structure showing Data Frame Header and Data Array.

data-transport-protocol specification will, when completed, essentially constitute a replacement for VSI-E. And though the VDIF specification makes no mention of data-transport protocol, it has been developed with an awareness of expected methods of data transport, including network transport using various standard protocols, as well as physical or electronic transport of standard disk files.

2 VDIF Task Force

The 2008 International e-VLBI Workshop, held 14-17 June 2008 in Shanghai, China, included panel and group discussions specifically targeting the subject of creation an international data-format standard. Those discussions led to the creation of a small, broadly-based international task force (subsequently known as the VDIF Task Force) to study the problem and make recommendations to the larger VLBI community.

3 Basic VDIF structure

The discussions at the Shanghai meeting supported the concept of a 'framed' data-stream format consisting of stream of "Data Frames", each containing a short self-identifying Data Frame Header, followed by a Data Array (containing the actual samples), as shown in Figure 1. A similar format is already used by several current and proposed disk-based recording systems.

Accordingly, the VDIF specification is based upon a basic self-identifying Data Frame, which carries a time segment of time-sampled data from one or more frequency sub-bands. The length of a Data Frame may be chosen by the user to best match the chosen transport protocol; for example, in the case of real-time network transfer, a VDIF Data Frame length would normally be chosen so that exactly one Data Frame is carried by each on-the-wire packet. It is important to emphasize that the VDIF Data Frame is fundamentally transport-protocol independent, so that exactly the same set of Data Frames can represent VLBI data through a network transfer or be stored to a physical disk file.

In some cases, an entire set of sampled frequency sub-bands (or "channels") may be carried in each Data Frame. In other cases, a single Data Frame may carry data from only a single data sub-bands (channel) from among a set of many, in which case a logically parallel set of Data Frames is needed to represent the entire data set. In the VDIF concept, each time-series of Data Frames from the same set of sub-band(s) is known as a "Data Thread", where each of the Data Frames within the Data Thread is identified by a "Thread ID" embedded in the Data Frame Header. For actual transmission over a serial-data network, or for storage on a disk file, the set of Data Threads that comprise the data set are merged into a single serial "Data Stream". Figure 2 show a schematic example of a Data Stream comprised of three Data Threads. The collection of Data Threads from the beginning to end of a particular observation, typically lasting seconds to minutes, is known as a Data Segment.

In normal usage, it is expected that two types of Data Streams will predominate: 1) a Data Stream consisting of a single Data Thread carrying multi-channel Data Frames or 2) a Data Stream consisting of multiple single-channel Data Threads, though mixing of single-channel and multi-channel Data Threads is not prohibited.

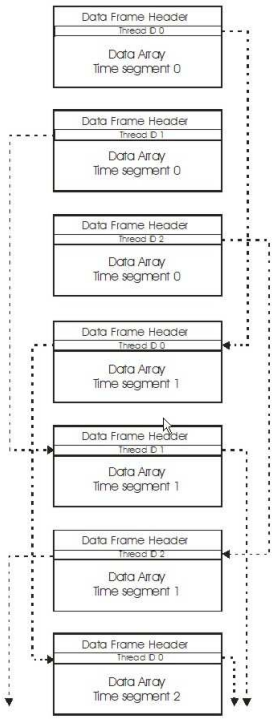

Figure 2. Illustration of Data Threads within a Data Stream.

4 VDIF attributes

The following considerations guided the creation of the VDIF specification:

1. The data in each Data Stream must be decodable using only information embedded within its constituent Data Frames.

2. A Data Thread may be discontinuous in time at the resolution of a Data Frame (e.g. transmit/capture Data Frames only during active part of a pulsar period)

3. Each Data Frame may carry single-bit or multiple-bit samples up to 32 bits/sample.

4. Up to maximum of 1024 Data Threads, each with a unique Thread ID, may be included in a single Data Stream.

5. A minimum of data manipulation should be necessary to move data between various data-transmission techniques (e.g. disk file or real-time transfer).

6. Data rates up to at least ∼100 Gbps should be supported.

7. The data overhead (e.g. embedded auxiliary information required to meet the VDIF requirements) must be as low as practical.

8. Observations over leap seconds and year boundaries must be transparently supported.

9. The VDIF data format must be compatible, in as natural way as possible, with all expected data-transport methods (e.g. network transfer, file transfer, etc).

10. Some limited amount of auxiliary user-defined data should be allowed in the Data Stream.

11. Within certain defined limits, out-of-time-order data within a Data Thread should be accommodated.

5 Data Frame Rules

The following rules govern each VDIF Data Frame within a given Data Thread:

Each Data Frame contains a Data Frame Header followed by a Data Array.

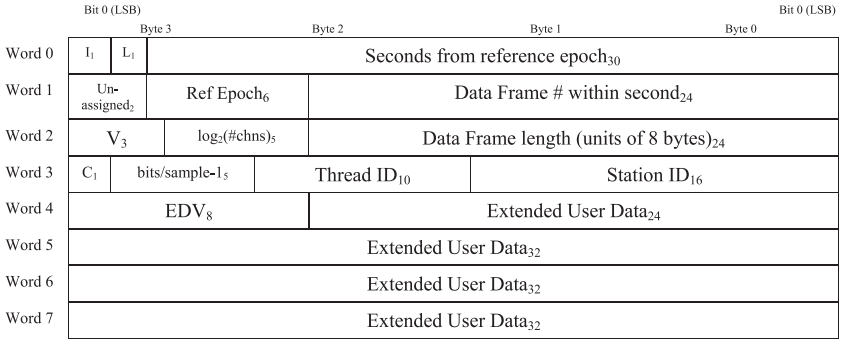

Figure 3. VDIF Data Frame Header format; subscripts are field lengths in bits; byte #s indicate relative byte address within 32-bit word (little endian format).

1. All Data Frames must have the same Data Frame Header length, Data Array length, #channels, #bit/sample and Station ID.
2. If a Data Frame contains data from multiple channels, the same time-tag must apply across channels.
3. If a Data Frame contains multiple channels, all channels must be sampled with the same number of bits/sample.
4. Each Data Array contains sample data from one or more channels with format (Section 9) and encoding (Section 10) specified by VDIF.
5. The Data Frame length (including Data Frame header) for each Data Thread must meet the following criteria:
   (a) Must be a multiple of 8 bytes (for maximum compatibility with various computer-memory-address schemes and disk-addressing algorithms).
   (b) Must be chosen so that an integer number of complete Data Frames are created in a continuous data flow of exactly one-second duration.
6. Data Frame #0 of each one-second period must contain, as its first sample, the data taken on a second tick of UTC; note that, in the case of time-discontinuous data, Data Frame #0 may not always be present.

These rules are intended to cover both "on-the-wire" e-VLBI data formats as well as disk-file formats. For "on-the-wire" real-time e-VLBI, it is expected that each transmitted non-fragmented packet will contain a single VDIF Data Frame as its data payload, in which case the Data Frame length is normally restricted to the range ∼64-9000 bytes. These restrictions do not apply to disk-file data format, for which the Data Frame length is limited (by the number of bits available to specify the Data Frame length) to 227 bytes (∼134 MBytes).

6 Data Frame Header

Each VDIF Data Frame carries header as shown in Figure 3, which may be either 16 or 32 bytes in length, depending on whether the Extended User Data words are included.

Details of the fields in the VDIF Data Frame Header are available in the VDIF specification.

7 Byte ordering

Byte ordering of both the Data Frame Header and Data Frame is little-endian (Intel x86 order) based on 32-bit words, which is consistent with most existing disk-based systems and software-based correlators.

8 Data Frame ordering

Data coming from a single data source (e.g. a single dBBC or DBE) will normally be transmitted in strict time order. If directly connected to a local recording device, the recorded data will almost certainly be recorded in exactly the same order. However, Data Frames transmitted through a switch or over a network are not guaranteed to arrive in order.

The VDIF specification does not mandate strict Data Frame ordering within a Data Thread, but a best effort should be made to so.

Some correlation equipment, particularly older types, may be sensitive to Data Frame order, in which case the requirements of Data Frame ordering will be dictated by the correlation equipment. Modern software correlators are generally rather tolerant of minor Data Frame re-ordering of the type that might occur.

9 Data Array formats

VDIF specifies the format of a Data Array based *solely* on the #channels and #bits/sample specified in the corresponding Data Frame Header. Since these two pieces of information are contained in each Data Frame Header, the samples in each Data Frame may be decoded with no external information.

The number of channels that can be accommodated in a multi-channel Data Array are limited to 2n, but it is expected that most users will prefer to use single-channel Data Array. The use of multiple single-channel Data Threads both allow the user to transmit an arbitrary number of channels, as well as being a more compatible format for the evolving generation of software correlators.

Any number of bits/sample from 1 to 32 are supported, though the Data Array may contain some pad bits for certain values of bits/sample.

Samples may either be "real" or may occur in "complex pairs", such are sometime used in standard digital-signal-processing algorithms.

10 Sample representation

VDIF-encoded data samples are represented by the desired number of bits in a fixed-point "offset binary sequence", beginning with all 0's for the most-negative sampled value to all 1's for the most-positive sampled value. For example, 2-bit/sample coding is (in order from most negative to most positive) 00, 01, 10, 11. This coding is compatible with existing Mark 5B, K5 and LBADR disk-based VLBI data systems, though bit-ordering may be different in some cases.

11 Summary

The VDIF specification is one more piece of the on-going effort to achieve standardization of Global VLBI. It will work, however, only if VLBI community members are convinced that VDIF is good both for them and the greater community. Indications to date are the VDIF is being well received. The authors, as members of the VDIF Task Force, are, of course, always open to constructive comments and suggestions that may strengthen VDIF further. The full VDIF specification is available at *http://www.haystack.edu/tech/vlbi/vsi/index.html*.

Plans for the Vienna VLBI Software VieVS

J. Boehm, H. Spicakova, L. Plank, K. Teke, A. Pany, J. Wresnik, S. Englich, T. Nilsson, H. Schuh
Institute of Geodesy and Geophysics, Vienna University of Technology, 1040 Vienna, Austria

T. Hobiger, R. Ichikawa, Y. Koyama, T. Gotoh, T. Kubooka
National Institute of Information and Communications Technology, Tokyo, Japan

T. Otsubo
Hitotsubashi University, Tokyo, Japan

Abstract. A new VLBI (Very Long Baseline Interferometry) data analysis software (called Vienna VLBI Software VieVS) is developed at the Institute of Geodesy and Geophysics in Vienna taking into consideration all present and future VLBI2010 requirements, e.g. phase delay solutions and a significantly denser observation schedule. The programming language Matlab is used, which considerably eases the programming efforts because of many built-in functions and tools. Matlab is the high-end programming language of the students at Vienna University of Technology and at many other institutes worldwide. Thus, the new software will attract students and scientists to get interested in VLBI and to contribute to VLBI analysis. Together with the National Institute of Information and Communications Technology (NICT, Japan) phase delay solutions will be implemented in VieVS and initial steps will be taken to equip the software with tools for spacecraft tracking and space VLBI. Furthermore, the gap existing between the correlator output and the presently used Occam software will be closed in the Vienna VLBI software. The common efforts will contribute to the new specification of the VLBI data format, which is defined within Working Group 4 on VLBI Data Structure of the International VLBI Service for Geodesy and Astrometry (IVS).

Keywords. VLBI software, Matlab

1 Introduction

So far, at the Institute of Geodesy and Geophysics (IGG) of the Vienna University of Technology, we have been using the Occam software package (Titov et al., 2004) for the analysis of Very Long Baseline Interferometry (VLBI) observations. Occam (previously called Bonn VLBI Software System, BVSS) has been in use since the beginning of the eighties, and many subroutines and source code lines have piled up which are obsolete and no longer necessary. Some technical Fortran-related details date back to the eighties, e.g. the use of COMMON blocks to exchange variables between the subroutines. Thus, the source code of Occam is rather difficult to read for persons who have not been involved in the development of the software.

As an Associated IVS Analysis Center, IGG Vienna is mostly dealing with research tasks and not with operational (routine) VLBI processing, i.e., we often make modifications to the source code by introducing new models and algorithms. Our students are experts in Matlab but they are not experienced in writing Fortran source code, which makes the work very difficult and time consuming for them (and consequently also for the other staff at IGG). This is our main motivation to develop new VLBI software (VieVS) in Matlab.

Another reason for developing new VLBI software is that right now we need to carry out several updates of our present VLBI software package Occam 6.1, and this task would be much easier in Matlab than in Fortran. In particular, we want to make the software fully consistent with the most recent IERS Conventions (McCarthy and Petit, 2003) (e.g., non-rotating origin and the corresponding partials for the nutation parameters), and for clarity we will remove all former models which are no longer necessary.

At the IGG Vienna, we have been using the classical Gauss-Markov least-squares adjustment of Occam 6.1 LSM which is based on piecewise linear functions using rates for the representation of zenith wet delays, clocks, or Earth orientation parameters. These rates do not correspond to intervals between integer hours as their first epoch

is arbitrary. With the new software VieVS, we estimate the paramters as piecewise linear offsets at integer hours (see below), which makes our results easier compatible with those from other space geodetic techniques like the Global Navigation Satellite Systems (GNSS) or Satellite Laser Ranging (SLR).

2 Why Matlab?

In many courses of their curriculum the students of the Vienna University of Technology and at many other universities use Matlab. Thus, new VLBI software in Matlab will attract more students to get interested in VLBI and to write their diploma or phd theses about VLBI related topics. The use of Matlab will ease the implemention of new ideas and models in the software (for them and their supervisors). Furthermore, Matlab has many built-in tools and functions which make the writing of the code much faster, and the source code is significantly shorter and more concise. Examples for built-in tools are:

- Matrix operations like matrix inversion and multiplication or matrix decomposition, but also easy addressing of columns/rows;
- Plots can be made easily and routines for graphical interfaces are available;
- Netcdf readers and writers;
- Structure arrays which are very useful to store scan-based information.

Of course, there are also arguments against using Matlab - the main of which is certainly that Matlab is a commercial software. However, many institutes worldwide have access to Matlab and use it. Alternatively, we can provide executables of VieVS which run on any machine (whithout having Matlab installed). Another possibility is the use of non-commercial counterparts of Matlab like Octave which will be tested in the next months. If possible, we will modify VieVS in a way that it can be run with Octave or other counterparts.

The other argument against Matlab is that it is slower than Fortran or C/C++. This is certainly true, but tests showed that this is not critical in our case. Even if VieVS takes twice as long as e.g. the Fortran-based Occam, we think that this is fast enough for most of the research purposes, but also for the determination of global solutions.

3 Concept

3.1 Occam to VieVS

We did not start from scratch when developing VieVS, but we heavily rely on the Occam 6.1 LSM software package. Occam LSM consists of five parts: *dtau0*, *pn*, *station*, *geomet*, *lsm*. At first, we made a 'line by line' transition from Fortran to Matlab to guarantee that we get identical results. In a second step we deleted all obsolete parts and comments, and we applied Matlab tools to shorten the source code considerably. Finally, we re-structured the code and the results were still identical to those of Occam. E.g., we connected *pn*, *station*, and *geomet* into one part called *vie_mod*. *dtau0* is now called *vie_init* and *lsm* becomes *vie_lsm*.

One important change with *vie_lsm* is that we are using piecewise linear offsets for all parameters which can be estimated. These piecewise linear offsets are estimated at integer hours (e.g., at 18 UTC, 19 UTC, ...), at integer fractions of integer hours (e.g., 18:20 UTC, 18:40 UTC, ...) or at integer multiples of integer hours (e.g. 18:00 UTC, 0:00 UTC, 6:00 UTC, ...). This representation is not only possible for troposphere zenith delays and gradients, station clocks, or Earth orientation parameters, but also for stations coordinates.

As an example Equation (1) shows the troposphere delay L at one station represented by piecewise linear offsets x_1 and x_2 of the zenith delays at the integer hours t_1 and t_2. $m(t)$ denotes the mapping function at the epoch t of the observation which is in between the integer hours. The partial derivatives which have to be entered in the design matrix are shown in Equation (2) and (3). This concept is similar for all parameters, and future combinations (at the normal equation level) with other space geodetic techniques will be easier with this kind of parameterization.

$$L(t) = m(t) \cdot x_1 + m(t) \cdot \frac{t - t_1}{t_2 - t_1} (x_2 - x_1) \quad (1)$$

$$\frac{dL}{dx_1} = m(t) - m(t) \cdot \frac{t - t_1}{t_2 - t_1} \quad (2)$$

$$\frac{dL}{dx_2} = m(t) \cdot \frac{t - t_1}{t_2 - t_1} \qquad (3)$$

As already mentioned, we will make VieVS fully compatible with the IERS Conventions (McCarthy and Petit, 2003), which is not the case with the Occam 6.1.

3.2 Related tasks

The Vienna VLBI Software (VieVS) comes at an appropriate time, because it is strongly related to many activities within the VLBI community and at IGG Vienna:

- **IVS WG4**: IVS Working Group 4 (chaired by John Gipson) is developing new VLBI data structures. We plan to fully incorporate the new format in VieVS and we also will contribute to the definition of the format. With the new Matlab software VieVS we are very flexible to consider any new development. E.g., if the new data structures will be based on netcdf, built-in Matlab tools will be available to read and write the data.

- **VLBI2010**: IGG Vienna has been contributing to the simulation studies for VLBI2010 (Petrachenko et al., 2009). We plan to continue these simulations with VieVS, and we will take advantage of the experience that we gained with our Occam simulations. E.g., we can use the generators of the turbulent delays and the clock values. In addition to the classical Gauss-Markov least-squares model *vie_lsm*, we plan to set up a Kalman Filter solution in VieVS as well.

- **SCHED2010**: We work on new scheduling software for geodetic VLBI which will be closely related to VieVS. In particular, we plan to use the simulation capabilities of VieVS to determine and validate optimized schedules.

A schematic workflow of VieVS and the related tasks are shown in Figure 1.

4 Co-operation between IGG and NICT

There will be close co-operation between the IGG Vienna and the National Center of Information and Communications Technology (NICT). Although NICT works on its own space geodetic software (for GNSS, SLR, and VLBI) which is based on Python and bindings to C/C++, both organizations will share their experience gained with the development of each software package.

Additionally, IGG Vienna can profit from NICT's experience concerning group delay ambiguity resolution and phase solutions. Presently, VieVS is using the 'NGS cards' as input files, but it is planned to also cover earlier steps in the processing chain when the new data structures are defined by the IVS WG4.

There are plans and ideas to equip VieVS with satellite tracking and space VLBI capabilities. In this respect, the co-operation between NICT and IGG will also be very beneficial and important.

5 Conclusions and outlook

The IGG Vienna is developing new VLBI software (VieVS) in Matlab. Presently, it has about the same capabilities as Occam 6.1, but by using Matlab the source code is more concise. VieVS will be improved and extended in many aspects,

- it will be equipped with satellite tracking and space VLBI capabilities (in co-operation with NICT),
- steps 'backwards' in the processing chain will be covered, such as group delay ambiguity resolution,
- it will get its own features to set up global solutions.

The Vienna VLBI Software (VieVS) will be made freely available to get feedback from as many groups as possible.

Acknowledgements Hana Spicakova is grateful to Mondi Austria Privatstiftung for financial support during her phd study at TU Vienna. Andrea Pany is recipient of a DOC-fForte fellowship of the Austrian Academy of Sciences at the Institute of Geodesy and Geophysics, Vienna University of Technology. Joerg Wresnik is grateful to the Austrian Science Fund (FWF) for supporting his work within project P21049, and Tobias Nilsson to the Deutsche Forschungsgemeinschaft (DGF) (project SCHUH 1103/3-1).

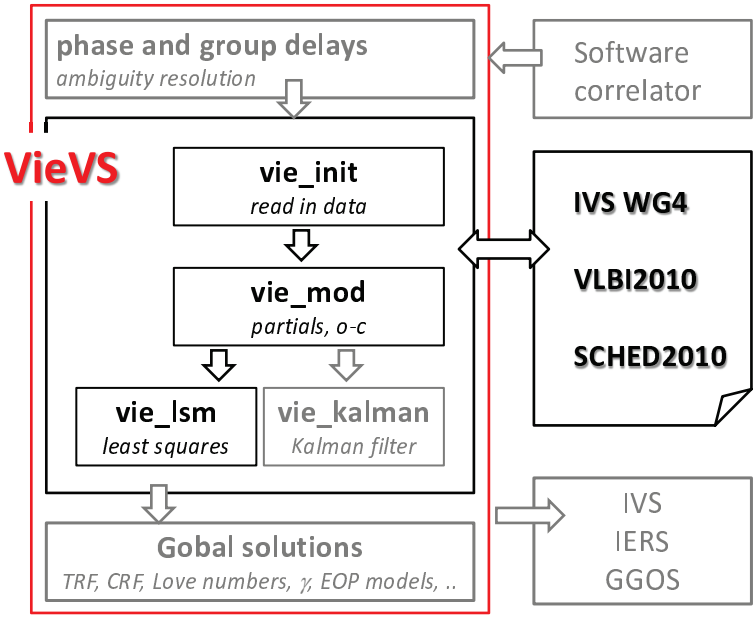

Figure 1. Schematic workflow for the Vienna VLBI Software VieVS. See the text for further details. Grey colour indicates that these tasks have not been started yet.

References

Titov O., Tesmer V. & Boehm J., 2004, OCCAM v.6.0 Software for VLBI Data Analysis, in: Vandenberg N.R. & Baver K. (eds.) International VLBI Service for Geodesy and Astrometry 2004 General Meeting Proceedings, NASA/CP-2004-212255, pp 267-271

Petrachenko B., Niell A., Behrend D., Corey B., Boehm J., Charlot P., Collioud A., Gipson J., Haas R., Hobiger T., Koyama Y., MacMillan D., Malkin Z., Nilsson T., Pany A., Tuccari G., Whitney A. & Wresnik J., 2009, Design Aspects of the VLBI2010 System, Progress Report of the IVS VLBI2010 Committee, in: Behrend D. & Baver K. (eds.) IVS Annual Report 2009

McCarthy D.D. & Petit G., 2003, IERS Conventions, IERS Technical Note 32

VLBI potential of the ALMA telescope in the millimetre

A. Baudry
Laboratoire d'Astrophysique de Bordeaux, Université de Bordeaux, CNRS/UMR5804, BP89, 33271 Floirac Cedex, France & European ALMA Project Office, ESO

Abstract. VLBI is not currently supported in the present ALMA construction plan. However, the ALMA high gain antennas are equipped with receivers spanning several frequency ranges of interest to perform future millimetre (mm)/submillimetre (submm) VLBI observations. The phased outputs of the full ALMA array or of subsets of the ALMA antennas will be supported in the future. In the mm/submm domain where spatial resolution is high but sensitivity is low in general, addition of the large ALMA collecting area to existing or future VLBI arrays would provide a definite detection or mapping advantage. Fine details of compact components in bright AGNs and highly redshifted sources could be revealed with good sensitivity −even though the brightest sources could remain unresolved with the longest terrestrial baselines. We briefly comment on the importance of relatively short VLBI baselines (in the 100–1000 km range) to: (i) map the mm/submm cosmic maser sources excited in evolved stars or galactic star-forming regions; (ii) perform high precision astrometry of nearby stars. Finally, on the basis of recent ideas discussed in the ALMA correlator team, we briefly comment on the ability of the ALMA correlator to support VLBI operation.

Keywords. mm/submm, ALMA telescope, VLBI, AGNs & cosmic masers

1 VLBI with ALMA antennas and receivers

The Atacama Large Millimeter/submillimeter Array (ALMA) is being constructed in the Atacama desert on a 5000 m high plateau of northern Chile under an international agreement involving Europe, North America, Japan and the host country Chile[1]. The main array consists of 50 12-m antennas (with an option up to 64) for observations in the range 30 GHz to 1 THz. The current electronics construction plan does not support VLBI observations. However, VLBI will be possible in the future with the phased array outputs from up to 64 antennas or from less antennas or just a single antenna in one sub-array. There is a minimum of 4 sub-arrays supported in the system. The ALMA Local Oscillator (LO) chain is designed in such a way that later substitution of the current master frequency standard by a hydrogen maser is possible. Other LO components are not meeting the VLBI requirements and there are two different routes for future VLBI with ALMA: either replace these components at a later stage, or add another sub-array to the existing ones to provide the adequate path for VLBI. The ALMA Compact Array (ACA), a set of 4 12-m antennas and 12 7-m antennas deployed in the inner part of the main array, is a major deliverable of the Japanese team. It will also perform VLBI as a stand alone element of

[1]The Atacama Large Millimeter/submillimeter Array (ALMA), an international astronomy facility, is a partnership of Europe, North America and East Asia in cooperation with the Republic of Chile. ALMA is funded in Europe by the European Organization for Astronomical Research in the Southern Hemisphere (ESO), in North America by the U.S. National Science Foundation (NSF) in cooperation with the National Research Council of Canada (NRC) and the National Science Council of Taiwan (NSC) and in East Asia by the National Institutes of Natural Sciences (NINS) of Japan in cooperation with the Academia Sinica (AS) in Taiwan. ALMA construction and operations are led on behalf of Europe by ESO, on behalf of North America by the National Radio Astronomy Observatory (NRAO), which is managed by Associated Universities, Inc. (AUI) and on behalf of East Asia by the National Astronomical Observatory of Japan (NAOJ). The Joint ALMA Observatory (JAO) provides the unified leadership and management of the construction, commissioning and operation of ALMA.

16 or less antennas.

The main array and the ACA are equipped with identical receivers. There are 10 ALMA bands (see Table 1) with receivers being fabricated in priority for bands 3, 6, 7 and 9. The receivers for bands 4, 5, 8 and 10 are under development. All ALMA bands provide two polarizations with linearly polarized receiver feeds. As of this writing, there are no firm plans to construct receivers for bands 1 and 2 although all 10 receivers can be assembled in a common cryostat for each antenna. Two frequency ranges falling in the ALMA bands 3 and 6 are of clear interest for future mm VLBI: (i) the 85–95 GHz range (ALMA band 3) where global mm VLBI observations have been performed successfully in several sources, especially at 86 GHz (Lee et al., 2008); (ii) the 210–230 GHz range (ALMA band 6) which has been opened to VLBI observations nearly 15 years ago (Greve et al., 1995) and has been further explored by different groups (Doeleman et al., 2008). ALMA bands 3 and 6 offer extreme sensitivity with SSB temperatures around 40–80 K. For bands 3 to 8 and for each polarization the upper and lower sidebands are separated (SSB mixers). The instantaneous bandwidth per polarization can be arranged as 4 GHz per sideband or as 8 GHz in a single sideband. We also note that the sensitivity achieved in bands 7 to 10 remains high (Table 1); it is thus conceivable that submm VLBI observations will be attempted in the future.

In the next 2 Sections we briefly comment on: the interest of mm VLBI to observe extragalactic continuum sources and galactic line sources; the sensitivity/imaging enhancement which would result from the addition of the ALMA antennas to existing or future mm/submm arrays. We conclude with remarks on the potential of the ALMA correlator for VLBI.

2 Mm/submm VLBI observations of continuum and line radio sources

Extragalactic radio sources are not, or are less self-absorbed in the millimetre than in the cm-wave domain. Therefore, at a given frequency the source flux density is directly proportional to the brightness temperature and to the source size squared. At the 10^{12} K Compton limit, even sources as bright as 1–0.5 Jy have sizes as small as about 8–12 and 3–4 microarcsec at 3 and 1 mm, respectively. Such sources are not resolved even with the longest terrestrial baselines. However, it was shown that several extragalactic sources are well below the Compton limit and can be imaged in the millimetre with a few thousand km VLBI baselines (Lee et al., 2008). Adding the ALMA sensitive array to a network of a few thousand km would clearly be of major interest. With 5 000 to 10 000 km baselines, resolutions of 40 to 20 microarcsec are achieved at 1 mm and fine structural details could be revealed in the most compact components of the brightest AGNs. In the direction of Sgr A* (right above the ALMA site) spatial scales close to the expected accretion disk around the central black hole (Doeleman et al., 2008) could be mapped accurately in the future. An alternative would be to image Sgr A* or other black holes with baselines much shorter than 5 000–10 000 km in the submm domain where the ALMA sensitivity is still high.

In our own Galaxy, relatively short VLBI baselines −around 100 to 1 000 km− are likely to bring new results in the direction of radio continuum stars. However, many new results are expected to be obtained in thousands of stars for baselines below 100 km with ALMA and the EVLA because these sensitive radio telescopes are able to investigate a broad variety of spatial scales ranging from the stellar photosphere of different stellar classes across the Hertzsprung-Russel diagram to the circumstellar expanding envelope of late-type stars. At 1 mm the ALMA broad band array will provide an r.m.s. sensitivity of 10 microJy in one hour, and, with its longest baselines (up to 15 km), will reach 13 milliarcsec resolution. On the other hand, maser line sources are favourable VLBI targets because of their compactness and of their high brightness temperature resulting from the coherent maser amplification process. Masing lines from OH, H2O, SiO, HCN CH3OH or H2CO have been observed in many evolved stars and star-forming regions of our Galaxy. Among these molecules, several SiO transitions accessible to mm VLBI arrays are most useful to probe the physical conditions and kinematics of the gas around late-type stars and in the Orion molecular core. But the most promising masing lines are perthaps those of water because: (i) it is a widespread species; (ii) several mm/subm transitions have already been detected with single dishes in stars and compact HII regions, including Orion and Sgr B2. Several of these water lines fall in the

Table 1. ALMA bands and receiver noise temperatures.

ALMA Band	Frequency (GHz)	Maximum noise temperature (K)
1	31 - 45	17 SSB
2	67 - 90	30 SSB
3	84 - 116	37 SSB
4	125 - 163	51 SSB
5	163 - 211	65 SSB
6	211 - 275	83 SSB
7	275 - 373	147 SSB
8	385 - 500	196 SSB
9	602 - 720	175 DSB
10	787 - 950	230 DSB

ALMA bands 7 and 8 in the 275 to 500 GHz frequency range; the relatively strong 183 GHz maser line of water falls in ALMA band 5. We further note that some of the brightest water vapour lines which would deserve VLBI observations with moderately extended baselines (100 to 1 000 km) could also be used to self-calibrate the images obtained with the connected ALMA array.

3 Sensitivity enhancement with ALMA and future facilities

The successful 3-mm VLBI observations performed with the IRAM radio telescopes together with other European and US antennas, and the more "experimental" detection at 1.3 mm of Sgr A* suggest that adding the sensitive ALMA antennas to existing VLBI networks would be beneficial to the VLBI science. We estimate that at 3 mm the detection threshold for any single baseline including the most sensitive antenna available in Europe now −the IRAM 30-m dish− would be improved by a factor of three if the phased sum of only 16 antennas of the ALMA array would replace the 30-m. The ALMA antennas would thus improve significantly the dynamic range of images obtained with the smaller dishes of existing mm VLBI arrays. At wavelengths shorter than 3 mm, including the ALMA antennas is even more advantageous because of the extremely good atmospheric transparency of the ALMA site; at 1.3 mm for example (ALMA band 6) the atmospheric transmission is better than 95% for 0.5 mm precipitable water vapour.

It is worth noting that several mm/submm telescopes close to, or very close to the ALMA site could also be outfitted with VLBI equipment in the future (e.g. APEX, ASTE, Cornell-Caltech Atacama 25-m telescope and other projects in discussion). Baselines around 100 km provide 1.5–2.5 milliarcsec resolution in the frequency range 230–370 GHz (ALMA bands 6 and 7). This would be ideal to image maser sources with transitions falling in the ALMA bands 6 and 7 or to investigate details in radio continuum stars and their immediate vicinity. Astrometric studies of stars performed with VLBI baselines longer than the ALMA baselines could provide the fine details missing in the data obtained with ALMA alone, and they could eventually reveal the presence of nearby planetary companions. However, the benefit of using a 100 km VLBI baseline with respect to astrometry performed at the same frequency with the longest ALMA baselines alone deserves careful examination because high signal-to-noise ratios will be achieved with the ALMA connected interferometer.

4 ALMA correlator for connected interferometry and VLBI

4.1 ALMA correlator

The ALMA digital correlator processes up to 64 antennas to form a single connected array for a digitized instantaneous bandwidth of 8 GHz (four 2 GHz basebands) per polarization. The correlator system consists of 4 identical and independent quadrants. Each quadrant processes up to 4 GHz (one polarization pair) and all 4 quadrants process a total bandwidth of 16 GHz for all 64 antennas. The input stage of the correlator is the digital filter bank subsystem which divides each input baseband into 32 sub-channels whose center frequencies are independently tunable across 2 GHz. The correlator part of the system consists of 32 "planes" where the corre-

lation coefficients are derived for each polarization product. Each plane processes at 125 MHz clock rate a frequency sub-channel or a "time slice" packet of digitized data. These two operating modes are named Frequency Divison Mode or Time Divison Mode, respectively; in the latter case the correlator is a pure XF machine. Details on the ALMA correlator specifications and requirements are given elsewhere (Escoffier, Webber & Baudry, 2008).

4.2 ALMA correlator for VLBI

Each quadrant of the ALMA correlator can provide the summed outputs for all antennas or a subset of antennas (subarray). Each correlator "plane" outputs four signal summations (8-bit precision) for two basebands in a quadrant, and each summation output (with LVDS drivers) corresponds to the selected number of phased antennas in the array. This number will be determined with a programmable "include/exclude" antenna mask which has to be developed. The respective advantages of the Frequency Division Mode and of a modified Time Division Mode are being discussed in the correlator team (Escoffier et al., 2008). Both modes could be used when the ALMA correlator is interfaced to a VLBI terminal.

There is some additional equipment to build in order to perform VLBI with the ALMA correlator (Escoffier et al., 2008). This is required to adapt the LVDS summation outputs from the correlator "planes" to a standard VLBI terminal or to an e-VLBI bandwidth. In addition, the 125 MHz ALMA clock rate must match the VLBI standard clock rate and this also requires a clock change logic design.

Acknowledgements A. Baudry wishes to thank University of Bordeaux/LAB and ESO for their support.

References

Doeleman S.S., Weintroub J., Rogers A.E.E. et al., 2008, Event-horizon-scale structure in the supermassive black hole candidate at the Galactic Centre, Nature, 455, 78

Escoffier R., Webber J. and Baudry A., 2008, 64-antenna Correlator specifications and requirements, ALMA Technical Memo ALMA-60.00.00.00-001-C-SPE, 2008-08-07

Escoffier R., Webber J., Lacasse R. et al., 2008, Proposed ALMA correlator VLBI, phased sum and pulsar support, ALMA Memo No. 584

Greve A., Torres M., Wink J.E. et al., 1995, 215 GHz VLBI observations: Detection of fringes on the 1147 km baseline Pico Veleta-Plateau de Bure, Astron. Astrophys., 299, 33

Lee S-S., Lobanov A.P., Krichbaum T.P. et al., 2008, A global 86 GHz VLBI survey of compact radio sources, Astron. J., 136, 159

Simulations of Different Antenna Velocities in VLBI Networks

S. García-Espada
Instituto Geográfico Nacional (IGN), Cerro de la Palera s/n, 19141, Yebes, Spain
Onsala Space Observatory, SE-439 92, Onsala, Sweden

F. Colomer
Instituto Geográfico Nacional (IGN), C/ General Ibañez de Ibero, 3, 28003, Madrid, Spain

R. Haas
Onsala Space Observatory, SE-439 92, Onsala, Sweden

Abstract. The new 40-m radiotelescope of the National Geographical Institute (IGN) in Yebes (code Ys) started to participate in IVS geodetic VLBI sessions in 2008. The azimuth and elevation slew velocities cause stress on the structure, and therefore has an impact on the expected life of the instrument; this calls for slow velocities and accelerations. However, high velocities are needed for better network geodetic results because, in principle, they allow more observations to be performed. In order to evaluate the optimum slew velocities for the new antenna, we used the scheduling software SKED and created schedules with different antenna velocities for Ys. We focussed on the two sessions EURO94 and R1331 and analyzed the schedules with SKED itself, and with the VLBI analysis software SOLVE, both with and without introducing simulated atmosphere and clock contributions. We found that the schedules with a fast Ys antenna (3°/s in az. and el.) give slightly better results than the ones with a slow Ys antenna (1°/s in az. and el.). For the studied EURO session the standard deviation of the estimated topocentric U-component for Yebes is similar for a fast and slow antenna. For the R1-experiment the standard deviations of all three topocentric station components improve for a fast antenna. The SKED-only results appear to be too optimistic, while the SOLVE results show more realistic estimates for the UEN components and sigmas. We found no significant difference in the UEN sigmas with or without introducing simulated atmospheric and clock contributions, although the wrms fit becomes slightly worse.

Keywords. VLBI networks, station velocities, SKED, SOLVE

1 Introduction

The National Geographical Institute (IGN) of Spain has participated in IVS geodetic VLBI sessions since 1995, by means of the 13.7-m radiotelescope in Yebes (code Yb). Till 2003, the antenna participated in 32 geodetic VLBI experiments, including 19 European sessions. The results of such participation are discussed in García-Espada et al. (2008).

IGN has built a new 40-m radiotelescope in Yebes (code Ys), which started to participate in the IVS geodetic VLBI sessions in 2008, it was necessary to determine the antenna slew velocity (in azimuth and elevation) in order to optimize its performance and the performance of the whole network participating in each IVS geodetic VLBI session.

Figure 1 shows a picture of the new IGN 40-m radiotelescope in Yebes (Spain).

Figure 1. New IGN 40-m radiotelescope in Yebes (Ys), Spain.

Table 1. Percentage of observation and idle time for a slow and a fast Yebes40m (Ys) station in the simulated EURO94 and R1331 sessions.

	SKED slow or fast	# stations in the session	Ys Observation time	Ys Idle time	Total # Obs	Ys Scans	Ys # scans/hour
EURO94	sked slow	7	19%	35%	3780	299	13
	sked fast	7	24%	45%	3933	327	14
R1331	sked slow	9	16%	26%	6034	317	13
	sked fast	9	19%	39%	6607	368	15

2 Simulations

To check the impact on the whole network performance of the velocity of a new antenna (Ys), we used the scheduling software SKED and we created new schedules from two already existing schedules from the IVS. We chose two kinds of typical geodetic VLBI experiments, EURO and R1, and we focused on the two sessions EURO94 an R1331. We introduced Ys station as a new participating station in the already existing networks. The participating stations for the simulated EURO94 session were: Crimea (Sm), Effelsberg (Eb), Metsähovi (Mh), Noto (Nt), Onsala60 (On), Wettzell (Wz) and Yebes-40m (Ys). The stations for the simulated R1331-session were: Badary (Bd), Hobart-26 (Ho), Kokee Park (Kk), Ny Alesund-20 (Ny), Tsukuba-32 (Ts), Westford (Wf), Wettzell (Wz), Yebes-40m (Ys) and Zelenchukskaya (Zc). We created various schedules for various Ys velocities: with a fast Ys antenna (3°/s in az. and el.) and with a slow Ys antenna (1°/s in az. and el.). We analyzed the new created networks and schedules with SKED itself, and with the VLBI analysis software SOLVE. In SOLVE we analyzed the sessions with and without introducing atmosphere and clock contributions (Nilsson & Haas, 2008) to make the simulations more realistic.

3 Results

We found that the schedules with a fast Ys antenna (3°/s in azimuth and elevation) give slightly better results than the ones with a slow Ys antenna (1°/s in azimuth and elevation). Figure 2 shows the standard deviations of the Yebes 40-m UEN position derived from the simulated schedules for a fast and slow Ys antenna and the SKED analysis and VLBI analysis software SOLVE. For the studied EURO-session the standard deviation of the estimated topocentric U-component for Yebes is similar for a fast and slow antenna. For the R1-session the standard deviations of all three topocentric station components improve for a fast antenna.

The SKED-only results appear to be too optimistic, while the SOLVE results show more realistic estimates for the UEN components and sigmas. We found no significant difference in the UEN sigmas with or without introducing simulated atmospheric and clock contributions, although the wrms fit becomes slightly worse. Figure 3 shows the values of the wrms delay for a slow and a fast Ys antenna using VLBI analysis software with and without simulated clock and atmosphere contributions (Nilsson & Haas, 2008).

Table 1 shows the percentage of observation and idle time for the Yebes station in each configuration. For Ys-fast the idle time increases more than the observation time, indicating that Ys-fast has to wait for the other slower telescopes in the network.

4 Summary

We have quantified the advantages of including a new slow (1°/sec) or fast (3°/sec) antenna into a typical geodetic VLBI schedule. The goal is to check whether it is worth to increase the slewing speed of the new IGN 40-m antenna in Yebes (Spain), which also increases the stress on its structure, to achieve a higher number of observations and/or a lower standard deviations of the antenna position.

A fast antenna improves the estimated topocentric components. However, the performance of an existing VLBI network does not really improve just by adding a new fast antenna; compared with the case of a slower one, this new antenna will have a higher idle time, as it waits for all the other antennas in the network to reach the source.

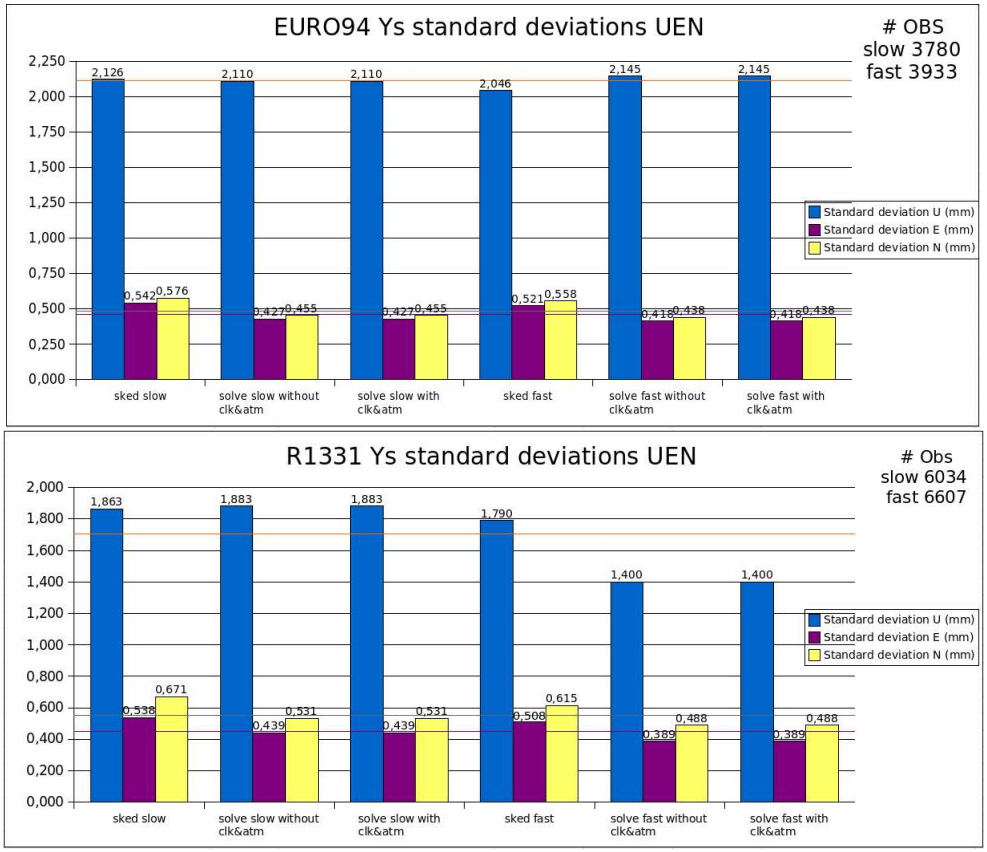

Figure 2. Standard deviations of the Yebes 40-m UEN position derived from simulated schedules with a fast or slow Ys-antenna in a typical EURO- and R1-session using the scheduling software SKED and VLBI analysis software SOLVE.

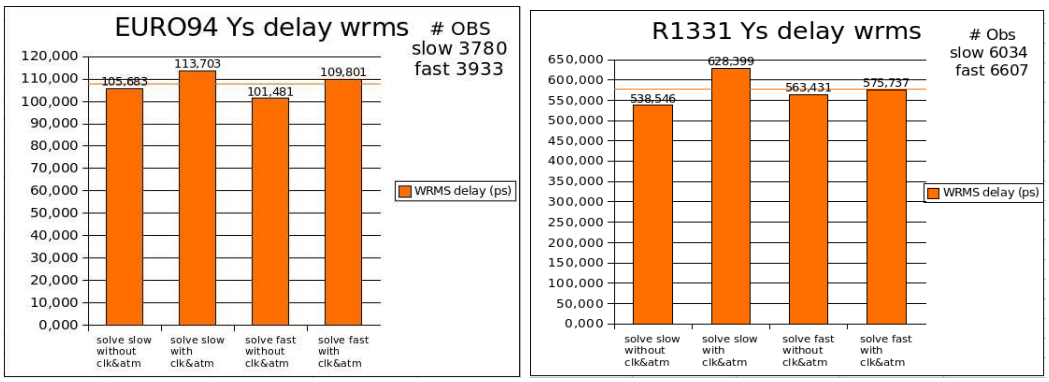

Figure 3. Values of the wrms delay for a slow and a fast Yebes 40-m telescope in typical EURO- and R1-sessions, using VLBI analysis software SOLVE with and without simulated clock and atmosphere contributions.

Acknowledgements S. García-Espada is grateful to Tobias Nilsson for his tropospheric delays based on his atmospheric turbulence models simulations.

References

García-Espada S., Haas R., Colomer F., 2008, Space Geodesy at Yebes: Station Motion from VLBI and GPS. The 5th IVS General Meeting Proceedings, 2008, p. 93-97

Nilsson T., Haas R., 2008, Modeling Tropospheric Delays with Atmospheric Turbulence Models, The 5th IVS General Meeting Proceedings, 2008, p. 361-370

Bordeaux IVS analysis center: Activities and future plans

G. Bourda, A. Bellanger, P. Charlot, A. Collioud, M. Zhang, A. Baudry
Université de Bordeaux, CNRS, Laboratoire d'Astrophysique de Bordeaux, BP89, 33271 Floirac Cedex, France

Abstract. The Bordeaux Observatory has been an associate Analysis Center of the International VLBI Service for geodesy and astrometry (IVS) since the very beginning of this service in 1999. At present, the Bordeaux Observatory IVS activities are focused on three different areas. The IVS data are regularly analyzed with the GINS software for determining the EOP (Earth Orientation Parameters) and the ITRF (International Terrestrial Reference Frame) in the framework of a project to combine the data of all space-geodetic techniques at the observation level. Additionally, the structure of the sources from the ICRF (International Celestial Reference Frame) is regularly monitored, through VLBI imaging along with the astrometric quality of these sources. Finally, the Bordeaux IVS analysis center is involved in more prospective studies comprising VLBI observing programs with the European VLBI Network (EVN) and Very Long Baseline Array (VLBA), and simulations for future VLBI network improvements (VLBI2010 project). This paper is aimed at presenting the current activities as well as the future plans of the Bordeaux VLBI team.

Keywords. VLBI, celestial reference frame, Earth orientation, Gaia, VLBI2010

1 VLBI analysis for EOP, ITRF and ICRF determination

Team: G. Bourda, A. Bellanger, P. Charlot

The Bordeaux IVS analysis center is involved in EOP (Earth Orientation Parameters) and ITRF (International Terrestrial Reference Frame) determination through a national collaboration within the French GRGS (Groupe de Recherches de Géodésie Spatiale). The GRGS is a consortium of several research institutes in France working in the fields of reference systems and geodesy. Within this group and in the framework of the IERS (International Earth Rotation and Reference Systems Service), a specific project has been set up to combine the GPS (Global Positioning System), DORIS (Doppler Orbitography by Radiopositioning Integrated on Satellite), SLR (Satellite Laser Ranging), and VLBI (Very Long Baseline Interferometry) normal equations with the software package GINS–DYNAMO (Meyer et al., 2000), in order to determine homogeneous EOP and ITRF (Coulot et al., 2007; Bourda et al., 2007; Gambis et al., 2009). In this respect, GINS is unique by its multi-technique capabilities.

In this framework, the Bordeaux IVS analysis center carries out regular analysis of the IVS data using the GINS software package. This work has three objectives: (i) to deliver the VLBI normal equations to the GRGS for the GINS multi-technique combination, (ii) to produce EOP time series solely from VLBI data, by analysis of the IVS-R1 and -R4 sessions (Figure 1), and (iii) to deduce geophysical interpretations, taking advantage of the GINS multi-technique combination which unifies reference systems. In 2008–2009, the GRGS group also participated to the ITRF2008 determination.

In the future, the Bordeaux group aims at becoming an IVS operational analysis center by participating in the IVS intra-technique combination, and at extending its products to the celestial frame, in order to extract information of potential interest for astrophysics from estimation of source positions.

2 VLBI imaging and astrometric source quality

Team: A. Collioud, P. Charlot, M. Zhang

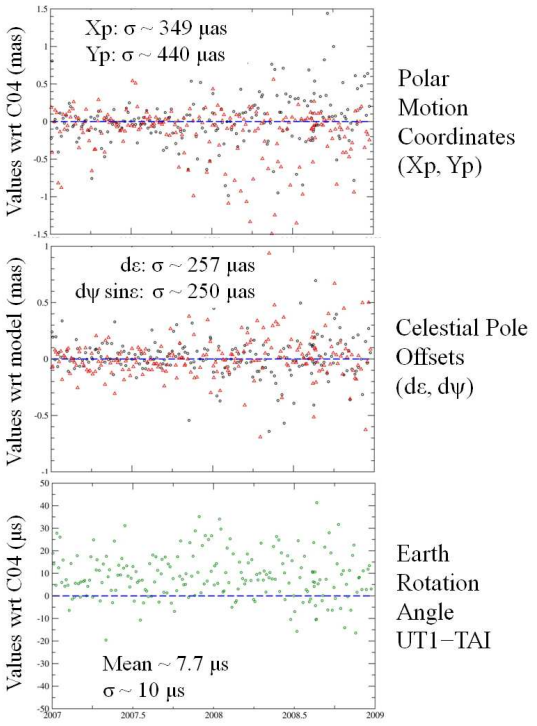

Figure 1. VLBI EOP time series (unweighted) for the years 2007–2008, as determined with GINS for the ITRF2008.

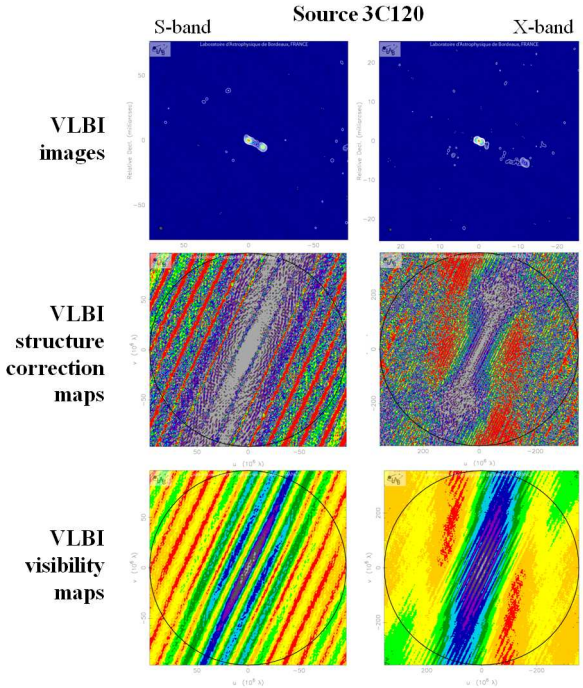

Figure 2. Excerpts from the Bordeaux VLBI Image Database for the source 3C120 at epoch 2008/04/02 (RDV68). Upper panels: VLBI images at S-band and X-band. Middle and lower panels: Structure correction maps and visibility maps.

The Bordeaux IVS analysis center is also involved in monitoring the VLBI structures of the radio sources from the ICRF (International Celestial Reference Frame; Ma et al., 1998; Fey et al., 2004). On the basis of these VLBI images, a structure index (SI) is determined for each radio source and each experiment (Fey & Charlot, 1997, 2000). This parameter is an indicator of the astrometric quality of the radio sources. The VLBI images produced so far, as well as the corresponding structure correction maps and visibility maps (see Figure 2 for an example), are available online through the Bordeaux VLBI Image Database (BVID; Collioud & Charlot, 2009).

The purpose of this database is (i) to help maintaining and improving the ICRF by providing an evaluation of the astrometric quality of the sources (structure indices), (ii) to refine VLBI astrometry by accounting for source structure effects in future VLBI analysis, and (iii) to deduce astrophysical interpretations based on source modeling.

In practice, the AIPS and Difmap software packages, supplemented with a pipeline of homemade scripts, are used to image all the sources observed in the bi-monthly RDV (Research and Development with the VLBA) sessions, which results in several hundreds of new VLBI images per year at X and S bands, along with the corresponding structure correction maps and visibility maps. From these, the structure index and source compactness at S-band and X-band are also calculated for each epoch of observation.

In the future, we aim at model-fitting all such VLBI images in an automatic way for astrophysical investigations (Zhang et al., 2009), determining continuous source structure indices, and developing further the Bordeaux VLBI Image Database, especially for the Virtual Observatory.

3 VLBI observing programs and VLBI technology

Team: G. Bourda, P. Charlot, A. Collioud, A. Baudry

In addition to the regular VLBI analysis mentioned above, the Bordeaux IVS analysis center has been involved in preparing and conduct-

ing VLBI observations for more research-oriented programs with the EVN (European VLBI Network) and VLBA (Very Long Baseline Array), as well as in simulations for future VLBI network improvements.

One such observational program was dedicated to densify the ICRF (see Charlot et al. 2005). Building on this expertise, a specific multi-step VLBI project for detecting, imaging and determining accurate positions of 447 weak extragalactic radio sources was initiated in June 2007 (Figure 3). This long-term program is intended to improve the alignment between the ICRF and the future Gaia optical frame by searching and characterizing proper radio sources suitable for this link (Bourda et al., 2008, 2009).

Furthermore, the Bordeaux IVS analysis center participates in the VLBI2010 project. This project is aimed at defining a new observing network for the IVS, based on small fast-moving antennas (12-meter diameter), uniformly distributed on Earth, and associated with broad band recording system. The Bordeaux contribution consists in studying the VLBI imaging capabilities of this future network by generating simulated images (Collioud & Charlot, 2008; Figure 4).

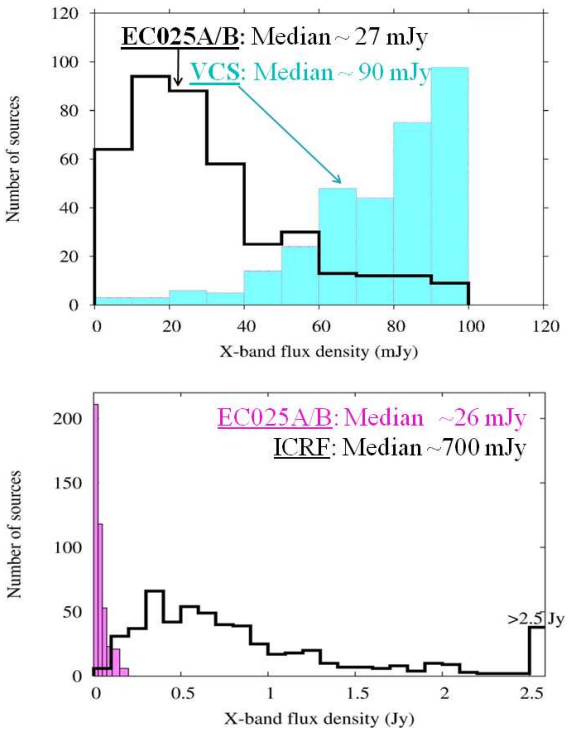

Figure 3. Mean correlated flux density distribution (at X band) for a sample of 447 weak extragalactic radio sources observed with the EVN in 2007 (experiments EC025A and EC025B), as part of a project dedicated to the ICRF-Gaia alignment. Upper panel: Comparison with the VCS catalogue (see Petrov et al., 2008 and references therein) after restricting the X-band flux density distribution to below 100 mJy. Lower panel: Comparison with the ICRF.

References

Bourda G., Charlot P. & Biancale R., 2007, GINS: a new tool for VLBI Geodesy and Astrometry, In: Proceedings 18th EVGA working meeting, edited by J. Boehm, A. Pany & H. Schuh (eds.), 59

Bourda G., Charlot P. & Le Campion J.-F., 2008, Astrometric suitability of optically-bright ICRF sources for the alignment with the future Gaia celestial reference frame, A&A 490, 403

Bourda G., Charlot P., Porcas P. & Garrington S., 2009, A VLBI survey of weak extragalactic radio sources to align the ICRF and the future Gaia celestial reference frame, In: The 9th European VLBI Network Symposium on The role of VLBI in the Golden Age for Radio Astronomy and EVN Users Meeting, edited by Proceedings of Science, (http://pos.sissa.it//archive/conferences/072/056/IX EVN Symposium_056.pdf)

Charlot P., Fey A.L., Jacobs C.S., Ma C., Sovers O.J. & Baudry A., 2005, Densification of the International Celestial Reference Frame: results of EVN+ observations, In: Fundamental astronomy: new concepts and models for high accuracy observations, Proceedings Journées 2004 Systèmes de Référence Spatio-Temporels, edited by N. Capitaine, 21

Collioud A. & Charlot P., 2008, Imaging Capabilities of the Next Generation VLBI System, In: Measuring the future, IVS 2008 General Meeting Proceedings, edited by A. Finkelstein and D. Behrend, 433

Collioud A. & Charlot P., 2009, The Bordeaux VLBI Image Database, this issue

Coulot D., Berio P., Biancale R., Loyer S., Soudarin L. & Gontier A.-M., 2007, Toward a direct combination of space-geodetic techniques at the measurement level: Methodology and main issues, J Geophys Res, 112, B05410

Fey A.L. & Charlot P., 1997, VLBA Observations of Radio Reference Frame Sources. II. Astrometric Suitability Based on Observed Structure, ApJS, 111, 95

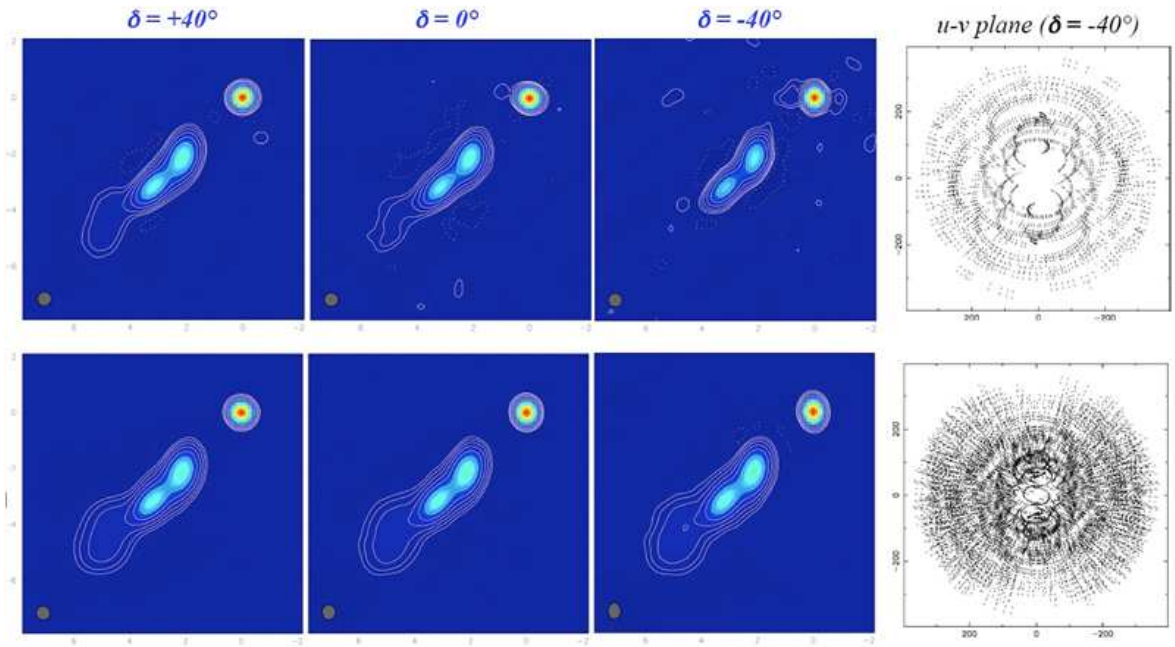

Figure 4. Reconstructed VLBI images at three declinations ($\delta = -40°$, $\delta = 0°$, $\delta = 40°$) and u-v plane coverage (for a declination of $-40°$) for typical VLBI2010 schedules with 16 stations (upper panels) and 32 stations (lower panels).

Fey A.L. & Charlot P., 2000, VLBA Observations of Radio Reference Frame Sources. III. Astrometric Suitability of an Additional 225 Sources, ApJS, 128, 17

Fey A.L., Ma C., Arias E.F., Charlot P., Feissel-Vernier M. et al., 2004, The Second Extension of the International Celestial Reference Frame: ICRF-EXT.1, AJ, 127, 3587

Gambis D., Biancale R., Carlucci T., Lemoine J.-M., Marty J.-C. et al., 2009, Combination of Earth Orientation Parameters and terrestrial frame at the observational level, In: Geodetic Reference Frames, edited by H. Drewes, IAG Symp, 134, 3

Ma C., Arias E.F., Eubanks T.M., Fey A.L., Gontier A.-M. et al., 1998, The International Celestial Reference Frame as Realized by Very Long Baseline Interferometry, AJ, 116, 516

Meyer U., Charlot P. & Biancale R., 2000, GINS: A new Multi-Technique Software for VLBI Analysis, In: International VLBI Service for Geodesy and Astrometry 2000 General Meeting Proceedings, edited by Nancy R. Vandenberg and Karen D. Baver, NASA/CP-2000-209893, 324

Petrov L., Kovalev Y., Fomalont E. & Gordon D., 2008, The Sixth VLBA Calibrator Survey: VCS6, AJ, 136, 580

Zhang M., Collioud A. & Charlot P., 2009, VLBI image model-fitting pipeline program, this issue

VLBI at OPAR: Analysis Service and Research

A.-M. Gontier, S. B. Lambert, C. Barache
Département Systèmes de Référence Temps Espace (SYRTE), Observatoire de Paris, CNRS/UMR8630, Paris, France

Abstract. We summarize the developments and research activities in relation to VLBI data and product exploitation within the VLBI group at the Paris Observatory.

Keywords. Reference frames, VLBI, Earth orientation

1 Operational Activities

1.1 VLBI Analysis

OPAR personnel produce global solutions every three months, reanalyzing all sessions since 1979. Latest solution, opa2009b, is made from 6.3 million delays. The corresponding Earth orientation parameters (EOP) time series are submitted to the IVS. Radio source coordinate catalogue and station coordinate and velocities are made available through the web site. These solutions differ from other analysis centers by the use of the 247 stable sources of Feissel-Vernier et al. (2006) as defining sources instead of the traditional 212 defining sources provided in the International Celestial Reference Frame (ICRF; Ma et al. 1998).

EOP series are updated by new data as soon as new experiment data bases are released. At the same time, daily SINEX files for IVS R1 and R4 experiments are generated and submitted to the IVS. For compability with other analysis centers' solutions, the solution for SINEX file generation is not aligned to the quarterly solution for the celestial frame, but to the 212 ICRF defining sources, avoiding to bias the combination.

Beside, UT1 series from intensives starting April 2006 are maintained and aligned to the ITRF 2005. Polar motion is forced by the IERS EOP 05 C 04 series. Radio source coordinate time series are also computed and completed regularly. Our web site provides plots for sources having a reasonable number of observations.

All the operational products can be found at http://ivsopar.obspm.fr.

1.2 Virtual Observatory

Lambert et al. (2008) summarize the activities of the French geodetic community in the frame of the Virtual Observatory (VO), an international proposal that provides uniform, convenient access to disparate, geographically dispersed archives of astronomical data from software which runs on the computer on the astronomer's desktop. VOTable is a XML-based format for representing astronomical data, and that takes advantage of computer-industry standards and uses standard software and tools. VO standards had initially been developed for Earth-centered or body-centered reference frames in order to extend the VO to Earth and planetary sciences. Nevertheless, some improvements had to be made to adapt the existing VO to geodesy. We recently proposed to the International Virtual Observatory Alliance (IVOA) the adoption of new standards relevant to Earth orientation data. OPAR products are now provided in VOTable format using these new standards. This includes terrestrial and celestial reference frames, station and radio source coordinate time series, and EOP. Thanks to the VOTable format, the VLBI-derived quasar positions can directly be viewed in VO-designed softwares like Aladin (http://aladin.u-strasbg.fr) with which various operations can be done in a few clicks (cross-identifications, superimposition of optical images, etc.).

2 Recent Research Achievements

2.1 Celestial Reference System

One of the goals of the next ICRF realization is to obtain a set of defining sources that is definitely more stable than the current 212 defining sources of the ICRF. In Gontier & Lambert (2008), we already presented a simple scheme, partly inspired from the work of Feissel-Vernier (2003), to obtain a set of core sources reaching this goal. In Lambert & Gontier (2009a), we improved the selection algorithm and applied it to source coordinate time series obtained from the analysis of 26 years of VLBI observations. The selection criterion considered the positional rms, the slope, and the observational history of the sources. Among the potentially suitable sources, we selected four frames made of 196, 200, 262, and 269 sources, respectively, showing a satisfactory sky coverage in both hemispheres. Our selections provide a frame stability improved by up to 40% with respect to the ICRF, and by 20% with respect to Feissel-Vernier et al. (2006). Reanalysis of data with respect to this frame gives astrometric catalogues aligned to the ICRF-Ext.2 within 17 μas. Effects on EOP estimates and terrestrial reference frame determination remain marginal.

Other source ranking algorithms were explored in the frame of the second realization of the ICRF (ICRF2) working group research (Lambert & Gontier, 2009b).

2.2 Test of General Relativity

Relativistic bending in the vicinity of a massive body is characterized by the post-Newtonian parameter γ within the standard parameterized post-Newtonian formalism, which is unity in General Relativity. We retrieved γ from the analysis of geodetic VLBI observations recorded since 1979. We compared estimates of γ and errors obtained using various analysis schemes including global estimations over several time spans and with various Sun elongation cut-off angles, and analysis of radio source coordinate time series. We concluded that γ cannot be estimated at better than 2×10^{-4}. The main factor of limitation is the uncertainty in the determination of radio source coordinates. A sum of various instrumental and modeling errors and analysis strategy defects, that cannot be decorrelated and corrected yet, is at the origin of the limitating noise (Lambert & Le Poncin-Lafitte, 2009).

2.3 Earth's Interior, Nutation and Precession

Observation of nutation allows one to determine some properties of the Earth's interior. In 2007, we examined whether the VLBI analysis configuration could have a substantial impact on determinations of the free core nutation (FCN) and free inner core nutation (FICN) frequencies (Lambert et al., 2008) that describe the free rotational modes of the fluid outer core and of the solid inner core, respectively. We concluded that the instability of the celestial reference frame could impeach one to constraint the FCN and FICN at better than 0.1 day and 100 days, respectively, which is smaller than the error arising from the internal noise of the EOP series. In 2008, we focused on the dissipation at the core-mantle boundary (CMB) that shows up observationally in the quality factor Q of the FCN. The dissipation factors estimated from VLBI nutation data and from local tidal variation of the gravity measured by superconducting gravimeters were known to be in disagreement, the latter being about 30% smaller than the former, leaving open questions about the values of possible dissipative torques emerging from electromagnetic or topographic couplings at the CMB. After a wise treatment of gravimetric data (especially concerning the ocean loading correction) and the use of optimized estimation methods, we obtained values of Q close to 17 000 for both techniques (Rosat & Lambert, 2009).

Theoretical formulation of the contribution to the nutation of the interaction between the tidal potential and the tides arising at the Earth's surface (Lambert & Mathews, 2006) have been reexamined for the precession part (Lambert & Mathews, 2008), and extended to the axial rotation of the planet (Mathews & Lambert, 2009). The additional terms, that emerge mainly from dissipation processes in the oceans, are at the level of current VLBI observational accuracy.

Fundamental aspects of the semi-analytical precession-nutation models that were adopted by IAU Resolutions in 2000 and 2006 have been discussed in Capitaine et al. (2009). In the same paper, we also report on the most recent comparisons of the models with VLBI observations. We showed that a combination of linear and 18.6-

Figure 1. The OPAR web page hosted at the Paris Observatory.

year corrections is the most credible model for explaining the currently observed residuals, but that a longer span of observations is required before the true character of the effect can be determined.

References

Capitaine N., Mathews P. M., Dehant V., et al., 2009, On the IAU 2000/2006 precession-nutation and comparison with other models and VLBI observations, Celest. Mech. Dyn. Astr., 103, 179

Feissel-Vernier M., 2003, Selecting stable extragalactic compact radio sources from the permanent astrogeodetic VLBI program, A&A, 403, 105

Feissel-Vernier M., Ma C., Gontier A.-M., & Barache C., 2006, Analysis strategy issues for the maintenance of the ICRF axes, A&A, 452, 1107

Gontier A.-M., & Lambert S. B., 2008, Stable radio sources and reference frame, In: N. Capitaine (Ed.), Proc. Journées 2007 systèmes de référence spatio-temporels, Observatoire de Paris, 42

Lambert S. B., & Mathews P. M., 2006, Second-order torque on the tidal redistribution and the Earth's rotation, A&A, 453, 363, and Erratum, A&A, 481, 833

Lambert S. B., Deleflie F., Gontier A.-M., et al., 2008, The astronomical Virtual Observatory and application to Earth's sciences, In: A. Finkelstein and D. Behrend (Eds.), IVS 2008 General Meeting Proc., 203

Lambert S. B., Dehant V., & Gontier A.-M., 2008, Celestial frame instability in VLBI analysis and its impact on geophysics, A&A, 481, 535

Lambert S. B., & Gontier A.-M., 2009a, On radio source selection to define a stable celestial frame, A&A, 493, 317

Lambert S. B., & Gontier A.-M., 2009b, On radio source selection and frame stability, this issue

Lambert S. B., & Le Poncin-Lafitte C., 2009, Determination of the relativistic parameter γ using very long baseline interferometry, A&A, 499, 331

Ma C., Arias E. F. Eubanks, T. M., et al., 1998, The International Celestial Reference Frame as Realized by Very Long Baseline Interferometry, Astron. J., 116, 515

Mathews P. M., & Lambert S. B., 2009, Effect of mantle and ocean tides on the Earth's rotation rate, A&A, 493, 325

Rosat S., & Lambert S. B., 2009, FCN resonance parameters from VLBI and superconducting gravimeter data, A&A, in press

IVSTrop: Status and recommendations of the IVS rapid troposphere combination

R. Heinkelmann
Deutsches Geodätisches Forschungsinstitut DGFI, Alfons-Goppel-Str. 11, 80539 München, Germany

Abstract. The paper presents the status and recommendations for the IVS rapid troposphere product. Analysis recomendations are given in order to achieve an improved internal consistency.

Keywords. IVSTrop, combination

1 Introduction

The IVS rapid troposphere product (DGFI, 2009) is a combination of zenith delay estimates provided by various IVS ACs. Currently the IVS-R1 and -R4 types of session within a calendrical week are considered. The combined solution is conventionally available from IVS DCs four weeks after the release of both, DB- and NGS-files. The rapid troposphere product serves for external comparisons, e.g. with EUREF, as well as for internal consistency checks. The tropospheric parameters are very sensitive to variations and discontinuities of the involved terrestrial reference frame, i.e. to station coordinates, which have to be estimated simultaneously to achieve highest precision. So far the analysis strategy was up to the individual AC, with the only agreement, that estimates are to be reported every integer hour during an observing session.

2 Status of the IVS rapid troposphere combination

Although the VLBI technique and the models are steadily improved, the standard deviations of the combined product were found to slightly increase over the past few years (see Fig. 1). The increase can be addressed to more and more differing analysis options, models, and catalogues used by the various ACs. For this reason and because at least some part of the analysis options can be considered objectively better or worse, I come up with the point to recommend the analysis strategy for the estimation of zenith delays. The recommendations are only meaningful for this purpose. If consequently applied, they will significantly better the external as well as the internal comparisons, outliers will be easily detectedable and systematic differences between ACs will be explaineable and traceable to their origin.

3 Recommendations

The following recommendations are for the determination of tropospheric parameters zenith wet delay (ZWD) and zenith total delay (ZTD) with hourly temporal resolution in the case the mathematical model is of Gauss-Markov type. If filter or other techniques are applied by the AC instead, please transform the recommendations, so that they serve correspondingly for your model.

3.1 Parameterization and external data

In order to estimate ZWD, the a priori zenith delay (ZD) should equal the zenith hydrostatic delay (ZHD), which is given by the IERS (2004):

$$ZHD\,[mm] = \frac{0.0022768 \cdot p[hPa]}{1 - 0.00266 \cdot \cos(2\varphi) - 0.00028 \cdot H[m]}$$

where p denotes the surface air pressure, φ the latitude, and H the orthometric height, i.e. the height referred to the geoid, of the theoretical reference point of the observing antenna. Values for the pressure can be usually taken from station log-files, or NGS-data cards, respectively. If the pressure record is missing (indicated by a reported pressure of $-999\,[hPa]$) or obviously wrong, please substitute a pressure value from an alternative source, such as a numerical weather model (NWM). The access

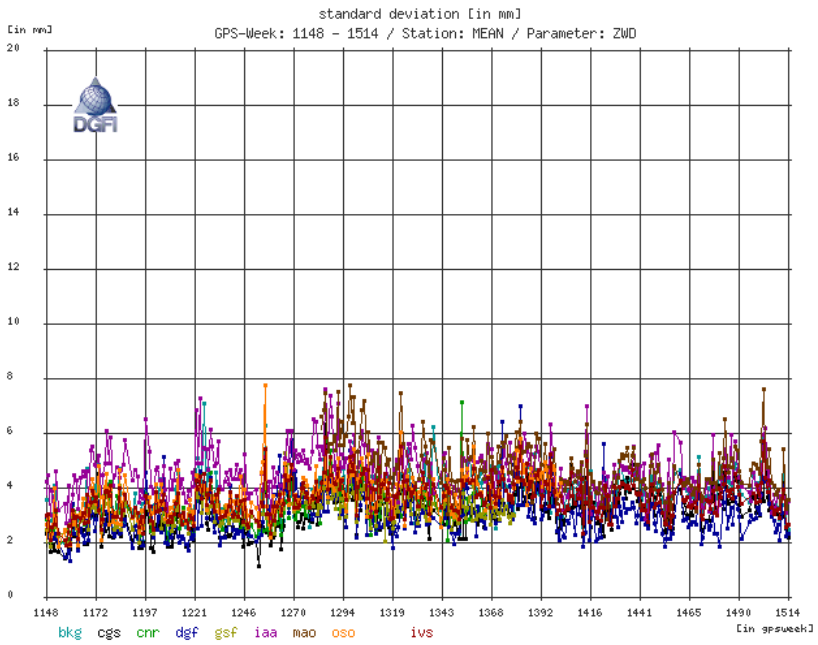

Figure 1. Mean standard deviation of $ZWD\,[mm]$ during the course of IVS rapid turnaround type of session

to data of a state-of-the-art NWM is described in more detail by Heinkelmann et al. (2008). If the pressure in the above equation differs by only $0.5\,[hPa]$, the estimated ZWD will be systematically affected in the order of $1\,[mm]$. Due to correlations some part will be absorbed by station coordinate adjustments, in particular of the height component. Thus, the accuracy of the air pressure is the limiting factor for the determination of ZWD (and ZTD) by space-geodetic techniques such as VLBI, or GNSS. Whereas, the station's latitutde and height only have to be known to about $400\,[m]$ (Davis et al., 1985) for the above model. ZWD and ZTD should be modeled as linear spline functions (piecewise linear continuous functions, PWLF). Please report the value at integer hours during the experiment. If possible, the rate of the linear spline is to be constrained adding a pseudo-observation of the first time derivative (the rate) equal to zero with a weight of $10\left[\frac{mm}{\sqrt{h}}\right]$. The relative clock is modeled by a 2nd order polynomial plus additional polynomials in the case of clock breaks. In addition the stochastic characteristics of the residual clock should be modeled as linear spline function with 1h-rates constrained with $30\left[\frac{mm}{\sqrt{h}}\right]$ weights. For the gradients (east and north) non-zero a priori values should be used from the Data Assimilation Office (DAO), available from GSFC ftp-server (GSFC, 2009), where available. For stations where no values are reported such as BADARY, TIGOCONC, SVETLOE, or ZELENCHK, please use mean total estimated gradients, or zero, if you have none available. Gradients should be modeled as PWLF, too, with 6h-resolution and $0.5\,[mm]$ constraint for the parameter, $2\left[\frac{mm}{\sqrt{h}}\right]$ constraint for its rate, respectively.

3.2 Mapping functions

The VMF1 mapping functions (Böhm et al., 2006a) are suggested for usage and are available from the IGG Server (IGG, 2009). As an alternative, GMF (Böhm et al., 2006b) can be used, which are easier to be implemented and which show no mean bias w.r.t. VMF1.

3.3 Observations under low elevation angles

The low observations are in particular valuable for the estimation of tropospheric parameters and therefore, should be used without cut-off or down-weighting for this purpose.

3.4 A priori catalogues and EOP

The a priori celestial reference frame does not play a significant role for the determination of tropospheric parameters, whereas the terrestrial frame can significantly and systematically affect tropospheric parameters, if station coordinates are not estimated simultaneously. Therefore, the station coordinates should be solved for simultaneously applying non-deforming (minimal) constraints, such as NNR/NNT for coordinates and velocities w.r.t. a priories. The choice of the a priori terrestrial frame is then of less importance. However, the a priori coordinates should not differ from the actual coordinates by more than about 1 $[dm]$. The current combined VLBI catalogue VTRF2008 (Nothnagel, 2009) certainly fulfils this limit. If the adjustment exceeds the limit, it can not be mitigated, that tropospheric estimates are affected as well. Celestial pole offsets, polar motion and dUT1 should be estimated simultaneously as well. Their parameterization appears to be non-significant for this purpose and can be set up according to standard estimation procedures.

4 Transition to the recommended solution set-up

The recommendations will be sent out once initially through the IVS-trop exploder and are open for discussion. Then, they will be finalized and distributed among the participating ACs. There will be no certain epoch or deadline for the transition. In the optimal case the participating ACs can change right away to the recommended solution settings. If one or some of the recommended options are not available right away, please still apply all the other transitions and go on with your preferred ones, but report what option or model you are using instead. Please make sure, that the transition is going to happen, when the necessary changes are made.

5 Update of recommendations

These recommendations consider currently available models and experience. If better models become available, the recommendations might be changed.

6 Contacts

If you have suggestions or want to discuss the aforementioned recommendations, please communicate via the IVS-trop exploder.

Acknowledgements I acknowledge the IVS for providing high quality VLBI data.

References

Böhm J., B. Werl, H. Schuh. JGR, Vol. 111, B02406, doi:10.1029/2005JB003629, 2006

Böhm J., A.E. Niell, P. Tregoning, H. Schuh. GRL, Vol. 33, L07304, doi:10.1029/2005GL025546, 2006

Davis J.L., T.A. Herring, I.I. Shapiro, A.E.E. Rogers, G. Elgered. Radio Science, Vol. 20, Nr. 6, 1593-1607, 1985

DGFI, 2009 `http://www.dgfi.badw.de/?194`

GSFC, 2009 `ftp://gemini.gsfc.nasa.gov/pub/misc/dsm/gradient/gsfc_dao_9095.mgr`

Heinkelmann R., J. Böhm, H. Schuh. In: Proceedings of the IVS General Meeting 2008, A. Finkelstein and D. Behrend (Edts), Nauka, Saint Petersburg, 188-192, 2008

IERS Conventions (2003). IERS Tech. Note 32, D.D. McCarthy and G. Petit (Edts), Frankfurt (M), 2004

IGG, 2009 `http://www.hg.tuwien.ac.at/~ecmwf1/`

Nothnagel A., p. comm., 2009

Scientific program
19th EVGA Working Meeting

March 24−25, 2009
Cap Sciences – Hangar 20 – Quai de Bacalan – Bordeaux (France)

Tuesday 24 March 2009

09:00−09:15	Opening of 19th EVGA working meeting	
Session 1: The VLBI celestial reference frame		**Chair: A. Nothnagel**
09:15−09:30	Preparations for the next ICRF	D. Gordon & D. MacMillan
09:30−09:45	Dependence of catalogue orientation parameters accuracy from sources set selection	S. Kurdubov & E. Skurikhina
09:45−10:00	X/Ka-band Global Astrometric Results	C.S. Jacobs & O.J. Sovers
10:00−10:15	Systematic effects in the radio source proper motion	O. Titov
10:15−10:30	On the connection of the apparent proper motion and the VLBI structure of compact radio sources	S. Frey, A. Moór & O. Titov
10:30−10:45	Apparent motion of quasars and its physical mechanisms	V.E. Zharov et al.
10:45−11:15	*Coffee break*	
Session 2: VLBI modeling		**Chair: H. Schuh**
11:15−11:30	Multi-technique approach for deriving a VLBI signal extra-path variation model induced by gravity: the example of Medicina	P. Sarti et al.
11:30−11:45	An assessment of Atmospheric Turbulence for CONT05 and CONT08	T. Nilsson & R. Haas
11:45−12:00	Modeling azimuthal asymmetries of the troposphere delay during a 14-days typhoon period in Tsukuba	A. Pany et al.
12:00−12:15	Atmospheric VLBI: A method to validate long time series of water vapour content	G. Elgered & R. Haas
12:15−12:30	Recent modeling improvements in SOLVE analysis	D. MacMillan & J. Gipson
12:30−14:00	*Lunch break*	
Session 3: Data acquisition and correlation		**Chair: R. Porcas**
14:00−14:15	The Mark 5C VLBI Data System	A. Whitney et al.
14:15−14:30	DBBC.2 Backend System: status report	G. Tuccari et al.
14:30−14:45	MPIfR/BKG correlator report	W. Alef et al.
14:45−15:00	e-VLBI and other developments at the EVN MkIV Data Processor at JIVE	R.M. Campbell & A. Szomoru
15:00−15:15	Current status of Chinese VLBI network software correlator	Z. Weimin et al.
15:15−15:30	Shanghai correlation system upgrade for geodetic application	S. Fengchun et al.
15:30−16:30	*Coffee break & **POSTER SESSION***	
Session 4: Terrestrial reference frame and Earth Rotation determination		**Chair: H. Hase**
16:30−16:45	Russian domestic QUASAR network – Participation in domestic and IVS observational programs	A. Finkelstein et al.
16:45−17:00	Geodetic research at IRA-INAF: recent results between a golden past and a gloomy future	M. Negusini et al.

17:00−17:15	The 2008 local-tie determination at the Onsala Space Observatory	M. Lösler & R. Haas
17:15−17:30	IVS contribution to ITRF2008 – Status and results	S. Böckmann et al.
17:30−17:45	IVS contribution to ITRF2008: preliminary analysis	X. Collilieux & Z. Altamimi
17:45−18:00	Monitoring UT1 using VLBI and GPS estimates	D. Gambis et al.
18:00−18:15	CONT08 – First results and high-frequency Earth rotation	T. Artz et al.

Wednesday 25 March 2009

Session 5: Progress and developments in VLBI technology — **Chair: W. Alef**

09:00−09:15	Status of the Twin Telescope Wettzell Project	H. Hase et al.
09:15−09:30	An Atlantic Network of Geodynamical Fundamental Stations (Project RAEGE)	J. Gómez-González & F. Colomer
09:30−09:45	Concepts for remote control of VLBI-telescopes and first experiences at Wettzell	A. Neidhardt et al.
09:45−10:00	VLBI2010: Next generation VLBI System for Geodesy and Astrometry	A. Niell et al.
10:00−10:15	VLBI2010 simulations at IGG Vienna	J. Wresnik et al.
10:15−10:45	*Coffee break*	
		Chair: R. Haas
10:45−11:00	Starting tests for the observation of GNSS-signals in view of the planned VLBI2010 system	V. Tornatore & R. Haas
11:00−11:15	VLBI Data Interchange Format	A. Whitney et al.
11:15−11:30	Report of Working Group 4 on Data Structures	J. Gipson
11:30−11:45	Plans for the Vienna VLBI Software VieVS	J. Boehm et al.
11:45−12:00	Closing of 19th EVGA working meeting	

12:00−13:00 *Lunch break*
13:30 *Departure by bus for Talence (Université Bordeaux 1 – salle Agora)*
14:30 *IVS 10th Anniversary Celebration*

15 Posters

Andrei *et al.*	Meeting the LQAC
Baudry	VLBI potential of the ALMA telescope in the millimetre
Bertarini *et al.*	Effects on the geodetic-VLBI measurable due to polarization leakage in the receivers
Bourda *et al.*	Bordeaux IVS Analysis Center activities and plans for the future
Collioud *et al.*	The Bordeaux VLBI Image Database
Finkelstein *et al.*	CONT08 – preliminary results
Garcia-Espada *et al.*	Simulations for different antenna velocities in a VLBI network
Gontier & Lambert	A snapshot of VLBI activities at the Paris Observatory
Johnston *et al.*	The Position Stability of Compact Radio Sources at 23 and 43 GHz
Kurdubov & Panafidina	Scale difference between various TRF solutions
Lambert & Gontier	On source selection and frame stability
Lösler & Eschelbach	Evolution and obtained expertise in reference point determination at the GIK
Tanir *et al.*	Analyses on the time series of the radio telescope coordinates of the IVS-R1 & -R4 sessions
Teke *et al.*	Piecewise linear offsets for VLBI parameter estimation
Zhang *et al.*	VLBI image model-fitting pipeline program

List of participants

Name	Affiliation	City	Country
Abbondanza, Claudio *c.abbondanza@ira.inaf.it*	IRA – INAF	Bologna	Italy
Alef, Walter *walef@mpifr-bonn.mpg.de*	MPIfR	Bonn	Germany
Andrei, Alexandre *oat1@on.br*	Observatorio Nacional/MCT Observatorio do Valongo/UF	Rio de Janeiro	Brasil
Artz, Thomas *artz@igg.uni-bonn.de*	Institute of Geodesy and Geoinformation	Bonn	Germany
Baudry, Alain *baudry@obs.u-bordeaux1.fr*	Laboratoire d'Astrophysique de Bordeaux European ALMA Project Office	Floirac	France
Böckmann, Sarah *boeckmann@uni-bonn.de*	Institute of Geodesy and Geoinformation	Bonn	Germany
Bedos, Reine *bedos@obs.u-bordeaux1.fr*	Laboratoire d'Astrophysique de Bordeaux	Floirac	France
Behrend, Dirk *Dirk.Behrend@nasa.gov*	NVI, Inc. – GSFC	Greenbelt, MD	USA
Bellanger, Antoine *bellanger@obs.u-bordeaux1.fr*	Laboratoire d'Astrophysique de Bordeaux	Floirac	France
Bertarini, Alessandra *abertari@mpifr-bonn.mpg.de*	Institute of Geodesy and Geoinformation	Bonn	Germany
Boboltz, David *dboboltz@usno.navy.mil*	USNO	Washington	USA
Boehm, Johannes *johannes.boehm@tuwien.ac.at*	Institute of Geodesy and Geophysics Vienna University of Technology	Vienna	Austria
Bolotin, Sergei *bolotin@mao.kiev.ua*	Main Astronomical Observatory National Academy of Sciences	Kiev	Ukraine
Bourda, Géraldine *bourda@obs.u-bordeaux1.fr*	Laboratoire d'Astrophysique de Bordeaux	Floirac	France
Campbell, Bob *campbell@jive.nl*	JIVE	Dwingeloo	Netherlands
Campbell, James *jcampbel@uni-bonn.de*	Geodetic Institute – University of Bonn	Bonn	Germany
Charlot, Patrick *charlot@obs.u-bordeaux1.fr*	Laboratoire d'Astrophysique de Bordeaux	Floirac	France
Cho, Jungho *jojh@kasi.re.kr*	Korea Astronomy & Space Science Institute	Daejeon	South Korea
Clark, Tom *K3IO@verizon.net*	NVI, Inc. – GSFC	Clarksville, MD	USA
Collilieux, Xavier *xavier.collilieux@ign.fr*	IGN/LAREG – GRGS	Marne La Vallée	France
Collioud, Arnaud *collioud@obs.u-bordeaux1.fr*	Laboratoire d'Astrophysique de Bordeaux	Floirac	France
Colomer, Francisco *f.colomer@oan.es*	Instituto Geografico Nacional	Madrid	Spain
Corey, Brian *bec@haystack.mit.edu*	MIT Haystack Observatory	Westford, MA	USA
Durepaire, Lydie *durepaire@obs.u-bordeaux1.fr*	Laboratoire d'Astrophysique de Bordeaux	Floirac	France

Name	Affiliation	City	Country
Elgered, Gunnar *kge@chalmers.se*	Chalmers University of Technology	Onsala	Sweden
Engelhardt, Gerald *gerald.engelhardt@bkg.bund.de*	BKG	Leipzig	Germany
Engen, Bjorn *bjorn.engen@statkart.no*	Statens kartverk	Honefoss	Norway
Eschelbach, Cornelia *eschelbach@gik.uka.de*	Geodetic Institut – Universität Karlsruhe	Karlsruhe	Germany
Fey, Alan *afey@usno.navy.mil*	USNO	Washington	USA
Fomalont, Ed *efomalon@nrao.edu*	NRAO	Charlottesville, VA	USA
Frey, Sandor *frey@sgo.fomi.hu*	FOMI Satellite Geodetic Observatory	Budapest	Hungary
Gambis, Daniel *daniel.gambis@obspm.fr*	Observatoire de Paris – SYRTE	Paris	France
Gaume, Ralph *rgaume@usno.navy.mil*	USNO	Washington	USA
Gipson, John *John.M.Gipson@nasa.gov*	NVI, Inc. – GSFC	Greenbelt, MD	USA
Gontier, Anne-Marie *Anne-Marie.Gontier@obspm.fr*	Observatoire de Paris – SYRTE	Paris	France
Gordon, David *David.Gordon-1@nasa.gov*	NVI, Inc. – GSFC	Greenbelt, MD	USA
Haas, Rüdiger *rudiger.haas@chalmers.se*	Chalmers University of Technology	Onsala	Sweden
Hanssen, Rune *rune.hanssen@statkart.no*	Statens kartverk	Honefoss	Norway
Hase, Hayo *hayo.hase@bkg.bund.de*	BKG	Bad Kötzting	Germany
Heinkelmann, Robert *heinkelmann@dgfi.badw.de*	DGFI	Munich	Germany
Himwich, Ed *Ed.Himwich@nasa.gov*	GSFC	Greenbelt, MD	USA
Jacobs, Christopher *Chris.Jacobs@jpl.nasa.gov*	JPL	Pasadena, CA	USA
Jike, Takaaki *jike@miz.nao.ac.jp*	Mizusawa VERA Observatory – NAOJ	Oshu City	Japan
Johnston, Kenneth *kjj@astro.usno.navy.mil*	USNO	Washington, DC	USA
Kingham, Kerry *kingham.kerry@usno.navy.mil*	USNO	Washington, DC	USA
Kobayashi, Hideyuki *hideyuki.kobayashi@nao.ac.jp*	NAOJ	Tokyo	Japan
Kurdubov, Sergey *ksl@quasar.ipa.nw.ru*	Institute of Applied Astronomy	St. Petersburg	Russia
Lambert, Sébastien *sebastien.lambert@obspm.fr*	Observatoire de Paris – SYRTE	Paris	France
Langkaas, Line *lanlin@statkart.no*	Norwegian Mapping and Cadastre Authority	Honefoss	Norway

Name	Affiliation	City	Country
Lanotte, Roberto *roberto.lanotte@telespazio.com*	Telespazio	Matera	Italy
Lösler, Michael *loesler@gik.uka.de*	Geodetic Institut – Universität Karlsruhe	Karlsruhe	Germany
Ma, Chopo *chopo.ma@nasa.gov*	GSFC	Greenbelt, MD	USA
Macmillan, Daniel *daniel.s.macmillan@nasa.gov*	NVI, Inc. – GSFC	Greenbelt, MD	USA
Mantovani, Franco *fmantovani@ira.inaf.it*	IRA – INAF	Bologna	Italy
Müskens, Arno *mueskens@mpifr.de*	Institute of Geodesy and Geoinformation	Bonn	Germany
Negusini, Monia *negusini@ira.inaf.it*	IRA – INAF	Bologna	Italy
Neidhardt, Alexander *neidhardt@fs.wettzell.de*	FESG – Munich Technical University Geodaetisches Observatorium Wettzell	Bad Kötzting	Germany
Niell, Arthur *aniell@haystack.mit.edu*	MIT Haystack Observatory	Westford	USA
Nilsson, Tobias *tobias.nilsson@chalmers.se*	Onsala Space Observatory	Onsala	Sweden
Nothnagel, Axel *nothnagel@uni-bonn.de*	Institute of Geodesy and Geoinformation	Bonn	Germany
Pany, Andrea *andrea.pany@tuwien.ac.at*	Institute of Geodesy and Geophysics Vienna University of Technology	Vienna	Austria
Petrachenko, Bill *Bill.Petrachenko@nrc.gc.ca*	Natural Resources Canada (NRCan)	Ottawa, ON	Canada
Plank, Lucia *lucia.plank@tuwien.ac.at*	Institute of Geodesy and Geophysics Vienna University of Technology	Vienna	Austria
Porcas, Richard *porcas@mpifr-bonn.mpg.de*	MPIfR	Bonn	Germany
Schlueter, Wolfgang *schlueter_wolfgang@t-online.de*	BKG	Bad Kötzting	Germany
Schuh, Harald *harald.schuh@tuwien.ac.at*	Institute of Geodesy and Geophysics Vienna University of Technology	Vienna	Austria
Schwegmann, Wolfgang *wolfgang.schwegmann@bkg.bund.de*	BKG	Frankfurt	Germany
Shu, Fengchun *sfc@shao.ac.cn*	Shanghai Astronomical Observatory Chinese Academy of Science	Shanghai	China
Skurikhina, Elena *sk-al@yandex.ru*	Institute of Applied Astronomy	St. Petersburg	Russia
Spicakova, Hana *hana@mars.hg.tuwien.ac.at*	Institute of Geodesy and Geophysics Vienna University of Technology	Vienna	Austria
Takashima, Kazuhiro *takasima@gsi.go.jp*	Geographical Survey Institute	Tsukuba	Japan
Tanir, Emine *etanir@ktu.edu.tr*	Karadeniz Technical University Engineering Faculty – Geodesy	Trabzon	Turkey
Teke, Kamil *kteke@mars.hg.tuwien.ac.at*	Institute of Geodesy and Geophysics Vienna University of Technology	Vienna	Austria
Titov, Oleg *oleg.titov@ga.gov.au*	Geoscience Australia	Canberra	Australia

Name	Affiliation	City	Country
Tornatore, Vincenza *vincenza.tornatore@polimi.it*	Politecnico di Milano – DIIAR	Milano	Italy
Tuccari, Gino *g.tuccari@ira.inaf.it*	IRA – INAF	Bologna	Italy
Ulvestad, James *julvesta@nrao.edu*	NRAO	Wallkill, NY	USA
Vondrak, Jan *vondrak@ig.cas.cz*	Astronomical Institute	Prague	Czech Republic
Wang, Guangli *wgl@shao.ac.cn*	Shanghai Astronomical Observatory	Shanghai	China
Warren, Steven *steven.w.warren@navy.mil*	USNO	Washington	USA
Weimin, Zheng *zhwm@shao.ac.cn*	Shanghai Astronomical Observatory	Shanghai	China
Whitney, Alan *awhitney@haystack.mit.edu*	MIT Haystack Observatory	Westford	USA
Wresnik, Joerg *wresnik@mars.hg.tuwien.ac.at*	Institute of Geodesy and Geophysics Vienna University of Technology	Vienna	Austria
Zhang, Ming *zhang@obs.u-bordeaux1.fr*	Laboratoire d'Astrophysique de Bordeaux	Floirac	France
Zhang, Xiuzhong *xzhang@shao.ac.cn*	Shanghai Astronomical Observatory	Shanghai	China

Abbreviations

BKG	Bundesamt für Kartographie und Geodäsie
DGFI	Deutsches Geodätisches Forschungsinstitut
DIIAR	Dipartimento di Ingegneria Idraulica, Ambientale, Infrastrutture Viarie, Rilevamento
ESA	European Space Agency
ESOC	European Space Operations Center
GRGS	Groupe de Recherche en Géodésie Spatiale
GSFC	Goddard Space Flight Center
IGN	Institut Géographique International
INAF	Istituto Nazionale di Astrofisica
IRA	Istituto di Radioastronomia
JIVE	Joint Institute for VLBI in Europe
JPL	Jet Propulsion Laboratory
LAREG	LAboratoire de REcherche en Géodésie
MIT	Massachusetts Institute of Technology
MPIfR	Max Planck Institute for Radioastronomy
NAOJ	National Astronomical Observatory of Japan
NRAO	National Radio Astronomy Observatory
SYRTE	SYstèmes de Références Temps-Espace
USNO	U.S. Naval Observatory